

CARBON, SILICON AND PHOSPHORUS REACTIONS
IN OXYGEN STEELMAKING

A Thesis submitted to
the University of London
for the degree of
DOCTOR OF PHILOSOPHY

by

SHAFI JAHANSHAH

Nuffield Research Group.
Department of Metallurgy and Materials Science,
Imperial College of Science and Technology,
London, S.W.7. 2BP

July 1980

To my parents

ABSTRACT

The electromagnetic levitation technique has been used to study the removal of carbon, silicon, and phosphorus from liquid iron alloys, in the presence or absence of a basic slag, by streams of oxidising, neutral or reducing gas mixtures.

The rates of decarburization of Fe-C alloys, by streams of CO_2 and O_2 was found to be controlled by mass transfer in the gas phase. These rates were found to be in excellent agreement with those predicted by the available correlations for mass transfer in the gas phase. The effects of 0.1 wt.% phosphorus on the rates of decarburization and vaporization of iron have been studied, and it has been found that phosphorus acts as a surface active element in the Fe-C alloys. Homogeneous nucleation of CO bubbles in levitated drops of Fe-C and Fe-C-P alloys has been observed before and after the main carbon boil. The presence of silicon, at concentrations of about 0.015 wt.% in the Fe-C alloy has a pronounced effect on the retardation of the rate of decarburization, and the promotion of the carbon boil.

The rate of removal of silicon from liquid Fe-Si drops, by a stream of oxygen-bearing gas was studied, and it was found that the rate of transport of silicate ions in the iron-silicate slag was the rate controlling step. The presence of 0.1 wt.% phosphorus showed no significant

effect on the rate of desiliconization of these drops.

The present investigations into the study of "dephosphorization" of Fe-P alloys in the absence of a basic slag, has shown that at oxygen partial pressures ranging from about 2.3×10^{-16} to 1.0 atm. in the gas stream passing levitated drops of Fe-P alloys, containing 0.1-2.0 wt.% phosphorus, the removal of phosphorus from the liquid iron does not take place via the formation of volatile species of sub oxides of phosphorus such as PO or PO_2 . Oxidation experiments of Fe-C-P alloys in a stream of CO_2 have shown that dephosphorization does not take place at high or low carbon concentrations in the metal by the formation of volatile phosphorus species. Furthermore vaporization experiments carried out on the levitated drops of Fe-P alloys, in streams of H_2/CO_2 and H_2 using nitrogen as a diluent, have revealed that the removal of phosphorus from liquid iron via the formation of volatile nitrides, hydrides, and hydroxides of phosphorus is unlikely.

Chemical equilibrium between levitated drops of iron and $CaO-P_2O_5-FeO$ slags had been achieved in a very short period of time, but thermal equilibrium may not have been achieved between the two phases. The equilibrium studies made have revealed that the effect of the miscibility gap in the system $CaO-P_2O_5-FeO$ on the dephosphorization power of the slags of high "FeO" content was beneficial. The rates of transfer of

phosphorus between the iron drops and basic slags was found to be very fast and the determined rates of transfer of phosphorus between these phases was between 1×10^{-5} to 5×10^{-5} moles $\text{cm}^{-2}, \text{s}^{-1}$. It was concluded that the rate of transport of phosphorus in the slag phase was controlling the rates of dephosphorization and re-phosphorization.

List of symbols

LIST OF SYMBOLS

A	surface area, cm ²
C _p	heat capacity of gas, cal.g ⁻¹ . °K ⁻¹
[C]	carbon concentration in metal, wt-%
DA/B	interdiffusion coefficient, cm ² . S ⁻¹
d	diameter of metal drop, cm
g	acceleration due to gravity, cm.S ⁻²
k	mass transfer coefficient, cm.S ⁻¹
k'	thermal conductivity of gas, cal.sec ⁻¹ cm ⁻¹ . °K ⁻¹
K	equilibrium constant
n	numbers of moles
N	mole fraction
JA, JB	fluxes of component A, B etc, mole.cm ⁻² S ⁻¹
[O]	oxygen concentration in metal, wt-%
P	total pressure, atm.
p _A , p _B	partial pressure of component A, B etc, atm.
[P]	phosphorus concentration in metal, wt.%
p	vapour pressure, atm
R	gas constant, cm ³ . atm. °K ⁻¹ . mole ⁻¹
[Si]	silicon concentration in metal, wt.%
T	absolute temperature, °K
T _f	'film' temperature, °K = $\frac{1}{2} (T_s + T_b)$
U	linear velocity of gas in tube approaching drop at temperature T _b , cm.S ⁻¹
V	volume of drop, cm ³
x	distance, cm
z	effective thickness of 'diffusion boundary layer', cm
ρ	gas density, g.cm ⁻³
μ	gas viscosity, g.cm ⁻¹ S ⁻¹
Sh	Sherwood number $\left(\frac{kd}{DA/B}\right)$
Gr ^m	Grashof number for mass transfer $\left(\frac{gd^3 \rho_f (\rho_s - \rho_b)}{\mu_f^2}\right)$
Gr ^h	Grashof number for heat transfer $\left(\frac{gd^3 \rho_f^2 (T_s - T_b)}{\mu_f^2 T_f}\right)$
Pr	Prandtl number $\left(\frac{\mu C_p}{k'}\right)_f$
Re	sphere Reynolds number $\left(\frac{\rho_f U d}{\mu_f}\right)$
Sc	Schmidt number $\left(\frac{\mu}{\rho DA/B}\right)_f$
\overline{Gr}	mean Grashof number $\left((Gr^m + (Sc/Pr)^{0.5} Gr^h)\right)$

SUBSCRIPTS, SUPERSRIPTS

b	property in bulk gas
C	property for carbon in metal
f	property at film temperature T _f
i	property at interface
s	property at surface of drop
G	property in gas phase
M	property in metal phase
O	property for oxygen in metal

CONTENTS

	Page
ABSTRACT	ii
LIST OF SYMBOLS	v
<u>CHAPTER 1. INTRODUCTION</u>	1
<u>CHAPTER 2.</u>	4
2-1. INTRODUCTION	4
2-2. ELECTROMAGNETIC LEVITATION	4
2-3. LEVITATION COIL MAKING	10
2-4. COIL DESIGN	15
2-4.1. Effect of varying the internal diameter of the coil.	15
2-4.2. Effect of varying the size of copper tubing.	18
2-4.3. Effect of varying the semi-apex angle of the suspension coil.	18
2-4.4. Effect of varying the number of turns of the levitation coil.	18
2-4.5. Further improvements	21
<u>CHAPTER 3.</u>	22
3-1. INTRODUOTION	22
3-2. TEMPERATURE MEASUREMENT AND PYROMETER CALIBRATION	22
3-3. PREPARATION OF ALLOYS	27
3-4. PREPARATION OF SLAGS	32
3-5. DESCRIPTION OF THE LEVITATION APPARATUS	36
3-5.1. Levitation coils	39
3-5.2. The gas train	41
3-5.3. Techniques for addition of slag	44
3-5.4. Photographic technique	47
3-5.5. Description of a typical levitation run	48
3-6. DESCRIPTION OF THE FREE FALL APPARATUS	49
3-6.1. Slag addition techniques	51
3-6.2. Quenching device	51
3-7. CARBON ANALYSIS	54
3-8. PHOSPHORUS ANALYSIS	54
<u>CHAPTER 4. KINETICS OF DECARBURIZATION OF LIQUID IRON ALLOYS BY STREAMS OF OXYGEN OR CARBON DIOXIDE</u>	58
4-1. INTRODUCTION	58
4-2. DECARBURIZATION OF IRON-CARBON ALLOYS	59

	Page
4-3. MASS TRANSFER BETWEEN A FLOWING GAS AND A STATIONARY SPHERE	60
4-4. EXPERIMENTAL METHOD	68
4-5. RESULTS	69
4-6.1 Decarburization by O ₂	77
4-6.2 Decarburization by CO ₂	79
4-7. DISCUSSION	81
4-7.1. Rate controlling step in the reaction of Fe-C and O ₂	81
4-7.2. Rate of Decarburization of Fe-C with CO ₂	85
4-7.3. Effect of 0.1 wt% P on the rate of ² decarburization	87
4-7.4. Effect of silicon on the rates of decarburization	94
4-7.5. Carbon boil	97
4-7.6. Comparison of the predicted and measures rates of decarburization	99
4-8. CONCLUSION	105
<u>CHAPTER 5. ENHANCED VAPORIZATION OF LIQUID IRON-PHOSPHORUS ALLOYS IN STREAMS OF OXIDISING OR REDUCING GAS MIXTURES</u>	107
5-1. INTRODUCTION	107
5-2. PREVIOUS WORK	107
5-3. FREE ENERGIES OF FORMATION OF VOLATILE PHOSPHORUS COMPOUNDS	109
5-4. EXPERIMENTAL	111
5-5. RESULTS	112
5-6. DISCUSSION	126
5-7. CONCLUSION	144
<u>CHAPTER 6. KINETICS OF DESILICONIZATION OF LIQUID IRON ALLOYS</u>	145
6-1. INTRODUCTION	145
6-2. PREVIOUS WORK	145
6-3. EXPERIMENTAL TECHNIQUE	150
6-4. RESULTS	152

	Page	
6-5.	INTERPRETATION OF THE RESULTS	155
6-6.	DISCUSSION	163
6-6.1.	Rate controlling step in the reaction of Fe-Si and O_2	163
6-7.	CONCLUSIONS	167
<u>CHAPTER 7. EQUILIBRIA AND KINETICS OF THE DEPHOSPHORIZATION OF LIQUID IRON</u>		168
7-1.	INTRODUCTION	168
7-2.	PREVIOUS WORK	169
7-2.1.	The equilibrium distribution of phosphorus between liquid iron and basic slags	169
7-2.2.	The $CaO-P_2O_5-FeO$ phase diagram	172
7-2.3.	Kinetics of transfer of phosphorus between liquid iron and basic slags	174
7-3.	EXPERIMENTAL TECHNIQUES	177
7-3.1.	Rate of establishing equilibrium	177
7-3.2.	Equilibrium distribution of phosphorus between metal and basic slags.	177
7-3.3.	Rates of transfer of phosphorus between liquid iron and basic slags	178
7-4.	RESULTS	179
7-5.	INTERPRETATION OF THE DATA	194
7-6.	DISCUSSION	195
7-6.1.	Rate of attainment of chemical equilibrium	195
7-6.2.	The distribution of phosphorus between the metal and slag	197
7-6.3.	The effect of CaF_2 on the distribution of phosphorus	205
7-6.4.	Kinetics of dephosphorization of Fe-P drops by a basic slag.	207
7-6.5.	Kinetics of transfer of phosphorus between the Fe-P drops and lime	211
7-6.6.	Reactions of Fe-C-P with basic slags	218
7-7.	CONCLUSIONS	222
APPENDICES:	1	224
	2	233
	3	234
ACKNOWLEDGEMENTS		237
REFERENCES		238

CHAPTER 1
INTRODUCTION

The molten iron produced by the blast furnace process contains many impurities such as carbon, manganese, phosphorus, silicon and sulphur, which have to be removed during the steelmaking processes in order that the product becomes a useful steel. The reactions occurring during steelmaking processes are basically oxidation and removal of such impurities, hence with the exception of sulphur, the impurities in the pig iron are removed by other selective oxidation, and some of the products separating as a slag phase.

By oxygen steelmaking, one usually refers to the two commonest processes, namely top blowing (L.D. or B.O.F.) or bottom blowing (Q-B.O.P. or O.B.M.). In these processes the oxygen is injected onto or into the molten metal respectively. The ultra-sonic top blown injection of oxygen causes a turbulent mixing of the metal and the slag, which in turn increases the rates of the reactions to a great extent, and hence difficulties arise in the control of such processes. From the economical and quality control points of view, the basic oxygen steelmaking processes should be controlled more exactly. In order to achieve a better control of the process, the details of the reaction mechanisms and the thermal behaviour in these processes require to be investigated carefully and extensively.

The aim of the present work was to obtain a better understanding of the phosphorus reaction in basic oxygen steelmaking processes, although some consideration was also given to the carbon and silicon reactions. These studies were made on levitated drops of iron alloys in the presence or absence of a slag phase, in streams of oxidising, neutral or reducing gases.

This thesis has been divided into several chapters, each of which describes a particular topic in detail. Chapter 2 deals with the tests performed on the levitation coil designs, to develop a coil capable of maintaining a stable droplet at lower temperature than has commonly been achieved by this technique. In Chapter 3 the basic experimental techniques used are described in some detail. The next chapter deals with the kinetics of oxidation and removal of carbon from levitated drops of iron alloys by streams of oxidising gases. This was used to study some aspects of mass transfer between a levitated drop and a flowing gas so that a better understanding of the system could be obtained. Some of the information gathered in Chapter 4 was used in the analysis of other kinetic studies, particularly those concerning a possible mechanism for the removal of the phosphorus from liquid iron by a gas/vapour phase reaction, which is described in Chapter 5. The kinetics of the oxidation and removal of silicon from liquid iron drops is described in Chapter 6, so that

the mass transfer between a levitated drop and a slag phase, together with the thermal behaviour of such a system could be studied. Finally in Chapter 7 the studies made on the equilibrium and kinetics of the phosphorus removal reactions from liquid iron alloys by basic slags are described.

CHAPTER 2

CHAPTER 2

2-1. INTRODUCTION

This chapter deals with the work carried out on testing several types of levitation coils in order to obtain the optimum design of the coil to give cool sample temperatures.

2-2. ELECTROMAGNETIC LEVITATION

Levitation of a metal is achieved by placing the metal in a correctly designed coil, carrying a high frequency alternating current. Eddy currents induced in the metal interact with the inducing field to give supporting (vertical) and stabilizing (lateral) restoring forces to the sample metal. The metal is then freely supported in space and due to the resistance of the metal, the eddy currents heat the specimen usually to above the melting point.

Excellent reviews of levitation melting techniques and their uses have been published by Peifer,⁽¹⁾ McLean,⁽²⁾ Rostron⁽³⁾ and Lewis⁽⁴⁾ while those of Hulsey,⁽⁵⁾ Okness et al.⁽⁵⁾ and Jenkins et al.⁽⁷⁾ deal more specifically with coil geometry and levitation force.

Large scale use of the technique of levitation melting on an industrial scale has not been used mainly due to the small masses of metal involved. However, extensive use has been made of it by many workers for physico-chemical studies at elevated temperatures and pressures.

The technique has many advantages and some disadvantages. It is specifically advantageous for gas-metal kinetics and equilibrium studies because:

- i) Crucible contamination of the melt is eliminated.
- ii) Homogeneity of the melt is achieved due to very efficient stirring.
- iii) Rapid attainment of equilibrium in gas-liquid metal systems is obtained due to the large surface area being exposed to the gas phase per unit volume of the melt.
- iv) The geometry of the levitated drop can be fairly accurately defined for gas-liquid metal kinetic studies.
- v) The gas phase surrounding the melt is easily controlled and can readily be changed for kinetic studies.

There are mainly three disadvantages associated with the technique and these are:

- i) Difficulties in temperature control and measurements.
- ii) Relatively high vaporisation rates.
- iii) Generally, the mass of the molten charge is limited to under 20 grams.

On considering the various characteristics of the technique it appears that the non-contamination from container materials, homogeneity of the melt, rapid attainment of equilibrium between gas-liquid metal system, well-defined geometry and relatively high vaporisation rates were all favourable for enhanced vaporisation studies. Furthermore the levitated drop may be considered as a bubble

turned "inside out" and so the results observed during the reaction with gases are relevant and analagous to reactions taking place during e.g. oxygen steelmaking.

The difficulties in controlling and measuring the temperature of levitated drops appears to be the most disadvantageous property of the technique. As far as the measurement of the temperature is concerned the difficulty arises from the fact that thermocouples cannot be conveniently used because the levitated molten drops cannot be probed by a thermocouple, and hence measurements of the surface temperature of a levitated metal drop necessitates the use of a pyrometric device sensitive to the energy emitted by the hot specimen. In these investigations a two colour radiation pyrometer was used to measure the surface temperature of the molten drops with a reasonable accuracy. Hence the control of the temperature remains the other main objection to the use of the technique. Generally keeping the temperature of the molten drop to within reasonable limits has been the main difficulty. There are several methods for controlling the temperature during levitation and these are listed overleaf.

In the past several workers^(1,6) have achieved temperatures as low as 1600°C with iron specimens in helium and/or hydrogen gas streams, but lowering the temperature of the sample below 1600°C at atmospheric pressure was thought to be very difficult until the work of Yavoskii et al.⁽⁸⁾ was published. According to their results it is

Variable	Effect
Coil design	Coils which produce more divergent fields produce lower temperature for a given power input and sample.
Power input	Variation of power input to the coil varies the specimen temperature. A minimum temperature is often obtained at a particular power input.
Sample mass	Increasing the mass of a levitated charge beyond about one gram usually increases the temperature.
Convection losses	By changing the surrounding gaseous environment (by addition of inert diluents such as argon or helium) the temperature of the sample may be altered.
Radiation losses	By altering the radiation environment the temperature of the sample may be altered.

possible to lower the temperature of iron specimens as low as 1300°C in an atmosphere of argon (which has a lower thermal conductivity than hydrogen or helium) at atmospheric pressure, by induction coils of appropriate geometry. If the new coil design by Yavoskii et al. had actually resulted in the temperature control of iron samples, then the worst problems associated with the levitation technique could be solved.

The principal difference between the coils used by Yavoskii et al. and the conventional type described by other authors is that the upper turns are connected in parallel instead of in series with the lower turns (as shown in Figures 2.1(a) and 2.1(b)). Hence according to Yavoskii "The induction coils, with turns wound on opposite sides were connected in parallel with the secondary winding of the high frequency transformer, thus solving the problem of independent power supply to the suspension and heating induction coils. The relationship between the current flowing through these coils could be adjusted according to number of turns in each of them."

It was consequently decided to construct and test various coil designs, where the two parts of the coils were connected in parallel. The following designs were tested on three different high frequency generators operating at different frequencies and maximum power output.

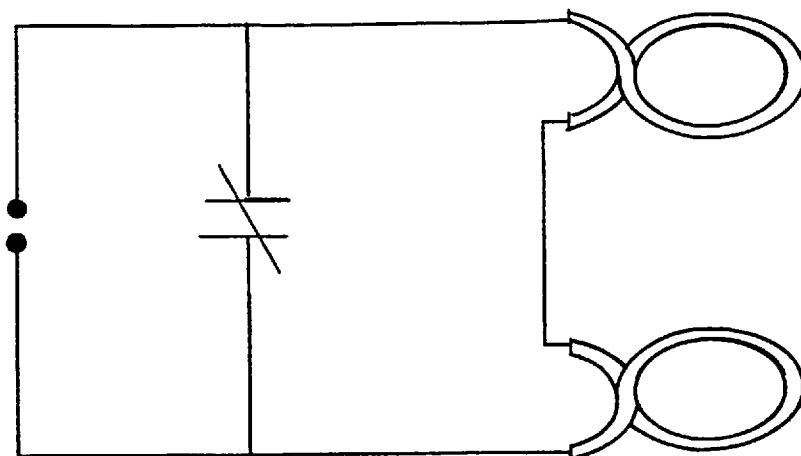


Fig.2.1(a) Conventional electrical circuit for levitation melting.

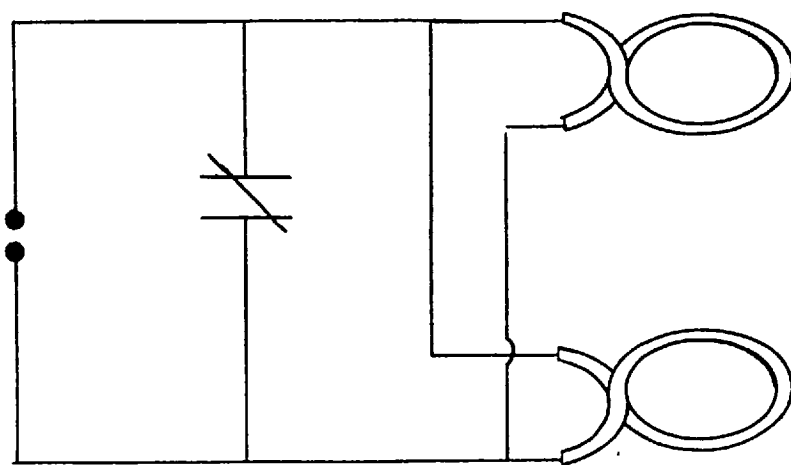
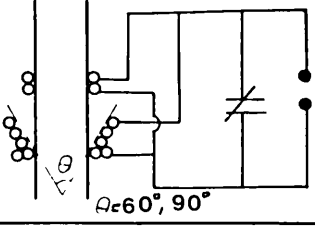
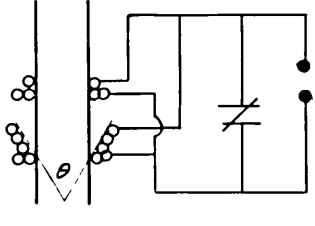
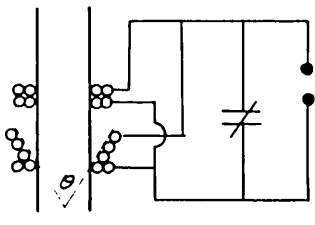
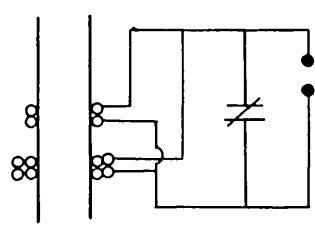
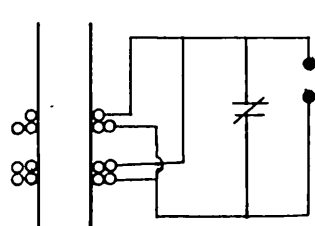
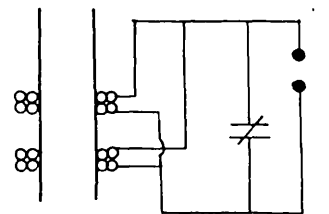
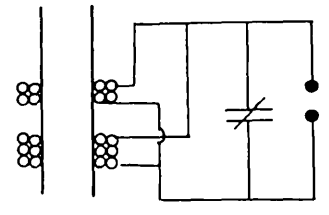
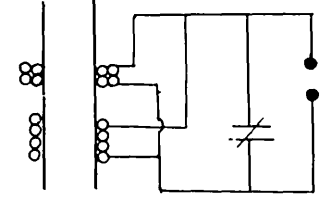
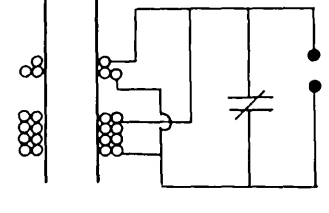
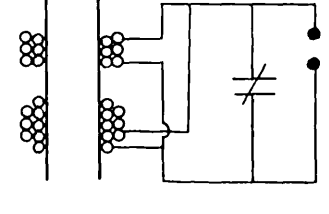
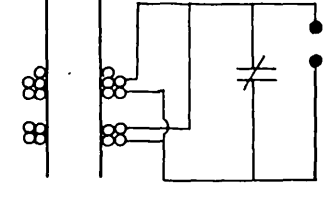


Fig.2.1(b) Modified electrical circuit by Yavoskii for levitation melting.

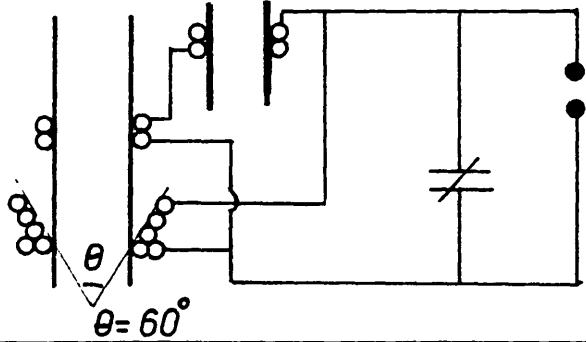
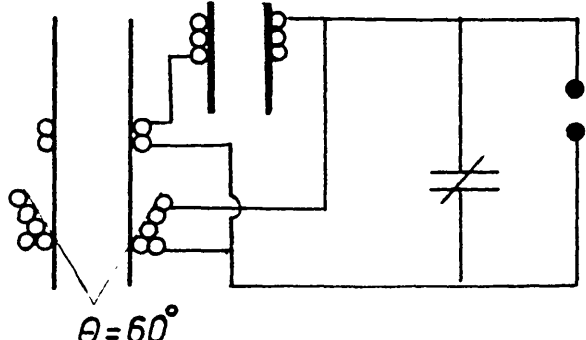
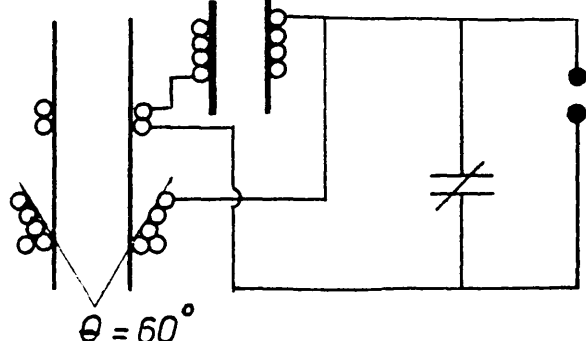
Table 2.1 Experimental results obtained on various coil designs tested with the two parts of the levitation coils being connected in parallel. All the designs were constructed in 3.2mm (1/8") copper tubing.

Coil	(450KHz, 15 KW) Radyne generator.	(450KHz, 12 KW) JJ generator.	(250KHz, 6 KW) Phillips generator.
	No levitation.	Maximum power required to levitate a 0.6g of copper.	No levitation.
	No levitation.	No levitation.	—
	No levitation.	—	—
	No levitation.	1g of copper was levitated with about 80% of the power.	No levitation.
	A small sample was levitated for a few seconds.	A 0.7g sample of copper was levitated, but $T > 1500^{\circ}\text{C}$.	—

cont.

<i>Coil.</i>	<i>Radyne gen.</i>	<i>JJ generator</i>	<i>Pillips gen.</i>
	No levitation.	0.86 g of copper was levitated with about 65% of the power.	No levitation.
	No levitation.	0.9 g of iron was levitated, but the coolest temperature achieved was 1850°C.	—
	No levitation.	—	—
	No levitation.	—	—
	No levitation.	—	—
	No levitation.	—	—

cont.

<p><i>These coils were wound in series with a secondary coil having an internal diameter of 15mm, so as to change the impedance of the coil.</i></p>	<p><i>Radyne generator (450 KHz, 15 KW)</i></p>
 <p>$\theta = 60^\circ$</p>	<p><i>No levitation.</i></p>
 <p>$\theta = 60^\circ$</p>	<p><i>No levitation.</i></p>
 <p>$\theta = 60^\circ$</p>	<p><i>No levitation.</i></p>

All these designs gave a very small lifting force to levitate samples of one gram or under of either copper or iron, and in a few cases where levitation was achieved the temperature of the molten sample was too high (about 1800°C in relatively high flow rates of helium). Hence it was concluded that the use of such coil design and electrical circuit to improve the control of the temperature of the molten levitated drop under our experimental conditions did not seem promising and it was decided to focus our attention on the conventional type of levitation coil designs and to attempt to bring about improvement in these.

2-3. LEVITATION COIL MAKING

In making a conventional coil copper tubing of 3.2 mm or 2.4 mm outer diameter with a wall thickness of 0.36 mm was used. After annealing, the tube was filled with dry sand and was wound using a "former". Each coil consisted of several turns of which usually five or six were wound in one direction and the others in the opposite direction. The two turns of the bottom coil were normally wound coplanar, the inner one having a set diameter of 17.5 or 15.6 mm and the remainder were wound on a cone of semi-apex angle of 30° or 45° . The top turns were normally wound coaxially on a 17.5 or 15.6 mm.

There are four possible ways in which the lower and upper turns of a levitated coil can be connected in series and with the upper turns wound in a reverse direction to the lower ones. These are illustrated in Figure 2.2.

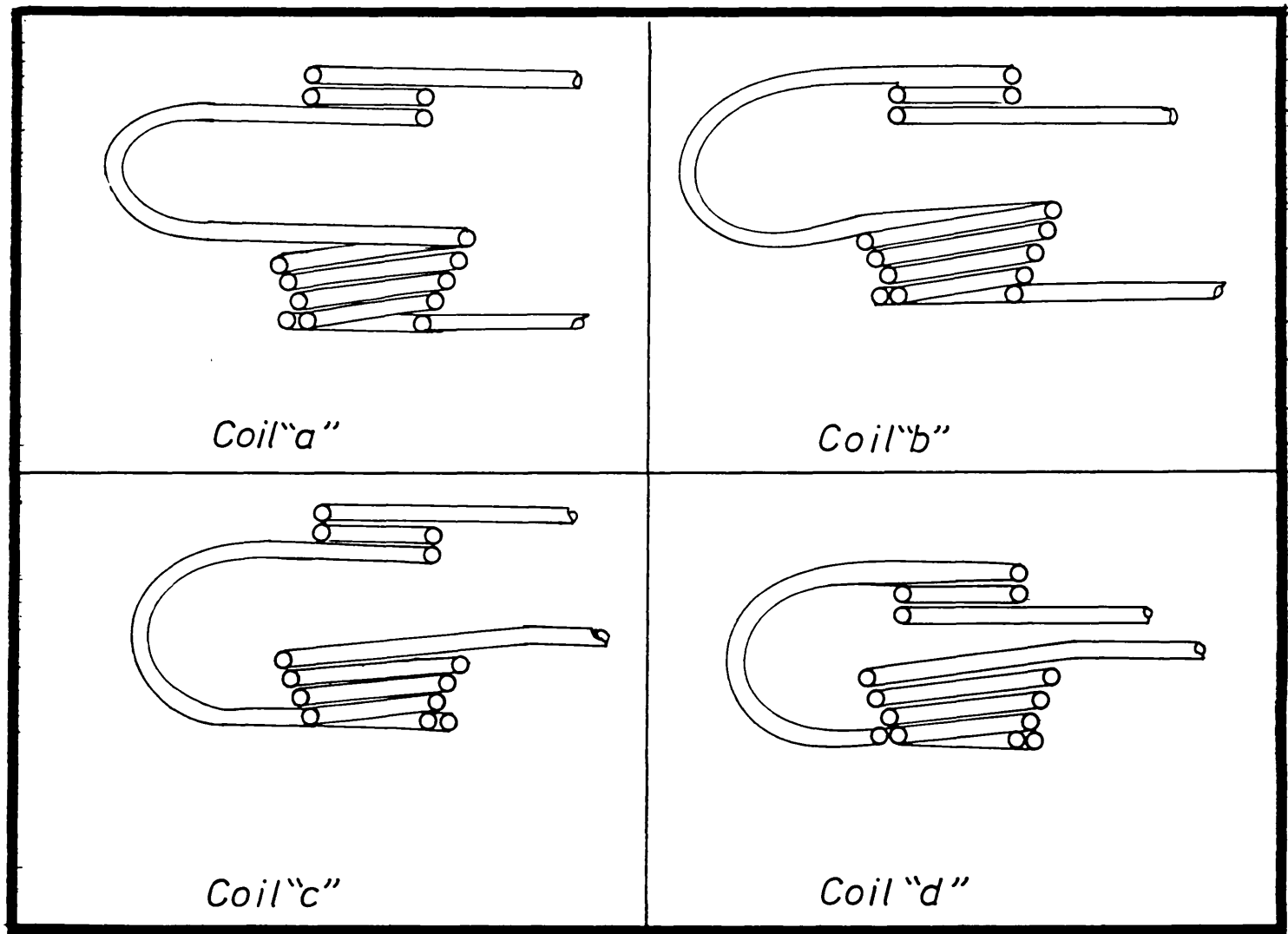


Figure 2.2

2-4 COIL DESIGN

Comparison of the results obtained on testing the four conventional types of coils under similar experimental conditions indicates that in coil "a", where the upper turns of the lower coil (suspension coil) is connected to the lower turns of the upper coil, produces the "hottest" levitation coil in which it is very difficult to keep down the temperature of the molten sample. The other extreme is illustrated by coil "d" in Figure 2.2., in which the lowest turn of the suspension coil is connected to the topmost turn of the upper coil. It is this construction which was found to give strong levitation force together with excellent temperature control. Coil conformations "b" and "c" show characteristics intermediate between "a" and "d".

The reason for these differences in behaviour are not well understood but one important factor is that coil "d" lends itself readily to close juxtaposition of the upper and lower turns.

2-4.1 Effect of varying the internal diameter of the coil

The results obtained indicate that decreasing the internal diameter of the coil causes the temperature of the molten drop to be lowered slightly under similar experimental conditions.

Table 2.2 Effect of coil design on iron specimen temperature

Generator ; Radyne (15 KW | 450 KHz)

Power ; maximum.

Mass of iron sample ; 1.2 ± 0.05 g.

Inner diameter of the coils ; 17.5 mm.

Semi-apex angle of the coils ; 30°

Coils were wound using 3.2 mm copper tubing.

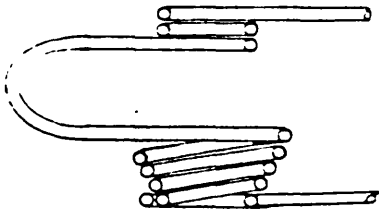
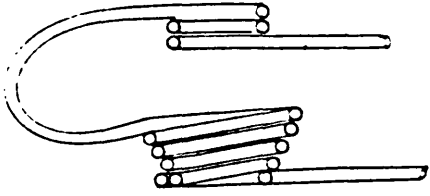
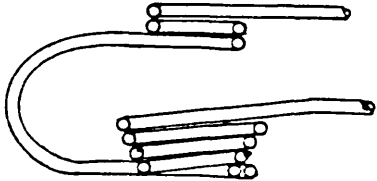
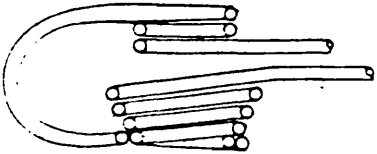
Design of the coil.	helium flow rate. (s.l.min ⁻¹)	steady temperature of the molten drop. (°C)
 <p>Coil "a"</p>	10.0	1570 ± 5
 <p>Coil "b"</p>	10.5	1560 ± 5
 <p>Coil "c"</p>	6.0	1560 ± 5
 <p>Coil "d"</p>	3.1	1570 ± 5

Table 2.3 Effect of coil design on iron specimen temperature.

Generator ; Radyne (15 KW/450 KHz)

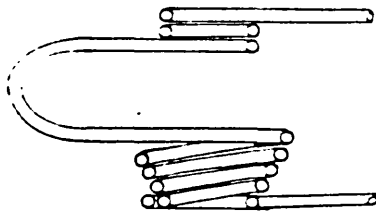
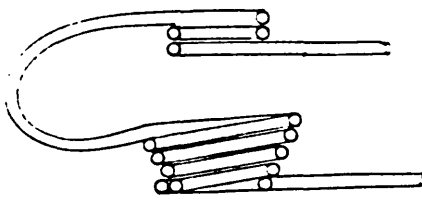
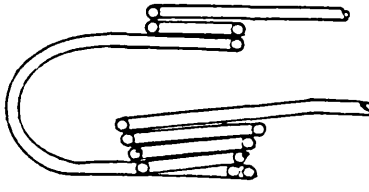
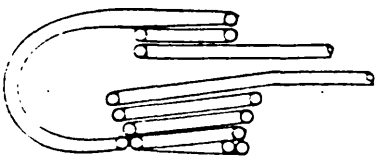
Power; maximum.

Mass of the iron sample; 1.2 ± 0.05 g.

Inner diameter of the coils; 15.6 mm.

Semi-apex angle of the coils; 30°

Coils were wound using 3.2 mm copper tubing.

design of coil	helium flow rate. (s.l. min ⁻¹)	steady temperature of the molten drops. (°C)
 <p>Coil "a"</p>	12.0	1560 ± 5
 <p>Coil "b"</p>	7.0	1590 ± 5
 <p>Coil "c"</p>	5.5	1579 ± 5
 <p>Coil "d"</p>	2.05	1580 ± 5

2.4.2 Effect of varying the size of copper tubing

From Table 2.4 and subsequently from Figure 2.3 it can be seen that on reducing the outer diameter of copper tubing from 3.2 mm to 2.4 mm (with wall thickness of 0.46 and 0.36 mm respectively) an appreciably cooler coil is obtained. This is because a smaller diameter of copper tubing yields more turns per unit length of the coil, hence resulting in a higher field strength and gradient. Thus minimum heating and maximum lifting force can be achieved. The main problem associated with this size of copper tubing was that in the absence of a back-up water pump, when the generator power was increased beyond 80% the coils suffered from "burning".

2.4.3 Effect of varying the semi-apex angle of the suspension coil

For the two angles used in this work, it was found that coils with a semi-apex angle of 30° gave a better lifting force and hence a cooler sample temperature. This observation is in agreement with the work of Jenkins et al. (7)

2.4.4 Effect of varying the number of turns of the levitation coil

The results obtained on varying this parameter are illustrated in Figure 2.3, from which it can be seen that for all cases studied the coolest coil appears to have the combination of two turns on the top and five turns on

TABLE 2.4: Effect of varying the number of turns, semi-apex angle and the O.D. of copper tubing of levitation coils on the specimen temperature.

Generator: Radyne (15Kw/450 KHz)
 Mass of iron samples: 1.1 + 0.05 gram
 Inner diameter of coils: 15.6 mm
 type of coil design: d.

O.D. of copper tubing/generator power setting	semi-apex angle of bottom coil	No. of turns on the top coil/no of turns on the bottom coil	helium flow rate to give ⁺ 1600°C (s.l.m)
2.4 mm /80%	45°	2/4	1.68
		2/5	1.14
		2/6	2.24
	30°	3/5	3.14
		2/5	0.65
		2/6	1.0
		3/6*	1.11
3.2 mm /100%	45°	3/5	4.8
		2/5	2.45
	30°	3/5	3.95
		2/5	1.65

⁺The results were sometimes adjusted to 1600°C from data at slightly different generator powers (75%-85%), giving temperatures in the range 1580-1610°C.

*No coplanar turn at the base.

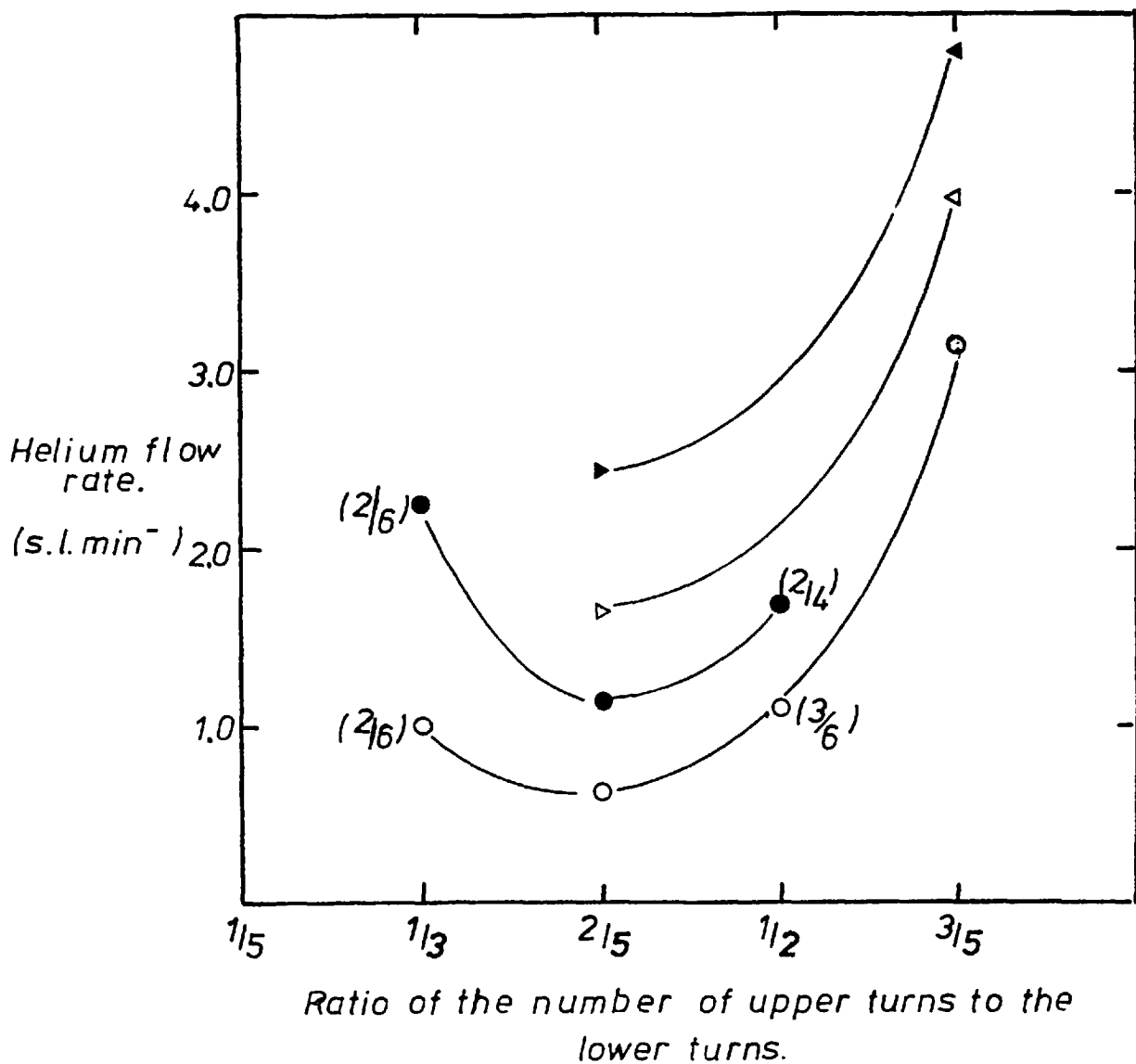


Figure 2.4 Variation of the No. of turns in the coils and the helium flow rate, to maintain a steady temperature of about 1600°C.

	OD. of copper tubing (mm)	semi-apex angle	generator power setting
◄	3.2	45°	100%
◁	3.2	30°	100%
●	2.4	45°	80%
○	2.4	30°	80%

the bottom. It is interesting to note that in the past most workers who managed to control the temperature of their molten iron alloys have used this particular combination of upper and lower turns.

2-4.5 Further improvement

Using silver tubing of 2.8 mm O.D. with a wall thickness of 0.25 mm instead of 3.2 mm copper tubing of 0.46 mm wall thickness, resulted in reducing the temperature of the molten drop by about 50°C , for an identical coil design. There are two reasons for such behaviour, first of all the silver tubing reduces the impedance of the levitation coil resulting in a relatively higher current and hence higher field strengths and gradient. The other contributing factor would be the wall thickness which results in a more efficient heat exchange between the radiating body and the cooling water.

The other contributing factor which alters the temperature of the molten sample slightly is to altering the radiation environment. It was found that dyeing the insulating sheeting of the tubing, tends to improve the heat losses by radiation, and hence a reduction of 10°C in temperature can be achieved.

CHAPTER 3

CHAPTER 3

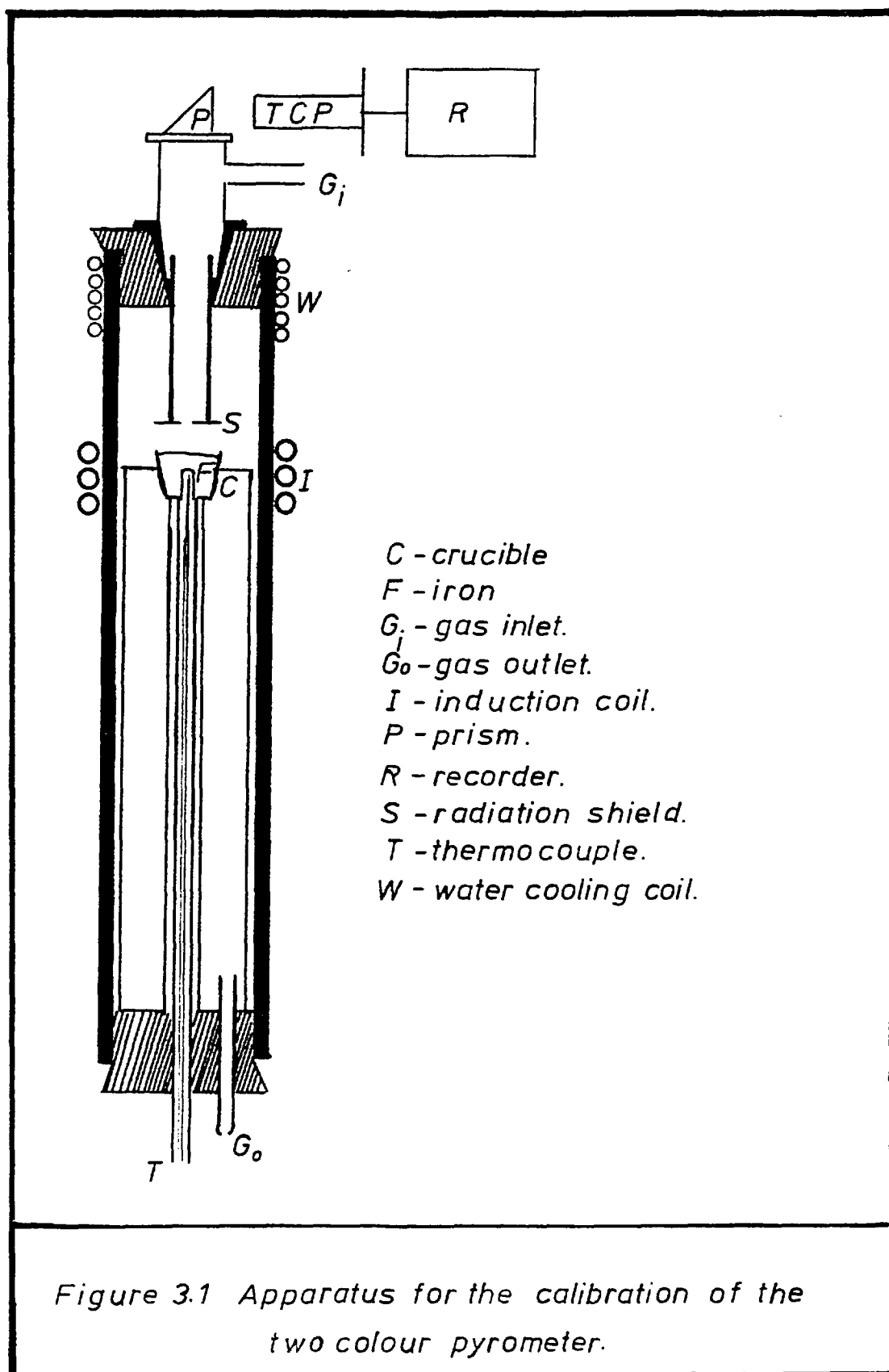
3-1. INTRODUCTION

The description of various experimental apparatus and techniques, that have been used in the course of this work are illustrated in some detail in this chapter. These include techniques that have been developed during the course of the work as well as those which have been adopted from others.

3-2. TEMPERATURE MEASUREMENT AND PYROMETER CALIBRATION

The accurate temperature measurement of a levitated drop is one of the difficult aspects of the technique. It has proved impossible to probe a levitated drop with a thermocouple, thus it is necessary to measure the surface temperature using optical means. Because of the tendency for the slag to collect at the bottom of the drop, it is possible to view the top metal surface of the drop without interference from the slag.

The pyrometer used for all the levitation experiments was an "Ardocol" two colour radiation pyrometer (TCP), connected to a "Kompensograph" continuous line potentiometric recorder. The pyrometer was calibrated as described in the next section, and was frequently checked against the melting point of "spec-pure" iron. In free fall experiments, however, the initial temperature of the metal surface



was measured using a milletron two-colour pyrometer, in this case the T.C.P. had only been calibrated against the melting point of "spec-pure" iron.

The TCP gives the measured temperature as a meter reading and a millivolt output to the recorder. Because the liquid iron does not behave as a black body, and the prisms together with the glass discs used in the optical path may not have the same effects on the intensity of both colours equally, calibration of the TCP was necessary.

The apparatus used for the calibration of the TCP is shown in Figure 3.1. Care was taken that the physical dimensions of the levitation cell light path were closely reproduced in the calibration apparatus. The area of the top surface of the metal in the crucible, used for calibration, was obviously much greater than that of a levitated drop, but the surface viewed by the pyrometer was similar owing to the aperture in the radiation shield. The crucibles used in the calibration were of recrystallized alumina with re-entrant thermocouple sheaths, (type N5029, manufactured by Morgan Refractories Ltd.).

Sufficient metal to fill the crucible was fused in it, in two stages, under an argon atmosphere. Simultaneous reading of the TCP and thermocouple were taken as the metal was heated, from its melting point to 1800°C. Similar readings were taken in stepwise manner, on cooling from 1800°C to 1350°C. The results obtained are summarized

TABLE 3.1. Variation of the measured temperatures between T.C.P. and Thermocouple : Pt/Pt-13%Rh

Thermocouple temperature (°C)	T.C.P. temperature (°C)
1613	1630
1616	1635
1619	1630
1636	1645
1643	1653
1646	1660
1651	1666
1664	1680
1673	1683
1690	1695
1711	1722
1723	1733
1741	1750
1756	1770
1770	1782
1789	1800
1766	1785
1743	1757
1728	1743
1717	1738
1705	1715
1685	1700
1675	1690
1650	1658
1631	1639
1603	1612
1566	1560
1531	1510
1520	1505
1516	1500
1494	1465
1424	1405
1372	1370
1302	1305
1309	1301
1309	1305
1300	1310

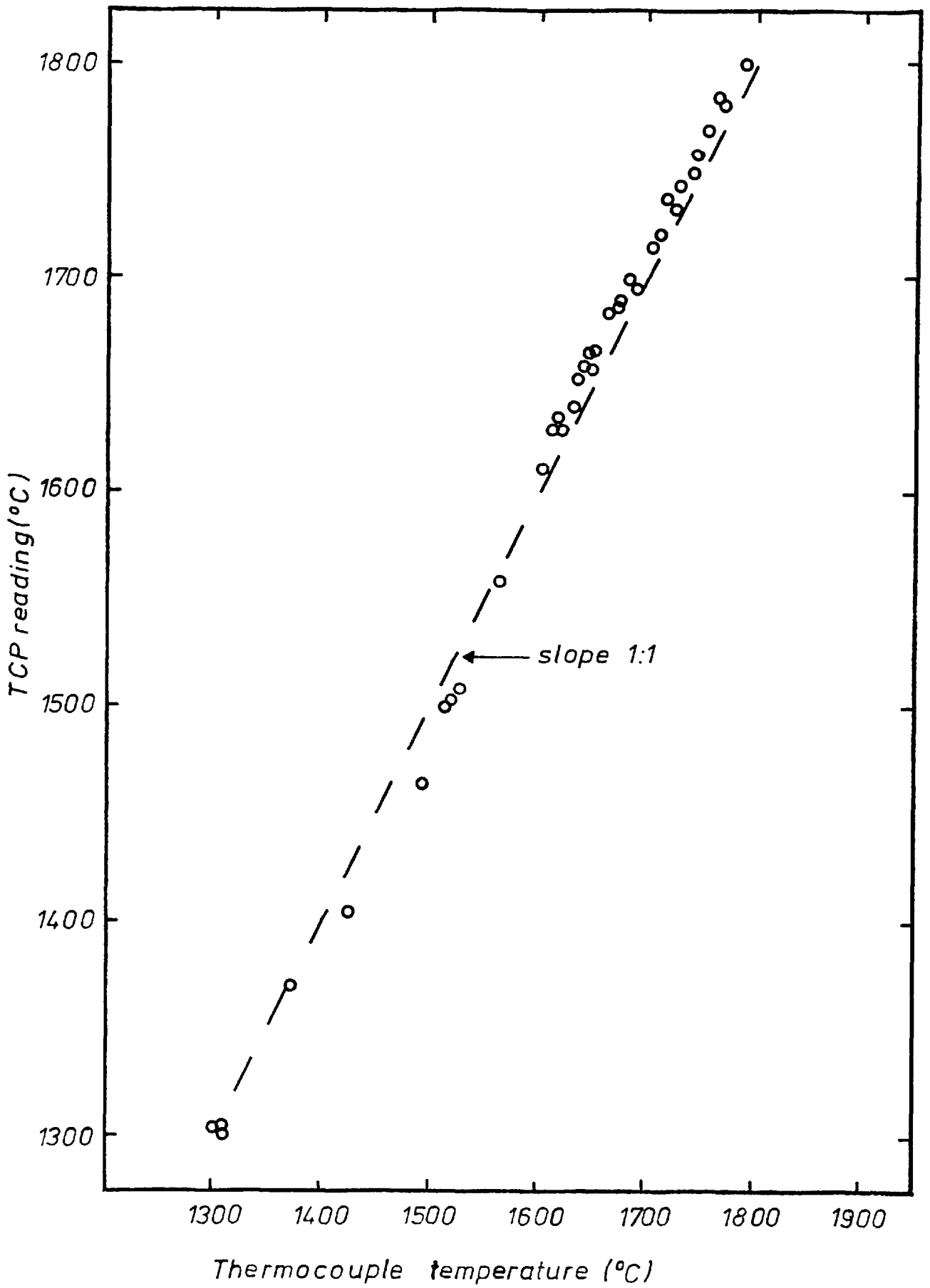


Figure 3.2 Calibration of the TCP against a Pt/Pt-13%Rh thermocouple.

in Table 3.1. and Figure 3.2. As it can be seen between the temperature range of 1560^oC and 1800^oC the discrepancy between the two measured values is small.

3.3. PREPARATION OF ALLOYS

In the preparation of alloys two techniques were used. Generally in order to avoid any contamination from the crucible to the iron-saturated with carbon melts a different technique was applied, the techniques used are described below.

Preparation of Fe-P, Fe-Si, Fe-Si-P, and Fe-C-Si alloys

For the preparation of these alloys the materials used were iron powder, (Grade: C/5010), ferric phosphide powder, silicon powder from "spec pure" silicon lumps, and carbon powder from "spec pure" graphite rods. The analyses of these starting materials are given in Table 3.2.

In a typical preparation, appropriate amounts of constituents totalling about 150-200 grams were placed in a "pure ox" recrystallized alumina crucible, and heated in an induction furnace under an atmosphere of helium or argon. On melting hydrogen was introduced to the gas stream, passing over the surface of the melt, to reduce any oxide that may have formed on its surface. After

TABLE 3.2. Materials used for preparation of alloys

Materials	C ppm	Si ppm	Mn ppm	Ti,V ppm	Ca ppm	Ni ppm	Cr ppm	Fe ppm	Al ppm	P ppm	Ca, Mg, B, Ag ppm	O ppm	N ppm
spec-pure iron-1	-	1	2	-	1	-	1	balance	-	-	<1	60	-
Iron carbonyl powder (C-grade)	1000	-	-	-	-	-	-	balance	-	-	-	3000	1000
Iron powder (Grade 6010)	<500	<1400	-	-	-	-	-	balance	-	<150	1	-	-
Spec-pure silicon lumps	-	balance	-	-	3	-	-	<1	-	-	<1	-	-
Electro graphite carbon blocks (EY9 106 grade)	balance	<50	<1	<50	<1	<50	-	<100	<50	-	<200	-	-
Ferric phosphate powder	The analysis of the sample was not available, but it was 99.8% pure.												

solidifying the melt, the alloy was remelted in an atmosphere of helium/argon to ensure the removal of absorbed hydrogen from the melt. Cooling the alloy in the crucible inside the apparatus, would have led to inhomogeneity in the product, in spite of the quite rapid cooling allowed by the use of induction heating. Thus after maintaining the alloy at 1650°C for 45 minutes, the temperature of the molten metal was decreased to about 40°C above its melting point and kept at that temperature for a further 10 minutes. A rapid current of argon/hydrogen gas was then passed into the silica outer tube, and allowed to escape through the open end (E) of the vertical central tube, as shown in Figure 3.3. A thin walled silica tube of about 5 mm inner diameter and about half a meter long was lowered through "E" until its lower end dipped into the melt, a sudden application (through a stopcock) of suction from a semi-vacuum bulb attached to the silica tube caused the molten metal to be sucked up into the tube, where it was rapidly solidified. The tube carrying the frozen rod of alloy was lifted out of the apparatus and was quenched immediately in water. This procedure was repeated until most of the crucible was emptied, usually out of 200 grams of the charge, about 150 grams of alloy could be drawn into rods by this method providing the temperature of the melt was close to its melting point. By cracking away the silica tube, the rods of alloys were obtained, which were then cut into 1 gram samples and then kept in a dry atmosphere. Any surface oxide formed was removed by light grinding or polishing.

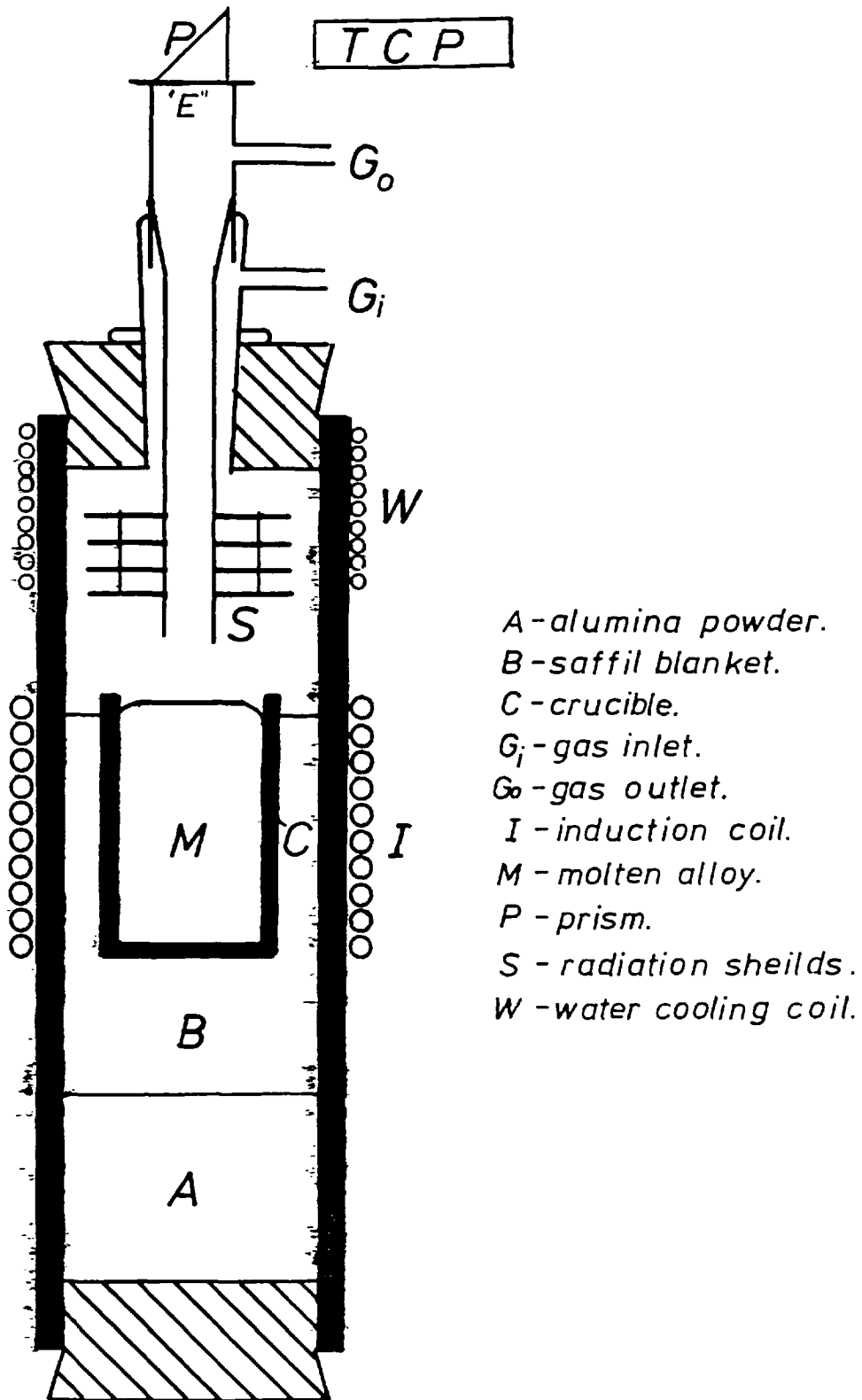


Figure 3.3 The apparatus for the preparation of alloys.

Electron microprobe analyses for phosphorus were conducted on longitudinal and transverse sections of the chilled alloys, which showed satisfactory constancy in phosphorus content. Chemical analysis of samples from different rods of the same batch, also showed a satisfactory constancy in phosphorus content of the alloys.

Preparation of Fe-C and Fe-C-P alloys

Graphite crucibles were made from graphite blocks (Ey9106 grade) and fired at 1000°C for half an hour to remove any volatile impurities. The crucibles were then filled with appropriate amounts of iron carbonyl powder (Grade C), graphite powder (Ey9 106 grade) and in some cases ferric phosphide. The crucible and its contents were then heated inductively till the charge was molten, then the temperature of the melt was slowly lowered to about 1200°C, so that the excess graphite would precipitate out of the solution and be acidised away by current of oxygen passed over the surface. After holding the melt at this temperature for half an hour the entire crucible and its contents were quenched in water. By cracking away the crucible, the cylindrical shaped ingot of alloy was obtained, about 8 mm of the outer shell was machined off, before sectioning into discs of 6 mm thick. After cutting the disc into 1 gram cubic samples, the samples were ground and lightly polished.

Preparation of Fe-P and Fe-P-O

The method used here was similar to those used in the preparation of Fe-C or Fe-C-P alloys. The difference being that "pure-ox" recrystallized alumina crucibles were used instead of graphite ones and also in the case of Fe-P alloys the melt was deoxidized by jetting forming gas over its surface. This method was adopted to ensure rapid quenching and hence homogeneity of the discs of the alloys, which could be used to produce small cubes of samples rather than cylindrical samples.

3-4. PREPARATION OF SLAGS

Seven batches of basic slags were prepared in the laboratory using a similar technique in each case. In all cases the basic component of the melts was lime; the other components were calcium fluoride with or without silica, or ferric oxide, ferrous oxide, or alumina. In preparing $\text{CaO-CaF}_2\text{-SiO}_2$ and $\text{CaF}_2\text{-CaO}$ melts, platinum crucibles were used, but in the other cases recrystallized alumina crucibles were used, since at high temperatures the iron oxide in the melt is very corrosive and can attack platinum ware. In these cases contamination from the crucible material was less than a few percent as was shown by the absence of any phase containing alumina on carrying out X-ray powder diffraction examination on the product.

Materials

In the preparation of these slags powdered calcium carbonate (Analar), calcium fluoride (Analar), quartz, ferric oxide, ferrous oxalate (Analar), and alumina (Analar) were used as the starting materials (the analyses of these are given in Table 3.4). The composition of each slag and its melting point is given in Table 3.3.

Method

The appropriate amounts of the constituents were thoroughly mixed using a ball mill, and then transferred into the crucible. The crucible was placed in a furnace and was heated to a temperature of about 50^oC above the melting point of the melt. One hour after melting had taken place the melt was poured out of the crucible on to a brass plate; when the solidification of the melts took place in a few seconds, the slags were then crushed and ground. A Tema mill was used for grinding the slag to a very fine particle size, and also to ensure good mixing. The procedure was repeated to ensure homogeneity of the product.

TABLE 3.3. The composition of the slags prepared.

Batch	Components						Melting point °c
	CaO wt.%	CaF ₂ wt.%	SiO ₂ wt.%	Fe ₂ O ₃ wt.%	FeO wt.%	Al ₂ O ₃ wt.%	
A	38.6	46.0	15.4	-	-	-	1240
B	20	-	-	77	3	<2	1200
C	20	-	-	17	63	<2	1200
D	16	84	-	-	-	-	1370
E	50	-	-	-	-	50	1420
F	30	-	-	70	-	<2	1360
G	39	-	-	61	-	<2	1430

TABLE 3.4. Chemical analysis of various materials used in the preparation of the slags.

Material	(PO ₄) ppm	Mg ppm	Cl ppm	Fe ppm	SO ₄ ppm	Pb ppm	SiO ₂ ppm	Na ppm	Ba ppm	Fe ₂ O ₃ ppm	Al ₂ O ₃ ppm
CaCO ₃	10	1000	10	10	50	-	100	200	200	-	-
CaF ₂	-	-	50	50	100	50	500	-	-	-	-
SiO ₂	-	- 1	-	-	-	- balance		3	-	1.5	45
Fe ₂ O ₃	10	1000	10	-	-	-	100	-	-	balance	-
Fe (CO ₂) ₂	-	-	50	-	-	-	-	-	-	5000	-
Al ₂ O ₃	-	-	50	50	50	-	-	-	-	-	balance

3-5. DESCRIPTION OF THE LEVITATION APPARATUS

A photograph of the apparatus and a drawing of its cross-section are given in Figures 3.4 and 3.5 respectively. The levitation cell consisted of a brass "well" in which a brass turntable with six "stations" could be rotated on thrust ball bearings. The turntable was designed so that the six "stations" could be rotated to positions that either they were individually, directly below an opening, which could be covered by a lid, or be directly below the silica tubing of reaction chamber. The turntable was rotated about its central axis by a lever fixed to it, and passed through an O-ring sealed flange. A spring loaded ball bearing in the turntable was used to locate the six "stations", when they were in position. One of the stations contained a small prism, with a glass disc covering it; when this "station" was directly below the silica tube, observation of the specimen could be made through an observation window fixed in the "well". Another observation window, with facilities for introducing gases was fixed directly above the silica tube. A brass plate with two holes, one directly below the silica tube, and the other at 180° to it, covered the "well" and the turntable. The first hole was connected to the silica tube by a gas sealed O-ring flange, and the other hole which could be covered by a gas sealed O-ring was used for introducing or removing samples from the station. Two pyrex tubes with sealed ends were used to push silica cups or copper moulds out of the stations either

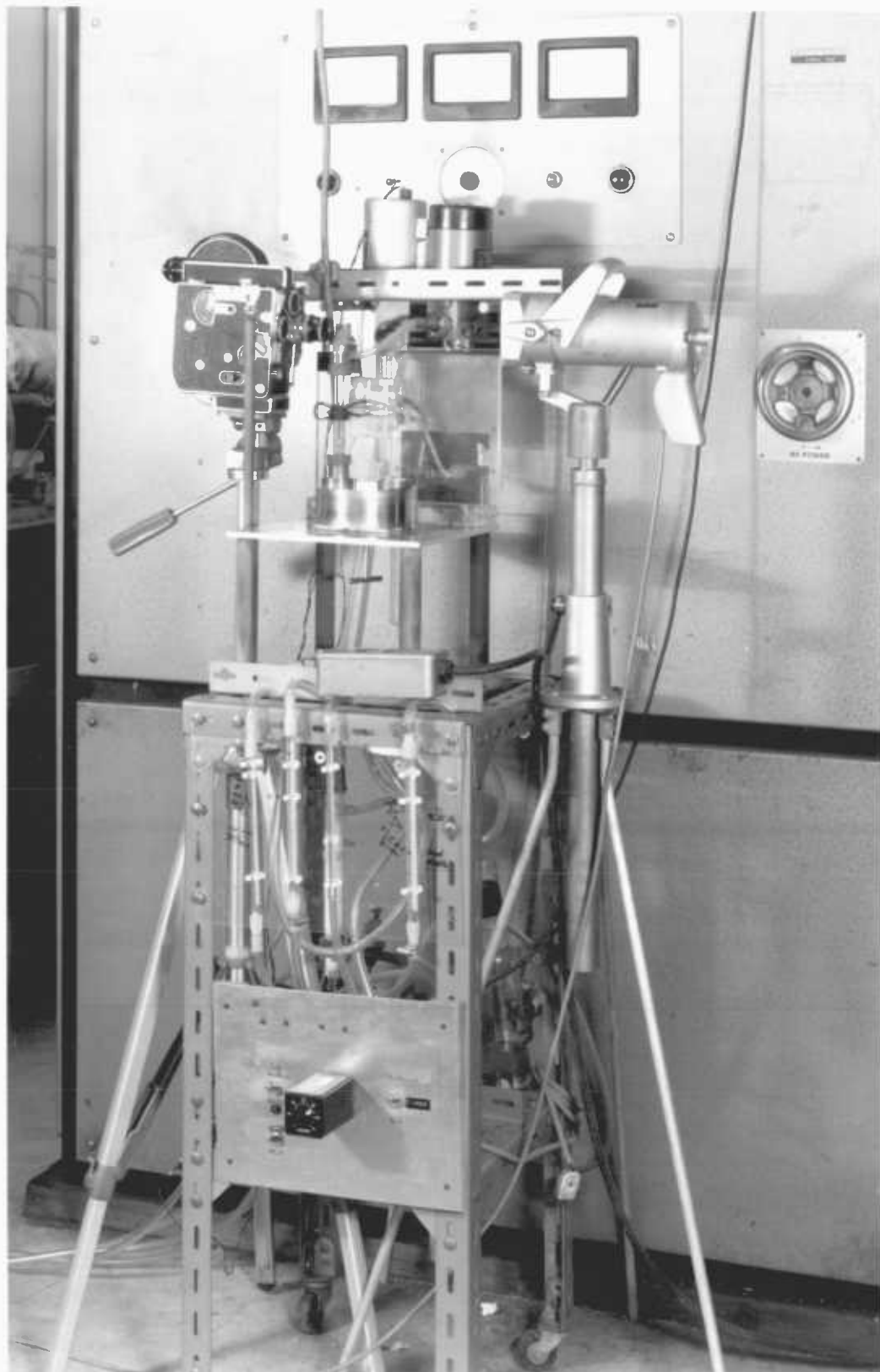


Figure 3.4 Photograph of the levitation apparatus and the gas train.

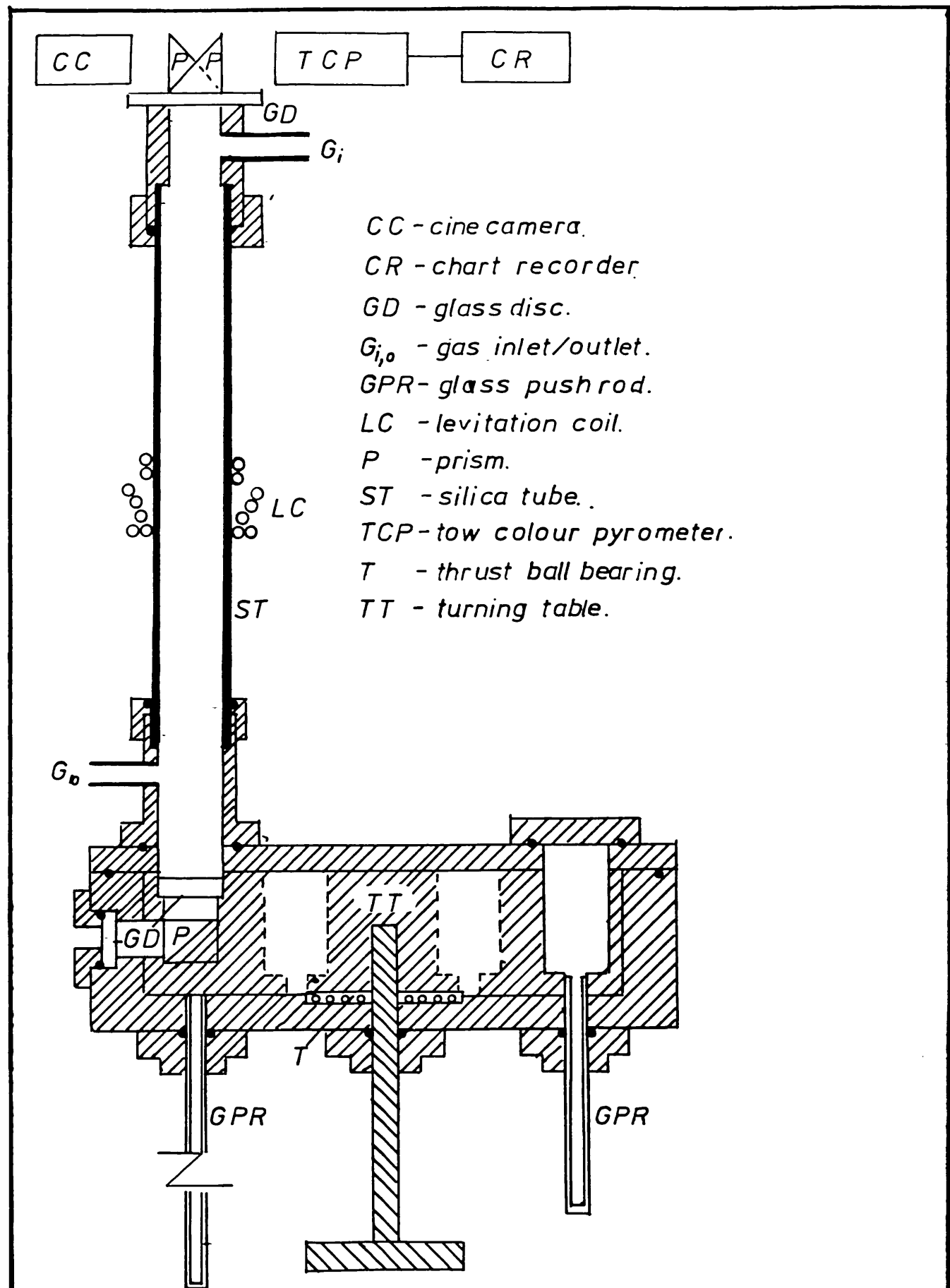
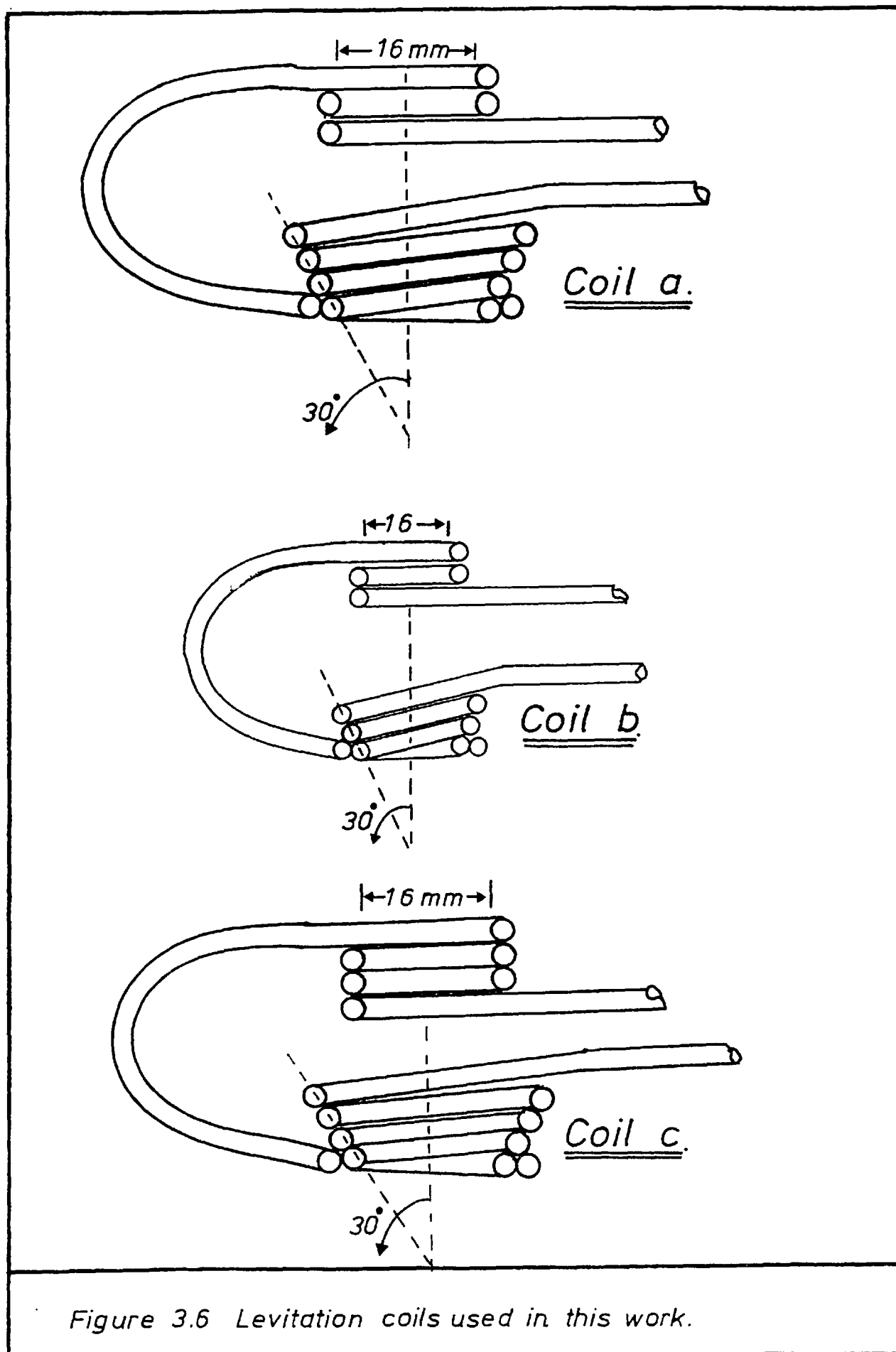


Figure 3.5 The levitation apparatus.

into the silica reaction chamber, or to the opening for introducing or removing samples.

3-5.1. Levitation coils

A 2.8 mm silver tubing of 0.25 mm wall thickness or a 2.4 mm copper tubing with a wall thickness of 0.36 mm was used in constructing levitation coils of "cool" characteristics. In designing levitation coils of "hot" characteristics a 3.2 mm copper tubing of 0.46 mm wall thickness was used. A number of successful levitation coil designs were produced with different characteristics, these have been described in Chapter 2. Three designs were chosen for use in the present work and are shown in Figure 3.6. These coils gave good lifting force and lateral stability. Coil "a" in Figure 3.6 consisted of seven turns, two lower turns being wound co-planar, while the other three formed a cone of 30° with the inner lower turn. The two reverse turns of 16 mm inner diameter were placed above the cone. Silver tubing was used in constructing this coil. Coil "b" consisted of six turns, two lower turns being wound co-planar, while the other three turns were wound to give a semi-apex angle of 30° , the inner diameter of the lower turn was 16 mm. Two reverse turns of 16 mm inner diameter were placed above the cone. Copper tubing of 2.4 mm O.D. was used for construction of this coil. Finally coil "c", made of 3.2 mm copper tubing was made for experiments with high flow rates of helium (10 l.min^{-1}).



This coil consisted of five lower turns, two being coplanar, and the other three at a semi-apex angle of 30° . The three reverse turns of 16 mm inner diameter were wound co-axial and placed above the cone. This coil gave very good lifting force, lateral stability and relatively high sample temperature.

3-5.2. The gas train

Figure 3.7 shows a sketch of the gas flow system used for oxidation experiments. Flow rates of gases were controlled with rotameters (incorporating blow-off columns). These rotameters had previously been calibrated for the gas concerned using a soap bubble meter for low flow rates of gases. For high flow rates the calibration charts supplied by the makers were used.

The gases were dried by passing through columns of silica gel and magnesium perchlorate. The gases were admitted to the levitation cell through two magnetic valves. The switching from one gas to another for a pre-set time was carried out automatically by an electronic time switch. The volume between the vacuum valves and the point at which the incoming gas made contact with the levitated specimen was kept to a practicable minimum, (i.e. about 5 ml), so that on assuming plug flow on changing from one gas to another, the gas occupying this space would have been swept out in a short time of 0.4 to 0.03 seconds depending on the flow

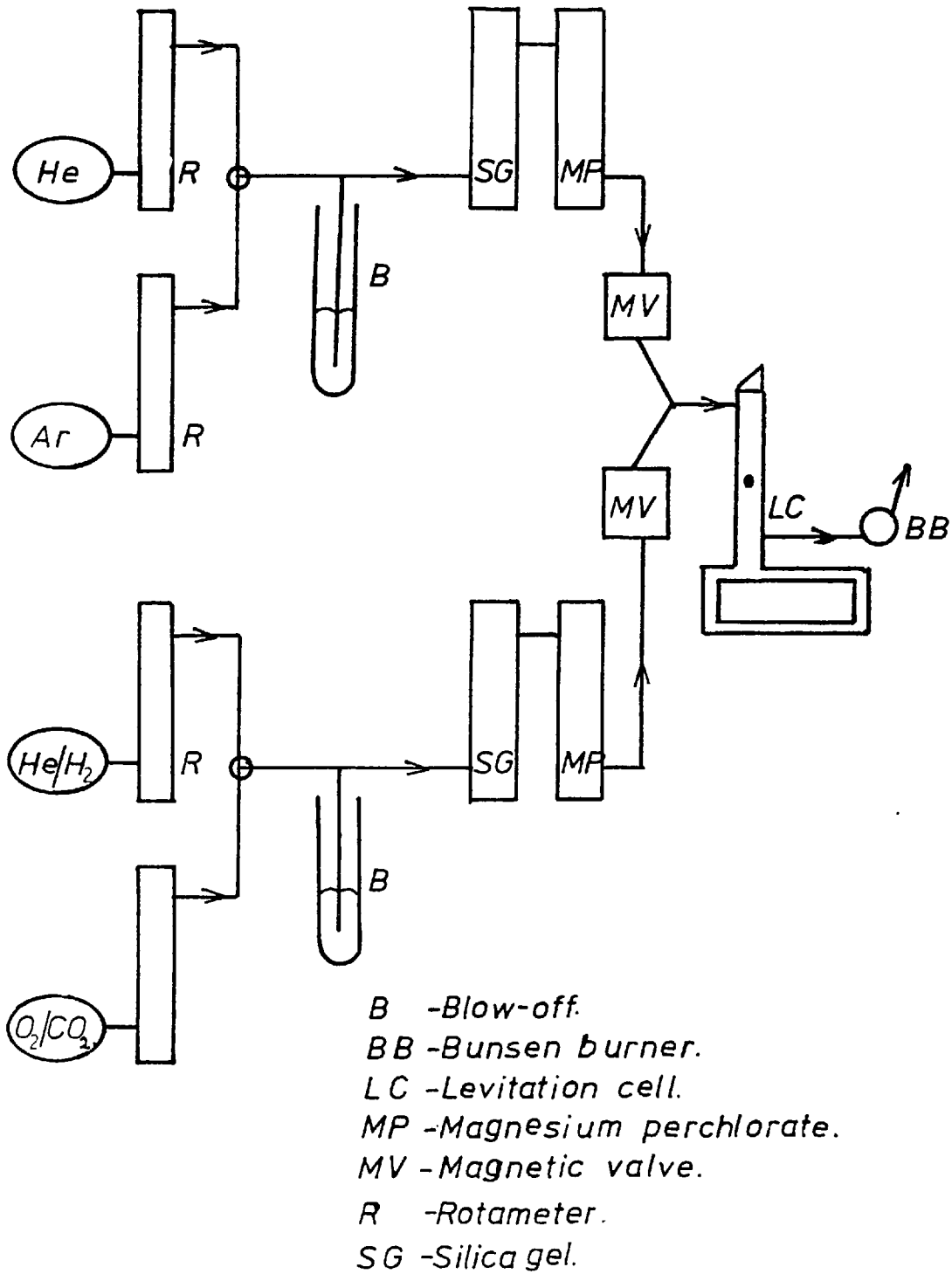


Figure 3.7 Gas train for the levitation apparatus.

rates of gases. Usually downward flow of gases were used, and hence gases left the levitation cell through the exit at the bottom. Whenever toxic gases (CO/CO_2) were used the exit gas was burnt using a specially designed Bunsen burner.

All gases used in levitation experiments and for analysis of carbon in samples were supplied by the British Oxygen Company Ltd. Table 3.5. gives the standard of the purity of each gas used.

TABLE 3.5

Gases	O_2 ppm	CO_2 ppm	CO ppm	N_2 ppm	H_2 ppm	H_2O ppm	Hydro- carbons
O_2	balance	<2	<1	<10	10-15	<50	<20
CO_2		balance	-	-	1	10	10
CO (CP grade)	10	10	balance	-	<300	5	<175
H_2	1-2	1		50-70	balance		1
N_2 -25% H_2	<8	5	<3			<3	<1
He (grade A)	<8	<1	-	10	<1	3	<1
Ar (H.P)	3.45	-	-	20	1	4	1

3-5.3. Techniques for addition of slag

Attempts were made to develop a relatively simple technique to add controlled amounts of slag to a levitated drop. In early experiments a silica cup containing the slag was raised near to the molten iron drop for a fixed period and it was hoped that the amount of slag picked up by the molten drops would be constant. When lime was attached the amounts picked up by the samples were about 18 ± 4 mg, and in the case of a $\text{CaO-CaF}_2\text{-SiO}_2$ slag the amounts were about 35 ± 6 mg. Thus the technique was unsatisfactory and it was thought that better results might be obtained by delivering the powdered slag to the levitated drop, using a stream of inert gas as a carrier. A gas tight apparatus with an Archimedian screw situated in it was designed for feeding the powdered slag into the gas stream. Figure 3.8. shows a drawing of a cross-section of the apparatus. It consisted of a brass cylinder with one end having an O-ring sealed flange, a glass tube of 6 mm O.D. passed through the flange and joined the gas stream at a T junction. The other end of the cylinder had the entry of the Archimedian screw, this was again O-ring sealed by another flange. The slag inside the cylinder was spring loaded, so as to aid even delivery of powder at a constant rotation rate of the Archimedian screw, which was driven by an electric motor fitted with a speed control. The trials carried out using this apparatus were once again unsatisfactory due to two reasons. First of all a constant feeding of powdered

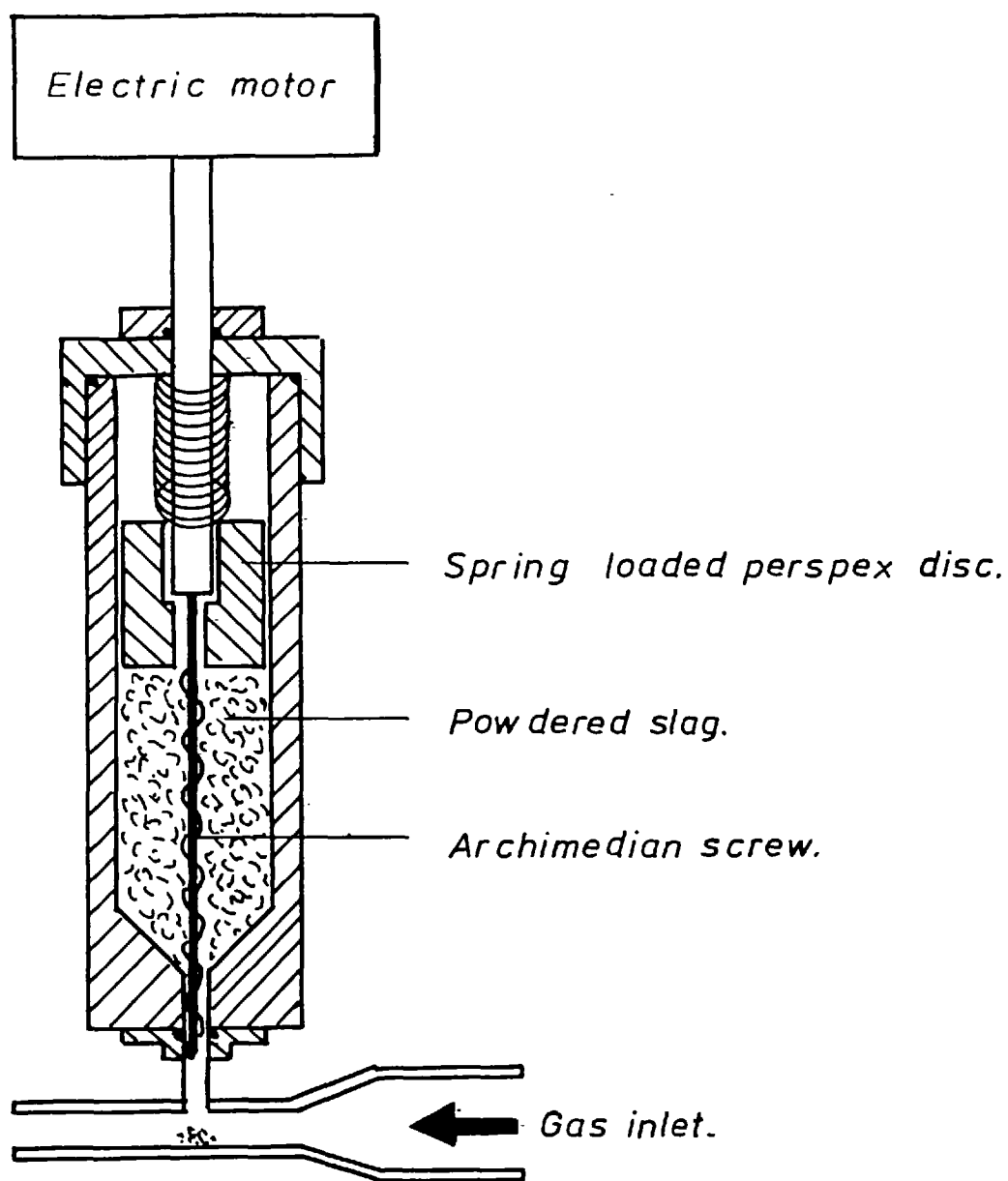


Figure 3.8 A cross-sectional drawing of the slag delivery apparatus.

materials was not achieved due to the blockage of the screw, when very fine powders were used. The coarse powders showed some improvements, but suffered from another point and that was the jet momentum of the gas, at flow rates of ~ 1.5 litres per minute through a nozzle of 2 mm in diameter, was not sufficient to carry all the particles into the gas stream.

A third method using a different principle was investigated. In this method about 1 gram of fine iron powder (710 microns) together with 20 mg of slag powder were pelletized in a $\frac{1}{4}$ " die under a pressure of 3000 p.s.i. The samples were then levitated in a stream of argon, but the method failed due to the fact that melting could not be achieved even at low flow rates. The reason for such failure of this technique partly lay in the fact that under the pressures used for pelletizing the samples, the overall density of the cylindrical samples were too low hence problems with melting the levitated drops arose. Further attempts to increase the pressure and hence reduce the pellet volume were unsuccessful, as the compressed pellets could not be retrieved from the die.

Finally the method of levitating capsules of iron containing the slag was used. This technique was time-consuming as individual capsules were made by machining a cavity in the iron cylinders of about 6 mm in diameter and 7 mm long. Lids of iron to fit tightly also had to be

machined so that once the cavity was filled with the slag the lid would prevent it from losing the slag before the sample was molten. This technique needed further improvement, since once the sealed capsule was levitated and heated, the expansion of the entrapped gas inside the cavity caused the lid to be ejected and hence loss of material occurred. This problem was overcome by introducing a small notch in the edge of the lid, to serve as a vent for the expanded gas. Thus apart from time consumption it was found that cylindrical specimens spinned on heating and levitating and three out of ten hit the silica tube, of the levitation cell, and were contaminated. Since cubic samples did not suffer from such behaviour, it was decided to cut the samples into small cubes, of 5 mm x 5 mm x 7 mm using a silicon carbide slitting wheel, and drilling cavities of 2.5 mm in diameter in the cubes. The slag powder was then compressed into the cavity. This method was less time-consuming, than machining cylindrical capsules with a lid, and was very satisfactory since none of the above mentioned problems arose.

3-5.4. Photographic technique

In studying the kinetics of reactions by a levitation technique it is sometimes necessary to determine any mechanism influencing the reaction by visual aids. A "Bolex" cine camera was used to record the events of the reactions. The maximum operating speed of the camera

was 64 frames per second. Use of a 75 mm "Cannon" lens and suitable close-up lenses were made to obtain suitable fields of view of the levitated drop. A photograph of the apparatus and the cine camera is given in Figure 3.8. Normally filming was carried out from the upper window, using a double prism arrangement, so that the temperature of the levitated drop could also be measured simultaneously. In some experiments filming was carried out from the bottom window, while the temperature was measured from the top one. At temperatures of 1600°C and above the drops were fairly luminous and use of a 0.9 neutral filter was made to photograph the events on Ilford Pan F (50 ASA), FP4(125 ASA) and Mark V (400 ASA) 16 mm black and white films. Depending on the film speed and temperature of the molten drop the aperture of the lens was set at f8 - f22.

3-5.5 Description of a typical levitation run

In a typical run, the apparatus was flushed with argon or helium, and then the specimen was levitated in the transparent silica tube, of 12.7 mm in internal diameter, under a stream of helium or argon. Once the sample was molten, the temperature of the molten drop was adjusted by altering the flow rate of the inert gas to the required level, and varying the power of the high frequency generator. On reaching a steady temperature, the sample was exposed to a stream of reacting gas, flowing at a

pre-adjusted rate. At the required time, the flow of the reacting gas was stopped, by the magnetic valves, and an inert gas (helium) at a similar pre-adjusted rate was introduced. In most experiments the molten drop was then quenched in a small copper mould, and in the case of a few experiments, the levitated drops were solidified in a stream of helium flowing at several litres per minute.

The entire sample was weighed, then the slag (if any) was removed physically, and the specimen was analysed for carbon, silicon or phosphorus.

3-6. DESCRIPTION OF THE FREE FALL APPARATUS

In order to determine the kinetics of some metal/slag and metal/slag/gas reactions, use of a free fall apparatus was made. A photograph of the apparatus is shown in Figure 3.9.

The apparatus consisted of a levitation zone, with optical arrangements for measuring the surface temperature of the metal, and a reaction zone which was separated by a thin film of "stretch and seal" membrane. The reactive gas, normally pure oxygen, was introduced near to the top of the tube using an L-piece glass tubing; the reactive gas escaped from the bottom of the column through a pin-hole in the membrane. The quenching device was placed at an angle near the bottom end of the reaction column,



Figure 3.9 Photograph of the free fall apparatus.

so that the sample could be quenched immediately after the reaction period had elapsed.

3-6.1. Slag addition techniques

In some experiments capsules of the alloys were filled with a known quantity of slag and then levitated, reacted, and quenched. In other experiments where attempts were made to measure the kinetics of the reactions between metal and slag, the above-mentioned technique could not be applied for obvious reasons, hence a thin layer of the powdered slag was placed over the upper membrane and after levitating and melting the samples in a stream of helium, the drops were allowed to fall freely through the membrane into the column, with hopes that during the free fall period some of the slag particles in contact with the metal would melt and hence reactions between the two phases would occur.

3-6.2. Quenching device

In the past many workers using the free-fall technique to study kinetics of reactions between levitated drops and oxidizing gas were faced with the problem of using a quenching device which would give very rapid rate of cooling the metal and to give good metal/slag separation. Up until recently the "mouse trap" device consisting of two vertical copper plates, which were brought together

horizontally, as the specimen fell between them, by a pair of springs, has been used for such studies. This device suffers from the difficulty in synchronising the movement of the copper plates and arrival of the specimen. The other objection to this technique arises from the difficulty in separating the metal phase from the slag by physical methods. Thus it was decided to use a rotating copper cylinder of about 12 cm long, at an angle to the exit end of the free-fall column. On using iron-phosphorus alloys of melting point about 1530°C , with a $\text{FeO-CaO-P}_2\text{O}_5$ slag attached, when the cylinder was put at an angle of 60° to the vertical and was rotated at speeds of about 3500 r.p.m. very good separation of metal from the slag was obtained. The metal usually solidified in a form of spiral, while the slag spread over a section of the metal surface. When alloys of iron containing appreciable amounts of carbon were used, the spreading was not achieved even at various angles and rotational speeds of the device. This behaviour was thought to be due to differences between the melting points of the alloys and their viscosities. A photograph of the quenching device is provided in Figure 3.11.

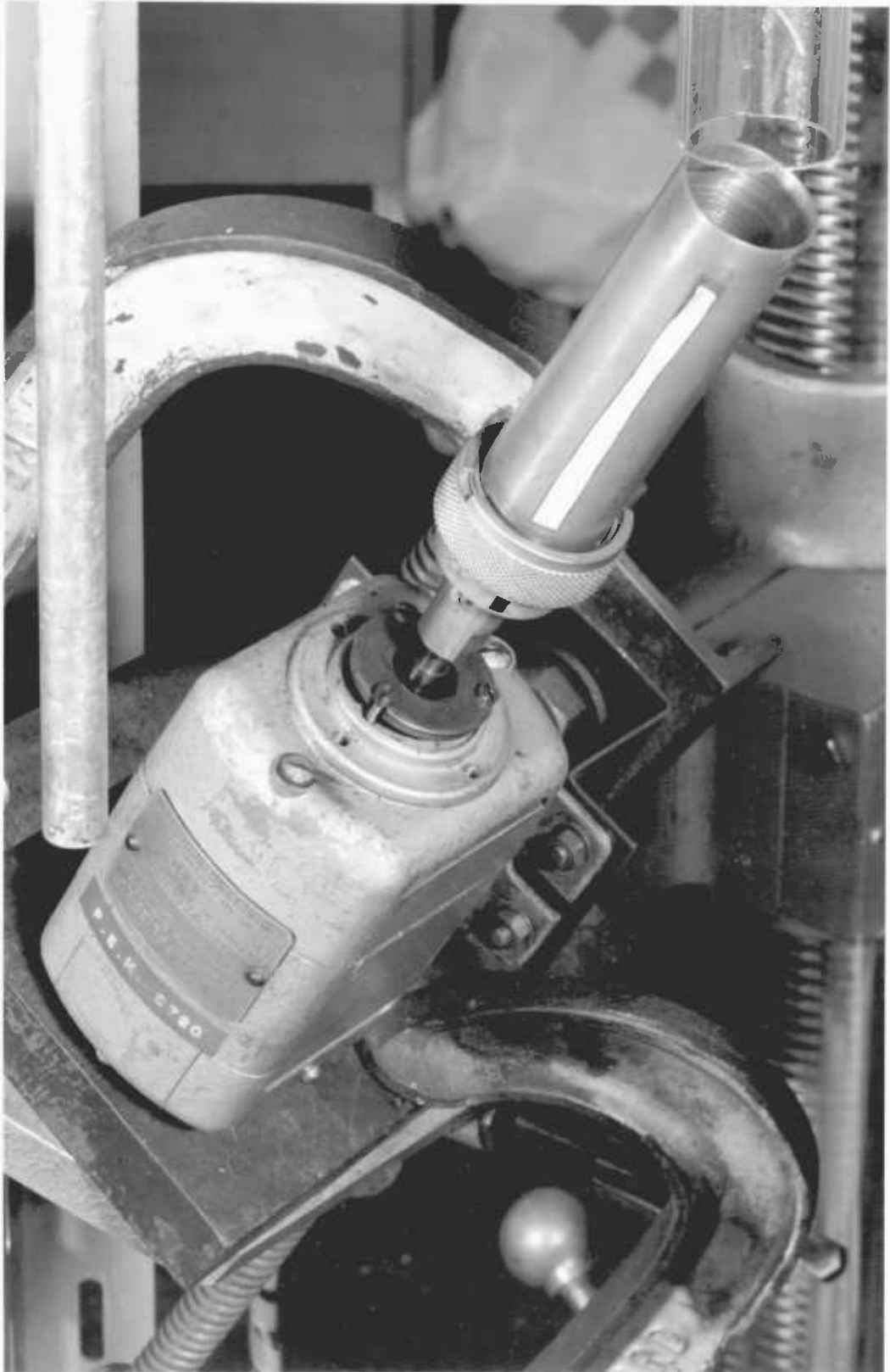


Figure 3.11 Photograph of the quenching device.

3-7. CARBON ANALYSIS

Samples were placed in a boat to which some lead was added as a fluxing agent and heated to 950°C , and ignited in a stream of oxygen previously purified with soda asbestos and silica gel. The product of the combustion, CO_2 , was then passed through chromic acid, conc. sulphuric acid, and magnesium perchlorate, before being absorbed in a Nesbitt bottle containing soda asbestos and magnesium perchlorate. The carbon content of the samples were calculated from the weight difference.

The fire clay boats used for the analysis were previously fired at 1100°C for 24 hours and kept in a dessicator. Blank determinations and analysis of British Chemical Standard iron and steel samples containing 2.79%C to 0.333%C gave an average error of 0.07 to 0.013% respectively.

3-8. PHOSPHORUS ANALYSIS

The method used for analysis of phosphorus in the samples, was a photometric one, in which after dissolution of the samples in an oxidising acid mixture, the phosphorus is converted to phosphovanado-molybdate in perchloric nitric acid solution. The complex phosphovanado-molybdate is extracted into isobutyl methyl ketone, and the phosphorus content is determined photometrically. This method is applicable to all types of iron and steel, although in the presence of other elements, such as tin,

vanadium, niobium, tantalum, or tungsten addition of other reagents is necessary to remove them from the solution because of interference.

Calibration

Into nine conical flasks, each containing 0.5 gram of "spec-pure" iron powder, various additions of the standard phosphorus solution were made so that a range of 0.00 to 0.40 mg (equivalent to 0.0 to 0.08 wt.%) phosphorus would be covered in steps of 0.05 mg. The contents of these flasks were then treated as described in the next section. From the readings obtained from their optical densities, a calibration curve was obtained.

The standard solutions of phosphorus were made by dissolving 0.4393 gram of potassium dihydrogen orthophosphate (previously dried to constant weight at 105°C) in water, the solution was cooled, transferred to a 1 litre calibrated flask, diluted to the mark and mixed. Then 100 ml of this solution was transferred into another 1 litre calibrated flask, diluted to the mark and mixed (1 ml of this solution contained 0.01 mg of phosphorus).

Procedure

The samples were weighed and then transferred into conical flasks where addition of 5 ml. of nitric acid (sp.gr. 1.42) and 5 ml of hydrochloric acid (sp.gr. 1.16)

were made. The conical flasks were then covered and heated till dissolution was completed. (For alloys containing more than 0.4 mg of phosphorus, the solution was cooled and diluted in a calibrated flask, and a suitable aliquot; not containing more than 0.4 mg of phosphorus was taken). 10 ml of perchloric acid (sp.gr. 1.54) were then added and the solution was evaporated to fuming, the fuming was continued for 5-10 minutes at such a temperature that a steady reflux of acid on the walls of the beaker was maintained. The solution was then cooled and 25 ml of nitric acid (20% v/v) and a few glass beads were added to it, before reheating. After boiling this solution for a few minutes 5 ml of potassium permanganate solution (1% w/v) were added to it and boiling was continued for another few minutes, before 10 ml of sodium nitrite solution (5% w/v) were added, and boiled until it was free from nitrous fumes. This solution was then cooled to room temperature, and then 10 ml of ammonium vanadate solution (0.25% w/v), together with 15 ml of ammonium molybdate solution (15% w/v) were added to it and allowed to stand for a minimum of 10 minutes to ensure a complete colour development. Once the colour was developed the solution was diluted to 100 ml and transferred into a 250 ml separating funnel, additions of 10 ml of citric acid solution (50% w/v) and 40 ml of isobuty methyl ketone were made, and shaken for a minute. The two immiscible liquids were allowed to separate, and the aqueous layer was discarded. The organic layer was filtered through a dry Whatman No. 541 paper into a small dry sample tube.

The optical density of the ketone was determined by using unispek photoelectric spectrophotometer, with the wavelength set at 4.25 nm. The cells used for the measurements of the optical densities were 2 cm quartz cells.

The accuracy of the method was checked by using two British Chemical Standard Steel Samples containing 0.055% and 0.029% phosphorus, which on average gave an error of 0.0035% and 0.0023%P respectively.

CHAPTER 4

CHAPTER 4KINETICS OF DECARBURIZATION OF LIQUID IRON
ALLOYS BY STREAMS OF OXYGEN OR CARBON DIOXIDE4-1 INTRODUCTION

Recent studies on surface chemistry have shown that the properties of surfaces of liquids containing surface active agents are noticeably different from those which do not. The surface active agents have great influence on the interfacial movement and mass transfer across the interface, particularly in the case of metal/gas interfaces. Hence in most metallurgical reactions chemisorption of surface active elements on the surface of the metals can greatly influence the kinetics of the reactions involved, and this factor has to be taken into consideration.

The present work was undertaken primarily to investigate the effect of phosphorus and silicon, at relatively low concentrations, on the kinetics of the decarburization of levitated drops of iron-carbon alloys in streams of oxygen or carbon dioxide. The other objective of this work was to analyse the results of the study of the kinetics of mass transfer between the levitated drops and a flowing gas, and hence to examine the available correlations for calculating the gas phase mass transfer coefficients.

4-2 DECARBURIZATION OF IRON-CARBON ALLOYS

The rate of decarburization of liquid iron-carbon alloys by CO_2 or O_2 has been the subject of numerous investigations.⁽⁹⁻¹⁸⁾ Many investigators, particularly those studying levitated drops, concluded that at carbon concentrations above 1 wt.% the rates are independent of the carbon concentration, and mass transfer through the gas film boundary layer near the surface of the liquid iron is the rate controlling step. The observed rates of decarburization were found to be in reasonable agreement with the predicted rates for gaseous diffusion mass transfer control.

Previous investigations into the kinetics of gas/metal reactions have shown that adsorption of impurities at the reaction interface can greatly affect the reaction rate and the rate controlling mechanisms. The influence of alloying elements on the rates of decarburization of iron and nickel alloys has also recently been receiving considerable attention. Fruehan and Martonik,⁽¹⁸⁾ in their decarburization studies of iron alloys, using crucible type experiments, have found that presence of 0.3 wt.%(S) reduced the rate by 10% indicating that a slow reaction on the surface is effecting the rate slightly when the surface is covered by sulphur atoms. Achari and Richardson,⁽¹⁹⁾ found that with levitated drops of iron and nickel the presence of sulphur, at concentrations above 0.03 wt.%, retards the rate of decarburization, although the rates

observed were in good agreement with the predicted rates for gaseous diffusion mass transfer control; they concluded that the rate of supply of carbon to the surface of the drop was effected by the presence of the sulphur. Furthermore, Sain and Belton^(20,21) studied the kinetics of decarburization of liquid iron under conditions where mass transport of the reactants was not the rate controlling step and found a remarkable effect of sulphur on retarding the rate of the reaction. They also concluded that presence of silicon and phosphorus at concentrations of up to 0.5 wt.% had no measurable effect on the decarburization rates of liquid iron. On the contrary Fruehan⁽²²⁾ studied the effect of phosphorus on the rate of decarburization of solid iron at 1140°C and under conditions of low carbon activity, he concluded that presence of 0.1 wt.% phosphorus reduces the rate by a factor of two. Furthermore in studies of the nitriding of solid and liquid iron,^(23,24) it has been shown that presence of phosphorus retards the rate of nitriding significantly.

4-3 MASS TRANSFER BETWEEN A FLOWING GAS AND A STATIONARY SPHERE

The subject of mass transfer between a single sphere and flowing gases has received considerable attention in the past, since many chemical engineering processes such as spray drying, humidification, adsorption, and desorption involves such mechanisms.

Mass (and heat) transfer from a sphere to a surrounding flowing gas can take place by any one or any combination of the following three mechanisms:

- a. Radial molecular diffusion
- b. Natural convection
- c. Forced convection.

These mechanisms can be expressed in terms of dimensionless groupings to correlate the overall mass transfer coefficient.

$$\text{e.g. } Sh = f(Gr, Pr, Re, Sc\dots)$$

a. Radial molecular diffusion

This occurs when no contribution is made to mass transfer by natural or forced convection.

i.e. when $Gr = Re = 0$.

Maxwell⁽²⁵⁾ first provided an analytical solution to radial diffusion from a sphere as:

$$K = \frac{2D}{d}$$

Langmuir⁽²⁶⁾ was first to express this behaviour in dimensionless form as:

$$Sh = 2.$$

This constant of $Sh = 2$ for radial diffusion has been experimentally verified by several investigators.⁽²⁷⁻³⁰⁾

b. Natural convection

Mass transfer accountable to natural convection results from inhomogeneities in the gas phase; concentration and temperature gradients yielding density differences in the fluid phase, i.e. natural convection occurs when $Gr > 0$.

When no significant temperature or concentration gradients are present in the gas phase, there would be no significant contribution to the overall mass transfer from natural convection sources, any small contribution being negligible in comparison with those from radial molecular diffusion or forced convection. Skelland and Cornish⁽³¹⁾ found that with vaporization from naphthalene spheres into flowing air the contribution due to natural convection was negligible at $Re > 15$.

In most metallurgical systems involving drops of metal, large temperature and/or concentration gradients are present and it is not reasonable to ignore mass transfer due to natural convection in these cases.

Ranz and Marshall⁽²⁷⁾ in their studies of evaporation of water drops into air streams at temperatures up to 200°C propounded the overall mass transfer correlation as:

$$Sh = 2 + 0.60 Re^{0.5} Sc^{0.33} \quad (4.3-2)$$

which ignores the separate contributions due to natural convection by combining them in the forced convection term. On the other hand a number of other investigators

have computed the contribution due to forced convection independent of natural convection and have supplied a further correlation for natural convection.

Contributions due to natural convection have been expressed in terms of Grashof numbers for many years. Suitable correlations suggested by Merck and Prins⁽³²⁾ and Piret et al.⁽³³⁾ for $Gr \cdot Pr < 10^8$ (laminar boundary flow) and $Pr > 0$ respectively,

$$Nu(Re = 0) = 0.597 (Gr^h, Pr)^{0.25} \quad (4.3-3)$$

$$\text{and } Sh(Re = 0) = 2 + 0.5(Gr^m, Sc)^{0.25} \quad (4.3-4)$$

These show that similar correlations apply both to heat and to mass transfer contributions for natural convection.

Mathers et al.⁽³⁴⁾ have provided the most rigorous treatment of natural convection. They have found that the simultaneous heat and mass transfer from a sphere affect one another, and that they therefore cannot be studied independently (mass transfer accompanied by heat transfer was in some cases twice as great as that expected from simple mass transfer theory).

They introduced a compound Grashof number, \overline{Gr} , incorporating both the Grashof number for heat transfer Gr^h , and that for mass transfer, Gr^m .

$$\overline{Gr} = Gr^m + A Gr^h \quad (4.3-5)$$

The "A" factor here compensates for the difference in the thickness of the heat and mass transfer boundary layers, t_h and t_m , respectively and it has been shown that

$$\frac{t_h}{t_m} = \frac{Sc}{Pr}^{0.5} = A \quad (4.3-6)$$

The contribution to the total mass transfer due to natural convection is therefore a function of:

- i) Concentration gradient - Gr^m
- ii) Temperature gradient - Gr^h
- iii) Mass transfer boundary layer - Sc
- and iv) Heat transfer boundary layer - Pr

Therefore natural convection mass transfer is governed by an equation of the form $f(Gr^m, Gr^h, Sc, Pr)$, and this has been found to be:

$$Sh = B (\overline{Gr} \cdot Sc)^C \quad (4.3-7)$$

The values of "B" and "C" obtained by Mathers et al. ⁽³⁴⁾ from their studies on the mass transfer from heated naphthalene spheres tend to vary depending on the product of \overline{Gr} and Sc . These are given below in equations 4.3-8 and 4.3-9.

$$Sh(Re = 0) = 2 + 0.282 (\overline{Gr} \cdot Sc)^{0.37} \text{ for } \overline{Gr} \cdot Sc < 10^2 \quad (4.3-8)$$

$$Sh(Re = 0) = 2 + 0.50 (\overline{Gr} \cdot Sc)^{0.25} \text{ for } 10^2 < \overline{Gr} \cdot Sc < 10^6 \quad (4.3-9)$$

Steinberger and Treybal⁽²⁸⁾ performed statistical analysis on the available data and obtained the following correlation:

$$\text{Sh}(\text{Re} = 0) = 2 + 0.569 (\overline{\text{Gr}}, \text{Sc})^{0.25} \text{ for } \overline{\text{Gr}}, \text{Sc} < 10^8 \quad (4.3-10)$$

Furthermore El-Kaddah⁽³⁵⁾ studied the heat transfer from levitated drops and found the following correlations for heat and mass transfer from such drops:

$$\text{Nu} = 0.78 (\overline{\text{Gr}}, \text{Pr})^{0.25} \text{ for } \text{Gr}/\text{Re}^2 > 7 \quad (4.3-11)$$

and by analogy

$$\text{Sh} = 0.78 (\overline{\text{Gr}}, \text{Sc})^{0.25} \text{ for } \text{Gr}/\text{Re}^2 > 7 \quad (4.3-12)$$

c. Forced convection

When a gas flows around a sphere there is a mass transfer contribution due to forced convection. Froessling⁽³⁰⁾ measured the evaporation rates of spheres of water and benzene into air, using boundary layer theory and derived the equation:

$$\text{Sh} = 2 + 0.552 \text{Re}^{0.5} \text{Sc}^{0.3} \quad (4.3-13)$$

Many investigators have confirmed that the contribution to the overall Sherwood number for mass transfer

due to forced convection is a function of Reynolds and Schmidt numbers.

$$\text{i.e. } Sh \text{ (forced convection)} = f(\text{Re}, \text{Sc}).$$

The Reynolds number giving the effect of gas velocity on the mass transfer, and the Schmidt number accounting for the momentum and diffusion boundary layer thickness.

Most investigators have used correlation of the type:

$$Sh \text{ (Gr} = 0) = 2 + n \text{ Re}^d \text{ Sc}^e \quad (4.3-14)$$

Steinberger and Treybal performed, in their review paper an extensive analysis of the "n", "d", and "e" values of previous workers and arrived at a correlation of:

$$Sh(\text{Gr} = 0) = 2 + 0.347 \text{ Re}^{0.62} \text{ Sc}^{0.31} \quad (4.3-15)$$

The correlation appeared to be a generally reliable one for forced convection mass transfer and can be fitted to most data with an average of 20% deviation.

Distin et al.⁽¹²⁾ found in their studies of decarburization of molten iron drops, that the value of "n" varied with the diameters of the spheres. They found 0.6 for 6 mm spheres and 0.44 for 8 mm spheres.

El-Kaddah⁽³⁵⁾ has found that for 1 gram levitated drops the correlation:

$$\text{Nu} = 0.8 \text{Re}^{0.5} \text{Pr}^{0.33} \quad (4.3-16)$$

to give the best agreement with his data on heat transfer for $\text{Gr}/\text{Re}^2 < 1.3$ and by analogy of heat and mass transfer the following relation was arrived at for the forced convection regime:

$$\text{Sh} = 0.8 \text{Re}^{0.5} \text{Sc}^{0.33} \quad (4.3-17)$$

Combined forced and natural convection

Steinberger and Treybal⁽²⁸⁾ used linear addition of natural and forced convection to correlate large quantities of data, and they obtained the correlation:

$$\text{Sh} = 2 + 0.569 (\overline{\text{Gr}} \cdot \text{Sc})^{0.25} + 0.347 \text{Re}^{0.62} \text{Sc}^{0.31} \quad (4.3-18)$$

El-Kaddah⁽³⁵⁾ used the criteria Gr/Re^2 to define the combined regime, and presented his result as a plot of Gr/Re^2 against $\text{Nu}/\text{Re}^{1/2}$. He observed that the combined forced and natural convection regime occurs at $1.3 < \text{Gr}/\text{Re}^2 < 7.0$ and noted that forced and natural convection components were not arithmetically additive. Although his results were scattered in the region of combined regime, he showed that the heat transfer which

resulted in this regime can be expressed purely as for natural convection.

$$\text{Hence } Sh = 0.78(\overline{Gr}, Sc)^{0.25} \quad (4.3-19)$$

4-4 EXPERIMENTAL METHOD

Decarburization of iron-carbon alloys

Alloys of Fe-C containing about 4 wt% C, with or without 0.1 wt% P or 0.015 wt% Si were made by the method described previously. Samples weighing about 1.1 gram were cut and used for the experiments. In this series of experiments, after flushing out the levitation cell with an inert gas, the samples were levitated in the silica tube of the cell (12.7 mm internal diameter) and melted in a stream of dried helium and/or argon. Initially the temperature was raised to about 1650°C to ensure rapid dissolution of the graphite; the sample temperature was then decreased to the required value and on reaching a steady temperature it was exposed to a stream of reacting gas (CO₂ or O₂) flowing at a preadjusted rate. At the required time, the flow of the oxidising gas was stopped, and an inert gas (helium or argon) with similar pre-adjusted rates were introduced; the switching from one gas to another for a pre-set time was carried out automatically by an electronic time switch. Finally, the samples were quenched into a copper mould, weighed and then analysed for carbon or phosphorus.

Results:

The results obtained on oxidation of Fe-C, Fe-C-P, and Fe-C-Si samples in streams of O_2 or CO_2 are shown in Tables 4.1 to 4.7.

List of symbols

M	= mass of the sample (gram)
T	= temperature of the sample ($^{\circ}C$) $\pm 15^{\circ}C$
t	= oxidation period (sec)
Δm	= loss in mass (mg)
Δc	= loss in carbon content (mg)
a	= surface area of the sample (cm^2)

Subscripts

i	= initial
f	= final

TABLE 4.1 Decarburization of Fe-4.42C in a stream of carbon dioxide flowing at 0.75 l. min^{-1}

Run	M_i gram	T_i °C ± 15	t sec	T_f °C ± 15	M_f gram	Δm mg	Wt.% [C]	Δc mg	a cm ²	$\Delta c/a$ mg-cm ⁻²
CR1	1.1240	1600	5	1625	1.1125	11.5	3.90	6.3	1.455	4.33
CR2	1.1501	1600	5	1625	1.1395	10.6	3.85	7.0	1.475	4.75
CR3	1.1277	1595	10	1633	1.1078	19.9	3.18	14.6	1.455	10.03
CR4	1.1665	1608	10	1645	1.1317	34.8	3.05	17.0	1.48	11.45
CR5	1.1652	1600	10	1640	1.1451	20.1	3.08	16.0	1.485	10.77
CR6	1.1296	1598	15	1638	1.1019	27.7	2.72	20.0	1.455	13.75
CR7	1.1320	1598	15	1637	1.1039	28.1	2.28	24.9	1.46	17.06
CR8	1.1662	1600	20	1685	1.1224	43.8	1.93	30.0	1.490	20.13
CR8	1.1701	1602	20	1688	1.1322	37.9	1.65	33.0	1.495	22.07
CR9	1.1202	1600	20	1685	1.0800	40.2	2.17	26.1	1.455	17.94
CR10	1.1465	1600	25	1695	1.0986	47.9	1.110	38.6	1.475	26.17
CR11	1.1677	1600	30	1660	1.1080	59.7	0.45	-	-	-
CR12	1.1255	1603	30	1665	1.0703	55.2	0.71	-	-	-
CR13	1.1044	1595	30	1654	0.9860	118.4	0.21	-	-	-

Comments:

1. The observed rate of decarburization = $8.33 \times 10^{-5} \text{ moles.cm}^{-2} \text{ s}^{-1}$
2. The commencement of the carbon boil at about 28 seconds.

TABLE 4.2 Decarburization of Fe-4.42%C in a stream of oxygen flowing at 3.0 l.min^{-1}

RUN	M_i gram	T_i $^{\circ}\text{C}$ ± 15	t sec	T_f $^{\circ}\text{C}$ ± 15	M_f gram	Δm mg	wt.% [C]	Δc mg	a cm^2	$\Delta c/a$ $\text{mg}\cdot\text{cm}^{-2}$	$\Delta m/a$ $\text{mg}\cdot\text{cm}^{-2}$
CR14	1.0878	1520	1	1605	1.0796	8.2	3.96	6.3	1.42	4.44	5.78
CR15	1.1607	1530	1	1615	1.1508	9.9	3.87	6.8	1.49	4.56	6.64
CR16	1.1146	1530	2	1700	1.0977	16.9	3.51	10.7	1.44	7.43	11.74
CR17	1.1614	1540	2	1715	1.1456	15.8	3.47	11.6	1.49	7.79	10.6
CR18	1.1071	1525	3	1785	1.0870	20.1	3.04	15.9	1.45	10.97	13.86
CR19	1.1853	1530	3	1805	1.1620	23.3	3.00	17.5	1.53	11.44	15.23
CR20	1.1745	1540	4	1800+	1.1464	28.1	2.56	22.6	1.51	14.97	18.61
CR21	1.1598	1520	4	1800+	1.1322	27.6	2.61	21.7	1.50	14.47	18.4
CR22	1.1340	1520	6	1800+	1.0899	45.1	1.23	-	-	-	-
CR23	1.0765	1525	6	1800+	1.0382	38.1	1.15	-	-	-	-

Comments:

1. The observed rate of decarburization = $3.08 \times 10^{-4} \text{ moles}\cdot\text{cm}^{-2}\cdot\text{s}^{-1}$
2. Commence of the carbon boil at about 5.2 seconds.

TABLE 4.3 Decarburization of the Fe-4.42%C in a stream of oxygen flowing at 5.0 l.min^{-1}

Run	M_i gram	T_i °C	t sec	T_f °C	M_f gram	Δm mg	wt.% [C]	Δc mg	a cm ²	$\Delta c/a$ mg-cm ⁻²	$\Delta m/a$ mg-cm ⁻¹
CR24	1.1461	1490	1	1585	1.1365	9.6	4.00	4.9	1.46	3.36	6.58
CR25	1.1316	1465	1	1555	1.1218	9.8	3.70	8.4	1.45	5.79	6.76
CR26	1.1596	1465	1	1555	1.1461	13.5	3.90	6.6	1.47	4.49	9.18
CR27	1.1268	1465	2	1694	1.1082	18.6	3.40	12.1	1.470	9.41	12.65
CR28	1.1567	1465	2	1695	1.1354	21.4	3.27	14.0	1.475	9.5	14.5
CR29	1.1630	1465	2	1697	1.1419	21.1	3.31	13.0	1.475	8.8	14.1
CR30	1.1627	1490	3	1815	1.1313	31.4	2.98	17.7	1.48	11.96	21.22
CR31	1.1680	1470	3	1810	1.1358	32.2	3.00	17.6	1.485	11.85	21.68
CR32	1.1605	1465	3	1805	1.1275	33.0	2.83	19.4	1.48	13.11	22.30
CR33	1.1410	1470	4	1800+	1.1025	38.5	2.36	24.2	1.47	16.46	26.19
CR34	1.1660	1495	4	1800+	1.1263	39.7	2.25	26.2	1.487	17.62	26.70
CR35	1.1596	1470	4	1800+	1.1280	31.6	2.41	24.1	1.48	16.28	21.35
CR36	1.1131	1490	6	1800+	1.0087	105.2	0.78	-	-	-	-
CR37	1.1138	1495	6	1800+	0.9934	119.6	0.66	-	-	-	-

Comments:

1. Commence of carbon boil at about 4.2 seconds.
2. Rate of decarburization = $3.5 \times 10^{-4} \text{ moles.cm}^2.\text{s}^{-1}$

TABLE 4.4 Decarburization of Fe-4.42%C in a stream of oxygen flowing at 10.3 l. min^{-1}

Run	M_i g	T_i $^{\circ}\text{C}$	t sec	T_f $^{\circ}\text{C}$	M_f g	Δm mg	wt% [C]	Δc mg	a cm^2	$\Delta c/a$ mg-cm^{-2}	$\Delta m/a$ mg-cm^{-2}
CR39	1.0518	1525	1	1665	1.0420	9.8	3.71	7.8	1.39	5.61	7.05
CR40	1.0366	1530	1	1665	1.0261	10.5	3.65	8.4	1.38	6.09	7.61
CR41	1.0509	1525	2	1695	1.0268	24.1	3.01	15.3	1.372	11.29	17.57
CR42	1.1598	1520	2	1690	1.1439	16.9	3.12	15.6	1.465	10.65	11.54
CR43	1.1346	1525	2	1696	1.1160	18.6	2.98	16.9	1.452	11.64	12.04
CR44	1.1655	1535	2.5	1750	1.1456	19.9	2.79	19.5	1.48	13.18	13.45
CR45	1.0758	1530	2.5	1745	1.0546	21.2	2.84	17.6	1.412	12.46	15.01
CR46	1.1231	1525	2.5	1747	1.0997	23.4	2.69	20.1	1.445	13.91	16.19
CR47	1.0750	1535	4	1800+	1.0407	34.3	1.51	-	-	-	-
CR48	1.0505	1535	4	1800+	1.0027	47.8	1.23	-	-	-	-

Comments:

1. Commence of Carbon boil at about 2.8 seconds.
2. The observed decarburization rate: $4.5 \times 10^{-4} \text{ moles.cm}^{-2} \text{ s}^{-1}$

TABLE 4.5 Decarburization of Fe-4.13%C - 0.1% P in a stream of oxygen flowing at 3.0 l.min^{-1}

Run	M_i g	T_i °C	t s	T_f °C	M_f g	Δm mg	wt% [C]	Δc mg	a cm ²	$\Delta c/a$ mg-cm ⁻²	$\Delta m/a$ mg-cm ⁻²
CR49	1.1501	1535	1	1635	1.1420	8.1	3.57	6.7	1.485	4.51	5.46
CR50	1.1312	1520	1	1625	1.1218	9.4	3.65	5.8	1.46	3.97	6.44
CR51	1.1522	1535	2	1725	1.1363	16.0	3.19	11.3	1.475	7.66	10.86
CR52	1.1275	1530	2	1720	1.1146	12.9	3.11	11.9	1.46	8.15	8.84
CR53	1.1405	1535	3	1805	1.1210	19.5	2.60	17.9	1.475	12.12	13.22
CR54	1.1608	1535	3	1805	1.1393	21.5	2.67	17.5	1.49	11.75	13.09
CR55	1.1004	1525	4	1800+	1.0735	26.9	2.18	22.1	1.435	15.40	18.75
CR56	1.1541	1525	4	1800+	1.1238	30.3	2.16	23.4	1.48	15.81	20.47
CR57	1.1278	1525	5	1800+	1.0825	45.0	1.36	-	-	-	-
CR58	1.0745	1520	5	1800+	1.0280	46.8	1.31	-	-	-	-

Comments:

1. The observed rate of decarburization = $3.25 \times 10^{-4} \text{ moles.cm}^{-2} \text{ s}^{-1}$.
2. The commencement of carbon-boil at about 4.5 seconds.

TABLE 4.6 Decarburization of Fe-4.13%C - 0.1% P in a stream of oxygen flowing at 10.3 l, min^{-1}

Run	M_i gram	T_i $^{\circ}\text{C}$	t sec	T_f $^{\circ}\text{C}$	M_f gram	Δm mg	wt.% [C]	Δc mg	a cm^2	$\Delta c/a$ $\text{mg}\cdot\text{cm}^{-2}$	$\Delta m/a$ $\text{mg}\cdot\text{cm}^{-1}$
CR59	1.1655	1535	1	1665	1.1563	9.2	3.65	5.9	1.485	3.97	6.2
CR60	1.1321	1530	1	1655	1.1213	10.8	3.55	7.0	1.46	4.79	7.4
CR61	1.1268	1530	2	1753	1.1117	15.1	3.01	13.1	1.455	9.0	10.4
CR62	1.1704	1532	2	1758	1.1551	15.3	3.03	13.3	1.485	8.96	10.3
CR63	1.1687	1530	2	1750	1.1524	16.3	2.94	14.4	1.485	9.69	11.0
CR64	1.1234	1527	2.5	1780	1.1056	17.8	2.65	17.1	1.45	11.79	12.3
CR67	1.1466	1535	2.5	1785	1.1275	19.1	2.72	16.7	1.47	11.36	13.0
CR68	1.1289	1530	2.5	1790	1.1105	18.4	2.65	17.2	1.455	11.82	12.65
CR69	1.1120	1530	3	1815	1.0778	34.2	2.13	-	-	-	-
CR70	1.1058	1535	3	1820	1.0732	32.8	2.14	-	-	-	-

Comments:

1. The observed rate of decarburization = $3.85 \times 10^{-4} \text{ moles}\cdot\text{cm}^{-2}\cdot\text{s}^{-1}$
2. The commencement of the carbon boil at about 2.8 seconds.

TABLE 4.7 Decarburization of Fe-3.65%C - 0.015%Si
in a stream of oxygen flowing at 0.75 l.min^{-1}

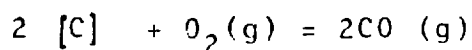
Run	M_i gram	T_i $^{\circ}\text{C}$	t sec	T_f $^{\circ}\text{C}$	M_f gram	wt% [C]
CR70	1.1325	1605	2	1665	1.1259	3.38
CR71	1.1355	1600	2	1663	1.0869	3.49
CR72	1.0890	1607	2	1670	1.0839	3.46
CR73	1.0805	1610	4	1670	1.0766	3.36
CR74	1.1217	1615	4	1680	1.1169	3.43
CR75	1.0750	1605	6	1690	1.0646	2.90
CR76	1.1023	1600	6	1695	1.0884	3.45
CR77	1.1003	1610	6	1715	1.0854	3.12
CR78	1.0960	1605	8	1730	1.0821	2.66
CR79	1.1360	1615	8	1780	1.0879	3.25
CR80	1.1682	1612	8	1730	1.1522	2.74

Comments:

1. Formation of high emissivity oxide layer on the surface.
2. Commence of carbon-boil at about 6 seconds after the oxidation had begun.

4-6.1 Decarburization by O₂

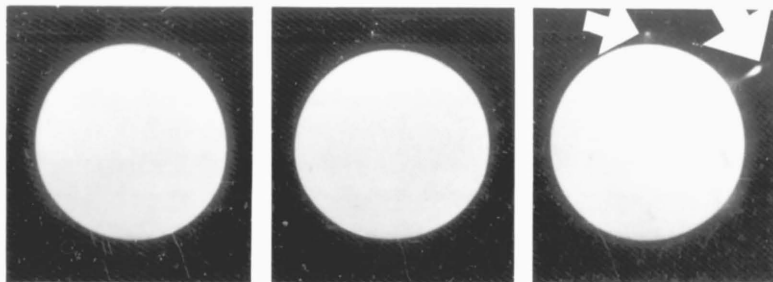
The overall reaction occurring between the dissolved carbon and the oxygen gas may be represented by the equation:



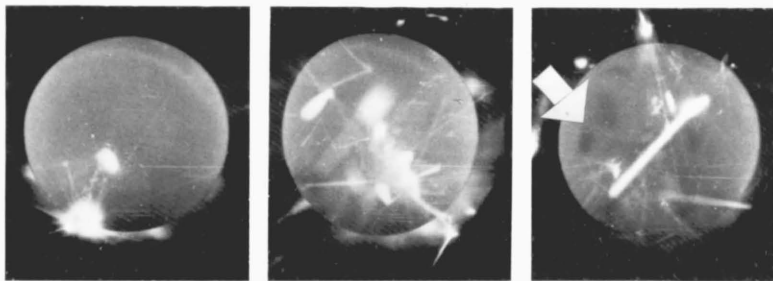
This reaction is exothermic and hence would tend to increase the temperature of the molten drop as reaction proceeds, however the rapid steady rise in the temperatures observed is partially due to the contributing effect of the thermal conductivities of oxygen and carbon monoxide as compared to that of helium.

In all experiments the drops started to boil in the absence of any oxide phase appearing on the surface of the molten drops, (see Figure 4.1): up to the commencement of the carbon boil there was no significant swelling in the drops, but once the boil began the diameter of the drops kept on increasing. At the end of the vigorous boil the drops' diameters had increased by about 5%. At the end of the oxidation, when the drops were kept levitated in a stream of helium prior to quenching, the most significant enlargement of the drops took place and on average the drops swelled to about 1.12 times their original diameters, appearance of dark spots on the surface of the drops were observed during this period, and rotation of the spots on the surface was followed by

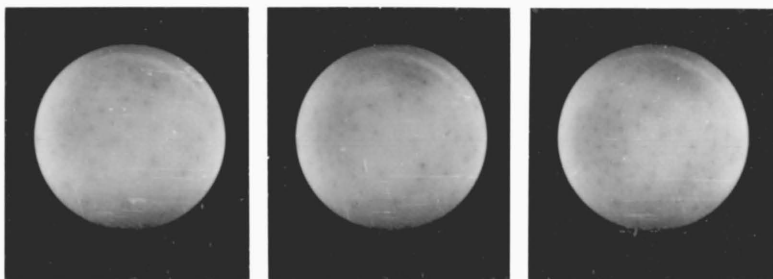
Frames



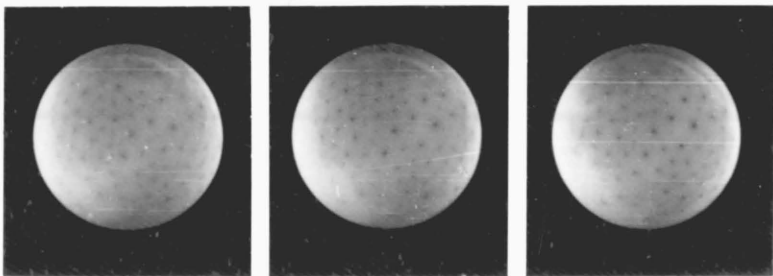
180-182 *First sign of boil.*



219-221 *Very violent boil, appearance of CO bubbles as large dark spots.*



257-259 *Nucleation of CO bubbles after the completion of the oxidation.*



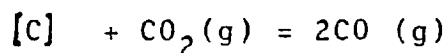
275-277
 Figure 4.1 *Illustrating the carbon-boil and "homogeneous" nucleation of CO. Alloy: Fe-C-P; Gas: oxygen. flow rate: 10.3 l.min⁻¹, oxidation period: ~3.5 cc. filming speed: 64 p.p.s.*

gradual decrease in the diameter of the drops. This sequence of events is illustrated in Figure 4.1.

The presence of phosphorus showed no significant effect on the appearance of the carbon boil, but its effect on the rate of decarburization was appreciable and will be discussed later.

4-6.2. Decarburization by CO₂

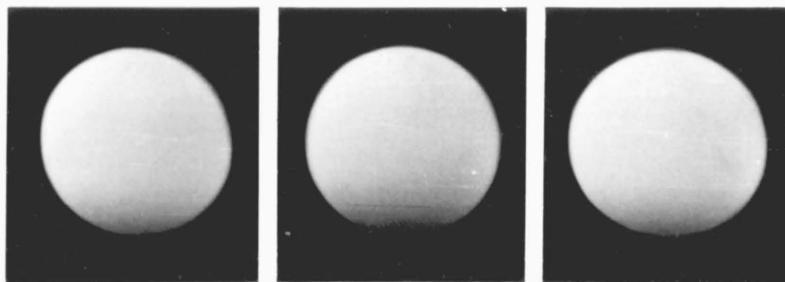
The overall reaction occurring between the dissolved carbon and the carbon dioxide gas may be represented by:



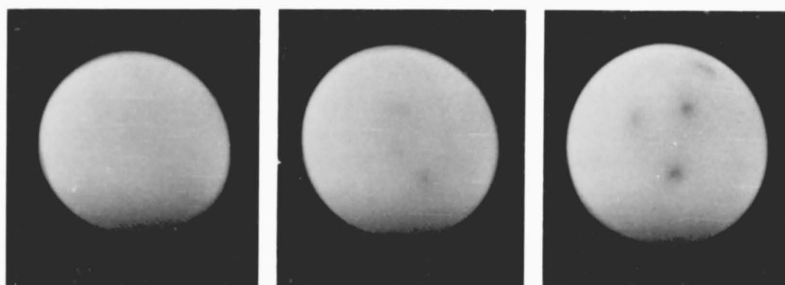
This reaction is slightly endothermic and hence it would be expected to decrease the temperature of the molten drop slightly as the reaction proceeds, but the observed sharp rise in the temperature of the samples is due to the differences in the thermal conductivities of He and (CO + CO₂) as was noted in the case of reaction with O₂.

In experiments where Fe-C alloys were oxidised, the drops started to increase in size and the diameters reached 1.12 times the original size before the commencement of the carbon boil. A few seconds before the boil started, appearance of dark "spots", presumably due to CO bubbles, were observed on the surface and these rotated about the

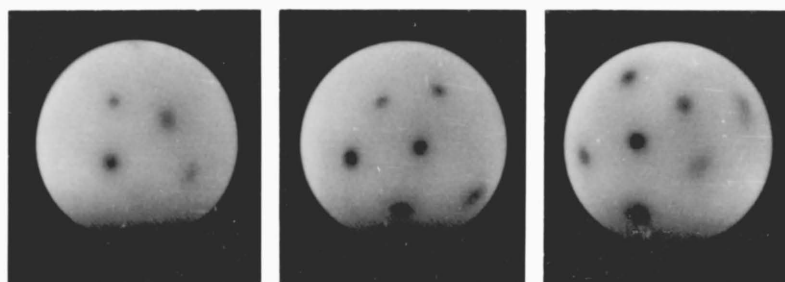
EXPERIMENT 8



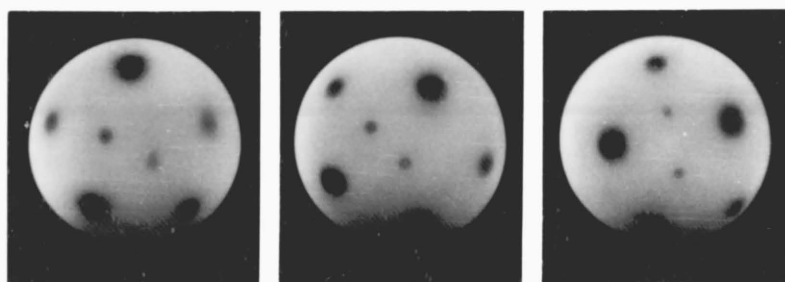
504-506 Illustrating the size of the levitated drop before nucleation of CO bubbles.



508-510 Start of the CO nucleation.



511-513 Nucleation of CO bubbles and their growth.



520-522 Growth and movement of CO-bubbles, just before the commencement of the carbon boil.

Figure 4.2 Illustrating the sequences of the events leading to homogeneous nucleation of CO bubbles and their enlargements, during oxidation of Fe-C alloy in a stream of CO_2 , flowing at 0.75 l. min^{-1} . filming speed: 16 p.p.s.

vertical axis and increased in size (see Figure 4.2.). Before and during the formation of the bubbles no oxide phase was observed on the surface. Ejection of material due to bursting of the CO bubbles caused the drops to lose their spherical shape and they became violently distorted.

In the presence of small amounts of silicon ($\approx 0.015\%$) the sequence of events was rather different. Once the oxidation had started, a high emissivity oxide layer nucleated on the top of the specimen and spread to cover the entire surface in a few seconds, about six seconds after the oxidation had begun the "early carbon-boil" commenced and carbon monoxide bubbles burst through the surface. The sequence of events is illustrated in Figure 4.3.

4.7. DISCUSSION

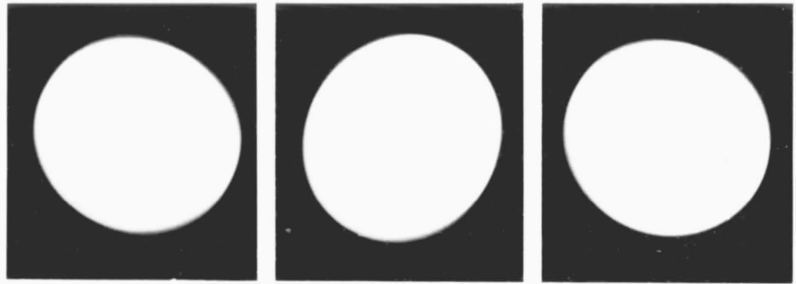
4-7.1. Rate Controlling Step in the Reaction of Fe-C and O_2

There are several mechanisms, which may control the rates of decarburization and these are:

- a. Transport of carbon to the metal/gas interface.
- b. Chemical reactions at the interface.
- c. Chemisorption of gaseous reactants and products.
- d. Transport of gaseous reactants and products to and from the interface.

With reference to Figure 4.4., it is evident that the linear rates of decarburization obtained, till the commencement of the carbon boil, are independent of carbon

Frames



6-8



72-74 The first signs of oxide formation



83-85 Spreading of the slag layer.



150-152 Surface coverage by the slag layer.

Figure 4.3 The sequence of the oxide formation, and spreading over the surface of a Fe-C-Si drop the commencement of the carbon boil. Reaction gas: CO_2 . Volume flow rate: 0.75 l.min^{-1} . filming speed: 24 p.p.s.

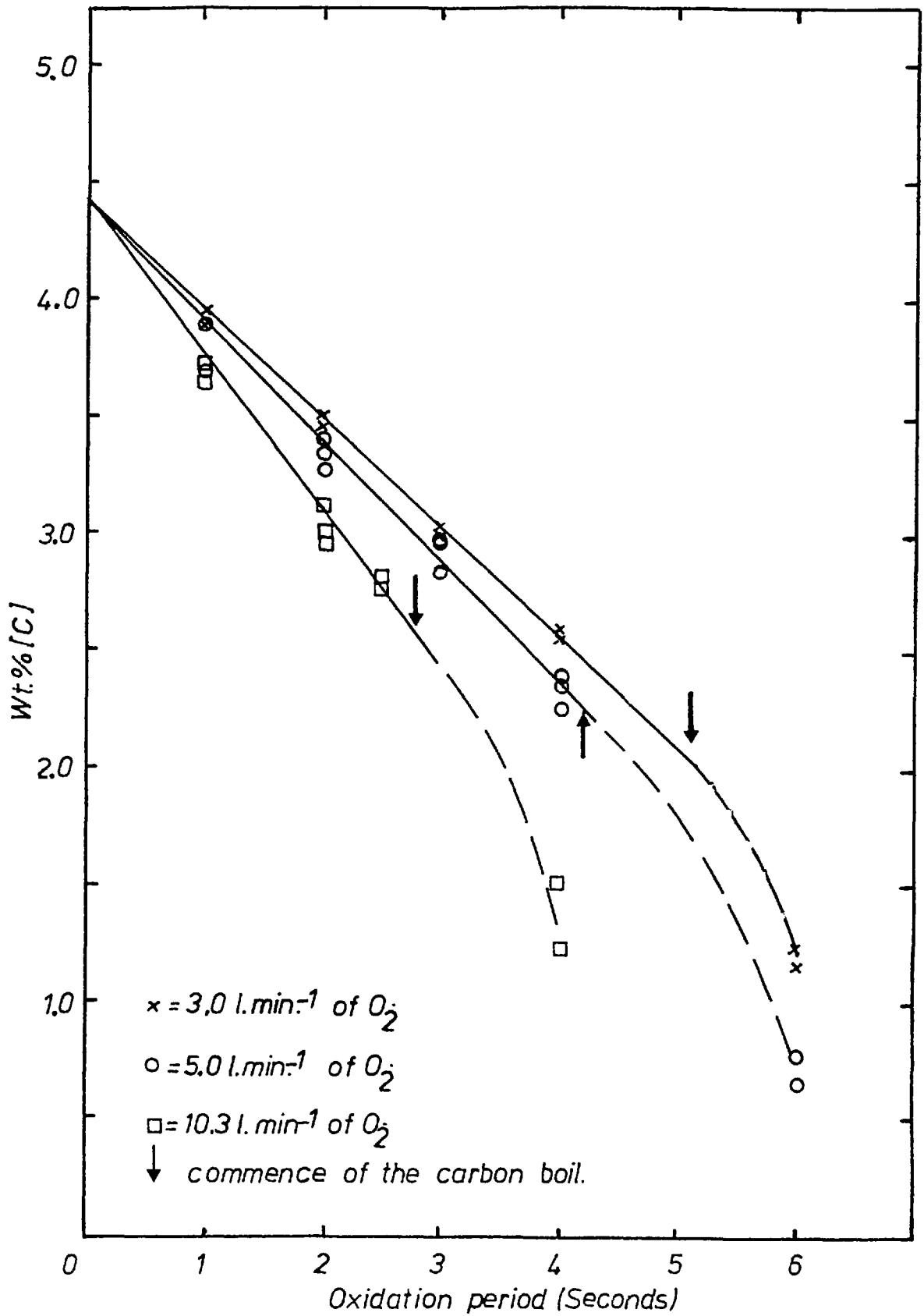


Figure 4.4 Decarburization of the Fe-C by streams of O₂.

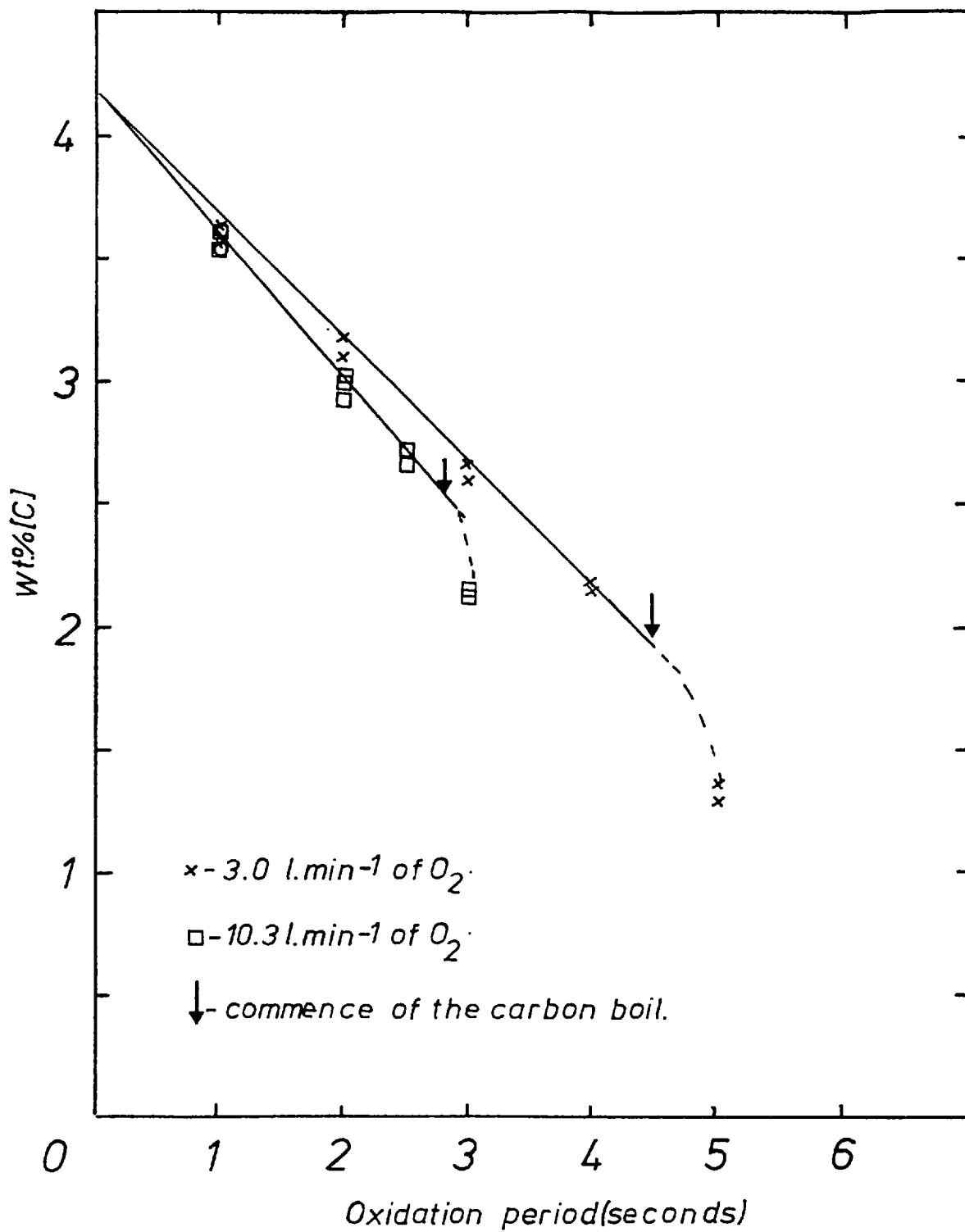


Figure 4.5 Decarburization of Fe-C-P by streams of O₂

concentrations at all flow rates of oxygen, hence the transport of carbon in the liquid phase is not a rate controlling step. The rates of chemical reaction, such as oxidation of carbon, are generally too rapid for these to be the rate controlling step. Thus in interpreting the results it was assumed that one or more of the other steps were rate controlling, and it was decided that if the result could not be interpreted in such a way then chemical reactions at the interface were rate determining. The effect of oxidant flow rate on the rate of decarburization indicates that the transport in the gas phase must be rate controlling, and the calculated rates based on the assumption that the mass transfer in the gaseous boundary layer is the rate controlling step, gives very good agreement with the observed rates (see Appendix 1). Finally in the case of oxidation of pure iron-carbon alloys, it may also be assumed that chemisorption of gaseous reactants and product onto and off the interface may not be rate controlling. However once the carbon concentration falls below that at which the carbon boil occurs, then transport in the liquid phase appears to be just as important as transport in the gas phase.

4-7.2. Rate of Decarburization of Fe-C with CO₂

Once again the linear decarburization rate observed until the commencement of the carbon boil was a good indication that transport in the liquid phase is not

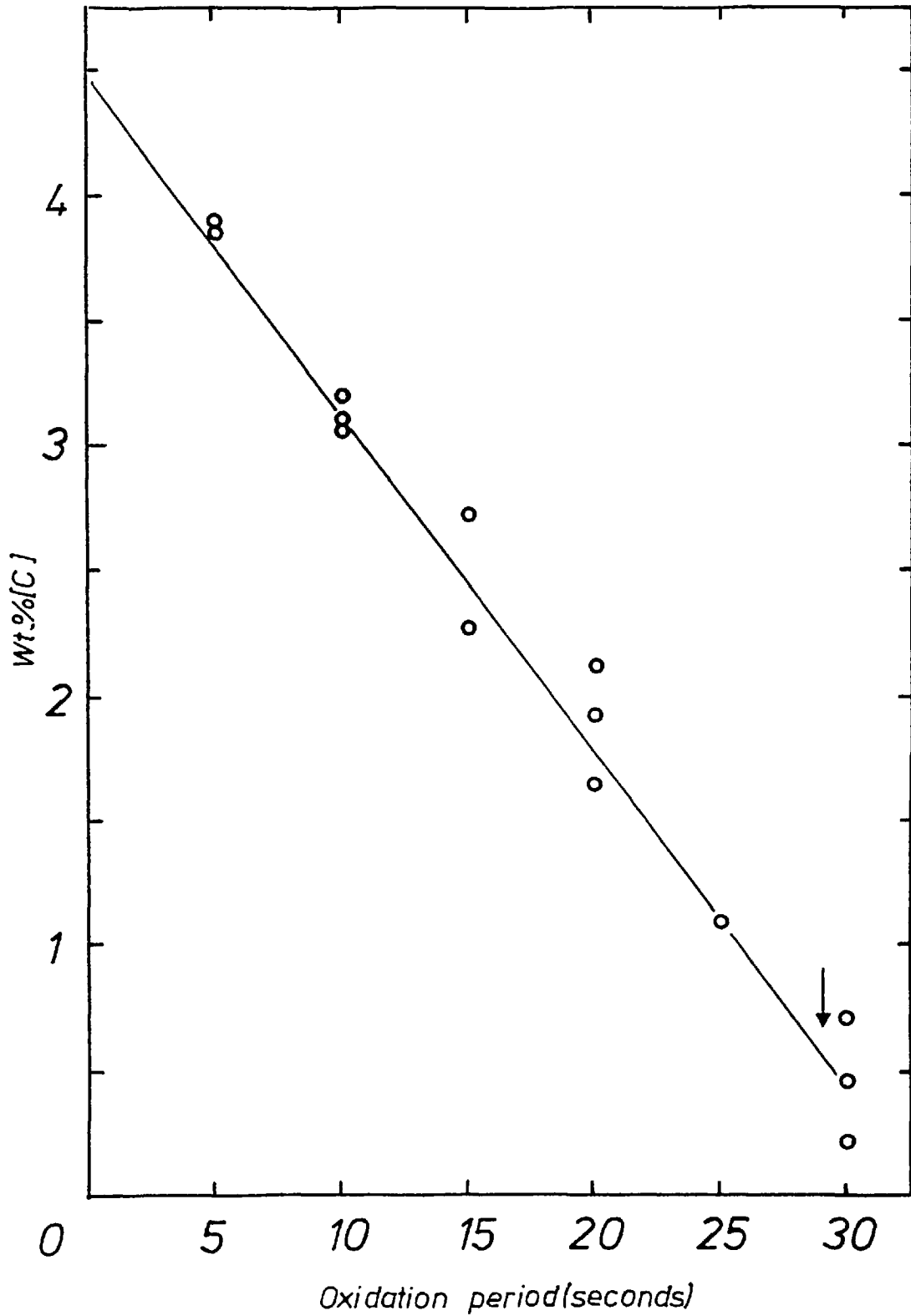


Figure 4.6 Decarburization of Fe-C by a stream of CO_2 flowing at 0.75 l min^{-1} .

the rate determining step and that the transport of the reactant and product to and from the interface is controlling the rate, since the observed rate is in good agreement with the calculated rates based on the assumption that the gaseous diffusion in the boundary layer is the rate controlling step.

The observed rate is about half the rate found by Baker et al.,⁽⁹⁾ who used drops of 0.7 gram at 1660°C in a stream of CO₂, flowing at 1 l.min⁻¹. The difference in the rates observed is due to several contributing factors, such as the flow rates of the reactant, which would have caused an increase in the rate. The other major contributing factor is the size of the drops used in this investigation as compared to those used by Baker et al. Their drops were smaller in size, this has the effect of increasing the area/unit mass for the smaller drops, as well as resulting in an increase in the mass transfer coefficient about the drops. Finally the slight difference between their reaction temperature (1660°C) and the mean temperature of the samples in this work (1645°C) probably contributed to the difference in the rates observed.

4-7.3. Effect of 0.1 wt% P on the Rate of Decarburization

The rates of decarburization of iron-carbon alloys in presence and absence of 0.1 wt% P in streams of O₂ flowing at 3.0, and 10.3 l.min⁻¹ are tabulated in Table 4.8.

TABLE 4.8 The observed and calculated rates of decarburization ($\text{moles}\cdot\text{cm}^{-2}\cdot\text{s}^{-1}$) of Fe-C and Fe-C-P in streams of oxygen.

Alloy	Flow rate of oxygen ($\text{l}\cdot\text{min}^{-1}$)		
	3.0	5.0	10.3
Fe-C	3.08×10^{-4}	3.5×10^{-4}	4.5×10^{-4}
Fe-C-P	3.25×10^{-4}	-	3.85×10^{-4}
Calculated*	3.09×10^{-4}	3.47×10^{-4}	4.27×10^{-4}

*See Section 4-7.6 below.

Comparison of the rates observed indicate that at low flow rate ($3.0 \text{ l}\cdot\text{min}^{-1}$) of oxygen, the apparent rates are slightly faster ($\sim 6\%$) in the presence of 0.1 wt% phosphorus. These rates are in excellent agreement with the predicted rates for gaseous diffusion control, hence any increase in the mass transfer coefficient, in the liquid phase, by the presence of phosphorus would not be expected to effect the overall rate. If it is supposed that the 6% rise in the measured rate is not due to experimental error, then the presence of phosphorus could influence the overall rate slightly by the following mechanism. In the absence of phosphorus, during the oxidation, some iron is being vaporized from the surface and the vapour reacts with some of the oxygen in the

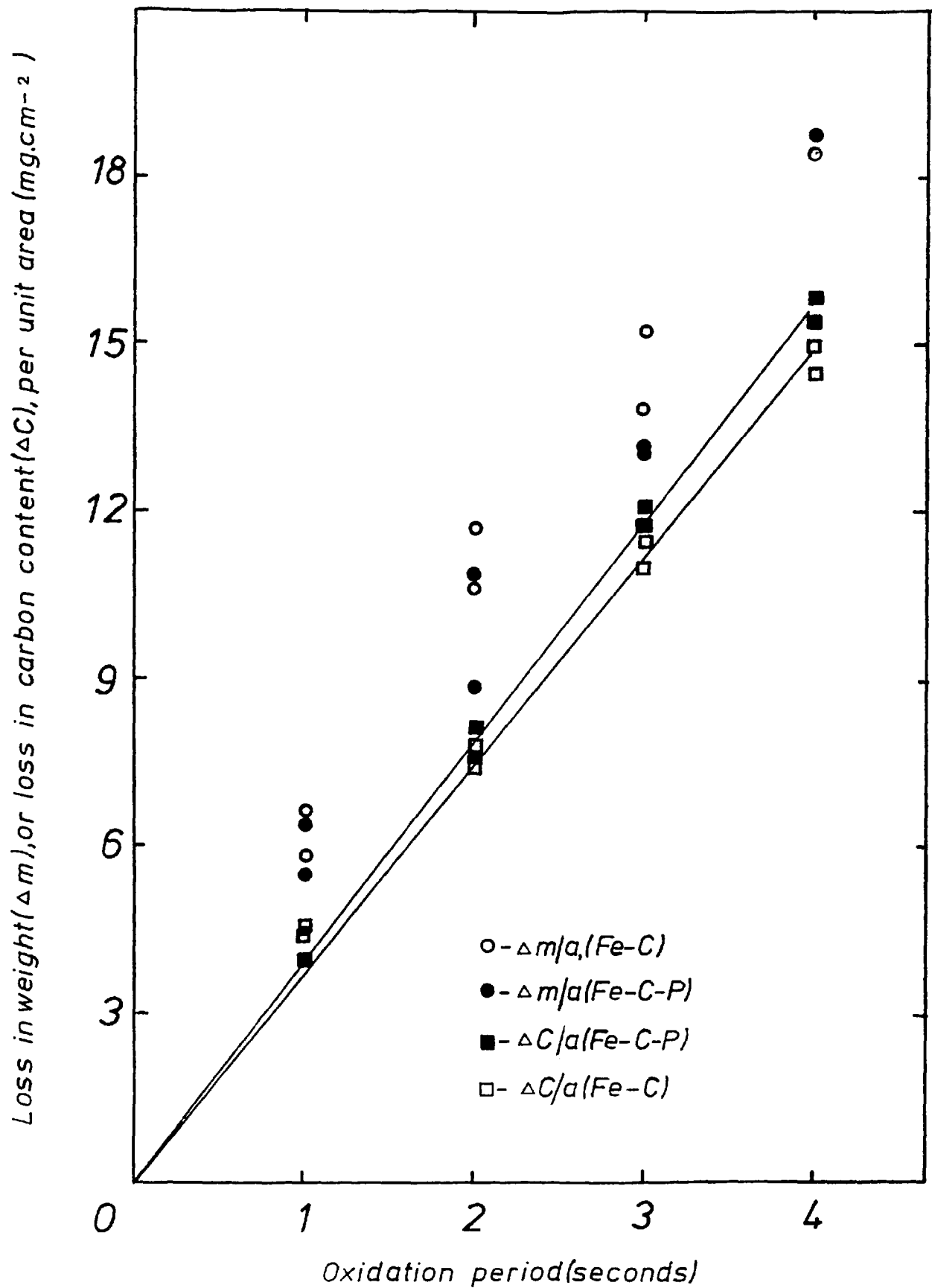


Figure 4.7 Oxidation of Fe-C and Fe-C-P in a stream of O_2 flowing at $3.0 \text{ l}\cdot\text{min}^{-1}$

gaseous boundary layer to form iron oxide, and then are carried away by the stream of the gas, hence resulting in the consumption of a portion of the oxygen available for decarburization. The net result is that not only less carbon is being oxidised away, but also the concentration of the remaining carbon in the molten drop is slightly effected. However in the presence of a "monolayer" of phosphorus on the surface the rate of vaporization of iron may be reduced, with the net result that slightly more oxidation of carbon occurs and a lower concentration of carbon in the molten iron drop results. The evidence to support the above hypothesis should arise from the inspection and comparison of Figures 4.7 and 4.8., where the total loss in weight (Δm), and the loss in carbon content (Δc) of the samples per unit area are plotted against oxidation period, for the two flow rates of oxygen. As can be seen from Figure 4.7. the lack of consistency in the data on the amount of iron lost by vaporization for each alloy makes such a hypothesis rather speculative, but nevertheless the results obtained at the higher flow rate of oxygen (10.3 l.min^{-1}) show less discrepancy and hence show some indication in favour of the above explanation.

Although the present investigations were not carried out with the intention of measuring the enhanced rates of vaporization of iron from alloys of different compositions, and the vaporization results are rather scattered, the postulated mechanism may be very important and applicable

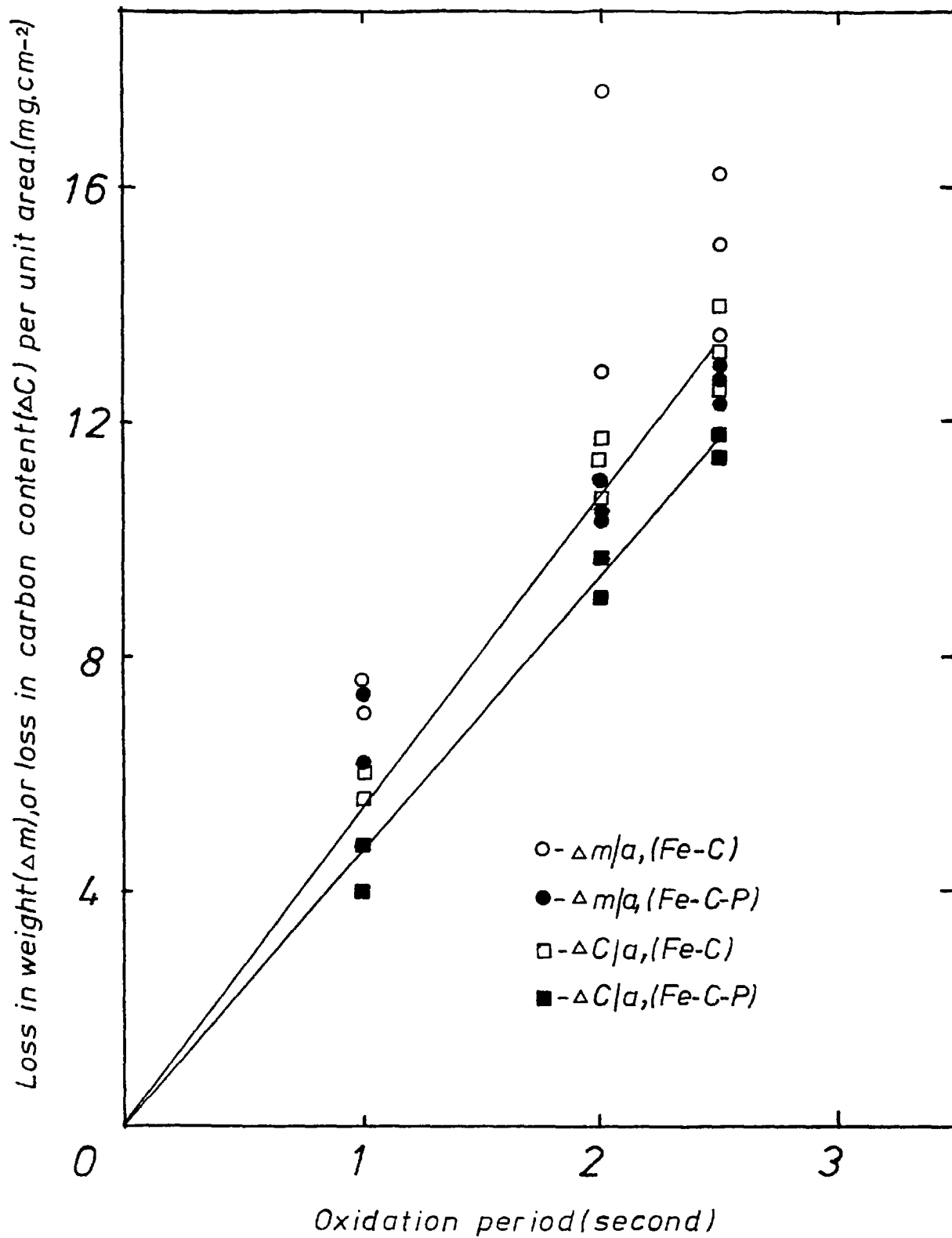


Figure 4.8 Decarburization of Fe-C and Fe-C-P by a stream of O_2 flowing at $10.3 \text{ l}\cdot\text{min}^{-1}$

when consideration is given to fuming observed in steel-making practice.

As can be seen from Table 4.8. and Figure 4.8. at higher flow rates, the situation changes and the presence of 0.1 wt% phosphorus apparently leads to the slowing down of the overall rate of decarburization by about 14%. Phosphorus has an affinity for a large amount of oxygen, and according to the work of Kor and Turkdogan⁽⁵⁶⁾ evolution of carbon monoxide from the surface of the melt may aid enhanced vaporization of phosphorus from the melt, in which case formation of volatile oxide species of phosphorus would take place. If such a reaction did occur then it is reasonable to consider the consumption of the available oxygen in the gaseous boundary layer to be the influencing factor on the inhibition of the carbon oxidation. However our investigations into the subject of enhanced vaporization of iron-phosphorus alloys in the absence and presence of carbon have clearly indicated that phosphorus does not leave the molten metal via vapour phase contrary to the above postulate (see Chapter 5).

An alternative explanation for the effect of phosphorus on the retardation of the decarburization rate would be of a mixed controlled regime, in which case both the interfacial reactions and the diffusion of the gaseous reactants and products play important roles in controlling the rate of decarburization. Under such

conditions it is likely that the adsorbed phosphorus would impede the carbon from penetrating to the interface, and hence the carbon-oxygen reaction would be prevented in the parts of the interface where the surface active material are fully adsorbed. It is reasonable to consider that the adsorbed phosphorus atoms are not occupying every available site at the interface, hence the reaction remains also dependent on the rate of transport of the gases in the gaseous boundary layer too.

The question arises as to why at the lower flow rate of oxygen, such retardation in the rate of decarburization was not observed. It seems likely that at low rates of supply of oxidant to the surface, the carbon flux to the active areas (phosphorus free) is sufficient to use up all the oxygen from the gas, and hence the reaction rate remains totally dependent on transport in the gases and the presence of the unreactive area would not affect the overall rate.

These findings are in accordance with those of other workers⁽²²⁻²⁴⁾ regarding the surface activity of phosphorus and appear to contradict the data of Kozakevitch.⁽⁴⁰⁾ According to the measurements made by Kozakevitch and Urbain^(41,42) in Groups III, IV and VI of the periodic table surface activity of the elements in liquid iron increases progressively with the atomic number of the element:

i.e. In > Al > 8
 or Te > Se > S > 0

But in Group V, there appears to be an exception and nitrogen is more surface active than phosphorus or arsenic. On the other hand the results of Hondros^(43,44) and Hayes et al.⁽²³⁾ show that phosphorus is as surface active as nitrogen in solid iron, hence by analogy it may be concluded that the results of Kozakevitch et al. on the surface activity of elements in Group V need verification.

4-7.4. Effect of Silicon on the Rates of Decarburization

The results obtained with drops weighing about 1.1 gram with and without 0.015 wt% silicon are shown in Figure 4.9. As mentioned previously in the absence of silicon, the observed rates are in very good agreement with those calculated for transport control in the gas phase, and the carbon boil occurs at about 0.6 wt% carbon in the melt, without any oxide particles being visible on the surface of the drops before the commencement of the boil. However with 0.015% silicon in the drops, the decarburization rate is retarded, and the carbon concentrations at the boil are much higher, about 3.1%C. Although the results obtained are scattered, due to the early carbon boil, the retardation of the carbon-oxygen reaction is clearly indicated. On the basis of visual

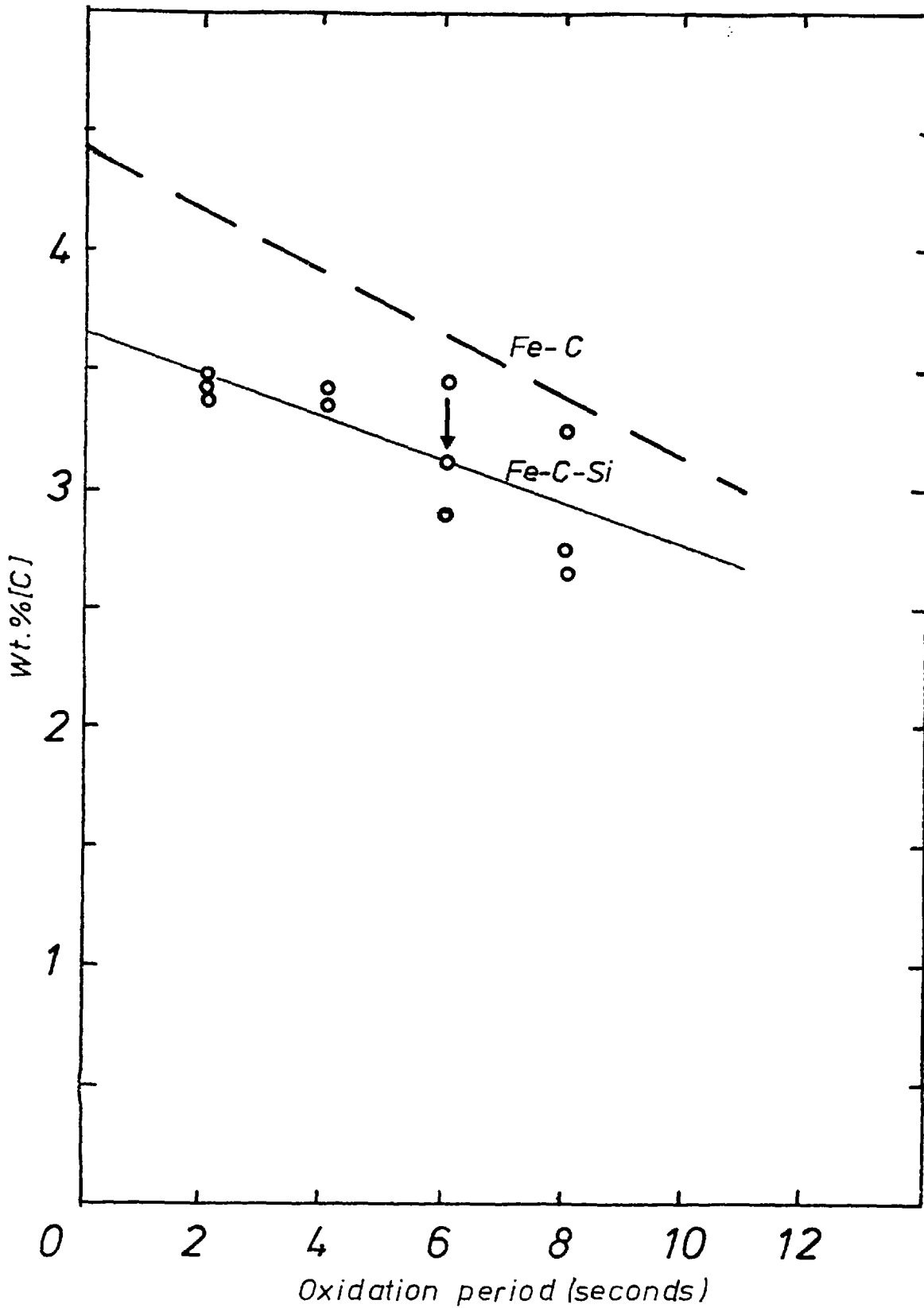


Figure 4.9 Decarburization of 1.15g drops of Fe-C and Fe-C-Si in a stream of CO_2 flowing at 0.75 l.min^{-1} (↓ indicates the commence of carbon boil)

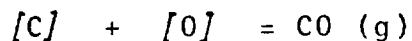
observations and the rates observed, the influence of the dissolved silicon may be explained in the following way: once the oxidation begins, formation of a "passive" oxide film, presumably silicate, takes place and the oxide film would cover the entire surface of the drop, hence transport of the oxidant to the interface would be controlled by diffusion of oxygen ions through the liquid oxide film to the metal/slag interface. At the interface the carbon-oxygen reaction takes place and carbon monoxide is formed. The presence of the passive film prevents desorption of the carbon monoxide from the melt and hence supersaturation of CO takes place. This would lead to nucleation and growth of CO bubbles at the metal/slag interface and eventually to the bursting of the bubbles through the surface.

These observations and deductions are consistent with those of Robertson⁽⁴⁶⁾ and See et al.⁽⁴⁷⁾ who oxidised iron-carbon drops containing a few wt% silicon. The question arises from the fact that these workers used high silicon contents in their melts and observed the formation of the passive film, while in this study the silicon activity in the drops was much lower, and hence on thermodynamic grounds it would be expected that the formation of the silica would take place at much lower carbon activities than observed. It seems likely that the formation of surface active compounds has affected the reactions in this case. Although carbon and silicon are generally known to be slightly surface active in liquid iron,⁽⁴²⁾ it is possible

that the interactions between the two non-active solutes, could produce a surface active soluble compound, as in the case of Fe-Cr-C, where chromium is not surface active in liquid iron, and carbon is only slightly active, but the surface tension is noticeably lowered when both solutes, are present.⁽⁴⁰⁾ Thus it is likely that the activity of silicon at the interface is increased by the presence of the surface active compound and hence oxidation of silicon takes place preferentially to carbon.

4-7.5. Carbon Boil

If a levitated drop is considered to be static, then it would be expected that a carbon concentration gradient to be set up within the drop once the initial period of decarburization at the surface has elapsed. Owing to the solubility of oxygen in liquid iron, the absorption of oxygen takes place simultaneously with the decarburization of the iron. The presence of dissolved carbon and oxygen in the molten drop would lead to formation of carbon monoxide:



the carbon monoxide formed being only slightly soluble in the liquid drop and hence would lead to supersaturation of CO in the liquid phase. Thus the CO formed in the liquid phase has to nucleate and then burst. If an oxide

phase such as FeO , Al_2O_3 , CaO or SiO_2 is present, then heterogeneous nucleation of the CO bubbles may occur at low super-saturation of CO, otherwise the super-saturation of CO in the liquid phase must be high enough to overcome the energy barrier for homogeneous nucleation.

Homogeneous nucleation of CO bubbles in levitated drops of iron has been studied by El-Kaddah and Robertson.⁽⁴⁹⁾ The critical super-saturation was found to be strongly dependent on the oxygen activity in molten iron. At 1600°C super-saturations of 10 and 72 atmospheres were required to initiate CO gas bubble nucleation, at oxygen potentials in the gas surrounding the drops corresponding to 8% CO_2 and 2% CO_2 in CO respectively. They have also concluded that the presence of surface active solutes affects the super-saturation required to bring about homogeneous nucleation of the bubbles by lowering the surface tension of the molten drop and hence lowering the energy barrier for the nucleation.

Distin et al.⁽¹²⁾ in their studies of decarburization of levitated iron drops in streams of pure CO_2 and O_2 have reported that nucleation of the bubbles took place after the formation of an oxide phase on the surface. On the other hand some other investigators^(10,46-48) have reported nucleation of CO bubbles before the formation of an oxide phase. The latter findings are in accordance with the present work. One reason for formation of an oxide phase before the boil reported by Distin et al., could be

the presence of oxide forming impurities, such as Al, or Si in their melts arising from contamination during the preparation of the alloys.

The question of when a carbon boil occurs in a levitated iron drop, in the absence of oxide phase remains the subject of conflicting evidence. (50)

4-7.6. Comparison of the Predicted and Measures Rates of Decarburization

The predicted rates of decarburization of Fe-C drops in streams of CO₂ or O₂ has been calculated using the model described in Appendix 1. In the evaluation of the gas phase mass transfer coefficients (K_g), use of different available correlations for different regimes of mass transfer in the gas phase has been made, and hence the flux of oxidant to the interface has been calculated using the following equations:

$$J_{O_2} = \frac{K_g CO/O_2}{RT_f} \cdot \ln \left(1 + P_{O_2}^b \right)$$

and

$$J_{CO_2} = \frac{K_g CO/CO_2}{RT_f} \cdot \ln \left(1 + P_{CO_2}^b \right)$$

and from the stoichiometry of the reactions the flux of carbon, i.e. the rates of decarburization have been calculated.

The estimated and measured rates in oxygen and carbon dioxide streams are listed in the following tables(4.9-4.12).

TABLE 4.9. Calculated and measured rates of decarburization of Fe-C in a stream of CO₂ flowing at 0.75 l.min⁻¹ D_{CO/CO₂} = 1.48 cm²/sec d = 0.68 cm \overline{Gr} = 1486 Pr = 0.76 Re = 9.0 Sc = 0.73 T_f = 1106^oK Gr^h = 394 Gr^m = 1100

Correlation	Calculated rate (moles.cm ⁻² .s ⁻¹)	Measured rate (moles.cm ⁻² .s ⁻¹)	J _c ^{calc} /J _c ^{meas.}
Sh = 2 + 0.569(\overline{Gr} .Sc) ^{0.25}	8.75 × 10 ⁻⁵	8.33 × 10 ⁻⁵	1.05
Sh = 2 + 0.5(\overline{Gr} .Sc) ^{0.25}	8.10 × 10 ⁻⁵	8.33 × 10 ⁻⁵	0.97
Sh = 0.78 (\overline{Gr} .Sc) ^{0.25}	7.44 × 10 ⁻⁵	8.33 × 10 ⁻⁵	0.89
Sh = 2 + 0.5 (\overline{Gr} .Sc) ^{0.25} + 0.52(Re ^{0.62} Sc ^{0.31})*	1.12 × 10 ⁻⁴	8.33 × 10 ⁻⁵	1.35
Sh = 0.78 (\overline{Gr} .Sc) ^{0.25} + 0.8(Re ^{1/2} .Sc ^{1/3})	1.10 × 10 ⁻⁴	8.33 × 10 ⁻⁵	1.32

*Modified Steinberger and Treybal by Distin et al. (12)

TABLE 4.10. Calculated and measured rates of decarburization of Fe-C in a stream of O_2 flowing at 3.0 l.min^{-1} $D_{CO/O_2} = 2.0 \text{ cm}^2 \cdot \text{s}^{-1}$ $d = 0.69 \text{ cm}$ $\overline{Gr} = 745$
 $Pr = 0.75$ $Re = 26.0$ $Sc = 0.74$ $T_f = 1133^\circ\text{K}$ $Gr^h = 217$ $Gr^m = 529$

Correlation	Calculated rate (moles $\cdot \text{cm}^{-2} \cdot \text{s}^{-1}$)	Measured Rate (moles $\cdot \text{cm}^{-2} \cdot \text{s}^{-1}$)	$J_c^{\text{calc}}/J_c^{\text{meas.}}$
$Sh = 2 + 0.347(Re^{0.62} Sc^{0.31})$	1.89×10^{-4}	3.08×10^{-4}	0.62
$Sh = 2 + 0.52(Re^{0.62} Sc^{0.31})^*$	2.41×10^{-4}	3.08×10^{-4}	0.79
$Sh = 2 + 0.552(Re^{\frac{1}{2}} Sc^{\frac{1}{3}})$	1.97×10^{-4}	3.08×10^{-4}	0.65
$Sh = 2 + 0.6(Re^{\frac{1}{2}} Sc^{\frac{1}{3}})$	2.06×10^{-4}	3.08×10^{-4}	0.68
$Sh = 0.8(Re^{\frac{1}{2}} Sc^{\frac{1}{3}})$	1.60×10^{-4}	3.08×10^{-4}	0.53
$Sh = 2+0.347(Re^{0.62} Sc^{0.31})+0.569(\overline{Gr}, Sc)^{0.25}$	3.09×10^{-4}	3.08×10^{-4}	1.02
$Sh = 2+0.347(Re^{0.62} Sc^{0.31})+0.5(\overline{Gr}, Sc)^{0.25}$	2.94×10^{-4}	3.08×10^{-4}	0.96
$Sh = 2+0.52(Re^{0.62} Sc^{0.31})+0.5(\overline{Gr}, Sc)^{0.25}^*$	3.46×10^{-4}	3.08×10^{-4}	1.14
$Sh = 0.8(Re^{\frac{1}{2}} Sc^{\frac{1}{3}}) + 0.78(\overline{Gr}, Sc)^{0.25}$	3.24×10^{-4}	3.08×10^{-4}	1.07

*Modified Steinberger and Treybal correlation by Distin et al. (12)

TABLE 4.11. Calculated and measured rates of decarburization of Fe-C in a stream of O_2 flowing at 5.0 l, min^{-1} $D_{CO//O_2} = 2.0 \text{ cm}^2, \text{ s}^{-1}$ $d = 0.69 \text{ cm}$ $\overline{Gr} = 745$
 $Pr = 0.75$ $Re = 43.4$ $Sc = 0.74$ $T_f = 1133^{\circ}\text{K}$ $Gr^h = 217$ $Gr^m = 529$

Correlation	Calculated rate (moles. $\text{cm}^{-2}, \text{ s}^{-1}$)	Measured rate (moles. $\text{cm}^{-2}, \text{ s}^{-1}$)	$J_c^{\text{calc}}/J_c^{\text{meas.}}$
$Sh = 2 + 0.347(Re^{0.62} Sc^{0.31})$	2.28×10^{-4}	3.5×10^{-4}	0.65
$Sh = 2 + 0.52(Re^{0.62} Sc^{0.31})^*$	2.98×10^{-4}	3.5×10^{-4}	0.85
$Sh = 2 + 0.552(Re^{\frac{1}{2}}, Sc^{\frac{1}{3}})$	2.30×10^{-4}	3.5×10^{-4}	0.66
$Sh = 2 + 0.6(Re^{\frac{1}{2}}, Sc^{\frac{1}{3}})$	2.42×10^{-4}	3.5×10^{-4}	0.69
$Sh = 0.8(Re^{\frac{1}{2}}, Sc^{\frac{1}{3}})$	2.07×10^{-4}	3.5×10^{-4}	0.59
$Sh = 2+0.347(Re^{0.62} Sc^{0.31}) + 0.569(\overline{Gr}, Sc)^{0.25}$	3.47×10^{-4}	3.5×10^{-4}	0.99
$Sh = 2+0.347(Re^{0.62} Sc^{0.31}) + 0.5 (\overline{Gr}, Sc)^{0.25}$	3.33×10^{-4}	3.5×10^{-4}	0.95
$Sh = 2+0.52(Re^{0.62} Sc^{0.31}) + 0.5 (\overline{Gr}, Sc)^{0.25}^*$	4.03×10^{-4}	3.5×10^{-4}	1.15
$Sh = 0.8(Re^{\frac{1}{2}}, Sc^{\frac{1}{3}}) + 0.78(\overline{Gr}, Sc)^{0.25}$	3.71×10^{-4}	3.5×10^{-4}	1.06

*Modified Steinberger and Treybal correlation by Distin et al. (12)

TABLE 4.12. Calculated and measured rates of decarburization of Fe-C in a stream of O_2 flowing at 10.3 l min^{-1} $D_{CO/O_2} = 2.0 \text{ cm}^2 \text{ s}^{-1}$ $d = 0.69$ $\overline{Gr} = 745$
 $Pr = 0.75$ $Re = 89.4$ $Sc = 0.74$ $T_f = 1133^\circ K$ $Gr^h = 217$ $Gr^m = 529$

Correlation	Calculated rate (moles.cm ⁻² .s ⁻¹)	Measured rate (moles.cm ⁻² .s ⁻¹)	$J_c^{calc}/J_c^{obs.}$
$Sh = 2 + 0.347(Re^{0.62} Sc^{0.31})$	3.08×10^{-4}	4.5×10^{-4}	0.68
$Sh = 2 + 0.52(Re^{0.62} Sc^{0.31})^*$	4.18×10^{-4}	4.5×10^{-4}	0.93
$Sh = 2 + 0.552(Re^{\frac{1}{2}} Sc^{\frac{1}{3}})$	2.92×10^{-4}	4.5×10^{-4}	0.65
$Sh = 2 + 0.6 (Re^{\frac{1}{2}} Sc^{\frac{1}{3}})$	3.08×10^{-4}	4.5×10^{-4}	0.68
$Sh = 0.8 (Re^{\frac{1}{2}} Sc^{\frac{1}{3}})$	2.97×10^{-4}	4.5×10^{-4}	0.66
$Sh = 2 + 0.347(Re^{0.62} Sc^{0.31}) + 0.569(\overline{Gr} \cdot Sc)^{0.25}$	4.27×10^{-4}	4.5×10^{-4}	0.95
$Sh = 2 + 0.347(Re^{0.62} Sc^{0.31}) + 0.5(\overline{Gr} \cdot Sc)^{0.25}$	4.13×10^{-4}	4.5×10^{-4}	0.92
$Sh = 2 + 0.52 (Re^{0.62} Sc^{0.31}) + 0.5(\overline{Gr} \cdot Sc)^{0.25}^*$	5.23×10^{-4}	4.5×10^{-4}	1.16
$Sh = 0.8(Re^{\frac{1}{2}} Sc^{\frac{1}{3}}) + 0.78(\overline{Gr} \cdot Sc)^{0.25}$	4.61×10^{-4}	4.5×10^{-4}	1.02

*Modified Steinberger and Treybal by Distin et al. (12)

Generally when such correlations are used to determine the mass or heat transfer coefficients, then the expected accuracy would be to about $\pm 20\%$. It appears from Table 4.9 that when the value of \overline{Gr}/Re^2 is greater than 7 the contribution due to forced convection is very little, and linear addition of the natural and forced convection terms increases the range over which the correlations hold. Although it is rather speculative to make such a judgement on one set of data, this conclusion is consistent with those of El-Kaddah. (35)

Comparison of the calculated and measured rates, which are summarized in Tables 4.10-4.12, indicate that for low values of \overline{Gr}/Re^2 ($\overline{Gr}/Re^2 < 1.3$) only the modified correlation of Steinberger and Treybal, by Distin et al. (12) gives agreements of within 20% and all other available correlations for mass transfer by forced convection give rates which are lower than the measured ones by a factor of about 35%. It is interesting to note that in the past most workers have ignored the contribution from the flame temperature arising from combustion of carbon monoxide in the aerodynamic boundary layer, and have obtained good agreements between the calculated rates and measured ones when contribution due to natural convection was arithmetically added to that of forced convection and the radial molecular diffusion. It can be seen that when the contribution due to natural convection is added to that of forced convection then the calculated rates become in

excellent agreement with the measured rates. Although such line of thoughts would lead to the conclusions that under the conditions where significant temperature and concentration gradients are present in the gas phase, there would be a significant contribution to the overall mass transfer by natural convection in comparison with that from radial molecular diffusion and forced convection, but the complications arising from the combustion of carbon monoxide causes the uncertainty of the concluded remarks, which is in disagreement with the suggestions to the contrary. (35)

4-8. CONCLUSION

The measured rates of decarburization of Fe-C alloys, under the conditions of the investigation were controlled by mass transfer in the gas phase. These rates were found to be in excellent agreement with those predicted by the correlations developed by Steinberger and Treybal, El-Kaddah, and Mather et al. under the conditions where the mass transfer was governed either by natural convection or by a combination of forced and natural convection in the gas phase.

The effect of 0.1 wt.% phosphorus on the rates of decarburization and vaporization of iron has been studied, and it has been found that phosphorus acts as a surface active element in iron-carbon alloys.

Homogenous nucleation of CO bubbles in levitated drops of Fe-C and Fe-C-P alloys has been observed before and after the carbon boil.

Finally the presence of silicon, at concentration of 0.015 wt.%, in an Fe-C alloy has a pronounced effect on the retardation of the rate of decarburization, and promotion of the carbon-boil.

CHAPTER 5

CHAPTER 5

ENHANCED VAPORIZATION OF LIQUID IRON-PHOSPHORUS ALLOYS IN STREAMS OF OXIDISING OR REDUCING GAS MIXTURES

5-1. INTRODUCTION

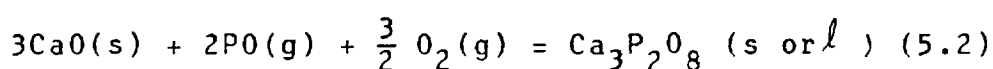
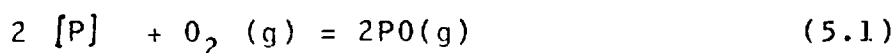
The removal of phosphorus from liquid iron by oxidation is one of the important reactions in steelmaking processes. The mechanism involved in removal of phosphorus from iron under the conditions of basic oxygen steelmaking is far from being clearly understood. The present work was undertaken to investigate a possible mechanism involving the formation of volatile species of phosphorus compounds.

This chapter describes the work carried out on studying the enhanced vaporization from levitated drops of iron-phosphorus alloys in various streams of gas mixtures. The influence of evolution of carbon monoxide, from the surface of the melt by decarburization, on the rate of removal of phosphorus from the melt has also been investigated and is described below.

5-2. PREVIOUS WORK

On a theoretical and experimental basis it has been shown by Turkdogan et al. (51-53) that the rate of vaporization of metals in a stagnant or a stream of neutral gas increases as the result of condensation of the vapour phase close to the surface of the molten metal.

Furthermore they have shown that the vaporization rate is enhanced on increasing the partial pressure of a reacting gas, such as oxygen. On considering the vaporization of a metal in a stream of oxygen bearing gas, the enhanced vaporization is basically a vaporization-oxidation process involving the counter diffusion of oxygen (or oxidising species) and metal vapours in the gaseous boundary layer. These interact to form a metal oxide mist in the gas close to the metal-gas interface. As the partial pressure of oxygen in the gas stream is increased, the thickness of the boundary layer of the metal vapour decreases, resulting in an increased rate of vaporization. This theory explained the formation and evolution of iron oxide fumes under steelmaking conditions,⁽⁵⁴⁾ but it was suggested by Turkdogan⁽⁵⁵⁾ that it may also play a major role in accounting for the reaction mechanism in the removal of manganese, phosphorus and silicon from iron under conditions of basic oxygen steelmaking as in the Q-BOP process. On considering dephosphorization of iron the work of Kor and Turkdogan⁽⁵⁶⁾ suggested that the phosphorus may be removed by the oxidation of phosphorus vapour to form volatile oxide species and that the rate of the reaction will be enhanced by a reaction of the vapour-phase with lime, such as:



These authors claimed that this hypothesis was experimentally verified by blowing a mixture of argon/oxygen on to the surface of a melt containing phosphorus at 1600°C , when some phosphorus loss from the metal to the magnesia crucible was observed.

5-3. FREE ENERGIES OF FORMATION OF VOLATILE PHOSPHORUS COMPOUNDS

In order to estimate the relative importance of the various gaseous compounds, which may be produced during the oxidation or reduction of phosphorus dissolved in iron, values of free energies of formation of four oxides and two hydrides of phosphorus, in the temperature range of interest in steelmaking were calculated, using the standard free energies of formation of the compounds, derived from spectroscopic data⁽⁵⁷⁾ and standard free energy of solution of phosphorus in liquid iron.⁽⁵⁸⁾ These values were plotted as an Ellingham diagram as shown in Fig. 5.1, for which the standard states are 0.1 wt% phosphorus in iron and 1 bar pressure for all gases.

It can be seen that all lines representing these reactions have positive slopes, i.e. negative entropies of formation. The lines representing the free energies of formation of PH_2 , PH_3 , and PO show positive free energies of formation in the temperature range considered and are endothermic processes, whereas the other possible

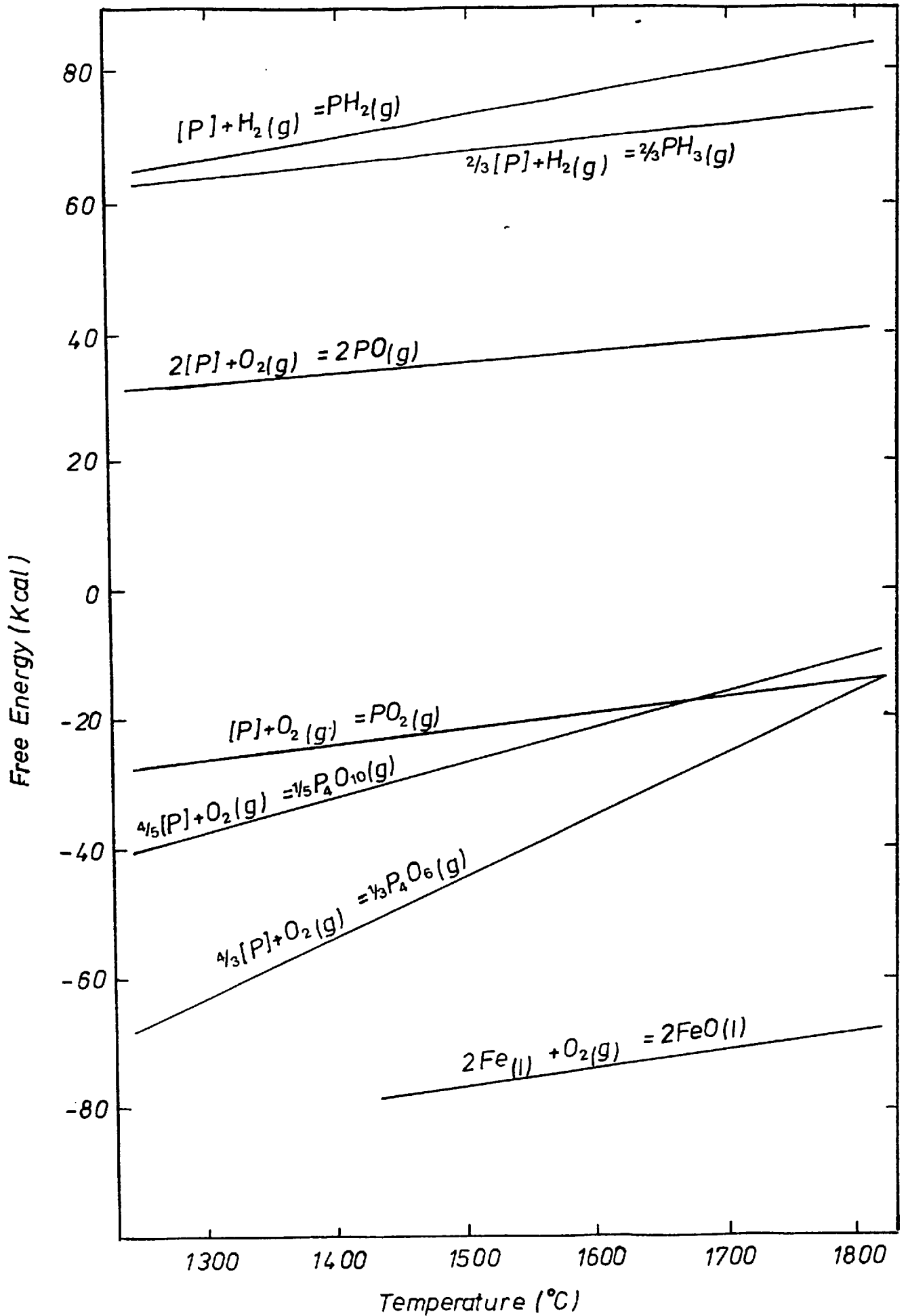


Figure 5.1 Ellingham diagram for volatile phosphorus compounds.

phosphorus eliminating reactions are exothermic. The degree of stability of the oxides are in the order $P_4O_6 > P_4O_{10} > PO_2 > PO$ up to the temperature of about $1670^{\circ}C$, and above $1830^{\circ}C$ the dioxide tends to become the most stable.

From the data obtained one may presume that the formation of volatile species may be possible during the dephosphorization reactions provided the energy requirements for the formation of the endothermic compounds are provided through other linked reactions.

5-4 EXPERIMENTAL

Alloys of Fe-P containing 2.0 to 0.1 wt% phosphorus, and Fe-C-P containing 3.7% and 0.7% C with 0.1 wt% phosphorus were prepared by the method previously described. Samples weighing about 1 gram were cut from the alloys and levitated and melted in a stream of

Helium and/or Argon. The samples were exposed for different periods to streams of oxidising or reducing gas mixtures of, O_2 , He- O_2 , CO_2 , CO- CO_2 , N_2 - H_2 - CO_2 or, N_2 - H_2 . The samples were finally quenched and analysed for phosphorus or carbon. The results obtained are tabulated in Tables 5.2-5.15, and Figures 5.2-5.15 respectively.

TABLE 5.2. Vaporization of iron-phosphorus alloy in a stream of He-O₂ at 1600°C.

Alloy: Fe-0.12% [P]

Reaction gas: He-O₂. Flow Rate: 5 l.min⁻¹ PO₂~3x10⁻⁴ Atm.

Run	Initial mass of (gram)	Initial temp. (°C) ± 15	Reaction period (min)	Final temp (°C) ±15	Final mass of (gram)	Wt.% [P] (±0.005%)
PR01	1.1535	1600	1	1600	1.499	.130%
PR02	1.1379	1600	2	1600	1.1344	.124%
PR03	1.1488	1600	4	1600	1.1448	.129%
PR04	1.1533	1600	6	1600	1.1483	.119%
PR05	1.1734	1600	8	1600	1.1680	.136%
PR06	1.1620	1600	10	1610	1.1556	.119%
PR07	1.1637	1600	12	1610	1.1563	.121%

Notes:

1. Samples were deoxidized initially by hydrogen.
2. Fumes of iron oxide were evolved and condensed in the silica tube of the levitation cell.

TABLE 5.3 Vaporization of iron-phosphorus in a stream
of He-O₂ at 1600°C

Alloy: Fe-2.0%[P]

Reacting gas: He-O₂ : total flow rate: 5 l.min⁻¹

P_O₂ = 3 × 10⁻⁴ Atm.

Run	Initial mass of sample (gram)	Initial temp. (°C)	Reaction period (min)	Final temp. (°C)	Final mass of sample (gram)	Wt.% [P] ±0.07%
PR08	1.1055	1600	1	1600	1.1027	1.98%
PR09	1.0932	1605	2	1605	1.0902	2.05%
PR10	1.1132	1605	4	1610	1.1105	2.00%
PR11	1.0926	1600	6	1600	1.0880	1.89%
PR12	1.1787	1600	8	1600	1.1723	1.93%
PR13	1.0819	1600	10	1600	1.0763	1.93%

Notes

1. Samples were deoxidised initially by hydrogen.
2. During the vaporization, whitish fumes which were evolved were condensed on the silica tube as brownish black deposits.

TABLE 5.4. Vaporization of iron-phosphorus alloy in a stream of CO/CO₂ at 1800°C.

Alloy: Fe-0.1 wt% [P]

Reaction Gas: CO/CO₂ with 10 ppm of CO₂*

Flow rate: 810 ml.min⁻¹

Run	Initial mass of sample (gram)	Initial temp. (°C)	Reaction period (secs)	Final temp. (°C)	Final mass of sample (gram)	Wt% [P] ±0.006%
PR14	0.9964	1550	20	1800+	0.9948	.105%
PR15	1.0359	1550	20	1800+	1.0338	.101%
PR16	1.1003	1550	20	1800+	1.1020	.090%
PR17	0.9520	1550	20	1800+	0.9515	.109%
PR18	1.0934	1550	20	1800+	1.0604	.097%
PR19	0.9543	1550	40	1800+	0.9528	.105%
PR20	0.9489	1550	40	1800+	0.9401	.112%
PR21	1.0984	1550	40	1800+	1.0942	.090%
PR22	1.0356	1550	40	1800+	1.0311	.103%
PR23	1.1116	1550	40	1800+	1.0249	.091%
PR24	1.0955	1550	60	1800+	1.0911	.095%
PR25	1.0827	1550	60	1800+	1.0755	.097%
PR26	1.0083	1550	60	1800+	1.0030	.107%
PR27	1.0777	1550	80	1800+	1.0690	.098%
PR28	1.1152	1550	80	1800+	1.1055	.098%
PR29	1.1049	1550	80	1800+	1.0937	.094%

Notes:

1. Soon after reaching temperatures above 1600°C white fumes were evolved from the surface of the drops.
2. Samples were carbonized as the result of the reaction:

$$2CO(g) = [c] + CO_2(g)$$

* $P_{O_2} \sim 2.3 \times 10^{-16}$ atm. at 1725°C

TABLE 5.5 Vaporization of iron-phosphorus alloy in a stream of CO/CO₂ at 1800°C.

Alloy: Fe-0.1 Wt%[P]

Reacting gas: CO/CO₂ $Q_{CO} = 760 \text{ ml, min}^{-1}$ $P_{CO} = 0.94 \text{ atm.}$

$Q_{CO_2} = 50 \text{ ml, min}^{-1}$ $P_{CO_2} = 0.06 \text{ atm.}$

$P_{CO}/P_{CO_2} = 15.7 *$

Run	Initial mass of sample (gram)	Initial temp. (°C)	Reaction period (secs)	Final temp. (°C)	Final mass of sample (gram)	Wt.% [P] ±0.006%
PR30	1.0387	1550	20	1800+	1.0364	0.10%
PR31	1.0896	1550	20	1800+	1.0878	0.10%
PR32	0.9710	1550	20	1800+	0.9703	0.09%
PR33	1.0414	1550	40	1800+	1.0379	0.11%
PR34	1.1247	1550	40	1800+	1.1202	0.11%
PR35	0.9872	1550	40	1800+	0.9841	0.10%
PR36	1.0663	1550	60	1800+	1.0609	0.11%
PR37	1.0529	1550	60	1800+	1.0471	0.11%
PR38	0.9321	1550	60	1800+	0.9278	0.09%
PR39	1.0148	1550	80	1800+	1.0080	0.11%
PR40	1.1208	1500	80	1800+	1.1117	0.11%
PR41	0.9916	1550	80	1800+	0.9903	0.10%

Notes.

1. Soon after reaching 1600°C, whitish fumes were evolved from the surface of the levitated drop, which condensed on the silica tube as brownish black deposits.
2. Samples were slightly carbonized as the result of the reaction $2CO (g) = C + CO_2 (g)$
3. Linear rate of vaporization = $8.6 \times 10^{-5} \text{ g/s.}$

* $P_{O_2} \sim 9.2 \times 10^{-9} \text{ atm. at } 1725^\circ\text{C}$

TABLE 5.6. Vaporization of iron-phosphorus alloy in a stream of $N_2/H_2/CO_2$ at $1800^\circ C$

Alloy: Fe - 0.1 wt.% [P]

Reacting gas: $N_2/H_2/CO_2$

$$Q_{N_2} = 5250 \text{ ml. min}^{-1} \quad P_{N_2} = .705 \text{ Atm.}$$

$$Q_{H_2} = 1750 \text{ ml. min}^{-1} \quad P_{H_2} = .235 \text{ Atm.}$$

$$Q_{CO_2} = 450 \text{ ml. min}^{-1} \quad P_{CO_2} = .060 \text{ Atm.}$$

$$P_{H_2}/P_{CO_2} = 3.92 (\equiv P_{O_2} = 5 \times 10^{-9} \text{ Atm.})$$

Run	Initial mass of sample (gram)	Initial temp. ($^\circ C$)	Reaction period (Secs)	Final temp. ($^\circ C$)	Final mass of sample (gram)	Wt% [P] $\pm 0.006\%$
PR42	1.0112	1600	30	1650	1.0105	.101%
PR43	1.0567	1600	30	1650	1.0560	.105%
PR44	1.0091	1600	30	1650	1.0080	.097%
PR45	1.1001	1600	60	1705	1.0988	.101%
PR46	1.0971	1600	60	1705	1.0952	.095%
PR47	1.0960	1600	60	1705	1.0951	.103%
PR48	1.0632	1600	90	1750	1.0612	.095%
PR49	1.0431	1600	90	1750	1.0416	.102%
PR50	1.0531	1600	120	1800	1.0491	.105%
PR51	1.0771	1600	120	1800	1.0730	.101%
PR52	1.0911	1600	200	1800+	1.0816	.092%
PR53	1.1211	1600	200	1800+	1.1142	.098%

Notes:

1. Soon after reaching temperature above $1600^\circ C$ fumes were evolved from the surface of the levitated drop and condensed on the silica tube.
2. Samples were slightly carbonized.

TABLE 5.7. Vaporization of iron-phosphorus alloy in a stream of forming gas

Alloy: Fe - 0.1% [P]

Gas: Forming gas (N_2 -25% H_2) total flow rate = 7 l.min⁻¹

Run	Initial mass of sample (gram)	Initial temp. (°C)	Reaction period (secs)	Final temp. (°C)	Final mass of sample (Gram)	Wt.% [P] ±0.005%
PR54	1.0071	1610	30	1630	1.0076	0.097%
PR55	1.0131	1610	30	1635	1.0123	0.093%
PR56	1.1031	1600	60	1690	1.1015	0.101%
PR57	1.0567	1610	60	1695	1.0551	0.097%
PR58	1.0421	1600	90	1750	1.0401	0.095%
PR59	1.0235	1600	90	1750	1.0214	0.097%
PR60	1.0300	1600	120	1800	1.0273	0.098%
PR61	1.0613	1600	120	1810	1.0582	0.099%

Notes: Vapours of iron evolved from the surface of the levitated drops were condensed on the silica tube.

TABLE 5.9 Oxidation of iron-carbon-phosphorus alloy in
a stream of CO₂

Alloy: Fe 3.5%[C] - 0.097%[P]

Reacting gas: Carbon dioxide $P_{CO_2} = 1 \text{ Atm.}$ $Q_{CO_2} = 1 \text{ l. min}^{-1}$

Run	Initial mass of sample (gram)	Initial temp. (°C)	Reaction period (secs)	Final temp. (°C)	Final mass of sample (gram)	Wt.% [P] ± 0.006%
PR62	0.7427	1600	5	1620	0.7092	0.097%
PR63	0.7500	1600	5	1640	0.7386	0.095%
PR64	0.7504	1600	5	1630	0.7403	0.097%
PR65	0.7443	1600	10	1645	0.7258	0.094%
PR66	0.7400	1600	10	1660	0.7234	0.104%
PR67	0.7415	1600	10	1660	0.7262	0.095%
PR68	0.7473	1600	15	1700	0.7210	0.107%
PR69	0.7545	1600	15	1700	0.7289	0.101%
PR70	0.7572	1600	15	1720	0.7288	0.104%
PR71	0.7121	1600	20	1700	0.6620	0.098%
PR72	0.7140	1600	20	1710	0.6417	0.095%
PR73	0.7187	1600	20	1690	0.6770	0.091%
PR74	0.7109	1600	20	1730	0.6664	0.106%

Notes:

1. Carbon boil commenced after about 13 seconds of oxidation.
2. White fumes were evolved from the surface of drop, which condensed on the silica tube as brownish-black deposits of iron oxide.

TABLE 5.9. Oxidation of iron-carbon-phosphorus in a stream of carbon dioxide

Alloy: Fe-3.5% [C]-0.097% [P]

Reaction gas: carbon dioxide, $P_{CO_2} = 1 \text{ Atm.}$ $Q_{CO_2} = 750 \text{ ml. min}^{-1}$

Run	Initial mass of sample (gram)	Initial temp. ($^{\circ}\text{C}$)	Reaction period. (Secs)	Final temp. ($^{\circ}\text{C}$)	Final mass of sample (gram)	Wt.% [C]
PR75	0.6498	1600	5	1650	0.5081	2.63%
PR76	0.6570	1600	5	1650	0.6453	2.24%
PR77	0.6655	1600	7	1660	0.6579	2.05%
PR78	0.6415	1600	7	1660	0.6314	1.86%
PR79	0.6570	1600	7	1660	0.6468	2.25%
PR80	0.6453	1600	10	1675	0.6195	1.45%
PR81	0.6501	1600	10	1675	0.6176	1.65%
PR82	0.6477	1600	15	1690	0.6181	0.74%
PR83	0.6589	1600	15	1690	0.6370	0.77%
PR84	0.6484	1600	15	1690	0.6149	0.75%
PR85	0.6487	1600	20	1730	0.5837	0.63%
PR86	0.6610	1600	20	1730	0.4625	0.313%
PR87	0.6489	1600	20	1720	0.5422	0.430%

Notes:

1. Carbon boil commenced about 17 seconds after the oxidation had begun.
2. Vaporization of iron continued to take place during the oxidation period.

TABLE 5.10 Oxidation of iron-carbon-phosphorus alloy in
a stream of carbon dioxide.

Alloy: Fe - 0.67%[C] - 0.10%[P]

Reacting gas: Carbon dioxide $P_{CO_2} = 1 \text{ Atm.}$ Flow rate: 750ml.min

Run	Initial mass of samples (gram)	Initial temp. ($^{\circ}\text{C}$)	Reaction period (Secs)	Final temp. ($^{\circ}\text{C}$)	Final mass of samples (gram)	Wt.% [P]
PR88	0.9694	1600	2	1680	0.9596	0.11%
PR89	0.9205	1600	2	1680	0.8615	0.10%
PR90	0.9500	1600	4	1700	0.9188	0.10%
PR91	0.9451	1600	4	1700	0.8435	0.09%
PR92	0.9617	1600	6	1730	0.7392	0.10%
PR93	0.9609	1600	6	1730	0.9315	0.11%
PR94	0.9760	1600	8	1690	0.8800	0.10%
PR95	0.9814	1600	8	1730	0.8237	0.09%

Notes:

1. Carbon boil began after 6 seconds.
2. Enhanced vaporization of iron was observed.

TABLE 5.11 Oxidation of iron-carbon-phosphorus in a stream of carbon dioxide.

Alloy: Fe - 0.67%C - 0.10%P.

Reacting gas: Carbon dioxide, $P_{CO_2} = 1 \text{ Atm}$. Flow rate: 750 ml. min^{-1}

Run	Initial mass of sample (gram)	Initial temp. ($^{\circ}\text{C}$)	Reaction period (secs)	Final temp. ($^{\circ}\text{C}$)	Final mass of sample (gram)	Wt.% [C]
PR96	0.9564	1600	2	1680	0.9536	0.67%
PR97	0.9566	1600	2	1680	0.9513	0.62%
PR98	0.9596	1600	4	1700	0.9528	0.55%
PR99	0.9538	1600	4	1700	0.9486	0.54%
PR100	0.9214	1600	6	1730	0.8219	0.48%
PR101	0.9558	1600	6	1730	0.6908	0.44%
PR102	0.9810	1600	8	1740	0.9264	0.46%
PR103	0.9770	1600	8	1740	0.9085	0.38%
PR104	1.0909	1600	8	1700	0.9226	0.44%

Notes:

1. Carbon boil commenced after 6 seconds.
2. Vaporization of iron was observed during the oxidation.

TABLE 5.12 Oxidation and vaporization of iron-phosphorus alloy in a stream of He - 5% O₂.

Alloy: Fe - 0.1 Wt% [P].

Reacting gas: He - 5% O₂:-

Helium Flow rate = 4750 ml.min⁻¹

Oxygen Flow rate = 250 ml.min⁻¹ (P_{O₂} = 5x10⁻² Atm)

Run	Initial mass of sample (gram)	Initial temp. (°C)	Reaction period (secs)	Final temp. (°C)	Final mass+ slag (gram)	Wt.% [P] ±0.006%
PR105	1.3705	1600	5	1690	1.3505	0.125%
PR106	1.3315	1600	10	1710	1.3479	0.125%
PR107	1.3297	1600	15	1725	1.3507	0.130%
PR108	1.3386	1600	20	1760	1.3527	0.136%
PR109	1.3589	1600	25	1800	1.3761	0.141%

Notes:

Although as soon as oxidation was started formation of liquid iron oxide took place, but the liquid phase did not cover the upper portion of the levitated drop and hence iron oxide vapours were evolved and condensed on the silica wall by enhanced vaporization from the base metal surface.

TABLE 5.13 Oxidation and vaporization of iron-phosphorus alloy in a stream of CO_2

Alloy: Fe - 0.52 Wt%[P].

Reaction gas: CO_2 , $P_{\text{CO}_2} = 1 \text{ Atm.}$ $Q_{\text{CO}_2} = 750 \text{ ml. min}^{-1}$

Run	Initial mass of sample (gram)	Initial temp. ($^{\circ}\text{C}$)	Reaction period (secs)	Final temp. ($^{\circ}\text{C}$)	Wt.% [P]
PR110	0.7207	1650	10	1800	0.552%
PR111	0.7037	1650	20	1800	0.637%
PR112	0.7290	1650	30	1800+	0.668%
PR113	0.7425	1650	30	1800+	0.692%

Notes:

On oxidation formation of a liquid iron oxide phase took place, but this liquid phase depended from the bottom of the drop. Vaporization of iron and condensation of iron oxide fumes were observed during the oxidation period.

TABLE 5.14 Oxidation and vaporization of iron-phosphorus alloy in a stream of He-O₂

Alloy: Fe - 0.12%[P]

Reacting gas: He - O₂ P_{O₂} = 5x10⁻¹ Atm. Q_{He} = 1 l.min⁻¹
Q_{O₂} = 1 l.min⁻¹

Run	Initial mass of samples (gram)	Initial temp. (°C)	Reaction period (secs)	Final temp. (°C)	Wt.% [P] ± 0.006%
PR114	0.9472	1550	1	1800	0.128%
PR115	0.8971	1550	2	1800+	0.133%
PR116	0.8851	1550	3	1800+	0.155%
PR117	0.8203	1550	4	1800+	0.154%

Notes:

On oxidation formation of a liquid iron oxide phase took place, but this liquid phase depended from the bottom of the drop. Vaporization of iron and condensation of iron oxide fumes were observed during the oxidation period.

TABLE 5.15 Oxidation and vaporization of iron-phosphorus alloy in a stream of oxygen.

Alloy: Fe - 0.12% [P].

Reaction gas: oxygen $P_{O_2} = 1 \text{ Atm}$. Flow rate: 3.5 l.min^{-1}

Run	Initial mass of samples (gram)	Initial temp. ($^{\circ}\text{C}$)	Reaction period (secs)	Final temp. ($^{\circ}\text{C}$)	Final of mass (gram)	Wt% [P]
PR118	0.9614	1600	2	1690	1.0103	0.147%
PR119	0.9860	1600	3	1800+	1.0160	0.156%
PR120	1.0396	1600	4	1800+	1.0752	0.173%
PR121	0.9580	1600	5	1800+	0.9992	0.182%

Notes:

On oxidation formation of a liquid iron oxide phase took place, but this liquid phase depended from the bottom of the drop. Vaporization of iron and condensation of iron oxide fumes were observed during the oxidation period.

5-6 DISCUSSION

On assuming that at the reaction front, in the gaseous/vapour boundary layer, at a distance " δ " away from the surface of the melt, all the available oxidising species are being consumed by the iron and phosphorus vapours. Then, the concentration profiles for the species involved may be represented by those in Figure 5.16.

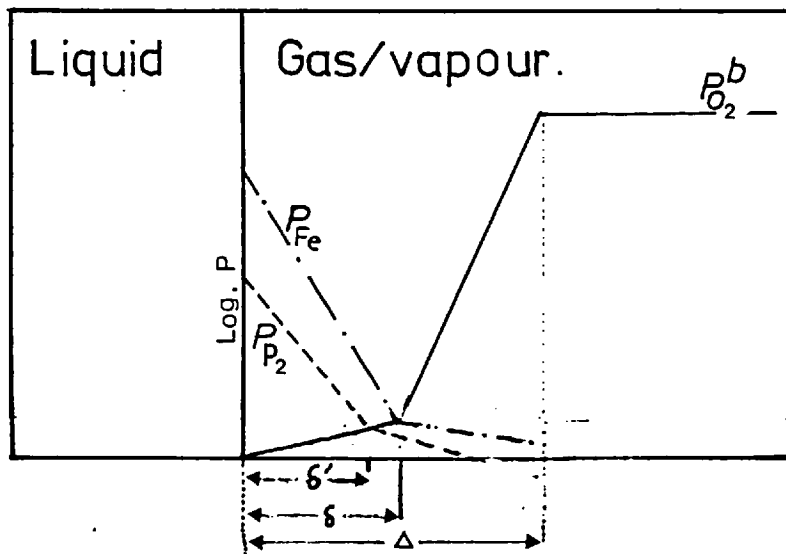


FIGURE 5.16. Schematic representation of the concentration profile in the gaseous boundary layer.

Under the above conditions, by Fick's law the counter flux of iron and phosphorus vapours and oxygen for a steady state is given by:

$$J_{Fe} = \frac{D_{Fe}}{RT_f} \times \frac{(\bar{p}_{Fe} - p'_{Fe})}{\delta} \quad (5.3)$$

$$J_{P_2} = \frac{D_{P_2}}{RT_f} \times \frac{(p_{P_2} - p'_{P_2})}{\delta'} \quad (5.4)$$

$$J_{O_2} = \frac{D_{O_2}}{RT_f} \times \frac{(p_{O_2} - p'_{O_2})}{(\Delta - \delta)} \quad (5.5)$$

where D_{Fe} = interdiffusivity of iron vapour and surrounding gas

D_{P_2} = interdiffusivity of phosphorus vapours and surrounding gas

D_{O_2} = interdiffusivity of oxygen and inert gas

p_{Fe} = vapour pressure of iron at the surface of the melt

p'_{Fe} = vapour pressure of iron at the reaction front

p_{P_2} = vapour pressure of phosphorus at the surface of the melt

p'_{P_2} = vapour pressure of phosphorus at the reaction front

p_{O_2} = partial pressure of oxygen in the bulk gas

p'_{O_2} = partial pressure of oxygen at the reaction front

R = gas constant, ($\text{cm}^3 \cdot \text{atm} \cdot \text{°K}^{-1}, \text{mol}^{-1}$)

T_f = film temperature, (°K) = $\frac{1}{2} (T_s + T_b)$

Since $p_{Fe} \gg p'_{Fe}$, $p_{P_2} \gg p'_{P_2}$, $p_{O_2} \gg p'_{O_2}$ and $\Delta \gg \delta$ then the above equations can be simplified to:

$$J_{Fe} = \frac{D_{Fe}}{\delta} \cdot \frac{p_{Fe}}{RT_f} \quad (5.6)$$

$$J_{P_2} = \frac{D_{P_2}}{\delta'} \cdot \frac{p_{P_2}}{RT_f} \quad (5.7)$$

and $J_{O_2} = \frac{D_{O_2}}{\Delta} \cdot \frac{p_{O_2}}{RT_f} \quad (5.8)$

It follows that in order to achieve dephosphorization the flux of phosphorus vapour must be increased. According to the theory of enhanced vaporization, the rate of vaporization from the surface of the melt may be enhanced when an oxygen-bearing gas is blown on the surface of the melt, but the question arises that to what extent could such a mechanism influence the rates of vaporization of iron and phosphorus vapours, and whether or not the rates are increased in proportion. Since the vaporization rates are functions of their vapour pressures and gaseous mass transfer coefficients $\frac{D_{Fe}}{\delta}$, $\frac{D_{P_2}}{\delta'}$, at a constant temperature.

$$\text{i.e. } \frac{J_{P_2}}{J_{Fe}} = \frac{D_{P_2}}{\delta'} \times \frac{\delta}{D_{Fe}} \frac{P_{P_2}}{P_{Fe}} \quad (5.9)$$

Since the vapour pressure of phosphorus at the surface of a melt containing 0.1 wt.% or 2.0 wt.% phosphorus is less than the vapour pressure of iron at the same temperature by several orders of magnitude (58-60), and the ratio of the diffusivities of phosphorus and iron vapours is inversely proportional to the square root of their molecular weights,

$$\text{i.e. } \frac{D_{P_2}}{D_{Fe}} \sim \sqrt{(M_{Fe}/M_{P_2})} \quad (5.10)$$

$$\text{hence } \frac{J_{P_2}}{J_{Fe}} = \frac{\delta}{\delta'} \times \text{constant} \quad (5.11)$$

hence it is reasonable to expect that any enhancement on the rates of vaporization of iron and phosphorus brought about by an oxygen-bearing gas stream, which is reactive with both species, would not cause dephosphorization of the melt, since the effective diffusional distances (δ , δ') are reduced proportionally, and hence $\frac{\delta}{\delta'}$ stays virtually constant.

Our calculations on the mass transfer coefficient in the gaseous diffusion boundary layer, and hence evaluation of the critical conditions for enhancement of vaporization rates, have set the maximum oxygen potential of the gas stream, passing a 1 gram levitated drop, at 1600°C, to be about 1.3×10^{-2} atm. of oxygen (see Appendix 2). The experimental results obtained on vaporization of iron-phosphorus alloys, containing 0.1 wt.% or 2 wt.% phosphorus under these conditions are given in Tables 5.2 and 5.3, and summarized in Figures 5.2 and 5.3 respectively. As can be seen, when using a gas mixture of helium-oxygen with a corresponding oxygen partial pressure of about 3×10^{-4} atm. enhanced vaporization is brought about by the mechanism discussed above, but the phosphorus concentration of the samples stay virtually constant. Furthermore, in experiments where CO/CO₂ gas mixtures were used, which had a corresponding oxygen partial pressures of about 1.8×10^{-26} atm. and 1.6×10^{-19} atm. at 910°C (film temperature) considerable fumes of iron were evolved from the surface of the levitated drops. However the phosphorus concentration

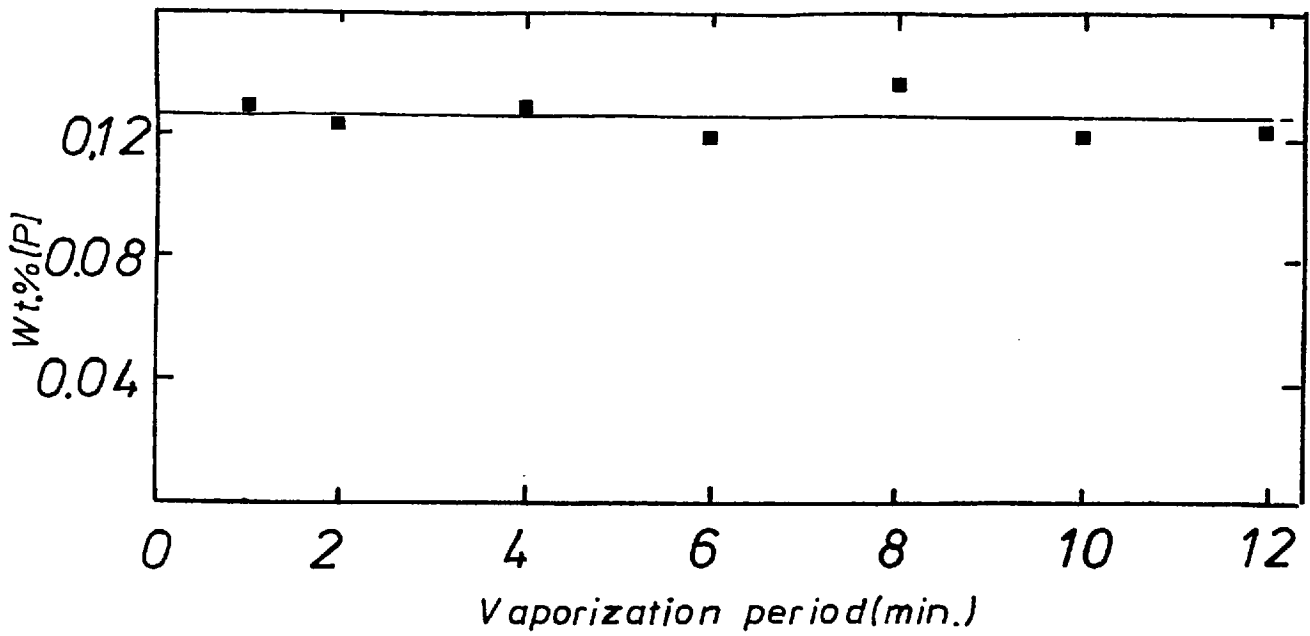


Figure 5.2 Vaporization of Fe-P in a stream of He-O₂
($P_{O_2} \sim 3 \times 10^{-4}$ atm.)

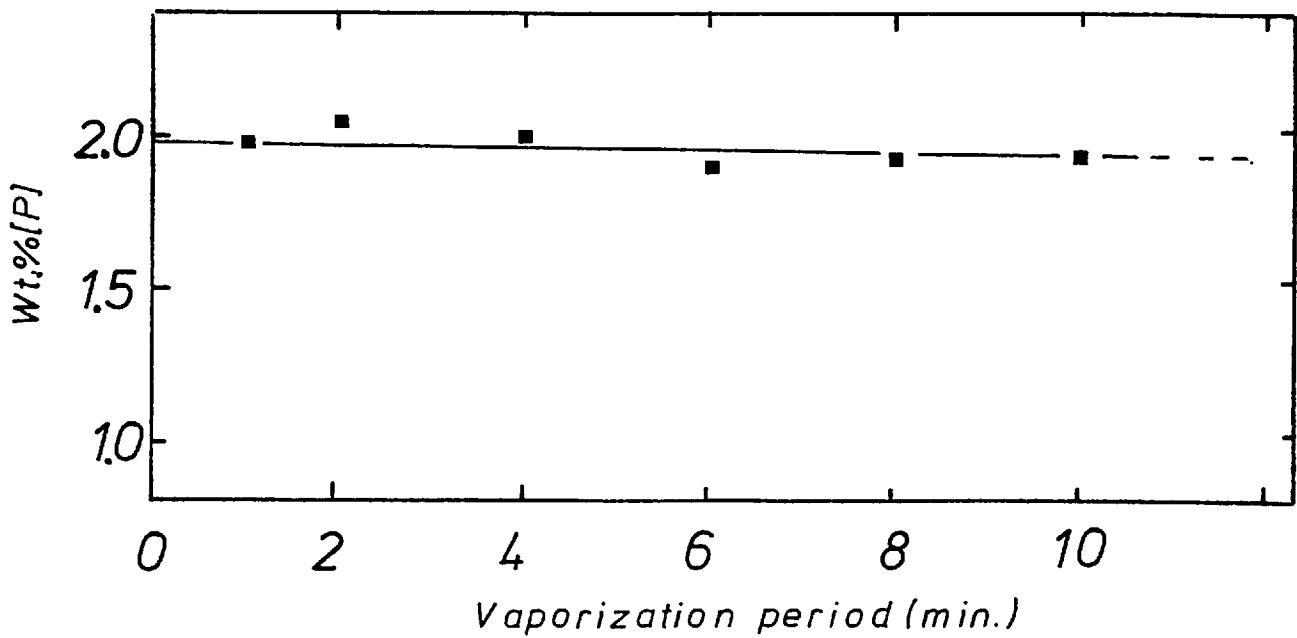


Figure 5.3 Vaporization of Fe-P in a stream of He-O₂
($P_{O_2} \sim 3 \times 10^{-4}$ atm.)

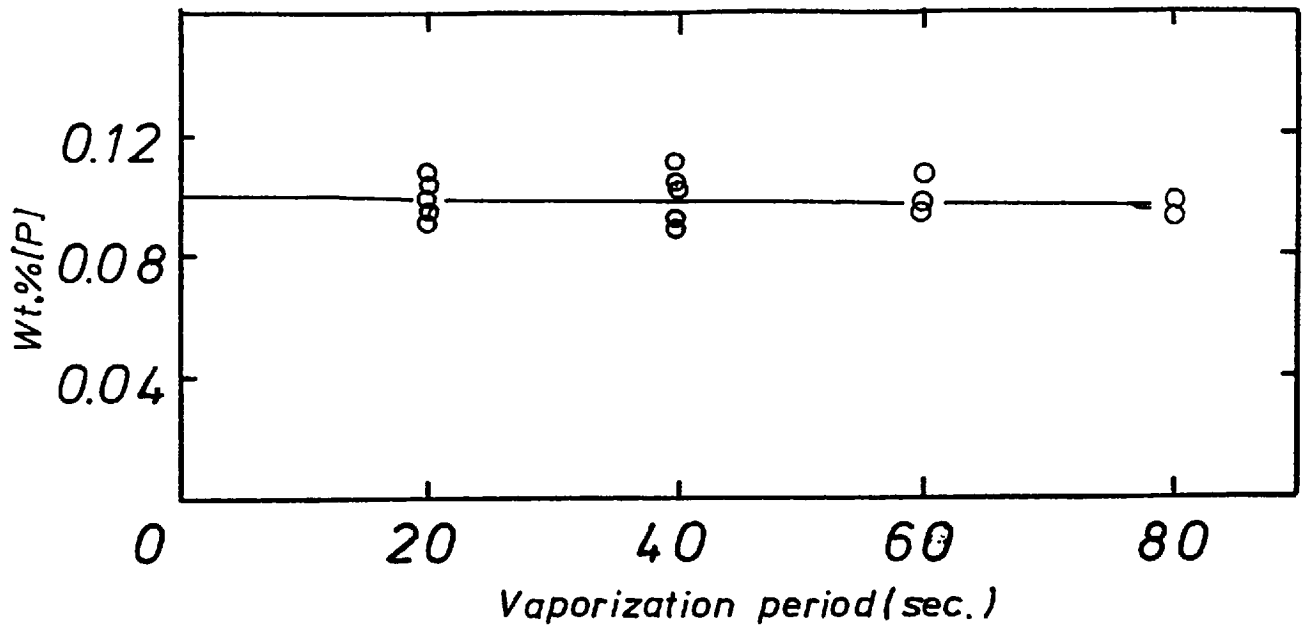


Figure 5.4 Vaporization of Fe-P in a stream of CO/CO₂
 ($P_{O_2} \sim 2.3 \times 10^{-16}$ atm. at 1725 °C)
 ($P_{O_2} \sim 1.8 \times 10^{-26}$ atm. at 910 °C)

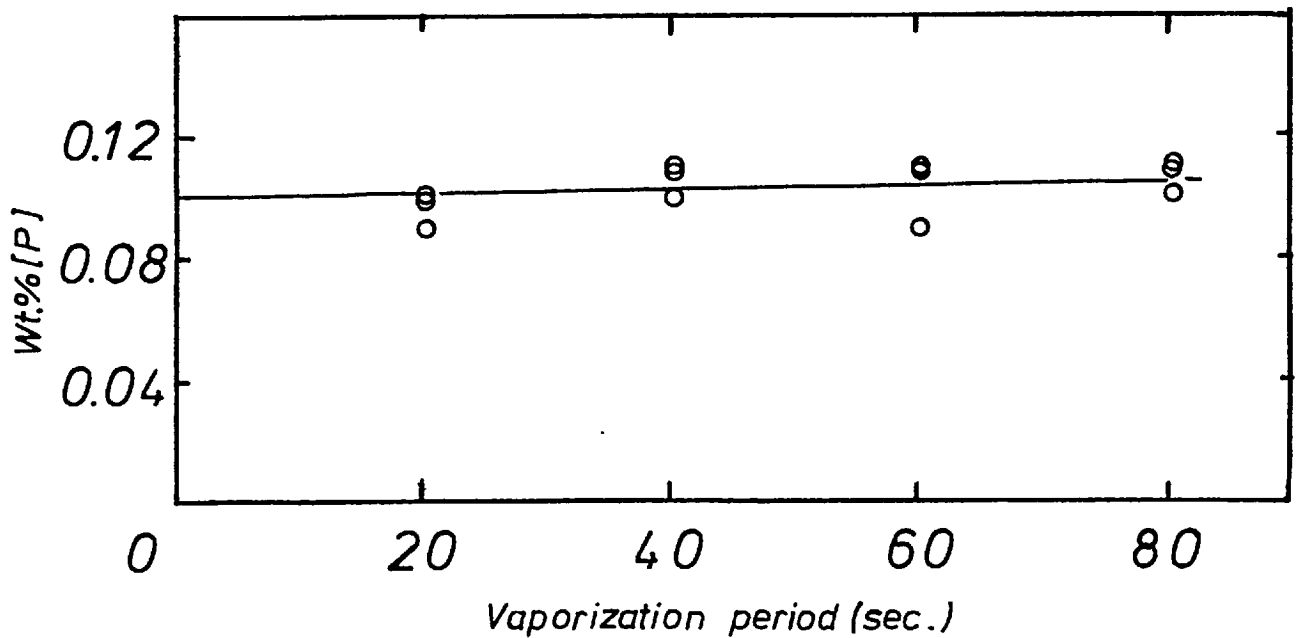
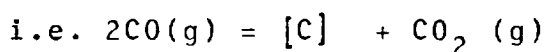


Figure 5.5 Vaporization of Fe-P in a stream of CO/CO₂
 ($P_{O_2} \sim 9.2 \times 10^{-9}$ atm. at 1725 °C)
 ($P_{O_2} \sim 7.6 \times 10^{-19}$ atm. at 910 °C)

of the samples stay virtually constant once again, (see Tables 5.4 and 5.5 and Figures 5.4 and 5.5 respectively). At the lower oxygen potential in the gas stream, apparently there is a slight decrease in the phosphorus concentration in the metal. This most probably is due to the dilution of the melt, as the result of the carburization of the melt at such elevated temperatures of the samples ($\sim 1800^{\circ}\text{C}$);



Thus these observations are consistent with the above predictions, and hence it may be concluded that any increase in the oxygen partial pressure of the gas stream would not lead to an increase in the gaseous mass transfer coefficient of the phosphorus vapours $\frac{D_{\text{P}_2}}{\delta'}$ compared to that of iron vapours $\frac{D_{\text{Fe}}}{\delta}$.

It follows from the foregoing discussion, that dephosphorization may be achieved by a vapour phase reaction, provided the gaseous mass transfer coefficient for phosphorus is greater than that of iron vapours, i.e.

$$\frac{D_{\text{P}_2}}{\delta'} > \frac{D_{\text{Fe}}}{\delta}$$

$$\text{or, } K_{\text{P}_2} > K_{\text{Fe}}$$

from equations 5.6 and 5.7

$$K_{P_2} = \frac{J_{P_2} \times RT_f}{p_{P_2}}$$

and
$$K_{Fe} = \frac{J_{Fe} \times RT_f}{p_{Fe}}$$

hence
$$\frac{J_{P_2}}{p_{P_2}} > \frac{J_{Fe}}{p_{Fe}} \quad (5.12)$$

Since at a particular temperature and concentration of phosphorus in the melt the values of p_{P_2} and p_{Fe} are constant, thus in order to satisfy the above conditions the rate of vaporization of phosphorus has to be increased to such an extent that the ratio of the rates of vaporization of phosphorus to that of iron becomes greater than the ratio of their partial pressures at the surface of the melt. Since the maximum rate of vaporization of a substance cannot exceed that in "Vacuo", the Langmuir equation can be used to determine the maximum rate of vaporization of phosphorus:

$$J_{P_x} = \frac{p_{P_x}}{\sqrt{(2\pi RT M_{P_x})}} \quad (5.13)$$

where: p_{P_x} = pressure of phosphorus (P_x)

M_{P_x} = molecular weight of phosphorus vapours

The vapour pressure of phosphorus at the surface of a melt containing 0.1 wt.% phosphorus is about

7.6×10^{-11} or 2.3×10^{-7} Atm^(57,58) at 1800°C as P_2 or P respectively. For iron at the same temperature is about 6.1×10^{-4} Atm^(59,60), inserting these values in equation 5.11 and 5.7 yields:

$$J_{P_2}^{\max} = 9.4 \times 10^{-12} \quad \text{moles.cm}^{-2} \text{ s}^{-1}$$

$$J_P^{\max} = 4.1 \times 10^{-8} \quad \text{moles.cm}^{-2} \text{ s}^{-1}$$

and $J_{Fe} = K_{Fe} \times 6.3 \times 10^{-9} \text{ moles.cm}^{-2} \text{ s}^{-1}$

hence $\frac{J_{P_2}}{p_{P_2}} = 0.124$, $\frac{J_P}{p_P} = 0.18$, and $\frac{J_{Fe}}{p_{Fe}} = 1.03 \times 10^{-5} \times K_{Fe}$

From estimating the values of D_{Fe} and " Δ " (because in the absence of a reacting gas $\delta \rightarrow \Delta$) as $5 \text{ cm}^2 \text{ s}^{-1}$ and 0.05 cm respectively, then the expected mass transfer coefficient (K_{Fe}) would be about 100 cm.s^{-1} , hence it can be seen that the above condition i.e.

$$\frac{J_{P_x}}{p_{P_x}} > \frac{J_{Fe}}{p_{Fe}} \quad \text{or} \quad K_P > K_{Fe}$$

can be satisfied, and hence dephosphorization of a melt by a vapour phase reaction is likely to occur on the kinetic grounds, under the conditions where the stream of the gas passing a levitated drop is reactive to phosphorus and less reactive with the iron vapour.

In order to test the validity of the proposed mechanism, experiments were carried out using streams of gas mixtures of $N_2/H_2/CO_2$, of relatively low corresponding oxygen^{potential} and forming gas ($H_2 - 25\% H_2$). The results obtained are given in Tables 5.6 and 5.7. From Table 5.6 and Figure 5.6 it is evident that there is practically no change in the phosphorus concentrations in the metal, although significant amounts of fumes were evolved during the experiments. Similarly in the experiments where forming gas was used, there was no significant change in the concentrations of the phosphorus. Thus indicating that iron and phosphorus were vaporized at a relative rate to their concentrations. It appears that the disagreement with the above prediction is mainly due to the thermodynamics of the systems studied, since the formation of oxides or hydrides of iron or phosphorus under these conditions are unlikely. However, if the gases used were reactive with phosphorus vapours at such temperatures and formed stable compounds such as nitrides or hydroxides, then dephosphorization could have been achieved, and hence accordance with the above predictions would have been obtained.

According to Kor and Turkdogan,⁽⁵⁶⁾ evolution of carbon monoxide from the surface of a melt containing carbon and phosphorus may enhance the rate of vaporization of phosphorus. For example, for a melt containing 1 wt.% carbon and 0.1 wt.% phosphorus with $p_{CO}/p_{CO_2} = 6.7$

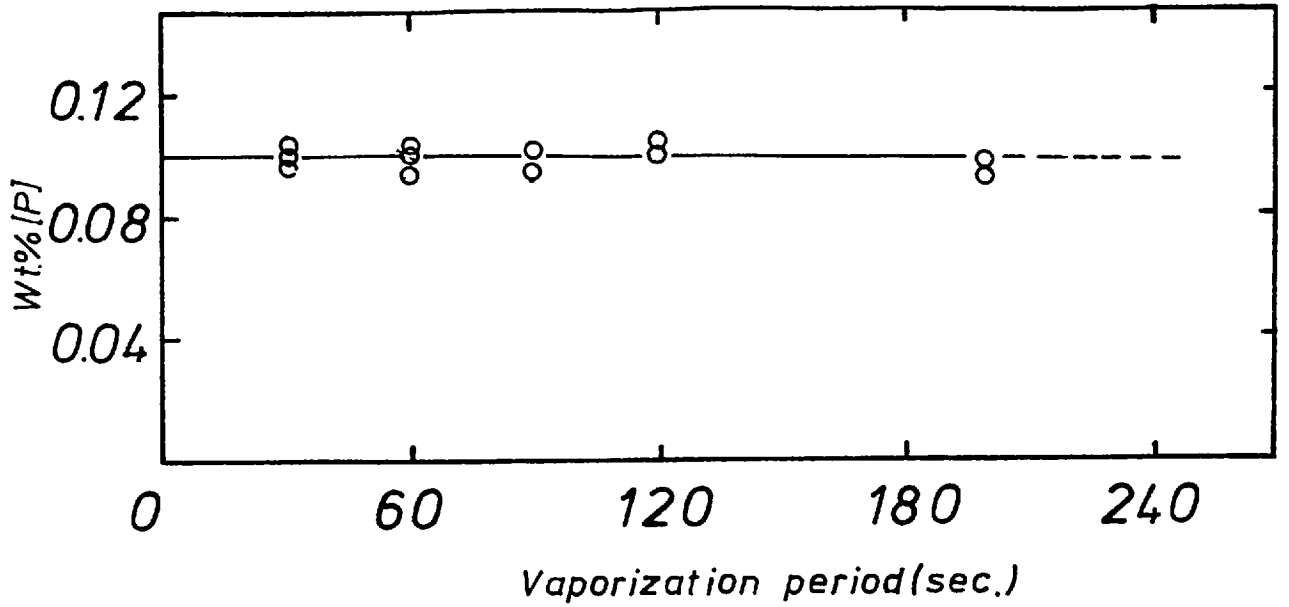


Figure 56 Vaporization of Fe-P in a stream of $N_2|H_2|CO_2$
 $(P_{O_2} \sim 5 \times 10^{-9} \text{ atm. at } 1725^\circ \text{C})$
 $(P_{O_2} \sim 8 \times 10^{-18} \text{ atm. at } 910^\circ \text{C})$

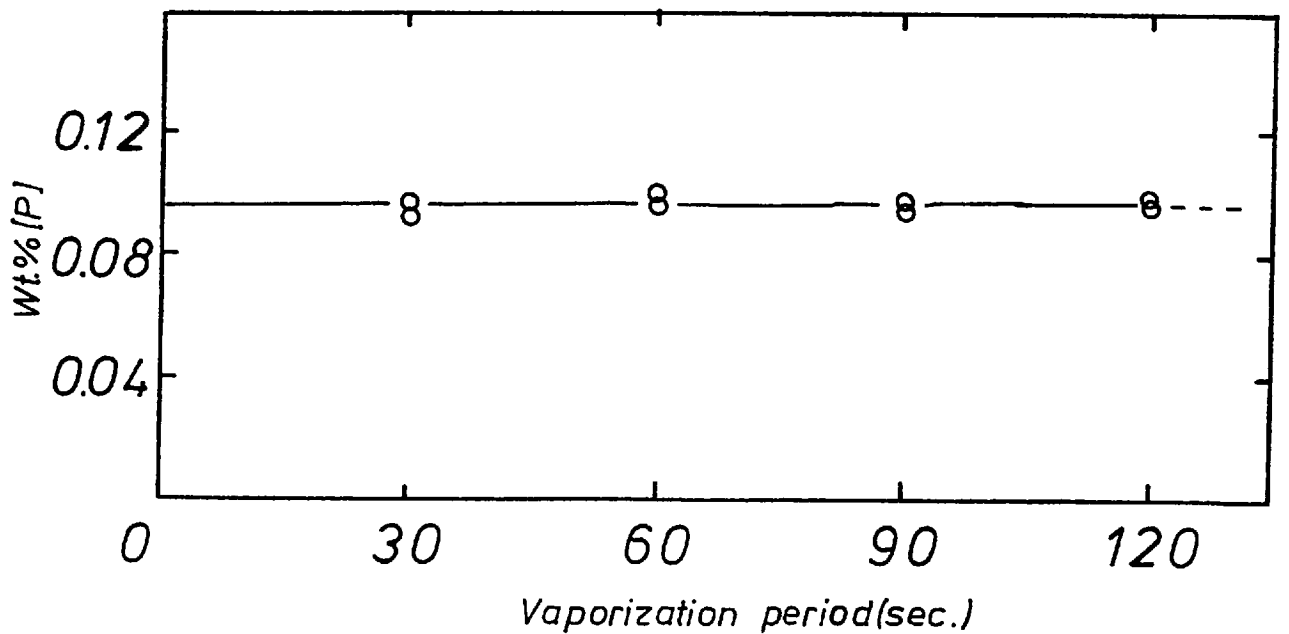
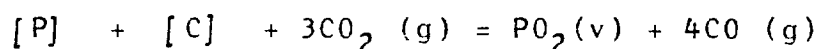
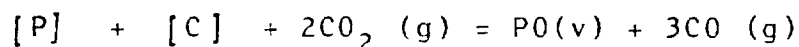
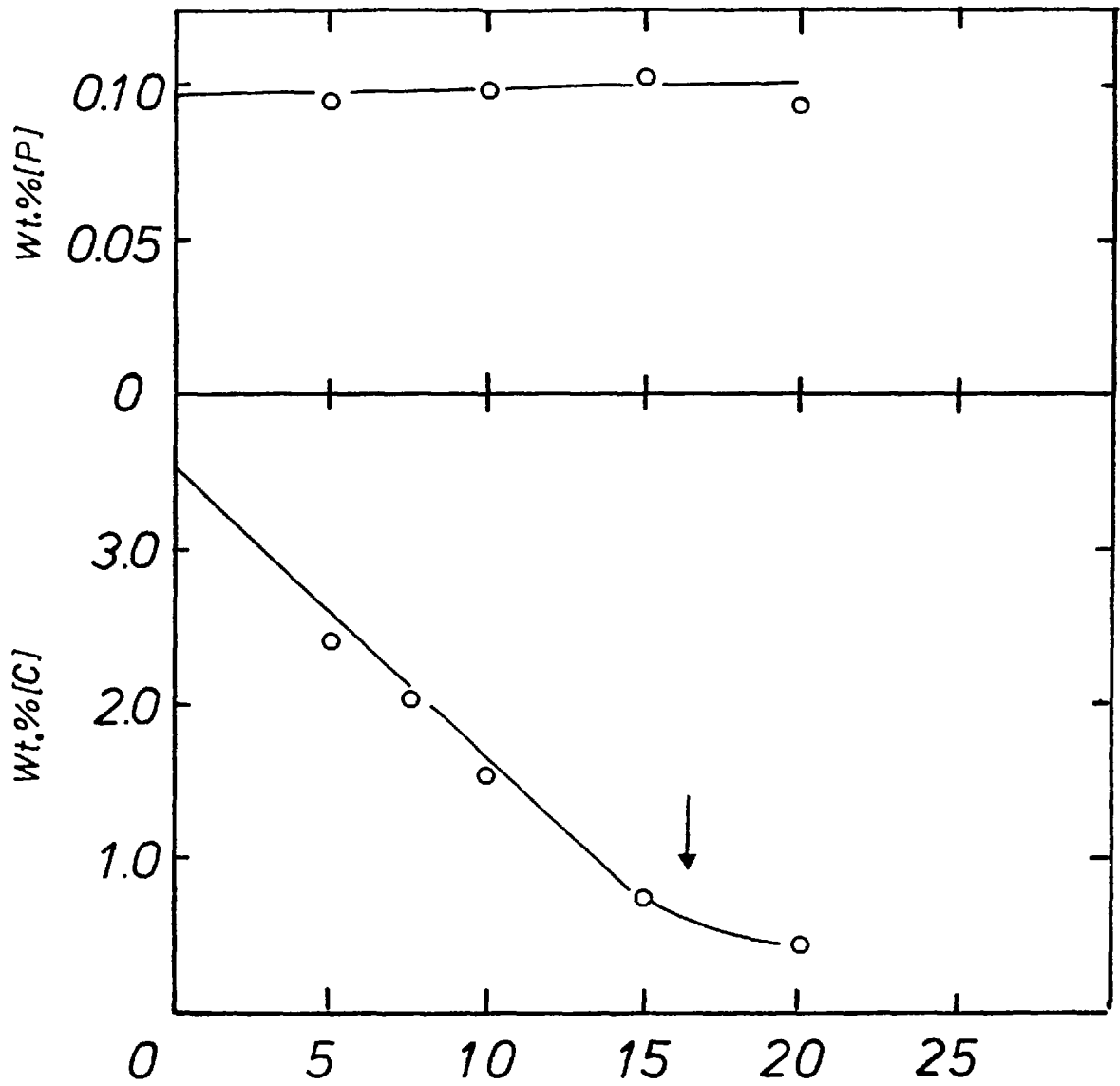


Figure 57 Vaporization of Fe-P in a stream of $N_2|H_2$
 $(P_{H_2} = 0.25 \text{ atm.})$

(corresponding to oxygen saturation at the surface of the melt at about 1620°C) the equilibrium values of PO and PO₂ are 6.9×10^{-5} and 10.9×10^{-5} atm. for the following reactions respectively:



These values are greater than the partial pressure of PO and PO₂ from a melt of iron-phosphorus by a factor of 10². Hence they concluded that comparison of these values indicates that removal of phosphorus from steel via the reactions given above would be greatly enhanced. The experimental results obtained on decarburization of Fe-C-P alloys in a stream of CO₂, have revealed that at high and low carbon levels in the melt, dephosphorization does not take place even under conditions that mass transfer in the gas phase is the rate-controlling step. These results are in accordance to the work of Kaplan and Philbrook⁽¹⁵⁾ who decarburized Fe - 4.7%C - 1.7%P melts in streams of He-O₂ at 2045°C by levitation. The experimental results of Kor and Turkdogan⁽⁵⁶⁾ on oxidation of Fe-C-P in magnesia crucibles also showed no loss of phosphorus from the melt, but this was thought to be due to low oxygen activity at the surface of their melts!



Oxidation & vaporization period (seconds)
Figure 5.8 & 5.9 Oxidation & vaporization of Fe-C-P
in a stream of CO_2 .

↓ Indicates the commence of the carbon boil.

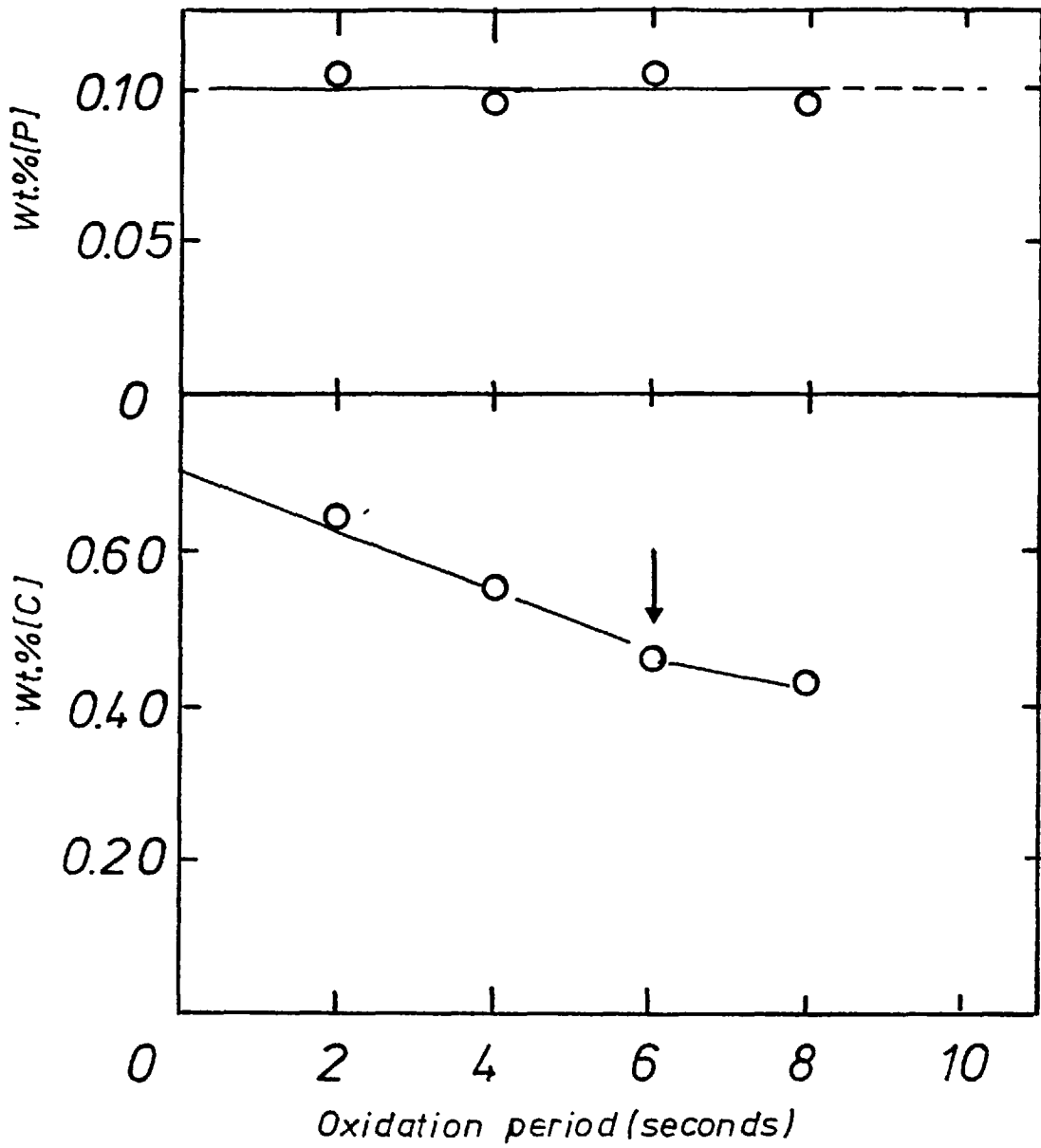


Figure 5.10 & 5.11 Oxidation of Fe-C-P in a stream of CO_2

↓ Indicates start of the carbon boil.

Oxidation and vaporization of iron-phosphorus alloys
at high oxygen partial pressures in gas streams

In order to verify the validity of the investigation of Kor and Turkdogan on the subject of dephosphorization of iron, oxidation and vaporization experiments were conducted on levitated drops of iron-phosphorus alloy in several gas mixtures with corresponding oxygen partial pressures greater than those which would bring about maximum rates of vaporization of iron leading to the formation of a liquid oxide phase on the surface of the melt. Although for the above-mentioned conditions one would expect vaporization to cease once the oxide phase is formed, because the flow of the gas passing the levitated drops was in a downward direction any oxide film formed accumulated at the bottom portion of the levitated drops by gravity, surface tension and the effect of the gas stream, the upper portion of the surface of the drops remained free of an oxide layer, and vaporization continued to take place even at such oxygen potentials.

The experimental results, which are summarized in Tables 5.12-5.15 and Figures 5.12-5.15 respectively indicate a rise in phosphorus concentrations in the metal. The rate of increase in the phosphorus concentration being proportional to the oxygen partial pressures in the gas stream, and hence to the rate of formation of an iron-oxide liquid phase at the metal interface. X-ray

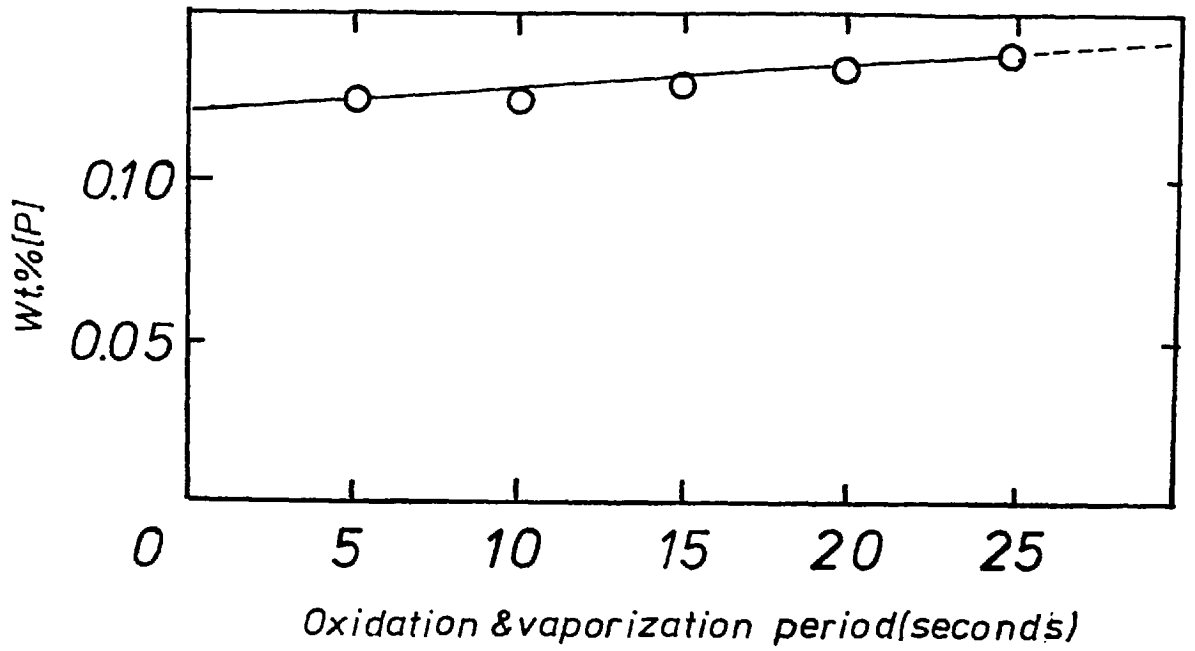


Figure 5.12 Oxidation & vaporization of Fe-P in a stream of He-O₂ ($P_{O_2} = 5 \times 10^{-2}$ atm.)

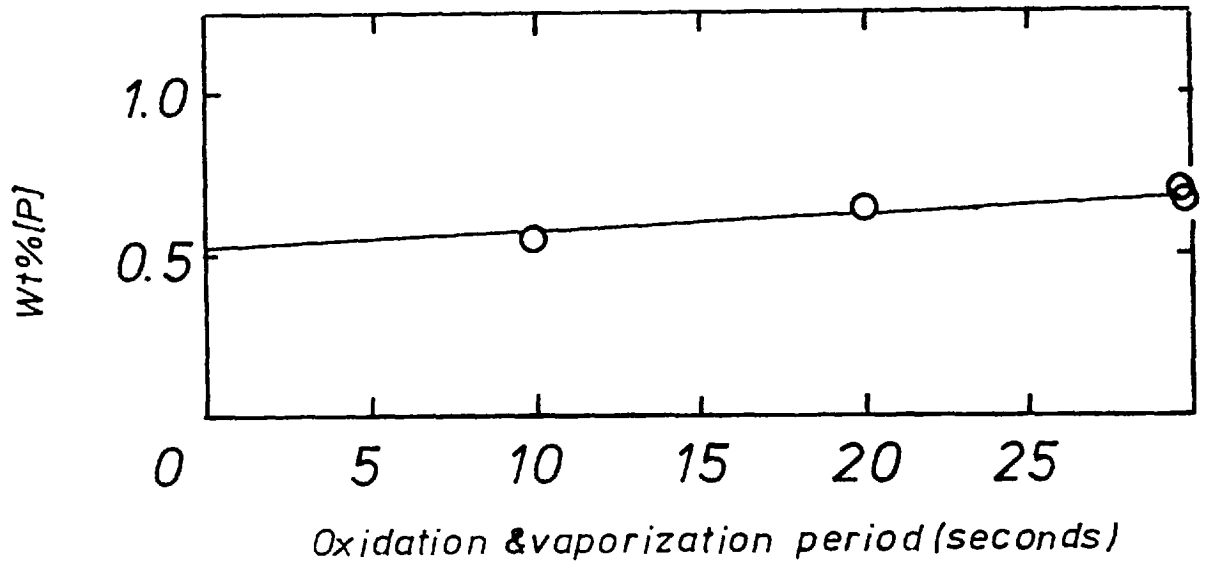


Figure 5.13 Oxidation & vaporization of Fe-P in stream of CO₂.

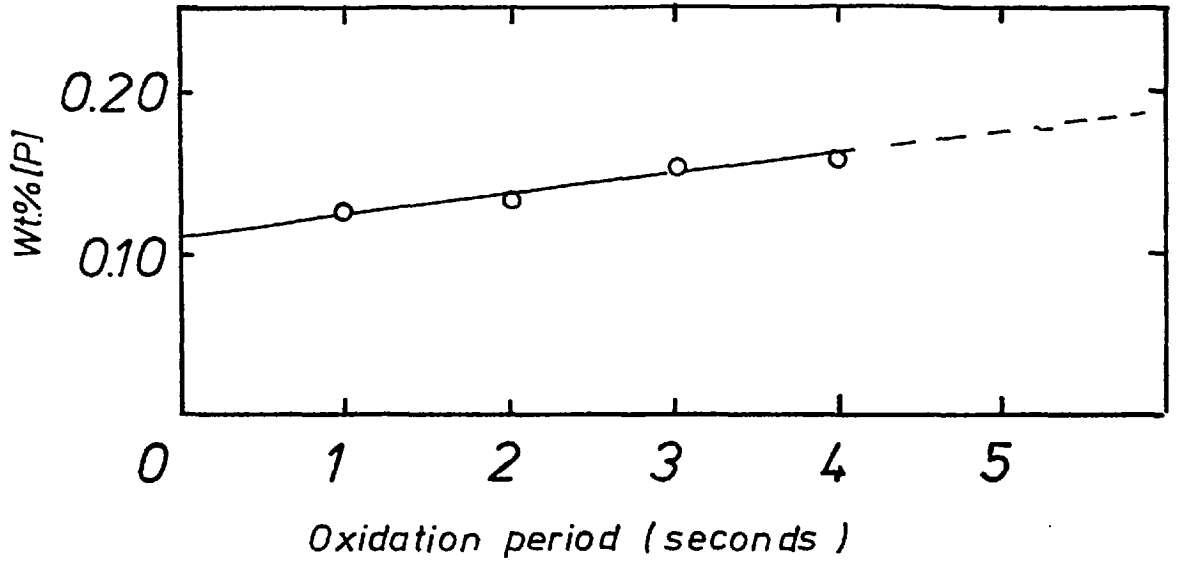


Figure 5.14 Oxidation & vaporization of Fe-P in a stream of He-O₂ ($P_{O_2}=0.5$ atm.)

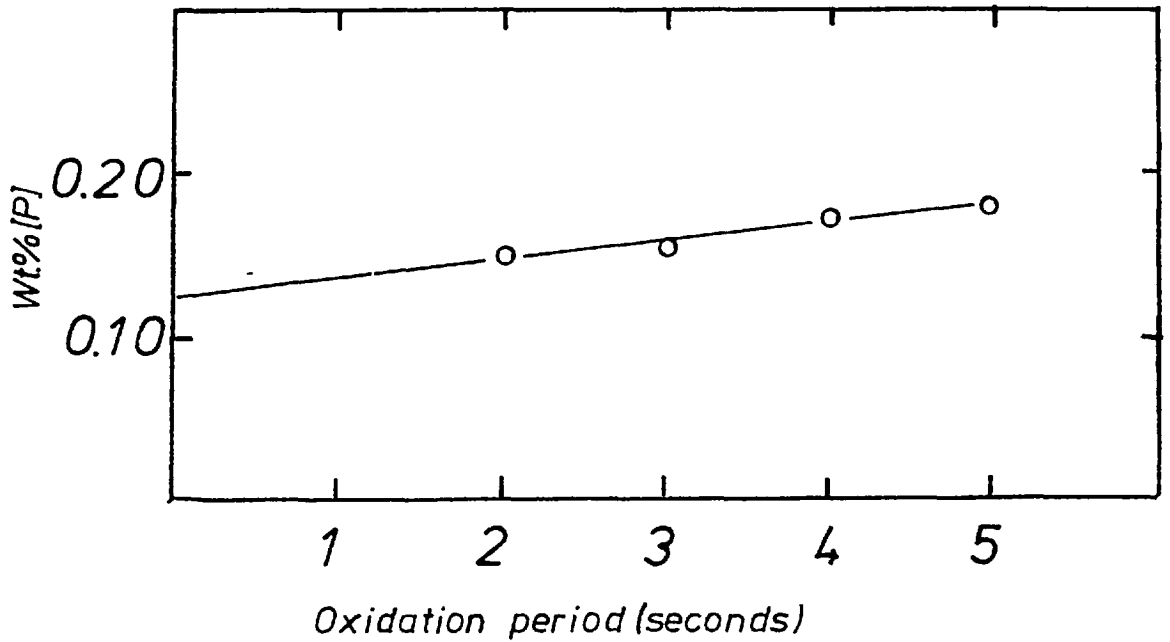


Figure 5.15 Oxidation & vaporization of Fe-P in a stream of O₂ ($P_{O_2}=1.0$ atm.)

diffraction examination of the condensate on the silica tube of the levitation cell, showed no presence of phosphorus compounds, and the deposits were identified as iron oxides. The rise in concentration of phosphorus in the metal can hence be expected to be due to low capacity of iron oxide "slag" for phosphorus pentoxide. In other words, as the oxidation takes place iron is being oxidised preferentially to phosphorus, so that the phosphorus concentration of the metal phase rises without significant loss as vapour. These results are not in accordance with those of Kor and Turkdogan,⁽⁵⁶⁾ and it is considered that this may be due to their experimental technique. They used magnesia crucibles; which may act as a basic slag when dissolved in liquid iron oxide. The phosphorus reaction could have taken place at crucible/metal interface rather than at the metal/gas interface. Magnesia is not a very good dephosphorizer and had relatively low solubility in liquid iron oxide ($\sim 4\%$). Such a slag would not dephosphorize iron alloys with low phosphorus concentrations ($\sim 0.1\%$),⁽⁶²⁾ but it is evident⁽⁶³⁾ that when in contact with melts of high phosphorus concentration it can reduce the phosphorus levels to some extent. Furthermore commercial magnesia crucibles contain a few percent of lime as an impurity, and on considering the ratio of the melt to the size of the crucible used by these workers, there appears to be sufficient calcium oxide to dephosphorize the alloy to lower levels of phosphorus. The supporting evidence for the above mechanism of achieving dephosphorization

in magnesia crucibles arises from the fact that practically no dephosphorization was achieved when carbon was present in the melt, since in the presence of carbon any iron oxide formed would be reduced by the carbon, and hence dissolution of magnesia and lime cannot take place, resulting in no phosphorus removal from the melt in such a case.

5-7 CONCLUSION

On the basis of investigations carried out on the "dephosphorization" of iron-base alloys in streams of oxidising and reducing gas mixtures it may be concluded that the removal of phosphorus from the liquid metal does not take place via the formation of any volatile species of sub-oxides of phosphorus such as PO or PO_2 in the presence or absence of carbon, or by formation of other volatile species such as hydrides, nitrides or hydroxides. It is also considered that phosphorus removal by the formation of iron phosphate by gas/vapour phase or at the metal/oxide interface does not occur.

CHAPTER 6

CHAPTER 6

KINETICS OF DESILICONIZATION OF LIQUID IRON ALLOYS

6-1. INTRODUCTION

The oxidation and removal of silicon from liquid iron is one of the important reactions in refining the blast furnace metal. The rate of desiliconization of liquid iron is thus an important factor in such processes as basic oxygen steelmaking.

The present investigation was undertaken primarily to study the behaviour of iron silicon alloys, at relatively low concentrations, during the course of oxidation and removal of silicon from the melt. The other objective of this work was to investigate whether phosphorus, at concentrations normally found in the hot metal leaving the blast furnace (~ 0.1 wt.%) had any affect on the rate of desiliconization of levitated drops of iron-silicon alloys in a stream of oxygen-bearing gas.

6-2. PREVIOUS WORK

Kaiser et al.⁽⁶⁴⁾ studied the oxidation of pure liquid silicon at about 1410°C , by a stream of oxygen bearing gas. Wagner⁽⁶⁵⁾ has used their results to show that at low oxygen partial pressures in the gas the formation of gaseous silicon monoxide (SiO) occurs at the surface of

the melt. The formation of silica takes place at the surface, when the oxygen partial pressure is raised to above a critical value. The critical oxygen potential to bring about the formation of $\text{SiO}_2(\text{s})$ at the interface is a function of the transport properties in the gas phase as well as the vapour pressure of the silicon at the surface of the melt (i.e. it is similar to that of the formation of a liquid iron oxide phase as in the case of enhanced vaporization, which has been discussed earlier in Chapter 5).

Sano et al.⁽⁶⁶⁾ used a levitation technique to study the kinetics of desiliconization of iron-silicon alloys, at temperatures of 1550°C - 1800°C , in streams of gas mixtures of CO_2 or O_2 in He. They found that gaseous SiO was formed as the reaction product, at high temperatures and low oxygen potentials in the gas stream. They concluded that under such conditions the rate of the reaction was controlled by gaseous diffusion of CO_2 and SiO to and from the interface. Although at silicon concentrations below 3 wt.% the rates appeared to be dependent on the silicon concentration in the metal. Their results are shown in Figures 6.1.-6.3. However at higher oxygen potentials in the gas stream and/or lower temperatures, the formation of a solid or liquid oxide phase was observed by these workers, and the transport of oxygen ions through the oxide layer was concluded to be the rate controlling factor. They also found in one experiment that presence of lime increased their desiliconization rates by a factor of 3.4. This was

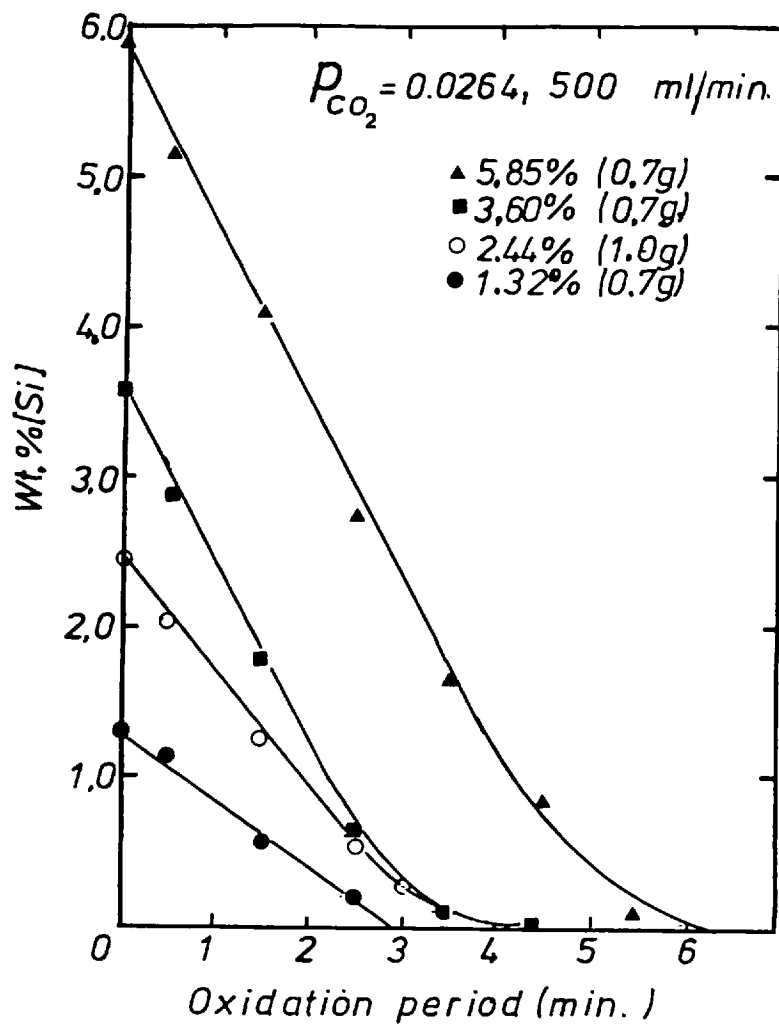
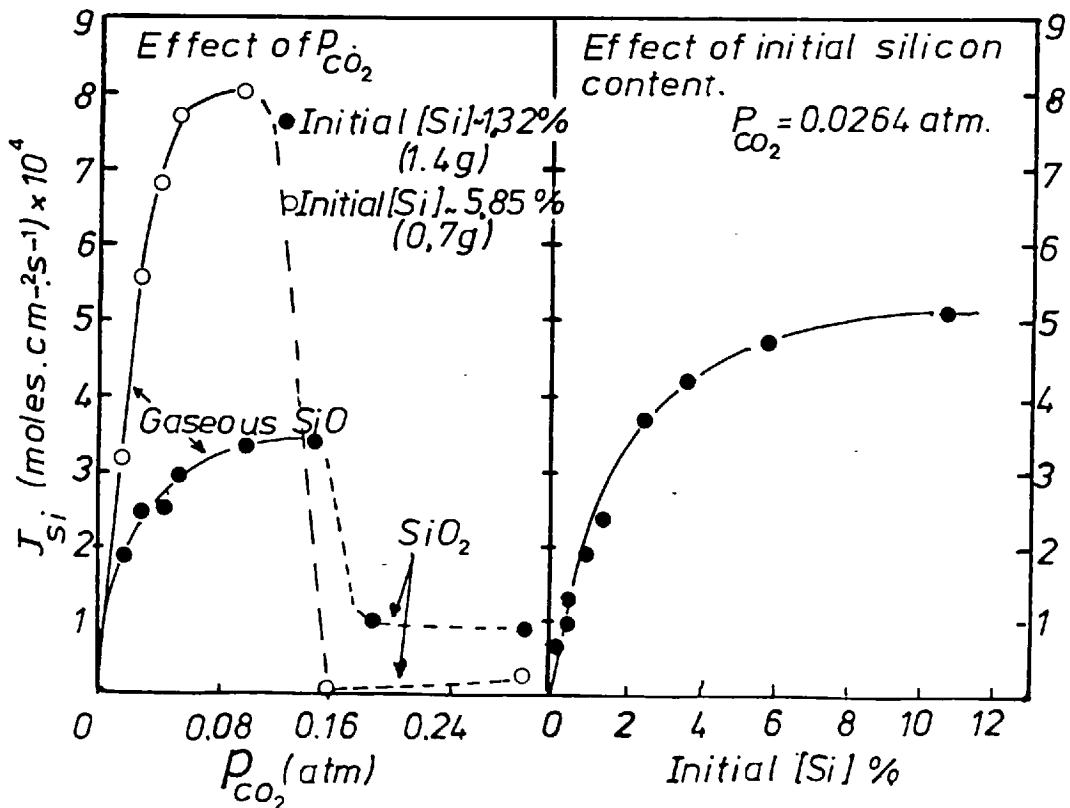


Figure 6.1 Effect of the composition of Fe-Si droplets on the oxidation rate of silicon at 1700°C.



Figures 6.2 & 6.3 Effect of P and initial [Si] concentration on the rate of desiliconization by vapour phase reaction.

explained in terms of the formation of a liquid oxide phase richer in FeO, and a higher concentration of oxygen ions in the basic slag as well as higher diffusivity of such ions in the slag formed.

Filippov et al.⁽⁶⁷⁾ oxidised Fe-Si by blowing Ar-O₂ mixtures on the surface of the melt. They found that at low flow rates, the efficiency of oxygen utilisation by the melt was about 75%, but at higher flow rates, the efficiency decreased significantly to about 30%, and the composition of their slag became richer in iron oxide. The behaviour was interpreted in terms of the formation of a viscous slag layer on the surface of the melt, which acted as a barrier to oxygen transfer to the metal surface.

Robertson⁽⁶⁸⁾ reacted 1 gram levitated drops of Fe-Si at 1660°C with pure O₂, or with mixtures of Ar-O₂ containing 10% or 20% O₂. He observed a reduction in the temperature of the sample once the thin layer of a passive slag was formed on the surface of the drops. The decrease in the temperature was accounted for by the higher emissivity of the slag layer compared with that of the clean metal surface, resulting in an increase in the rate of heat loss by radiation.

Baker⁽⁶⁹⁾ studied the oxidation of Fe-Si drops, with an initial temperature of about 1600°C, containing 1-7wt.% silicon, in pure oxygen during free fall. He found that at initial silicon contents of 3 wt.% and below,

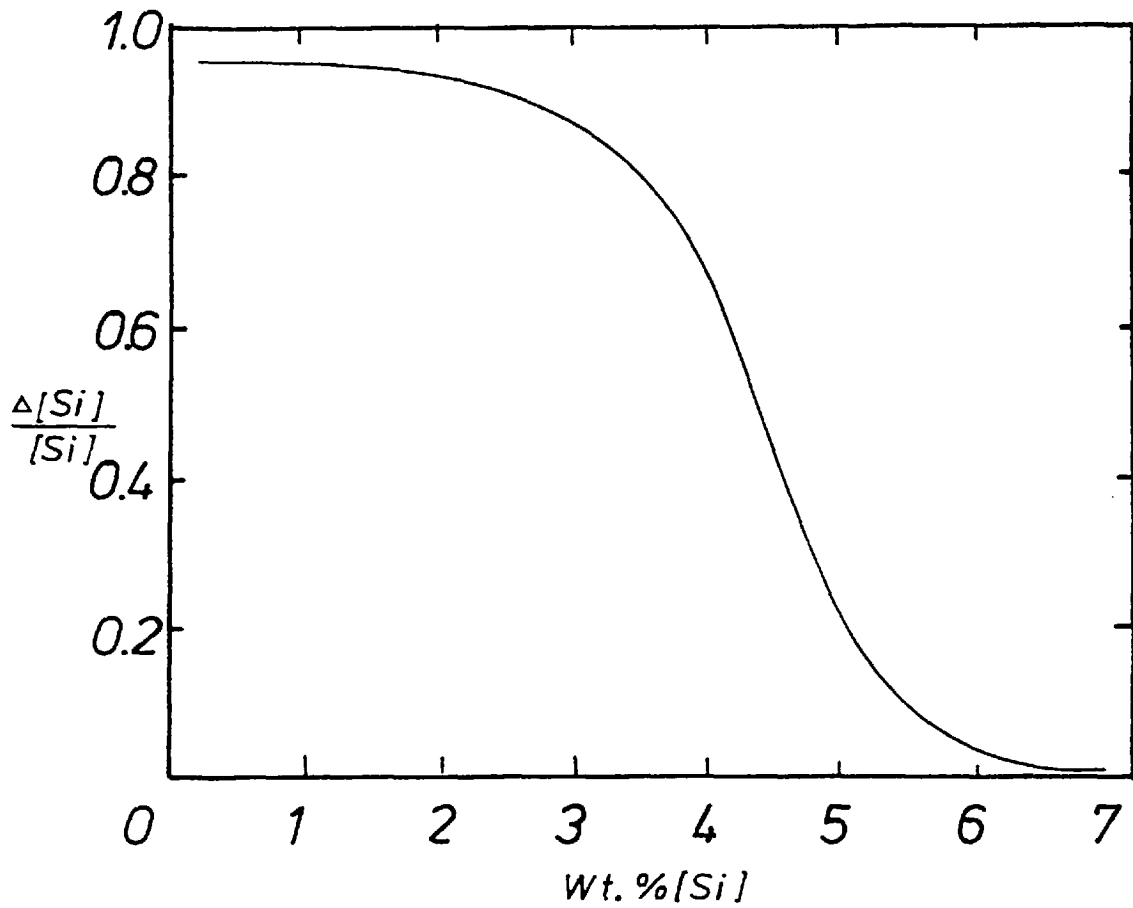


Figure 6.4 Results obtained by Baker on desiliconization of Fe-Si drops expressed as a function of the original silicon content.

rapid oxidation and removal of silicon took place, while a gradual transition to a passive behaviour of the slag occurred between 3 and 6 wt.% silicon in the metal. In alloys containing more than 6 wt.% silicon initially the rate of removal of silicon reached a minimum level, and he reported a decrease in the temperature of these drops. His results are shown in Figure 6. On the other hand it has been shown by many workers,⁽⁷⁰⁻⁷²⁾ that solution of oxygen in levitated drops of copper and nickel from an oxidising gas is often retarded or completely prevented by a barrier film on the surface of the drops. The nature of the film was found to be associated with the formation of a surface silica film from the indigenous silicon in the metal. Furthermore, Harvey⁽⁷³⁾ found that the presence of a few ppm of silicon in levitated drops of copper does lead to the formation of the passive film of silica.

6-3. EXPERIMENTAL TECHNIQUE

Two batches of alloys containing silicon and phosphorus at different concentrations were made by the method described previously. 1 gram samples were cut from the rods of alloys, levitated in a stream of forming gas until molten and deoxidized. The samples were then kept levitated in a stream of helium and on reaching a steady temperature of 1690°C, they were exposed to a stream of oxidising gas (He-5%O₂) flowing at a pre-adjusted rate of 1 l.min⁻¹. At the required time the flow of oxidising

gas was stopped, and an inert gas (helium) at a similar pre-adjusted rate was introduced. The drops were then solidified in a stream of helium. After removing the oxide layer from the samples, the entire sample was analysed for silicon or phosphorus.

6-4. RESULTSTABLE 6.1.

Run	Initial mass of metal (gram)	Initial temp. of metal (°C)	Oxidation period (secs)	Maximum temp. (°C)	Final temp. (°C)	Final mass of metal (gram)	wt % [Si]
SR01	1.0820	1690	0	1690	1690	1.0796	0.15
SR02	1.9681	1690	0	1690	1690	0.9676	0.12
SR03	1.0880	1690	2	1740	1710	1.0831	0.12
SR04	1.1557	1690	2	1750	1710	1.1472	0.12
SR05	1.1513	1690	4	1750	1640	1.1455	0.12
SR06	1.0417	1690	4	1745	1635	1.0386	0.13
SR07	0.9751	1690	8	1740	1620	0.9673	0.11
SR08	1.0208	1690	8	1740	1610	1.0133	0.10
SR09	1.1263	1690	10	1760	1610	1.1188	0.09
SR10	1.1834	1690	10	1755	1610	1.1751	0.10
SR11	1.1998	1690	15	1740	1730	1.1764	0.05
SR12	1.1820	1690	15	1745	1735	1.1628	0.05

Oxidation of Fe-0.12% Si-0.015% P in a stream of He-5% O₂, in absence of lime.

Gas flow: 1.0 l.min⁻¹

I.D. of tubing: 12.7 mm

TABLE 6.2

Run	Initial mass of metal (gram)	Initial temp. of metal (°C)	Oxidation period (secs)	Maximum temp. (°C)	Final temp. (°C)	Final mass of metal (gram)	wt% [Si] _{Fe}
SR13	1.0386	1700	0	1800	--	1.0353	0.174
SR14	1.0612	1700	0	1700	--	1.0613	0.179
SR15	1.0836	1695	2	1750	1735	1.0928	0.183
SR16	1.0970	1695	2	1750	1730	1.0933	0.178
SR17	1.0972	1690	5	1745	1660	1.0918	0.156
SR18	1.0929	1690	5	1745	1660	1.0909	0.174
SR19	1.0472	1690	7	1760	1620	1.0424	0.134
SR20	1.0778	1690	7	1760	1625	1.0734	0.121
SR21	1.1061	1690	10	1760	1615	1.0973	0.082
SR22	1.0850	1690	10	1760	1620	1.0780	0.083
SR23	1.0810	1690	15	1760	1725	1.0646	0.038
SR24	1.0420	1690	15	1760	1730	1.0724	0.047

Oxidation of Fe-0.179% Si-0.11% P in a stream of He-5% O₂ in absence of lime.

Gas flow rate: 1.0 l. min⁻¹

I.D. of tubing: 12.7 mm

TABLE 6.3

Run	Initial mass of metal (gram)	Initial temp. ($^{\circ}\text{C}$)	Oxidation period (secs)	Maximum temp. ($^{\circ}\text{C}$)	Final mass of metal (gram)	wt% [P] _{Fe}
SR25	1.0423	1690	2	1745	1.0398	0.111
SR26	1.0965	1695	5	1750	1.0896	0.114
SR27	1.0909	1690	7	1760	1.0644	0.106
SR28	1.0609	1690	10	1750	1.0530	0.108
SR29	1.0660	1670	15	1740	0.8981	0.108

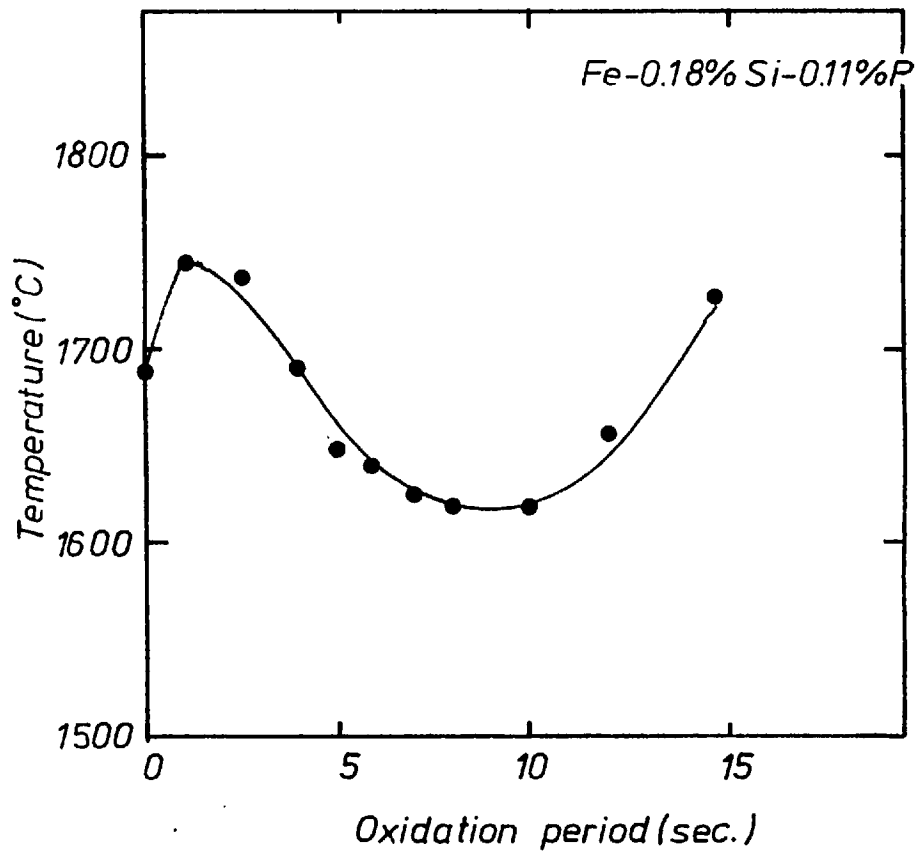
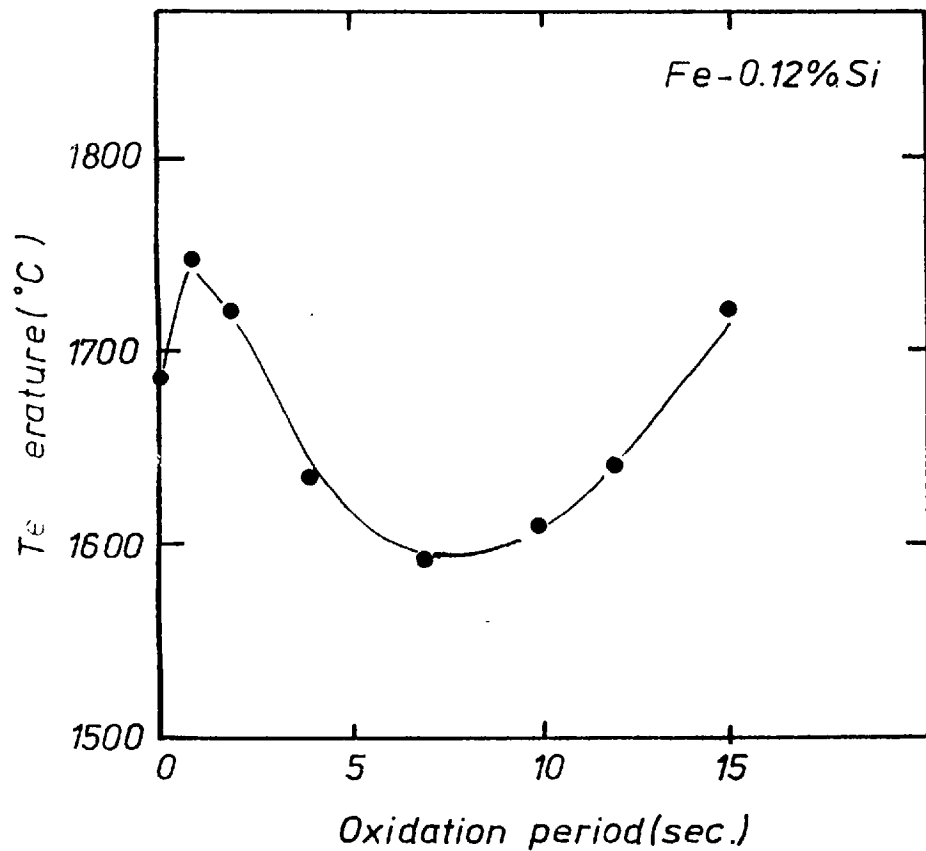
Oxidation of Fe-0.179% Si-0.11% P in a stream of He-5% O₂ in absence of lime.

Gas flow rate 1.0 l. min⁻¹

6-5. INTERPRETATION OF THE RESULTS

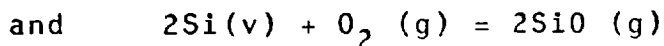
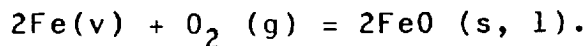
In order to interpret the kinetics of the oxidation and removal of silicon from iron based a knowledge of the sequence of events taking place is necessary. Thus on carrying out oxidation experiments, cine photography was used to record the observed sequence of the events occurring and the variation in the temperature of the levitated drop was measured by the T.C.P. and recorded. In the following section combinations of these data are used to explain the behaviour of the levitated drops during the course of desiliconization.

On considering the variation in the measured temperature of the levitated drops, the results obtained on oxidation of the two batches of the alloys were similar, as can be seen from Tables 6.1.-6.3. and Figures 6.5. and 6.6. They all represent a cycle in which an initial increase in temperature is followed by a decrease, and finally an increase in the temperature of the drops; as oxidation proceeds. The initial increase of about $60 \pm 10^{\circ}\text{C}$ can be expected to occur due to exothermic reaction as well as a small decrease in the thermal conductivity of the oxidising gas as compared to that of the inert gas. An important observation made during these oxidation reactions was the formation of a high-emmissivity oxide layer on the surface of the drops rather than evolution of fumes from them. In order to verify this observation, a model of the enhanced vaporization of iron and silicon was considered.



Figures 6.5 & 6.6 Variation in the temperature during the oxidation of Fe-Si & Fe-Si-P drops in a stream of He-5%O₂

The maximum rates of vaporization of iron and silicon were calculated using the data of Fruehan⁽⁷⁴⁾ on the activity of silicon in liquid iron. The vapour pressures of iron and silicon from a melt containing about 0.2 wt.% silicon were thus evaluated using the known values of the vapour pressures of the pure components at 1700°C.^(59,60,75) The results obtained indicate that at 1700°C the maximum rates of vaporization of iron and silicon from a melt containing 0.2 wt.% Si are 2.33×10^{-5} and 3.6×10^{-10} moles.cm⁻².s⁻¹, respectively. Our estimated flux of oxygen to the interface was found to be about 2.30×10^{-5} moles.cm⁻².s⁻¹. From the stoichiometry of the reactions:



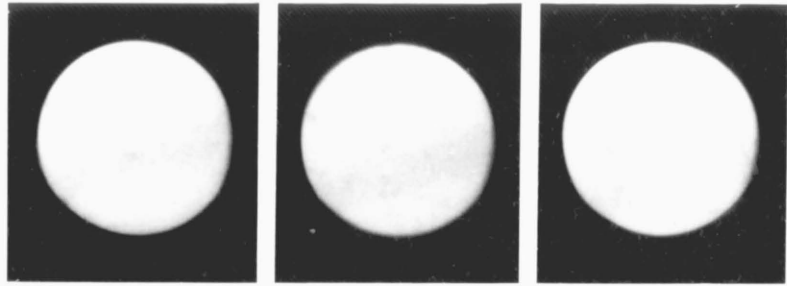
It can be expected that when:

$$J_{\text{O}_2} \geq \frac{1}{2} (J_{\text{Fe}} + J_{\text{Si}})$$

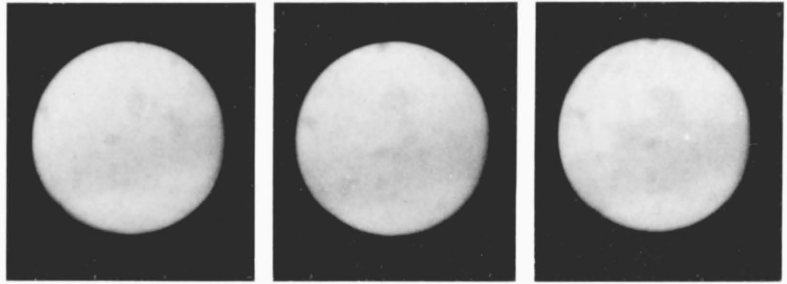
formation of an oxide layer on the surface of the molten drop takes place and hence vaporization should cease. It can be seen that the calculated flux of oxygen is about twice as much as that required to bring about oxide formation on the surface and inhibit the vaporization process.

In order to explain the observed decrease in the temperature of the samples, use of the series of photographs

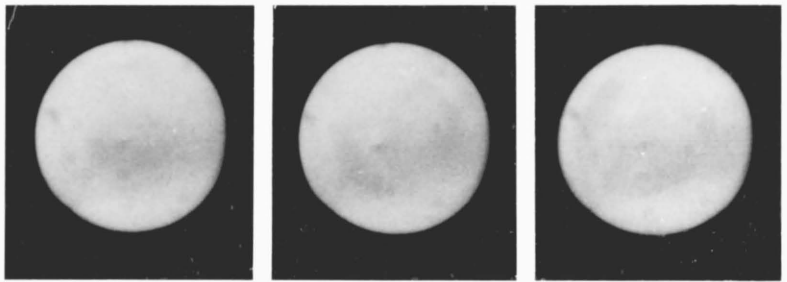
Frames



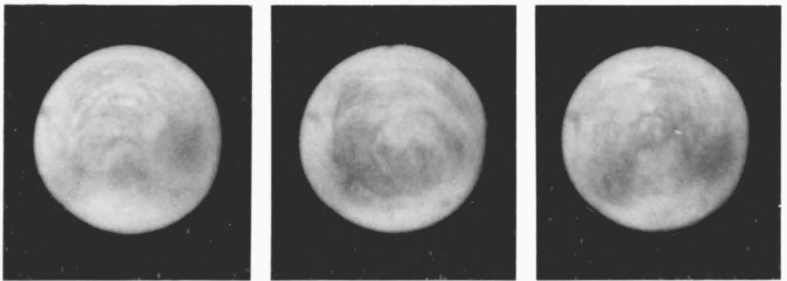
9-11 First sign of oxidation and surface coverage by an oxide phase.



16-18 Breakdown of the slag into two liquids.

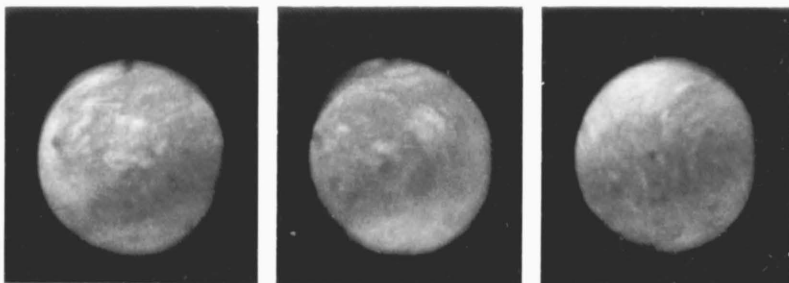


26-28 Formation of more slag on the surface.

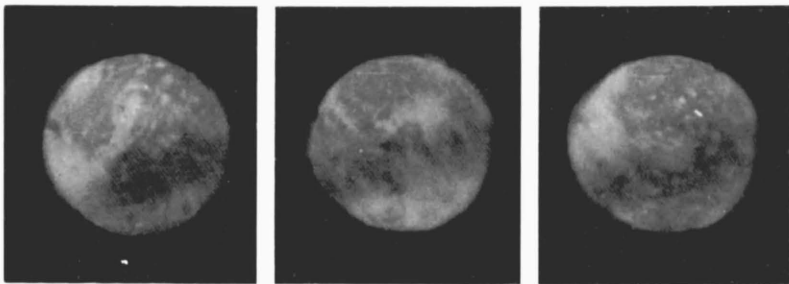


45-47 Spreading of the slag, and the gradual decrease in the brightness.

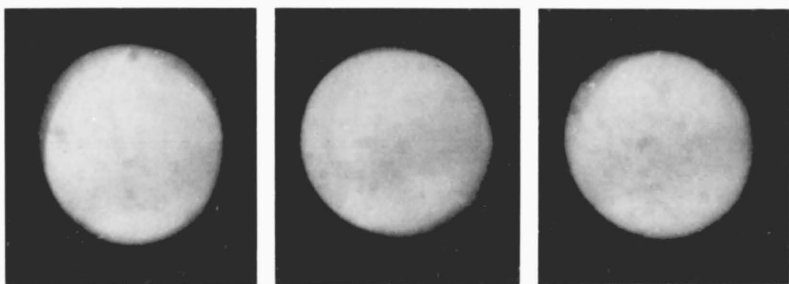
Frames



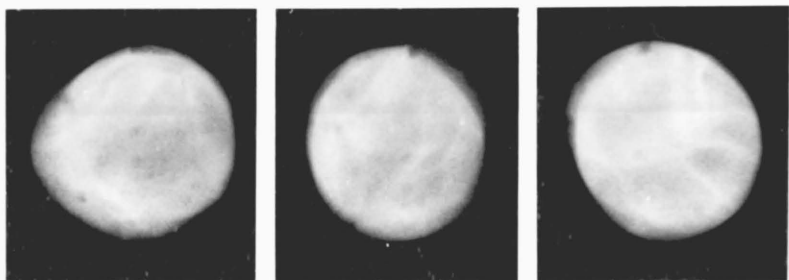
59-61 Formation of the second phase and further decrease in brightness.



144-146 Comparitively much less active slag phase (silicate) is present.



160-162 ~~Decrease~~ Increase decrease in brightness.

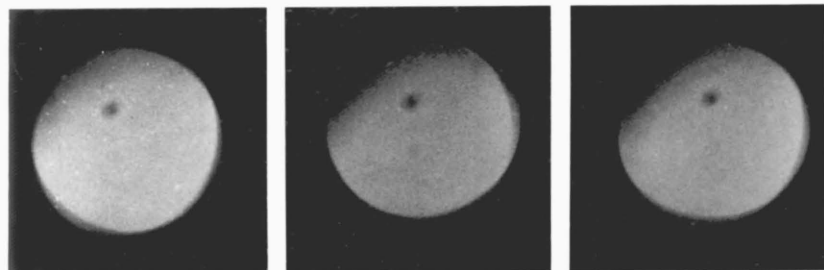


266-268 Iron burning on the surface, and the brightness increases.

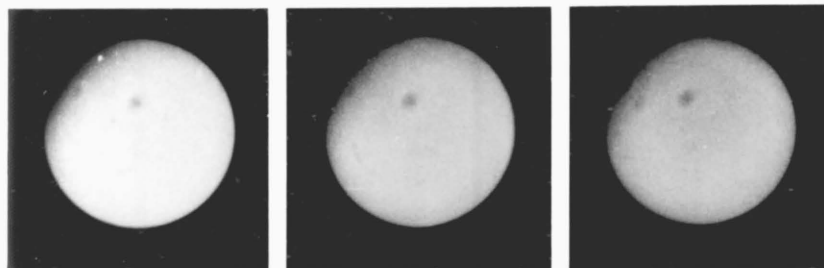
Figure 6.7 Top view of the events during oxidation of a Fe-0.18% Si-0.1%P drop in a stream of He-5%O₂, oxidation period ~30 seconds. filming speed \approx 16 p.p.s. (Prints were enlarged using the same conditions to illustrate the change in brightness during oxidation).

Frames

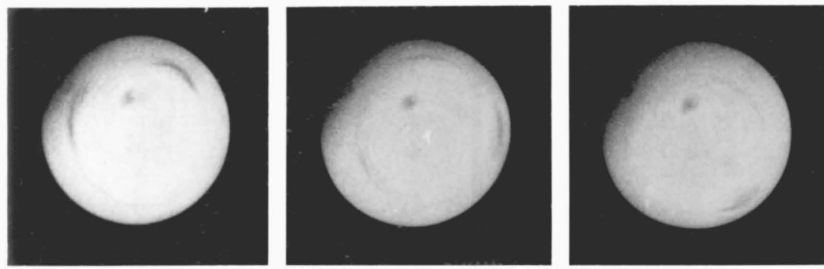
2-4



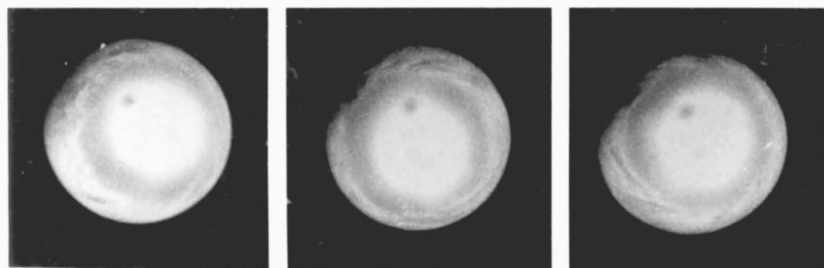
9-11



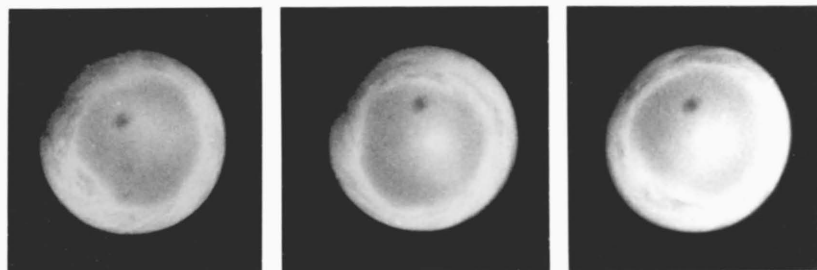
59-61



144-6



177-9



243-5

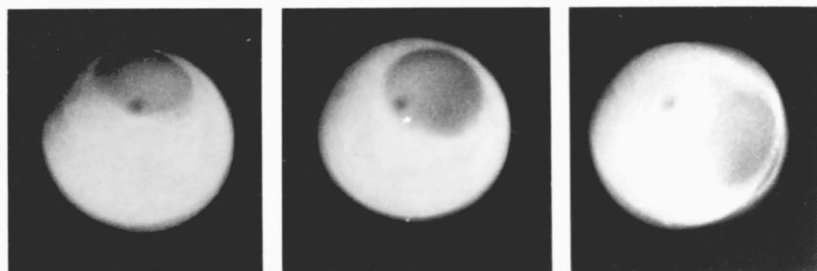


Figure 6.8 The sequence of the events at the bottom portion of the drop during oxidation of 1 gram Fe-Si-P in a stream of He-5%O₂ flowing at 1.0 l.min⁻¹. oxidation period ~30 secs. filming speed: 16 p.p.s. (prints were enlarged under the same conditions to illustrate the change in the brightness).

taken from the top and the bottom of the levitated drops during the oxidation process is made. With reference to Figures 6.7. and 6.8., it can be seen that in less than one second after the oxidation had commenced, surface coverage by an oxide phase takes place, and that soon after, the breakdown of the slag into two liquids takes place. Further oxidation leads to the formation of more slag on the surface and its spreading. This results in the gradual decrease in the brightness due to the lowering of the temperature of the molten drop. In order to explain this behaviour a heat balance must be drawn up. We may write that for a steady state, the heat generated by eddy currents (Q_{EC}) and chemical reactions (Q_{CR}), must be equal to the heat lost by convection (Q_{CONV}) and radiation (Q_{RAD}).

$$Q_{EC} + Q_{CR} = Q_{CONV.} + Q_{RAD}$$

$$= K' A (T_s - T_b) + e A \sigma (T_s^4 - T_b^4)$$

where K' = mean heat transfer coefficient.

A = surface area of the drop.

T_s = surface temperature of the drop.

T_b = bulk gas temperature

e = emmissivity

and σ = Stefan-Bomann constant

Although it is possible to calculate the values for Q_{EC} from the steady temperature of the drop (1690°C) when levitated in the stream of inert gas (helium), and the thermal properties of the gas, i.e. when $Q_{CR} = 0$

$$Q_{EC} = Q_{CONV} + Q_{RAD}$$

a problem arises in estimating the value of rate of heat generated when chemical reactions are taking place, since the amount of iron oxidised at any time is not known. An exact prediction of the rate of decrease in the temperature of the molten drop cannot therefore be made. However it has been shown by Robertson⁽⁶⁸⁾ that once a thin layer of passive slag has been formed on the surface of a levitated drop, the heat lost by radiation increases by about 50% due to the high emissivity of the slag layer ($e_{slag} \sim 0.8$) compared to that of a clean iron surface ($e_{Fe} \sim 0.4$). For such a case if there is no heat generated by chemical reactions a decrease of about 200°C would be expected. Due to the fact that chemical reactions at the surface of the drops were occurring in our experiments, it is thus estimated that the balance between the heat liberated by chemical reactions and that lost by radiation leads to a net decrease of about $18^{\circ}\text{C.s}^{-1}$ over a period of about 8 seconds.

The other interesting behaviour observed in these series of experiments was that on oxidising the drops beyond

9 seconds a gradual increase in the temperature of the drops was observed. This effect can be explained by the inspection and comparison of Figures 6.7 and 6.8, which illustrate that the slag formed tends to become more fluid and collects at the bottom of the levitated drop. This results in a reduction in the rate of heat lost by radiation, since a smaller portion of the surface area of the drop is covered by the high emissivity slag layer, so that the net result would be a gradual rise in the temperature of the levitated drop.

6-6. DISCUSSION

6-6.1. Rate Controlling Step in the Reaction of Fe-Si and O₂

There are several mechanisms, which may control the rate of desiliconization, and these are:

- a. Chemical reactions at the interface.
- b. Transport of gaseous reactants to the interface.
- c. Transport of ionic species across the slag layer.
- d. Transport of silicon to the interface.

The rate of chemical reactions, such as the oxidation of silicon are generally too rapid for these to be the rate controlling step. Thus in interpreting the results it is assumed that one or more of the other steps were rate controlling.

When the reaction taking place results in the formation of a slag phase on the surface of the melt; as

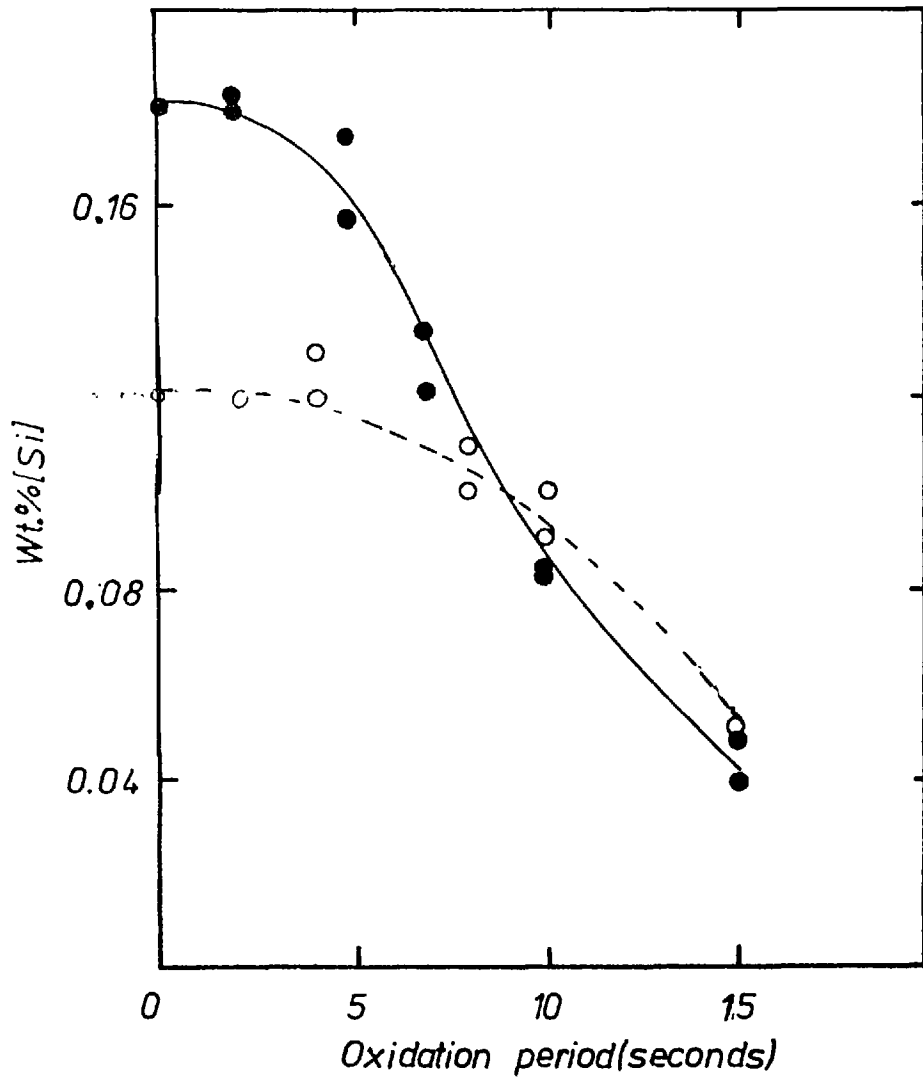


Figure 6.9 Oxidation of Fe-Si-0.015%P(○) and Fe-Si-0.11%P(●) in a stream of He-5%O₂.

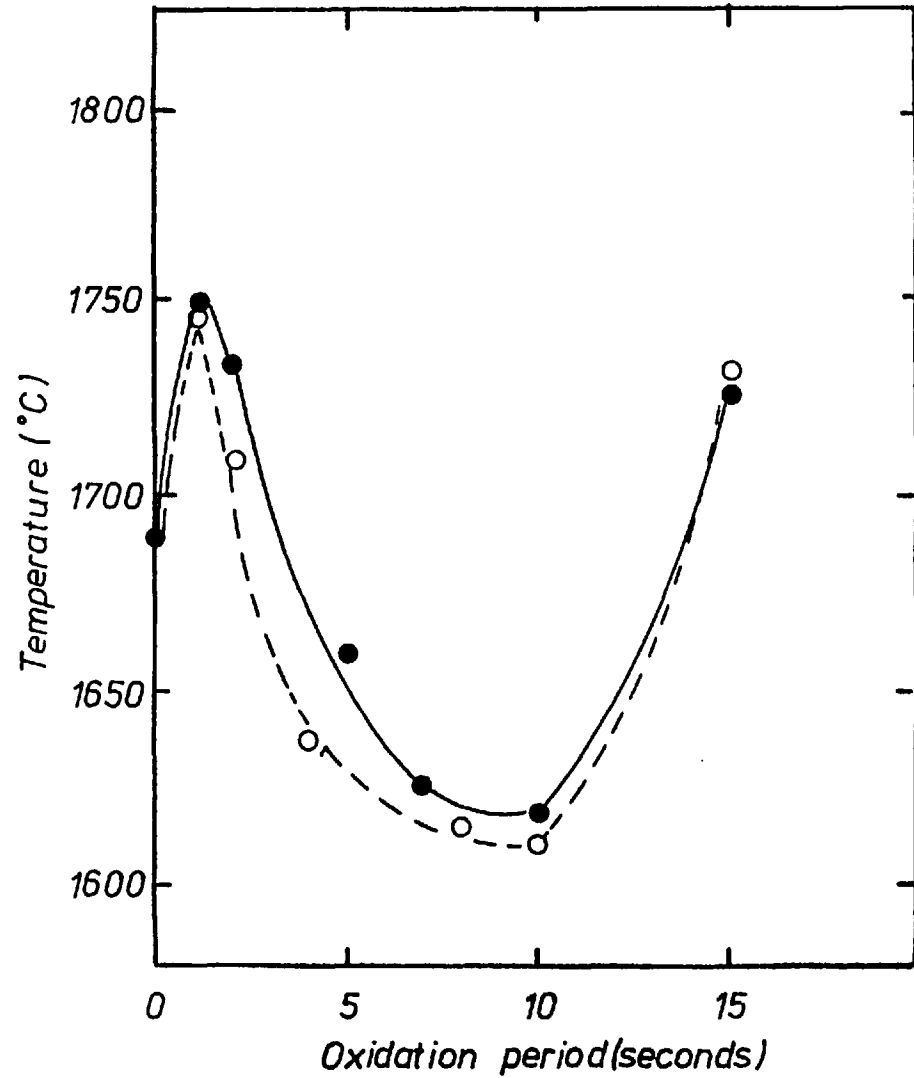


Figure 6.10 Variation in the temperature of the Fe-Si-0.015%P(○) and Fe-Si-0.11%P(●) drops.

was observed in this case, it is reasonable to suppose that if the rate is being controlled by gaseous diffusion, it will be the supply of oxygen to the surface which would be controlling, since under these conditions there would be no counter diffusion of gaseous products. Our calculation on the predicted rate of supply of gaseous oxygen to the surface of the drops has shown that if all the oxygen were used up for oxidation and removal of silicon from the melt, then the rate would be about 4.6×10^{-5} moles.cm⁻².s⁻¹. The measured overall rate of desiliconization was about 1.6×10^{-6} moles.cm⁻².s⁻¹, so that it is evident that the rate of supply of gaseous oxygen to the surface of the drop was not the rate controlling step. Furthermore, the X-ray examination of the slag phase showed appreciable amounts of iron oxide, so that it appears that most of the oxygen supplied to the drop was not used up in oxidising the silicon.

With reference to Figure 6.9., the non-linear behaviour of the desiliconization rates supports the view that transport of silicon to the metal/slag interface and/or the diffusion of silicate ions through the slag phase could have been controlling the rate. The rate of transport of materials within a levitated drop has been shown to be very rapid, hence it seems reasonable to assume that equilibrium between the metal and slag has been achieved and hence the transport of ionic species are more important in determining the rates. In order to discuss the effect of species involved any further, it is necessary to consider

the presence of phosphorus in the metal, so that comparison of the two series of the experiments can be made.

The chemical analysis of the samples containing 0.11 wt.% phosphorus showed no significant loss of phosphorus from the metal (see Table 6.3.), and the X-ray examination of the slag phase confirmed this. Thus the presence of phosphorus in the metal, should not affect the transport of ionic species in the slag phase. Furthermore, the effect of phosphorus in raising the activity coefficient of silicon⁽⁷⁶⁾ appears to be too small to influence the rates to a significant extent, therefore it may be concluded that presence of phosphorus in the alloys plays no role on the kinetics of silicon removal, and the increase in the apparent rate of desiliconization is due to other influencing factors.

The clue to the rate determining step may be in the comparison of the two sets of data obtained which are summarized in Figure 6.9. As can be seen samples containing initially 0.18% [Si], show a smaller incubation period and a greater rate of silicon removal during the first 9 seconds of oxidation than the samples initially containing 0.12 wt.% [Si]. The rates become very similar to one another during the period of 10-15 seconds of the oxidation. Hence it is evident that the rates are influenced by the initial concentration of silicon in the metal. It follows that a higher activity of silicon in the metal leads to a higher activity of silicate ions at the metal/slag

interface, so that the concentration gradient in the slag phase increases and hence the rate of diffusion of silicate ions increases. Since the diffusion of the silicate ions, is accompanied by the counter diffusion of ferric ions, thus it may be considered that the rates of diffusion of ferric ions may be as important. It is thought that the rate of transport of free ferric ions is important during the "incubation" period, where a passive layer of silica is being formed on the surface, and the oxidation is retarded. But once this period has elapsed, not only silicon is being oxidised away, but increasing amounts of iron oxide are also formed. Therefore it is reasonable to consider that the rate of transfer of ferric ions during the course of desiliconization is in excess of the rate of transfer of silicate ions, so that it may be concluded that the rate controlling step is the diffusion of silicate ions in the slag layer.

6-7. CONCLUSIONS

The removal of silicon from liquid iron-silicon alloys by using a stream of He-O₂ was found to be controlled by the transport of silicate ions in the iron-silicate slag phase. In the absence of a basic slag, oxidation of iron-silicon-phosphorus leads to no removal of phosphorus from the metal.

CHAPTER 7

CHAPTER 7
EQUILIBRIA AND KINETICS OF THE DEPHOSPHORIZATION
OF LIQUID IRON

7.1. INTRODUCTION

Phosphorus is generally considered as an undesirable element in steel, except in a very few cases where some phosphorus may be added to aid machinability or to stiffen carbon steel. Thus the desire to reduce as much as possible the content of this element in the steel has been the driving force for a large number of investigations, on the thermodynamics of the systems involved. On the other hand due to the complexity of the systems, little attention has been given to the kinetics of dephosphorization until recently.

The object of this work was to study the kinetics of the dephosphorization reaction, although some consideration was given to the effect of the composition of various slags on the equilibrium phosphorus concentration in the liquid iron, so that a better understanding of the complex reactions occurring between liquid steel and basic slags could be achieved.

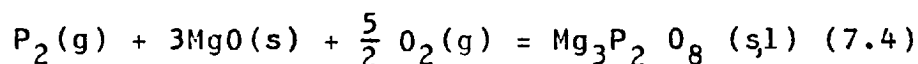
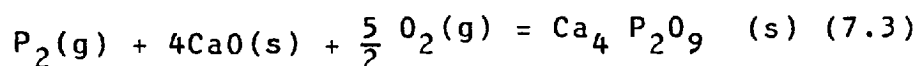
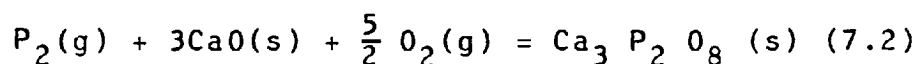
7-2. PREVIOUS WORK

7-2.1. The Equilibrium Distribution of Phosphorus between Liquid Iron and Basic Slags

Since the development of the basic open-hearth steelmaking process, the equilibrium distribution of phosphorus between liquid iron and slags of various compositions has been the subject of numerous investigations. Until the 1940's, in most of the studies, the phosphorus contents of the metal and slag samples taken from industrial furnaces have been determined, and attempts were made to correlate the distribution of phosphorus between the two phases. The interpretations became difficult and varied, due to the complexities of the reactions occurring under such conditions. As a result many workers decided to carry out their investigations under controlled laboratory conditions. The works of Zea,⁽⁷⁷⁾ Winkler and Chipman,⁽⁷⁸⁾ Balajiva and co-workers,⁽⁷⁹⁻⁸¹⁾ and that of Fisher and Vom Ende⁽⁸²⁾ form the basis of the studies made on the subject. These workers tended to use basic slags containing up to eight components, equilibrated the slags with iron-phosphorus alloys at various temperatures, and carried out detailed analyses of the metal and slag samples. Hence the effect of each component on the equilibrium distribution of phosphorus between the liquid metal and the slag had to be considered. Although these workers agreed on the conditions for improvement of dephosphorization: namely lower operating temperatures, high contents of lime

and oxides of iron, manganese, and magnesium, and low silica contents of the slag, but the equilibrium constants arrived at for dephosphorization of the molten iron by such slags were rather varied.

Bookey^(83,84) determined the free energies of formation of tetracalcium, tricalcium, and magnesium phosphates, and hence one of the obstacles, namely lack of knowledge of the equilibrium constants for the following reactions in the absence of other impurities was removed;



Turkdogan and Pearson⁽⁸⁵⁾ and recently Healy⁽⁸⁶⁾ applied this information to the results obtained by others,⁽⁷⁸⁻⁸²⁾ from laboratory studies, and some plant data, and so by adopting the Flood and Grjotheim⁽⁸⁷⁾ theory, obtained correlations expressing the distribution constant of phosphorus between the metal and the slag phase, but they did not take into account the effects due to co-existing liquid phases in their slags.

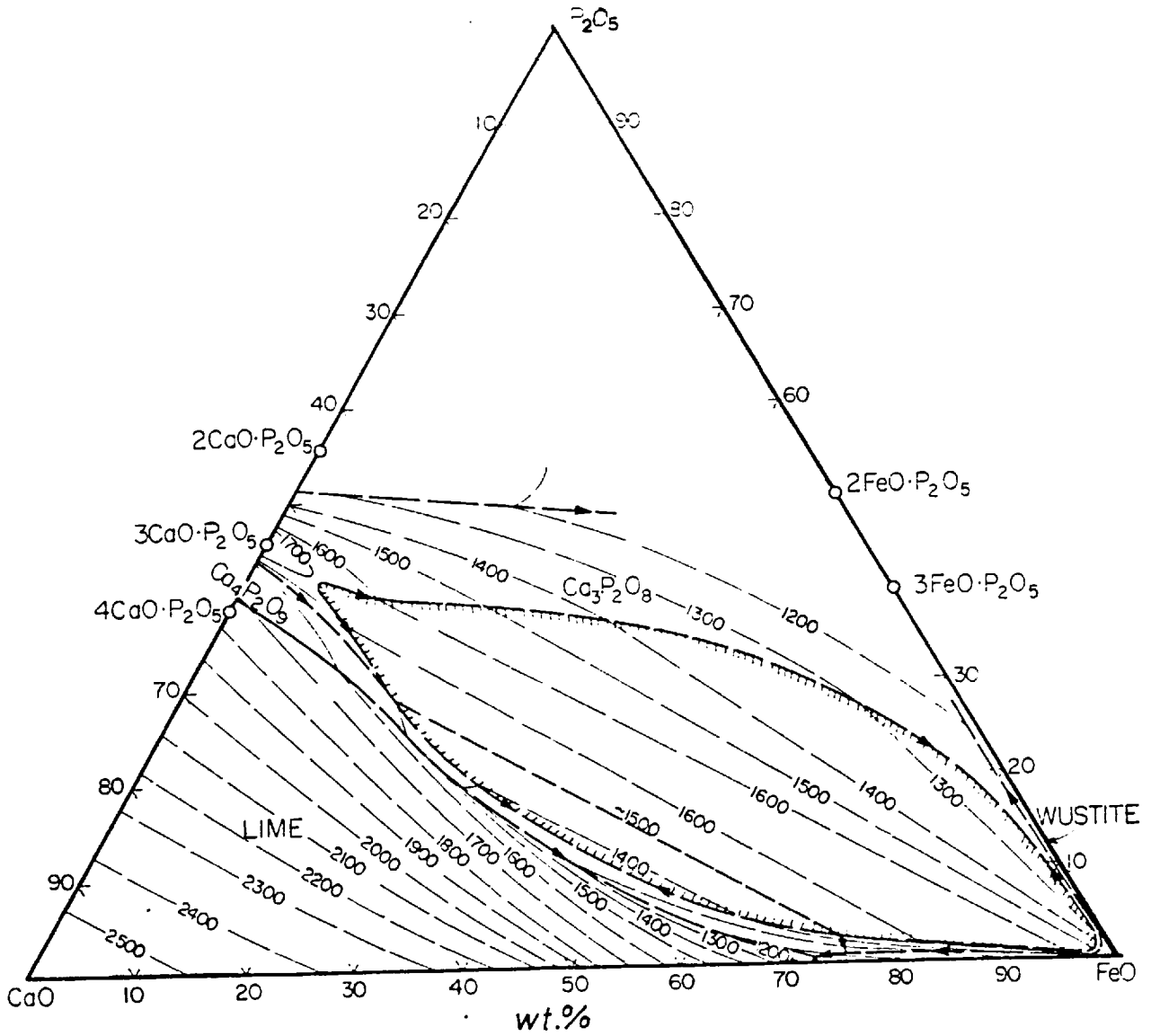


Figure 7.1a Phase relation at liquidus temperature_l in the system $\text{CaO}-\text{P}_2\text{O}_5-\text{FeO}$ in contact with metallic iron.(88-90)

7-2.2 The CaO-P₂O₅ -"FeO" Phase Diagram

From the work of Trömel and co-workers⁽⁸⁸⁻⁹⁰⁾ it is evident that there is a liquid immiscibility area, which dominates the central part of the CaO-P₂O₅-"FeO" system as shown in Figure 7.1a. The diagram shows the complexity of the system due to the high melting points of the phases such as Ca₄P₂O₉ and Ca₃P₂O₈. Therefore as can be seen the miscibility gap is separated by regions of solid and liquid phase (s) at temperatures up to 1670°C. The extent of the miscibility gap tends to decrease as the silica content of the slag increases, and as was shown by Drewes and Olette⁽⁹¹⁾ the liquid miscibility gap will disappear when the silica content of the slag exceeds 15 wt.%. This is illustrated in Figure 7.1b. The effect of the ferric ions in the slag on the extent of the miscibility gap was studied by some workers^(92,93) and it was concluded that the concentration of the ferric ions in the slag has rather little effect on the extent of the immiscibility area. The presence of other oxides such as MgO, MnO, and Al₂O₃ on the phase relations in the system CaO-P₂O₅-"FeO" has not been quantitatively studied, but it is evident from the X-ray and petrographic examinations of the slag samples taken from the melts of Balajiva and co-workers⁽⁷⁹⁻⁸¹⁾ that the presence of such constituents in their slags did not cause the miscibility gap to close.

It follows that although the available correlations for the determination of the phosphorus distribution

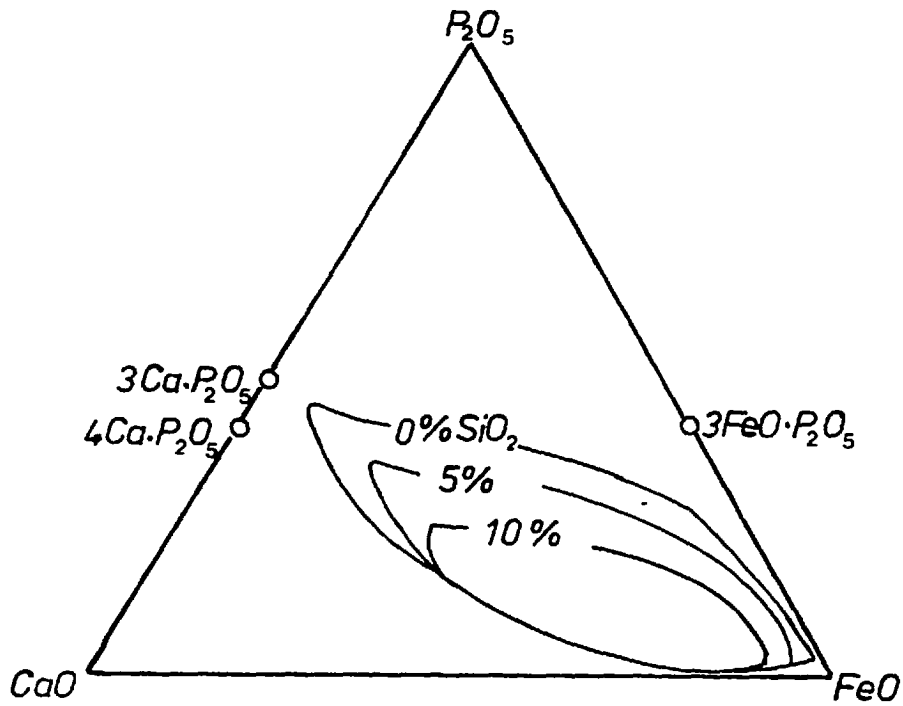


Figure 7.1b Sketch showing the estimated effect of SiO_2 on the liquid miscibility gap in the system $\text{CaO}-\text{P}_2\text{O}_5-\text{FeO}$ in contact with liquid iron(91).

constants in complex slags has been found to be in good agreement with the observed values under some conditions, but these may be rather speculative when applied to simple $\text{CaO-P}_2\text{O}_5\text{-FeO}$ slags. Hence a knowledge of the influence of the miscibility gap on the phosphorus distribution constant is essential, when studies are made on dephosphorization of liquid iron by lime.

7-2.3 Kinetics of Transfer of Phosphorus between Liquid Iron and Basic Slags

The rate of dephosphorization of liquid iron by lime crucibles under atmospheres of gas mixtures of various oxygen potentials has been measured by Kawai et al.⁽⁹⁴⁾ and Yoshii et al.⁽⁹⁵⁾ They found that the rate of dephosphorization increased with increasing oxygen potential of the gas atmosphere, and the temperature of the metal, although the rates were found to be a comparatively low function of the temperature. Kawai et al.⁽⁹⁶⁾ extended their studies in the field by measuring the rates of removal of phosphorus from iron by slags of FeO-CaO of various compositions. They have reported that the rates were dependent on the lime concentration in the slags and also on the phosphorus concentration in the metal. Fuji et al.⁽⁹⁷⁾ found that their rates of dephosphorization were proportional to the metal phosphorus concentrations up to 0.2 wt.%, and that the rates were also dependent on the lime content of

their slags as well as the rate of supply of oxidant to the slag.

The kinetics of transfer of phosphorus between liquid iron alloys and slags containing CaO , FeO , P_2O_5 and SiO_2 were studied by Aratani and Sanbongi;⁽⁹⁸⁾ they have reported that the rate constants for the dephosphorization reaction was found to be one quarter of that for rephosphorization, so that they concluded that the reaction was chemically controlled at the interface. However no detail of the chemical mechanism was given.

Recently some attention has been given to the kinetics of dephosphorization of Fe-C-P alloys in the presence of lime or a basic slag. Kawai et al.⁽⁹⁴⁾ found that when carbon was present in their liquid iron held in lime crucibles, the oxidation of carbon at the metal/gas interface took place preferentially to that of the phosphorus at the metal/crucible interface, until very low carbon concentrations (~ 0.01 wt.%) were reached. On the other hand Fuji et al.⁽⁹⁷⁾ used magnesia crucibles and added the lime to the surface of the liquid Fe-C-P alloy prior to the commencement of the oxidation by an oxygen jet blown on the surface of their melts. They have reported that simultaneous oxidation and removal of carbon and phosphorus was achieved at carbon concentrations of about 1.5 wt.% in the absence of iron oxide in their slag phase. Their rates of

7-3. EXPERIMENTAL TECHNIQUES

7-3.1. Rate of Establishing Equilibrium

Since some of the data gathered in this investigation were to be treated as equilibrium data, it is clear that it was necessary to ensure that equilibrium existed at the time of quenching the samples. To arrive at the time required for achievement of equilibrium, capsules of Fe-P alloy with 30 mg of slags "B" or "C" were levitated, melted and kept molten in a stream of He/Ar for various periods, then quenched, weighed and analysed for phosphorus in the metal. These results are shown in Tables 7.1 and 7.2. It will be noted that slag/metal equilibrium is achieved within 15 seconds.

7-3.2. Equilibrium Distribution of Phosphorus between Metal and Basic Slags

Capsules of either spec-pure iron or iron-phosphorus alloys, weighing about 1 gram were filled with the required amounts of the pre-melted slags, or pre-fired calcium phosphate, or lime, and then levitated in a stream of He/Ar till melting occurred, the temperature of the samples were then adjusted to the required value, and oxidation of the samples in streams of He-O₂ gas mixtures flowing at pre-adjusted rates were carried out. The samples were then allowed to react and reach equilibrium at a constant temperature, for a period of 3 or 10 minutes.

They were then quenched, weighed and analysed for phosphorus in the metal. In few cases the entire metal and slag were analysed for phosphorus, in order to check the mass balance of the phosphorus in the experiments. The mass balances were found to be satisfactory.

7-3.3 Rates of Transfer of Phosphorus between Liquid Iron and Basic Slags

In determining the kinetics of the phosphorus reaction two methods were used, namely levitation and free fall.

Levitation technique

This technique was used when studies of reaction periods between 1 to 50 seconds were made. In most experiments, capsules of Fe-P or Fe-C-P alloys containing known amounts of a basic slag were used, and in other series approximately 20 mg of lime or 35 mg of a basic slag was attached to the levitated samples, so that the interfacial area between the two phases could be increased. These samples were oxidised for a pre-determined period, quenched and analysed for phosphorus or carbon in the metal.

Free fall technique

This technique was employed for studying the rates of some rapid reactions. Two methods of slag addition

were used. In studying the rates of rephosphorization of iron drops by $\text{CaO-P}_2\text{O}_5\text{-FeO}$ slags, capsules of spec-pure iron containing known amounts of calcium phosphate (previously dried to constant weight) were levitated and melted in a stream of He/Ar, and on reaching chemical equilibrium between the two phases, the drops were then allowed to fall freely through a column of Ar or O_2 before being quenched into foils. In other experiments where attempts were made to measure the rates of dephosphorization of Fe-P alloys by $\text{Fe}_2\text{O}_3\text{-CaO}$ mixtures of various compositions, the samples were levitated and melted in a stream of He/Ar and on reaching the required temperature were allowed to fall through the membrane (separating the reaction column from levitation cell) and into the column of Ar before quenching. A thin layer of powdered slag was placed on the membrane prior to each run, so that as the drop contacted the membrane it would pick up some of the powdered slag and reaction could proceed at the metal/slag interface during the free fall period.

7-4. RESULTS

TABLE 7.1. Attainment of equilibrium between Fe-P and a basic slag in a stream of He/Ar at 1650°C

Alloy: Fe-0.12% [P]

Slag: \hat{C}'' (63% FeO-20%CaO-17% Fe₂O₃)

Run	initial mass of capsule (gram)	initial mass of slag (gram)	initial temp (°C)	Reaction period (sec)	Steady temp. (°C)	Final mass of metal & slag (gram)	wt.% [P]
PR125	1.0780	0.0300	1540	15	1650	1.1070	0.064
PR126	1.1114	0.0306	1540	30	1655	1.1420	0.063
PR127	1.0986	0.0293	1540	60	1660	1.1277	0.067
PR128	1.0426	0.0307	1540	60	1640	1.0728	0.054
PR129	1.1113	0.0292	1540	100	1655	1.1397	0.060
PR130	1.1087	0.0294	1540	200	1650	1.1329	0.056
PR131	1.0986	0.0283	1540	240	1645	1.1246	0.060
PR132	1.1014	0.0293	1540	360	1650	1.1338	0.060
PR133	1.0470	0.0341	1540	420	1650	1.0786	0.062
PR134	1.1064	0.0296	1540	500	1655	1.1329	0.062
PR135	1.1017	0.0283	1540	900	1650	1.1271	0.060

TABLE 7.2. Attainment of equilibrium between Fe-P and a basic slag in a stream of He/Ar at 1600°C
 Alloy: Fe-0.12%P, Slag: B (77% Fe₂O₃-20%CaO-3%FeO), Reaction atmosphere: He/Ar (PO₂ ~ 10⁻⁶ atm).

Run	initial mass of capsule (gram)	initial mass of slag (gram)	initial temp. (°C)	Reaction period (sec)	Steady temp. (°C)	Final mass of metal & slag (gram)	wt.% [P]
PR136	1.1194	0.0310	1540	15	1610	1.1368	0.037
PR137	1.1016	0.0328	1540	15	1600	1.1338	0.035
PR138	1.1274	0.0295	1540	25	1605	1.1569	0.027
PR139	1.1211	0.0282	1540	55	1610	1.1404	0.041
PR140	1.1013	0.0292	1540	110	1600	1.1307	0.038
PR141	1.1210	0.0324	1540	360	1615	1.1500	0.042
PR142	1.1260	0.0282	1540	600	1605	1.1535	0.030
PR143	1.1196	0.0323	1540	660	1610	1.1518	0.032

slag composition*		
wt.% (FeO)	wt.% (P ₂ O ₅)	wt.% (CaO)
69.8	7.6	22.6
71.2	7.0	21.9
66.7	9.9	23.4
76.0	6.5	17.5
70.5	7.9	21.6
72.3	6.0	21.6
65.5	10.7	23.8
69.7	7.9	22.4

*calculated from mass balance.

TABLE 7.3.

Alloy: Fe-0.23%O-0.12%P, Slag: CaO, oxidising gas: He-5%O₂ (5 l.min⁻¹), Reaction atmosphere He.

Expected rate of oxygen pick up during the oxidation period - 1.34 mg.s⁻¹

Run	initial mass of capsule (gram)	initial mass of time (gram)	oxidation period (sec.)	Reaction period (min)	steady temp. (°C)	Final mass of metal & slag (gram)	wt.% [P]	expected mass of O ₂ supplied (mg)	wt.% (FeO)	wt.% (P ₂ O ₅)	wt.% (CaO)	Log% (CaO)	Log K _p '
PR143	1.2733	0.0287	0	10	1600	1.2989	0.018	0	5.8	9.0	85.2	1.93	0.63
PR144	1.2470	0.0290	5	10	1600	1.2793	0.001	6.7	46.7	5.6	47.7	1.68	-1.60
PR145	1.2179	0.0292	7	10	1600	1.2532	0.004	9.4	55.5	4.4	40.1	1.60	-3.28
PR146	1.2695	0.0291	9	10	1600	1.3079	0.012	12.1	62.0	3.7	34.3	1.54	-4.55
PR147	1.2513	0.0291	12	10	1600	1.2938	0.017	16.1	68.5	2.9	28.6	1.46	-5.18
PR148	1.2176	0.0301	15	10	1600	1.2649	0.020	20.1	72.7	2.3	25.0	1.40	-5.55
PR149	1.2460	0.0292	20	10	1600	1.2991	0.035	26.8	78.9	1.7	19.4	1.29	-6.34
PR150	1.2418	0.0290	25	10	1600	1.2848*	0.052	33.5*	82.7	1.2	16.1	1.21	-6.94
PR151	1.1638	0.0272	25	10	1600	1.2222	0.109	33.5	84.6	0.3	15.2	1.18	-8.24
PR152	1.1070	0.0284	25	10	1600	1.1650	0.099	33.5	83.93	0.44	15.63	1.19	-7.97

TABLE 7.4

Alloy: Spec-pure iron, Slag: 56.55%CaO-43.45%P₂O₅, oxidising gas: He-5%O₂ (5l/min), Reaction gas He.

Expected rate of oxygen pick up during the oxidation period = 1.34 mg. s⁻¹

Run	initial mass of capsule (gram)	initial mass of slag (gram)	oxidation period (sec)	Reaction period (Min.)	steady temp. (°C)	Final mass of metal & slag (gram)	wt.% [P]	expected mass of O ₂ supplied (mg)	wt.% (FeO)	wt.% (P ₂ O ₅)	wt.% (CaO)	Log% (CaO)	Log K _p '
PR153	1.0034	0.0218	1	10	1605	1.0201	0.039	1.34	19.7	32.9	47.4	1.68	-2.14
PR154	1.0034	0.0214	2	10	1610	1.0219	0.038	2.68	35.1	26.6	38.2	1.58	-3.46
PR155	0.9916	0.0195	5	10	1610	1.0123	0.056	6.70	60.9	15.5	23.6	1.37	-5.23
PR156	1.0379	0.0124	5	10	1605	1.0506	0.061	6.70	76.9	8.1	15.1	1.18	-6.09
PR157	1.0647	0.0119	7	10	1600	1.0790	0.078	9.38	82.9	6.0	11.4	1.06	-6.59
PR158	1.0266	0.0115	9	10	1605	1.0443	0.084	12.06	86.4	4.4	9.2	0.96	-6.89
PR159	1.0373	0.0102	12	10	1600	1.0562	0.094	16.08	90.1	3.3	6.6	0.82	-7.20

TABLE 7.5 Equilibrium studies on Fe-O-P and (CaF₂-CaO-"FeO"-P₂O₅) slag at 1600°C in a stream of Helium

Alloy: Fe-0.23%O-0.12%P

Slag: D (84% CaF₂-16%CaO)

Oxidising gas: He-5%O₂ (flowing at 5.0 l.min⁻¹)

Run	mass of capsule (gram)	mass of slag (gram)	oxidation period (sec.)	reaction period (min)	steady temp. (°C)	final mass of metal & slag (gram)	wt.% [P]
PR160	1.1628	0.0289	0	3	1600	1.1906	0.005
PR161	1.1561	0.0256	5	3	1590	1.1871	0.016
PR162	1.1467	0.0263	7	3	1605	1.1811	0.017
PR163	1.1560	0.0319	10	3	1605	1.1999	0.021
PR164	1.1366	0.0286	15	3	1600	1.1833	0.036
PR165	1.1532	0.0293	20	3	1610	1.2084	0.030
PR166	1.1625	0.0300	25	3	1605	1.2248	0.025

Comments: The expected rate of oxygen pick up = 1.34 mg.s⁻¹ during the oxidation period.

TABLE 7.6. Oxidation of Fe-P with approximately 20 mg of lime attached in a stream He-5%O₂

Alloy: Fe-0.52%P (prepared under a forming gas atmosphere)

Slag: Fine powdered lime (previously fired at 1300°C)

Oxidising gas: He-5%O₂ (flowing at 0.75 l.min⁻¹)

Run	mass of sample (gram)	initial temp. (°C)	Reaction period (sec.)	Final temp. (°C)	wt.% [P]
PR167	0.8967	1605	4	1675	0.465
PR168	0.9115	1600	7	1685	0.461
PR169	0.9051	1600	9	1700	0.432
PR170	0.8911	1605	10	1710	0.4210
PR171	0.9012	1600	10	1705	0.405
PR172	0.9132	1600	14	1720	0.382

TABLE 7.7. Oxidation of Fe-P with approximately 20 mg of lime attached in a stream of He-5%O₂

Alloy: Fe-0-12% P (prepared under a forming gas atmosphere)

Slag: Fine powdered lime (previously fired at 1300°C)

Oxidising gas: He-5% (flowing at 0.75 l.min⁻¹)

Run	mass of sample (gram)	initial temp. (°C)	Reaction period (sec.)	Final temp. (°C)	wt.% [P]
PR174	0.8269	1600	5	1670	0.046
PR175	0.8484	1600	10	1700	0.027
PR176	0.8765	1600	20	1700	0.019
PR177	0.8818	1600	35	1780	0.020
PR178	0.8504	1600	40	1780	0.017
PR179	0.8668	1600	50	1780	0.007

TABLE 7.8. Oxidation of Fe-P with approximately 20 mg of lime attached in a stream of He-50%O₂

Alloy: Fe-0.12%P (prepared under an atmosphere of forming gas)

Slag: Fine powdered lime (previously calcined at 1300°C)

Oxidising gas: He-50%O₂ (flowing at 2.0 l.min⁻¹)

Run	mass of sample (gram)	initial temp. (°C)	Reaction period (sec.)	final temp. (°C)	wt.% [P]
PR180	0.8179	1550	1	1790	0.076
PR181	0.8130	1550	1	1790	0.075
PR182	0.7634	1550	2	1800	0.005
PR183	0.7950	1550	2	1800+	0.009
PR184	0.8171	1550	2.5	1800+	0.014
PR185	0.8680	1550	3	1800+	0.034
PR186	0.8468	1550	3	1800+	0.038
PR187	0.9586	1550	3.5	1800+	0.081
PR188	0.7227	1550	4	1800+	0.098

TABLE 7.9. Oxidation of Fe-P with about 20 mg of slag "A" in a stream of He-33%O₂

Alloy: Fe-0.12%P (prepared under an atmosphere of forming gas)

Slag: 38.6% CaO-46%CaF₂-15.4%SiO₂

Oxidizing gas: He-33%O₂ (flowing at 0.75 l.min⁻¹)

Run	mass of capsule (gram)	mass of slag (gram)	initial temp. (+15) (°C)	oxidation period (sec.)	final temp. (+15) (°C)	final mass of metal & slag (gram)	wt.% [P]
PR190	0.7166	0.0181	1600	2	1660	0.7370	0.012
PR191	0.7513	0.0148	1600	2	1660	0.7558	0.030
PR193	0.7515	0.0183	1600	4	1680	0.7125	0.001
PR194	0.6613	0.0219	1600	4	1670	0.6923	0.010
PR195	0.6713	0.0200	1600	6	1740	0.7001	0.010
PR196	0.5975	0.0193	1600	6	1750	0.6264	0.005
PR197	0.7200	0.0183	1600	6	1740	0.7514	0.004
PR198	0.5936	0.0188	1600	8	1800+	0.6273	0.001
PR199	0.6102	0.0196	1600	8	1800+	0.6505	0.007
PR200	0.7160	0.0194	1600	8	1800+	0.7654	0.038
PR201	0.6920	0.0138	1600	10	1800+	0.7289	0.058
PR202	0.6567	0.0168	1600	10	1800+	0.6932	0.038

TABLE 7.10 Oxidation of Fe-P with approximately 35 mg of slag
"A" attached in a stream of He- O_2

Alloy: Fe-0.12%P (prepared under an atmosphere of forming gas)

Slag: 38.6% CaO-46%CaF₂-15.4%SiO₂

Oxidising gas: He-50% O_2 (flowing at 2.0 l.min⁻¹)

Run	mass of sample (gram)	initial temp. (°C)	Reaction period (sec.)	Final temp. (°C)	wt.% [P]
PR203	0.8590	1550	1	1730	0.007
PR204	0.8370	1550	2	1780	0.008
PR205	0.8910	1550	2.5	1800+	0.014
PR206	0.8510	1550	3	1800+	0.0144

TABLE 7.11 Kinetics of rephosphorization of Fe-P drops by
CaO-P₂O₅-FeO slags at 1600°C

"Alloy": spec-pure iron.

Slag: 56.55%CaO-43.45%P₂O₅

Oxidising gas: O₂

Run	mass of capsule (gram)	mass of slag (gram)	initial temp. (°C)	free fall height (m)	oxidation period (sec.)	wt.% [P]
PR207	1.0293	0.0093	1605	-	0	0.021
PR208	0.9972	0.0113	1605	-	0	0.027
PR209	1.0222	0.0139	1600	-	0	0.035
PR210	1.0285	0.0158	1595	-	0	0.039
PR211	1.0152	0.0178	1595	-	0	0.041
PR212	0.9928	0.0205	1590	-	0	0.047
PR213	1.0555	0.238	1600	-	0	0.052
PR214	1.0497	0.0124	1600	0.42	0.170	0.040
PR215	1.0160	0.0131	1605	0.42	0.170	0.042
PR216	1.0261	0.0140	1610	0.42	0.170	0.045
PR217	1.0677	0.0149	1605	0.42	0.170	0.046
PR218	0.9542	0.0158	1590	0.42	0.170	0.052
PR219	1.0769	0.0126	1595	0.70	0.252	0.044
PR220	1.0213	0.0135	1605	0.70	0.252	0.051
PR221	1.0387	0.0144	1605	0.70	0.252	0.053
PR223	1.0636	0.0149	1600	0.70	0.252	0.051
PR224	1.0387	0.0159	1605	0.70	0.252	0.055
PR225	0.8956	0.0195	1590	0.70	0.252	0.063

- Comments:
1. initial free fall height before entering the oxidation column was about 14 cm.
 2. The delay time due to the membranes was about 0.002 sec.
 3. On quenching the samples, the slag separated out into a blackish liquid phase (probably iron oxide rich phase) and a brownish solid phase (phosphate phase).

TABLE 7.12. Oxidation of levitated drops of Fe-C-P with about 27 mg of slag "E" in a stream of oxygen.

Alloy: Fe-4.13%C-0.11%P

Slag: 50%CaO-50%Al₂O₃

Oxidising gas: O₂ (flowing at 5.0 l. min⁻¹)

Run	mass of capsule (gram)	mass of slag (gram)	initial temp. (°C)	levitation period (min)	oxidation period (sec.)	final temp. (°C)	wt.% [C]	wt.% [P]
PR226	1.2277	0.0214	1600	10	0	1600	4.07	-
PR227	1.1450	0.0316	1520	10	0	1535	4.04	-
PR228	1.1281	0.0292	1600	10	0	1600	-	0.097
PR229	1.2715	0.0269	1600	10	0	1590	-	0.103
PR230	1.1466	0.0236	1590	3	1	1710	3.82	-
PR231	1.2263	0.0304	1615	3	1	1730	3.73	-
PR232	1.1327	0.0223	1570	3	1	1700	-	0.099
PR233	1.1783	0.0289	1620	3	1	1740	-	0.094
PR234	1.2117	0.0269	1575	3	2	1800+	-	0.092
PR235	1.1234	0.0254	1520	3	2	1810	-	0.106
PR236	1.1984	0.0310	1570	3	2	1800	3.0	-
PR237	1.1421	0.0271	1550	3	2	1800+	1.4	-

- Comments: 1. When the samples and the slags were levitated in a stream of Ar/He for periods longer than 5 minutes, reduction of Al₂O₃ was accompanied by generation of CO(g) at the metal/slag interlace.
2. On oxidation of these drops spreading of the slag film on the surface was followed by ejection of particles (metal and slag) from the surface within half a second.

TABLE 7.13 Oxidation of levitated drops of Fe-C-P with about 28 mg of slag D in a stream of oxygen.

Alloy: Fe-4.13%C-0.11%P.

Slag: 16%CaO-84%CaF₂.

Oxidising gas: O₂ (flowing at 5.0 l, min⁻¹)

Run	mass of capsule (gram)	mass of slag (gram)	initial temp. (°C)	levitation period (min.)	oxidation period (sec.)	final temp. (°C)	wt.% [C]	wt.% [P]
PR238	1.0593	0.0265	1500	5	0	1510	4.10	-
PR239	1.0160	0.0296	1500	5	0	1515	4.16	-
PR240	1.0848	0.0308	1550	5	0	1550	-	0.11
PR241	1.1014	0.0291	1500	5	2	1765	-	0.104
PR242	1.1058	0.0279	1520	5	2	1770	-	0.11
PR243	1.1212	0.0275	1520	5	2	1780	2.33	-
PR244	1.0666	0.000	1490	6	2	1710	3.19	-

- Comments:
1. No CO(g) evolution was observed at the metal/slag interface, when drops were levitated in streams of Ar/He.
 2. On oxidising the samples, ejection of particles from the surface commenced after about 0.5 seconds. This was then followed by a vigorous carbon boil. Once the oxidation period had elapsed, the ejection of particles from the surface continued for a further 1.5 seconds.
 3. After the "carbon-boil" had ceased, a portion of the slag phase was still attached to the drops.

TABLE 7.14. Kinetics of dephosphorization of Fe-P drops by CaO-Fe₂O₃ slags at 1600°C.

Alloy: Fe-0.23%O-0.12%P.

Slags: B (77% Fe₂O₃ - 20% CaO-3%"FeO").

F (70%Fe₂O₃ - 30% CaO).

G (61% Fe₂O₃ - 39% CaO).

Amount of slag picked up in each run: ~15 mg.

Run	Mass of sample (gram)	initial temp. (°C)	slag	Reaction period (sec.)	wt.% [P]
PR245	1.2031	1600	B	0.252	0.121
PR246	1.1561	1605	B	0.252	0.119
PR247	1.1673	1610	B	0.252	0.116
PR248	1.1713	1605	F	0.170	0.118
PR249	1.1816	1590	F	0.170	0.123
PR250	1.1632	1600	F	0.170	0.116
PR251	1.1931	1610	F	0.252	0.122
PR252	1.1312	1610	F	0.252	0.119
PR253	1.2010	1600	F	0.252	0.120
PR254	1.1871	1595	G	0.252	0.124
PR255	1.1651	1595	G	0.252	0.116
PR256	1.1431	1600	G	0.252	0.115

7-5. INTERPRETATION OF THE DATA

In order to investigate the distribution of phosphorus between the metal and the slag, a knowledge of the composition of the slag is necessary. Although chemical analysis of the slags would normally be the most conventional and reliable method of obtaining such information, due to the difficulties and errors arising when such methods of analysis are carried out on small quantities of slags, which may separate into two or more phases, it was decided to calculate the slag composition by mass balance on the constituents involved. Under these experimental conditions it is possible to determine the quantities of lime and phosphorus in the slags fairly accurately provided the initial quantities of each one is known. In determining the iron oxide content of the slag, when oxidation had been carried out, the rate of adsorption of oxygen by the metal from the oxygen bearing gas stream had to be evaluated. This was achieved by a series of calibration runs, where spec-pure iron samples weighing about 1 gram, were first deoxidised in a stream of He-N₂-H₂, then weighed, oxidised and re-weighed. The losses in weight by vaporization were also determined by reducing the entire metal and the oxide in a stream of He-N₂-H₂. The difference in weights were reproducible within ±6% and gave a fairly accurate linear rate of oxygen pick up.

In calculating the slag composition some knowledge of the activity of iron oxide in the slags is necessary

in order to determine the amount of oxygen dissolved in the metal, and hence the amount of iron oxide in the slag. Thus the activity of iron oxide was initially estimated and an approximate composition of the slag was calculated. This calculated composition was used in conjunction with the results of Bookey et al.⁽⁸⁴⁾, or Trömel et al.⁽⁸⁹⁾ to arrive at a closer value of the activity of iron oxide. The latter procedure was repeated several times so that a better estimate of the activity of iron oxide could be obtained.

7-6. DISCUSSION

7-6.1. Rate of Attainment of Chemical Equilibrium

The attainment of chemical equilibrium between levitated drops of metal and a thin layer of the attached slag is expected to be rather rapid due to high mass transfer rates brought about by the electromagnetic field as well as the relatively large interfacial area between the metal and the slag phase (i.e. about one third of the surface area of the metal drop is in contact with the slag). The results obtained on the rate of establishing equilibrium are summarized in Tables 7.1 and 7.2 and Figure 7.2. As noted above chemical equilibrium had been achieved between the two phases in less than 15 seconds. Knight and Perkins⁽¹⁰¹⁾ found that equilibrium was achieved in about 30 seconds, when larger amounts of slag (greater than 30 mg) were used.

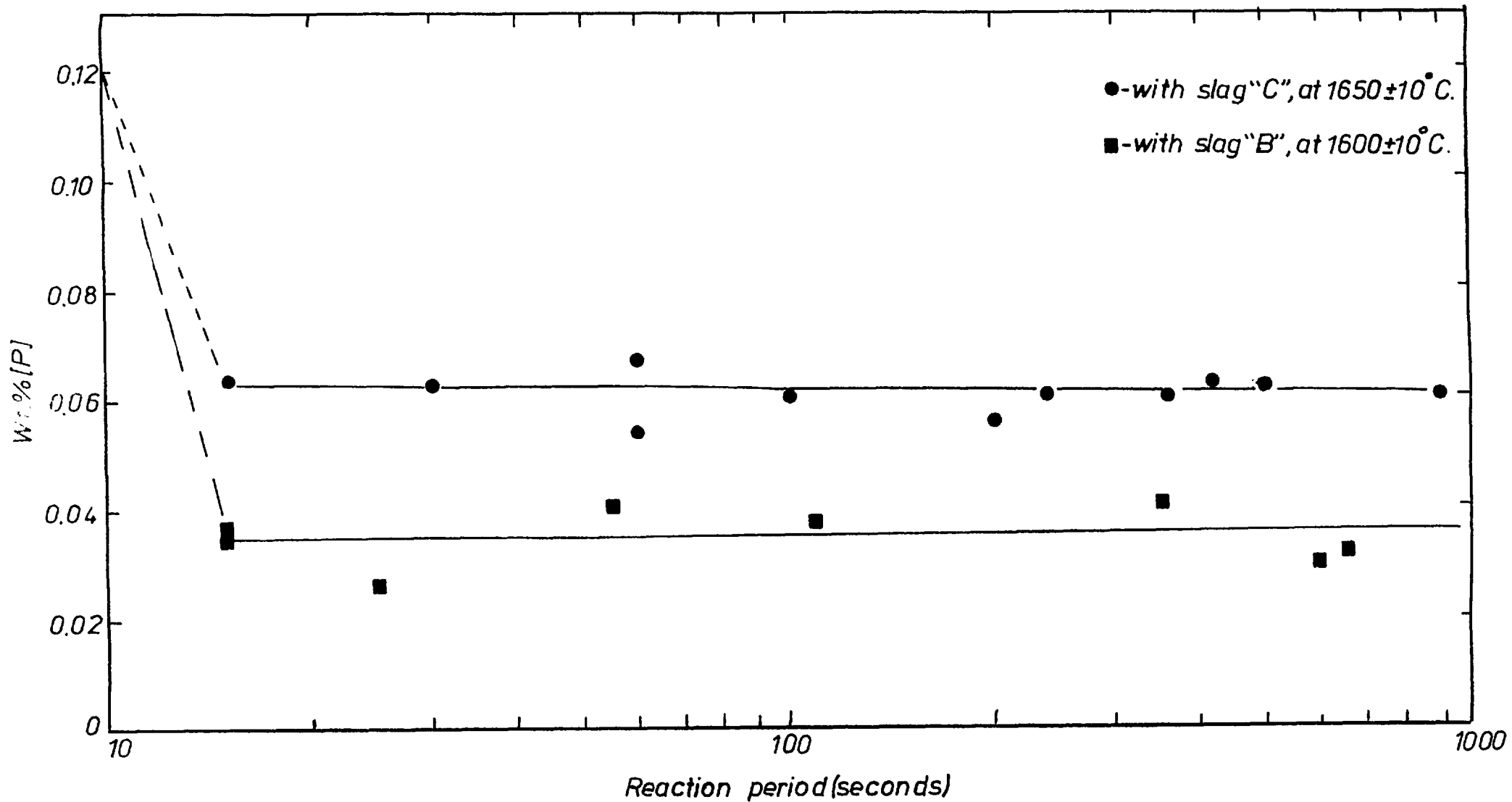


Figure 7.2 Rate of approach of equilibrium between levitated drops of Fe-P and $\text{CaO-P}_2\text{O}_5\text{-FeO}$ slag.

The main doubt about a true attainment of chemical equilibrium arises from the temperature difference between the metal and slag, since the slags are not inductively heated, and receive their heat from the metal at the metal/slag interface. Since the heat losses by radiation from the slag is greater than that of the metal and the thermal conductivity of the slag is rather poor, a temperature gradient is expected to exist in the slag phase, which may cause a concentration gradient across it. However since the present work was undertaken to estimate the effect of the miscibility gap on the distribution of phosphorus between the metal and the slag, it was decided, as an approximation, to assume that the thermal equilibrium between the metal and the slag phases had been attained.

7-6.2. The Distribution of Phosphorus between the Metal and Slag

With reference to points a-d in Figure 7.4 and 7.5 it is evident that the phosphorus content of the metal reaches a minimum value (0.001 wt.%) when the slag phase is very rich in lime and in liquid. The progressive enrichment of the slag with iron oxide leads to a lowering of the activity of lime and subsequently the phosphate capacity of the slags fall, resulting in reversion of phosphorus from the slag to the metal. Further oxidation and hence enrichment of the slag with iron oxide has led to further reversion of phosphorus, but as

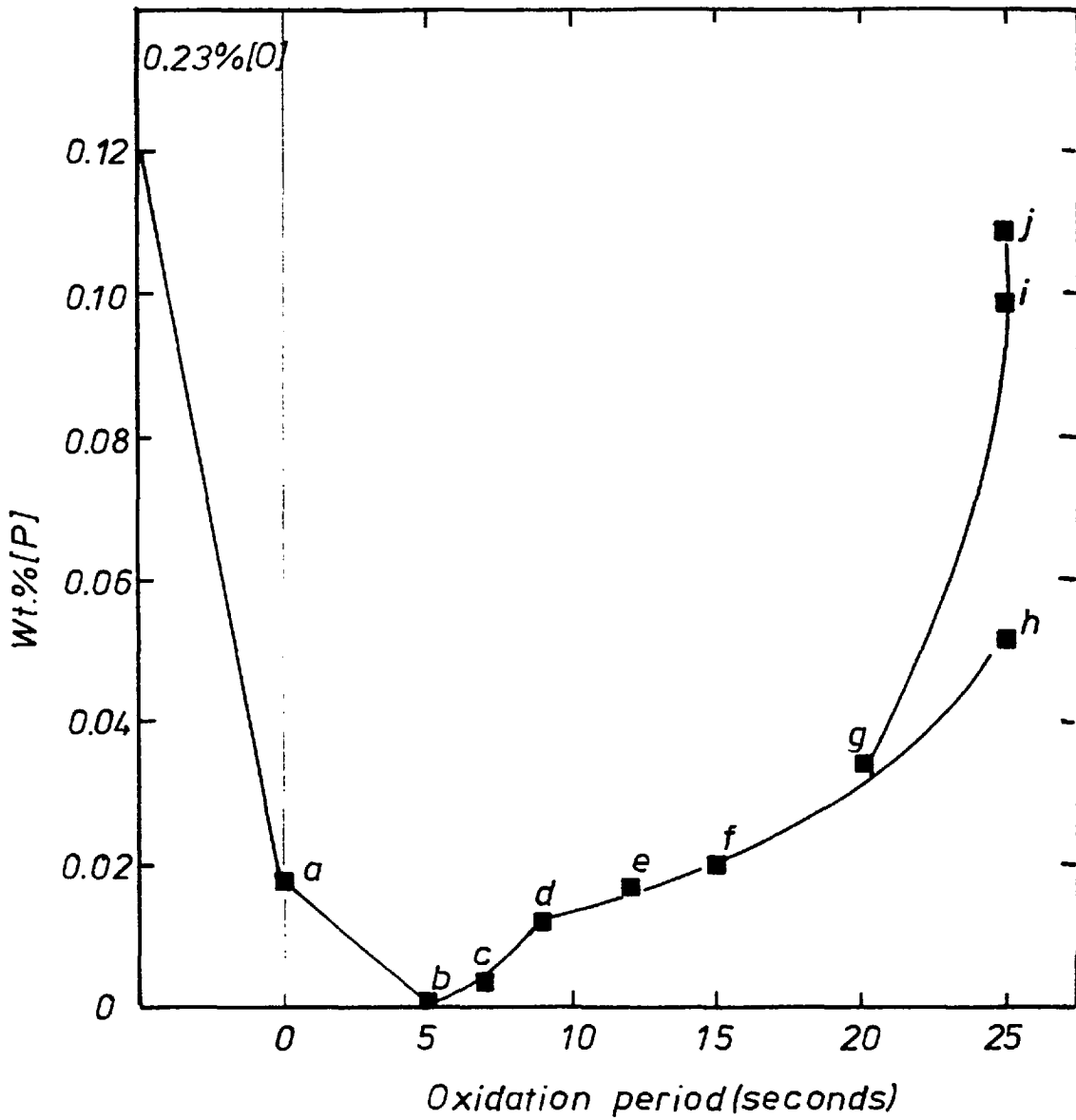
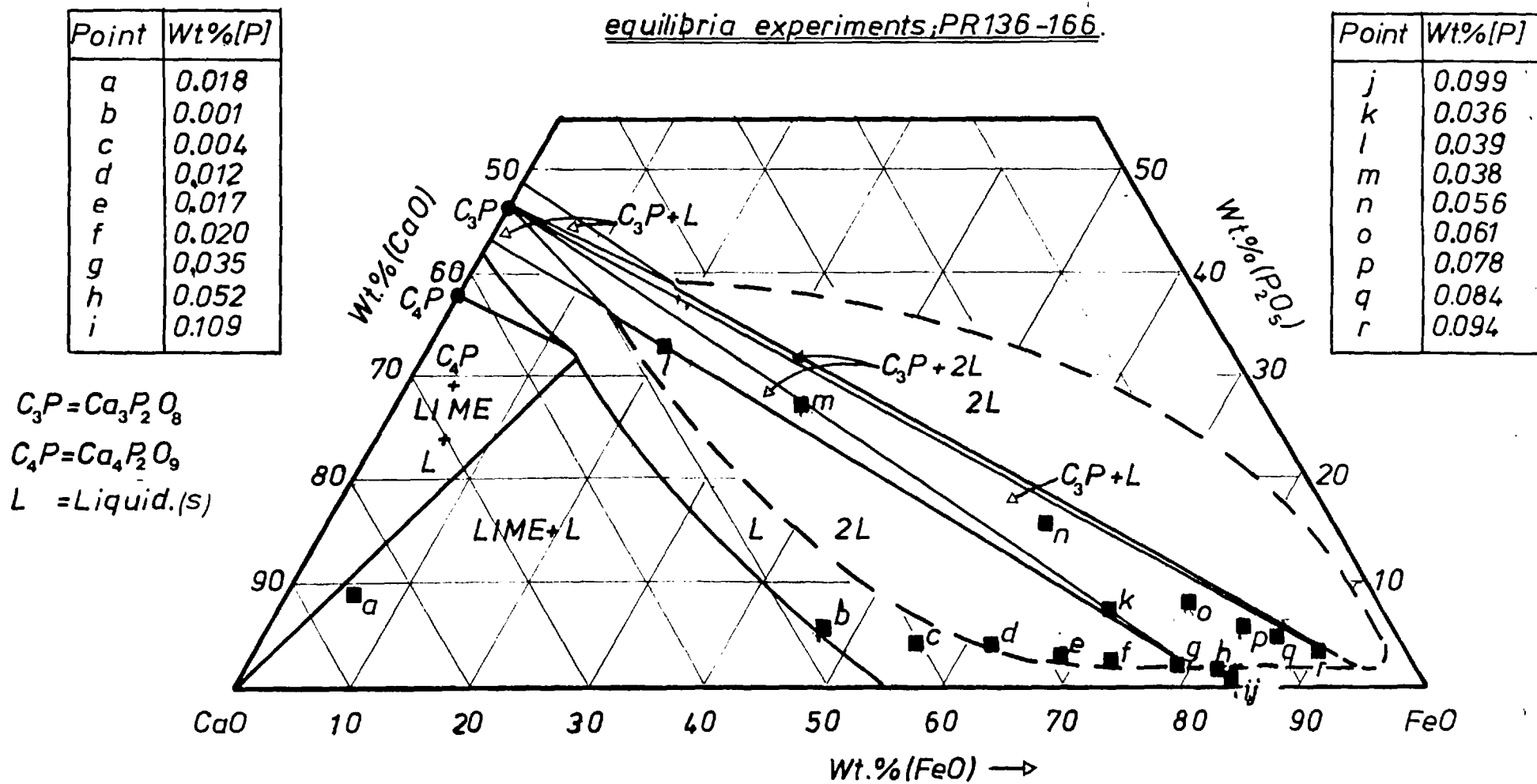


Figure 7.4 Variation of the phosphorus concentration in liquid iron drops in equilibrium with $\text{CaO-P}_2\text{O}_5\text{-FeO}$ slags at "1600 °C"

Figure 7.5 The metal and slag compositions of the equilibria experiments; PR136-166.



is shown by points d-g in Figure 7.5, the slag composition enters the two liquid phase region of the miscibility gap. The question arises as to what extent does the separation of the slag into two liquid phases influence the reversion. In order to show the effect of the miscibility gap on the phosphate capacity of the slag it was decided to plot the phosphorus distribution constant (K_p') against the concentration of the lime in the slag.

$$\text{where } K_p' = \frac{\%(\text{P}_2\text{O}_5)}{\% [\text{P}]^2 \times \%(\text{FeO})^5} \quad (7.10)$$

It is evident from Figure 7.6, that as the slag composition enters the miscibility gap the slope of the line becomes less steep i.e. for a given lime concentration the distribution constant becomes greater if the slag composition lies within the two liquid phase region of the miscibility gap rather than in the single phase region, hence less reversion occurs. This is because once the slag separates into the two liquid phases, the activities of the phosphate and iron oxide may change considerably, and exhibit the activities of these constituents in the respective liquid phases, which are in equilibrium with one another. Thus the ratio of $a_{(\text{P}_2\text{O}_5)}/a_{(\text{FeO})}^5$ is very different to that of a single phase slag of similar composition. Further evidence to support the above reasoning arises from the comparison of

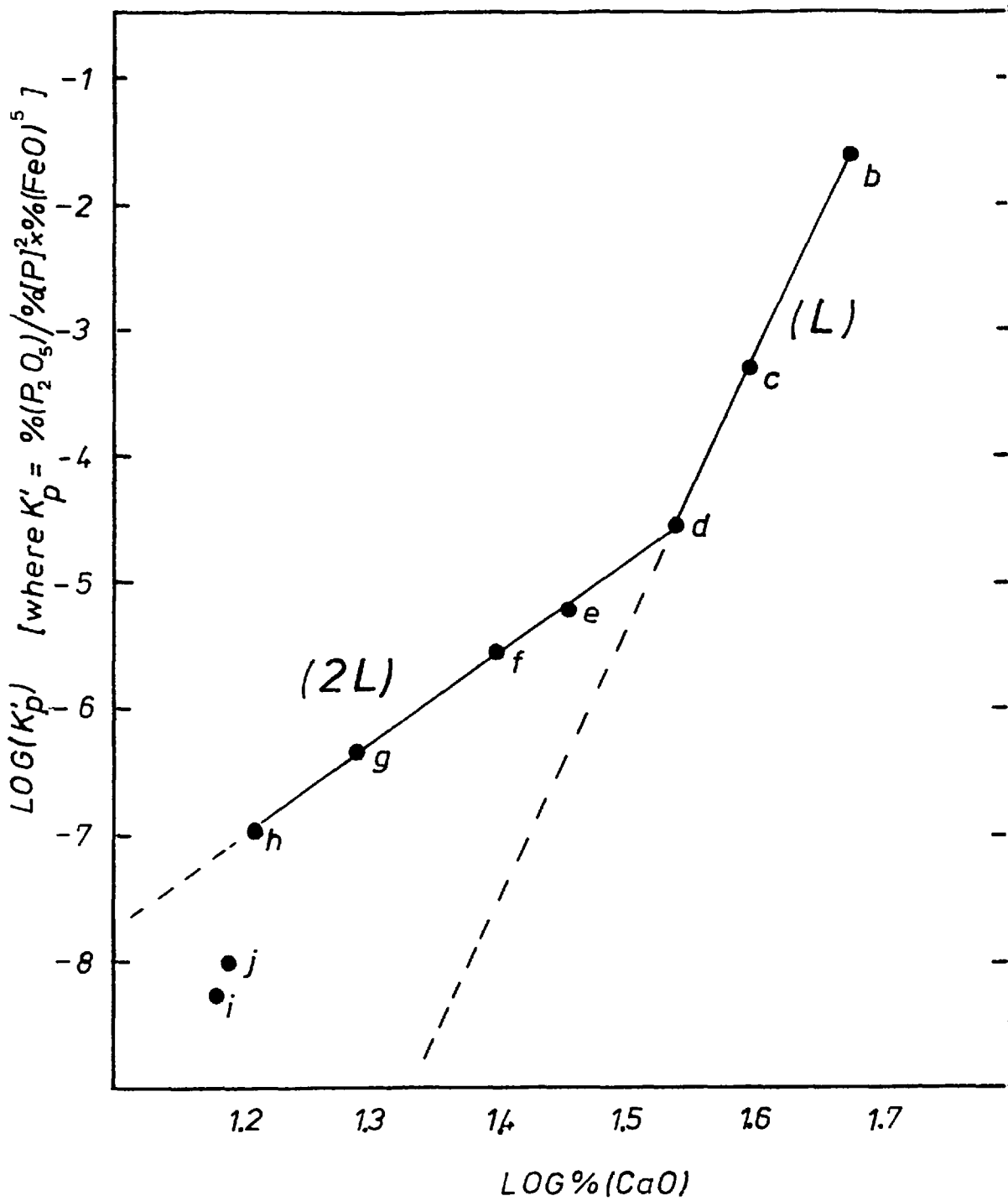


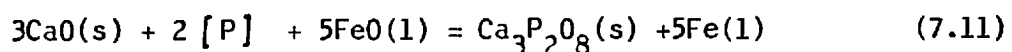
Figure 7.6 Variation of the phosphorus distribution constant (K'_p) with lime concentration in the slag.

points, g, k, l and m in Figure 7.5 which show that although the variation in their slag compositions is considerable, because all these slags lie in a three phase region of two liquids and a solid ($\text{Ca}_3\text{P}_2\text{O}_8$), the activities of the $\text{Ca}_3\text{P}_2\text{O}_8$, CaO and FeO are constant, so that the corresponding phosphorus concentrations in the metal phase are very close to one another. The slight variation ($\pm 0.0016\% [\text{P}]$) is most probably due to the errors involved in analysis of the metal phosphorus contents. The other important conclusion that may be drawn from these sets of data is that equilibrium is being achieved between the liquid metal and the slag regardless of the presence of a solid phase in the slag.

However, it follows from the foregoing discussion that once the slag composition moves outside the miscibility gap and enters the single liquid phase region of similar composition, then a significant rise in the activity of P_2O_5 in the slag occurs, and consequently a severe reversion of phosphorus from the slag to the metal should result. This is shown to be the case, when points h, i, and j are taken into consideration. Although one would expect that when the distribution constant for points i, and j are plotted against the concentration of lime in Figure 7.6 then they should lie on a line passing through points b, c, and d, but as can be seen they do not. This is because under these conditions the mass of the slag is almost twice as much as in the case in the points b, c, and d, hence a greater temperature gradient would

be expected to exist across the slag layer, which in turn would influence the distribution constant of the phosphorus.

The other interesting effect observed, is that shown by points g, h, n-r in Figure 7.5. Here the slags are in equilibrium with a solid phase of $\text{Ca}_3\text{P}_2\text{O}_8$, and a liquid phase which is rich in iron oxide. The activity of the tricalcium phosphate remains constant as the activities of lime and iron oxide vary. It is therefore to be expected that as the activities of iron oxide and lime increase and decrease respectively, reversion of phosphorus should occur. Although both the present work and that of Trömel et al.⁽⁸⁹⁾ record this effect, the degree of reversion observed differs by a factor of about 6. Our calculations of the equilibrium constant (K_p) for the reaction:



and hence the variation of the metal phosphorus concentrations in equilibrium with slags of compositions corresponding to the liquid phases, which are in turn in equilibrium with $\text{Ca}_3\text{P}_2\text{O}_8$ at 1600°C , are in good agreement with the results of the present investigation, provided that the composition of the liquid phase in equilibrium with point "r" has the same composition (see Appendix 3). Thus the disagreement between the present work and that of Trömel et al. would be on the extent of

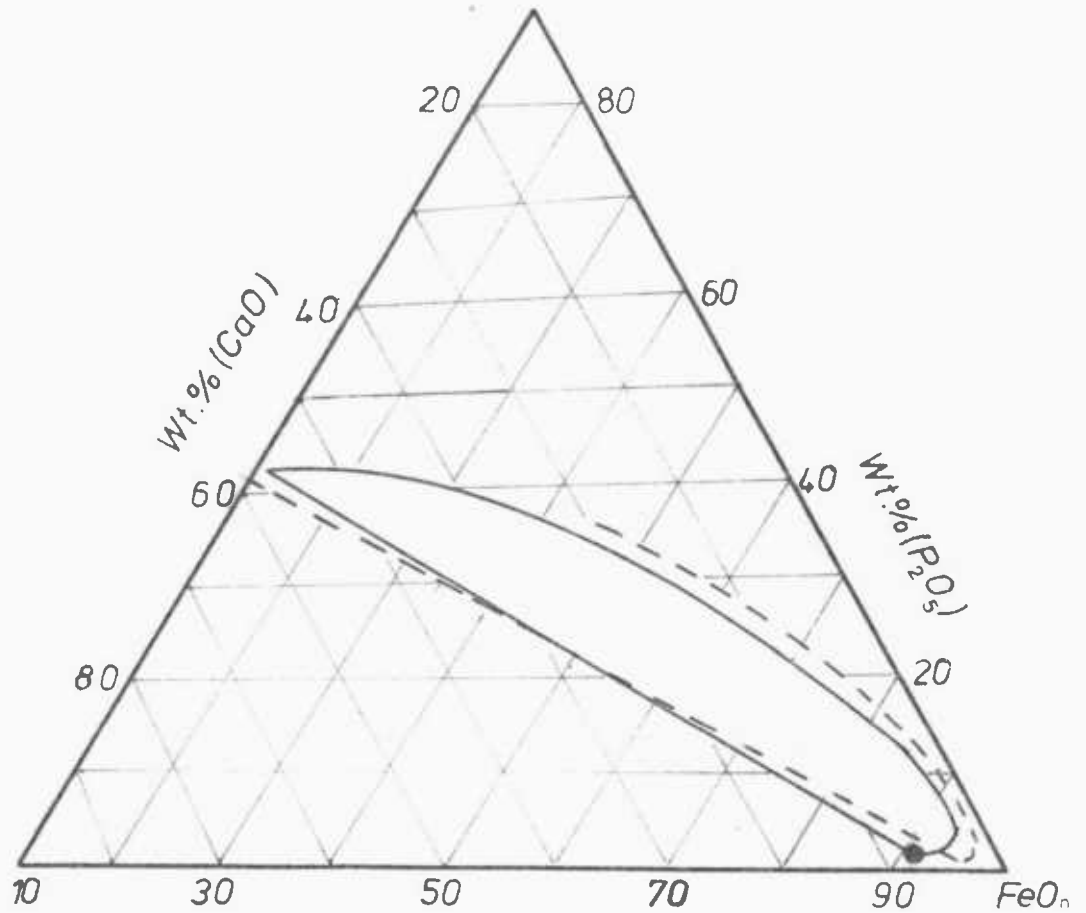


Figure 7.7 The upper portion of the miscibility gap in the $\text{CaO}-\text{P}_2\text{O}_5-\text{FeO}$ system at 1600°C .

----- after Trömel and Fritz (89,90)

————— after Olette et al. (93)

● point "r" (this investigation)

the miscibility gap. It is interesting that Olette et al.⁽⁹³⁾ also found a similar disagreement with the phase diagram constructed by Trömel et al. as shown in Figure 7.7.

Finally it is reasonable to expect that neither of the available correlations for evaluation of the phosphorus distribution constant should be valid when applied to a simple ternary slag system of $\text{CaO-P}_2\text{O}_5\text{-"FeO"}$. On the other hand the available correlations were derived for conditions of steelmaking slags, which normally contain sufficient silica to close the miscibility gap. But since the majority of the data used in deriving these correlations were those obtained by Balajiva and co-workers, as well as those by Winkler and Chipman, then the correlations become even more speculative since some, but not all of the results obtained by these workers indicate the presence of a miscibility gap in their system. Nevertheless the agreement between Healy's correlation and the measured phosphorus distribution constant of the steelmaking slags has been reported to be generally good.

7-6.3 The Effect of CaF_2 on the Distribution of Phosphorus

The phase relation existing in the systems CaO-"FeO"-CaF_2 and $\text{Ca}_3\text{P}_2\text{O}_8\text{-CaF}_2$ are quantitatively known from the work of Oelsen and co-workers,^(102,103) these are shown in Figures 7.8 and 7.9 respectively.

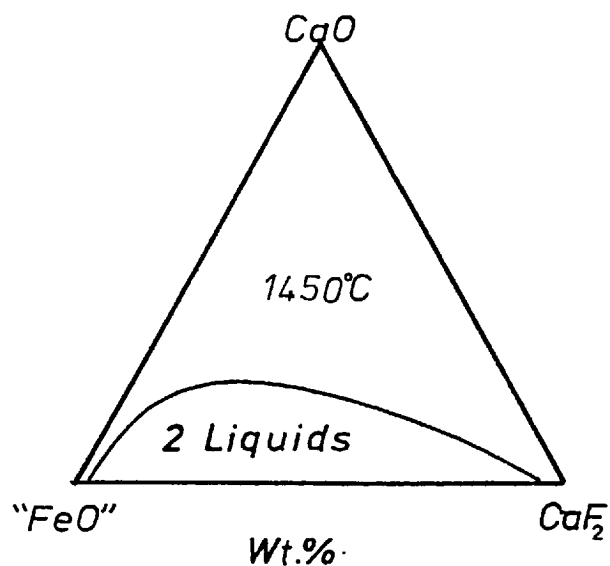


Figure 7.8 Phase diagram for the system
FeO -CaO -CaF₂ .

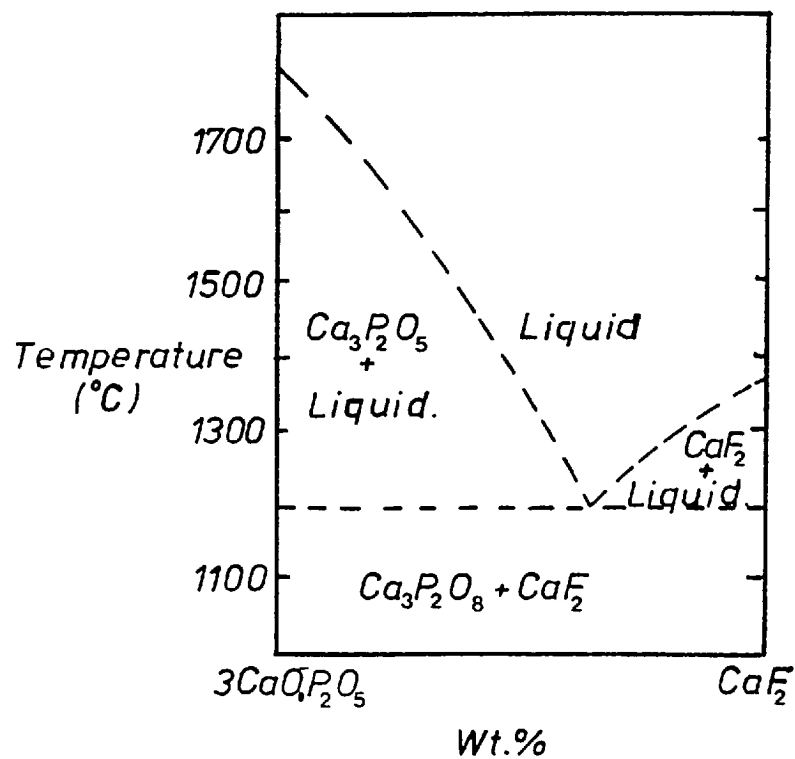


Figure 7.9 Phase diagram for the system
3CaO.P₂O₅-CaF₂ .

As can be seen there is a pronounced dissimilarity between the two systems, which includes an extensive miscibility gap in the CaO-FeO-CaF_2 system, and in contrast there is complete miscibility in the $\text{Ca}_3\text{P}_2\text{O}_8\text{-CaF}_2$ system. It is difficult to construct a phase diagram for the system $\text{CaO-P}_2\text{O}_5\text{-FeO-CaF}_2$ from the existing information on its ternary systems. It may be reasonable however to suppose that the calcium fluoride in the slags of the type considered is present partly in an iron oxide rich phase and partly in a phosphate rich phase. Its effect would be to increase the phosphate capacity of the slag by forming a very stable fluoroapatite phase and simultaneously to increase the oxygen potential in the iron oxide rich phase. Our results on the equilibrium distribution of phosphorus between the metal and slags of the type $\text{CaO-P}_2\text{O}_5\text{-FeO-CaF}_2$ have shown that at low concentrations of FeO in the slag, a very high degree of dephosphorization is achieved, whereas as the concentration of the iron oxide is raised some reversion of phosphorus occurs as shown in Figure 7.10. Due to lack of information on the quaternary system, we are unable to explain this behaviour.

7-6.4. Kinetics of Dephosphorization of Fe-P Drops by a Basic Slag

The results obtained on oxidation of the levitated drops of Fe-0.12%P with a liquid basic slag

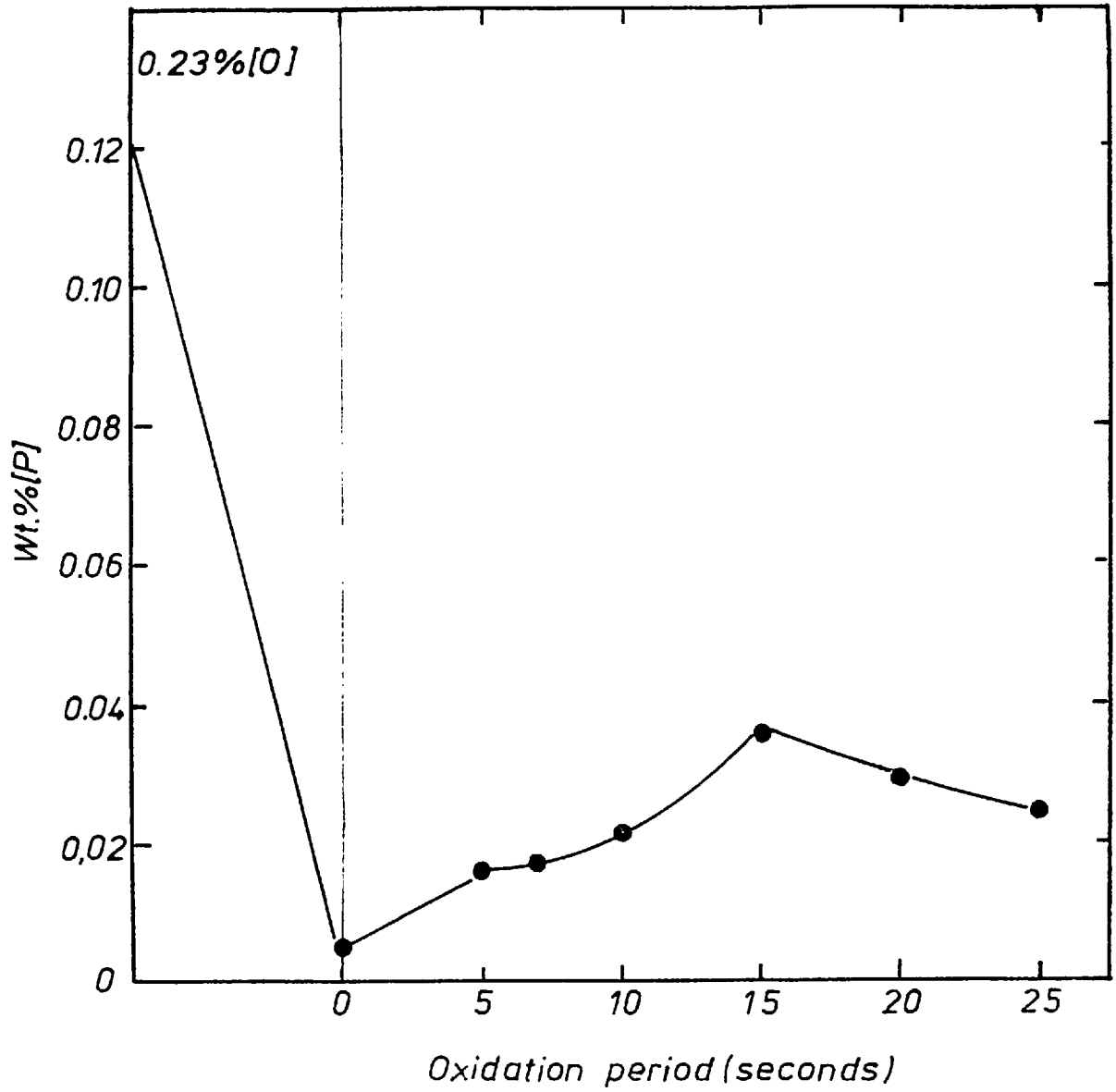
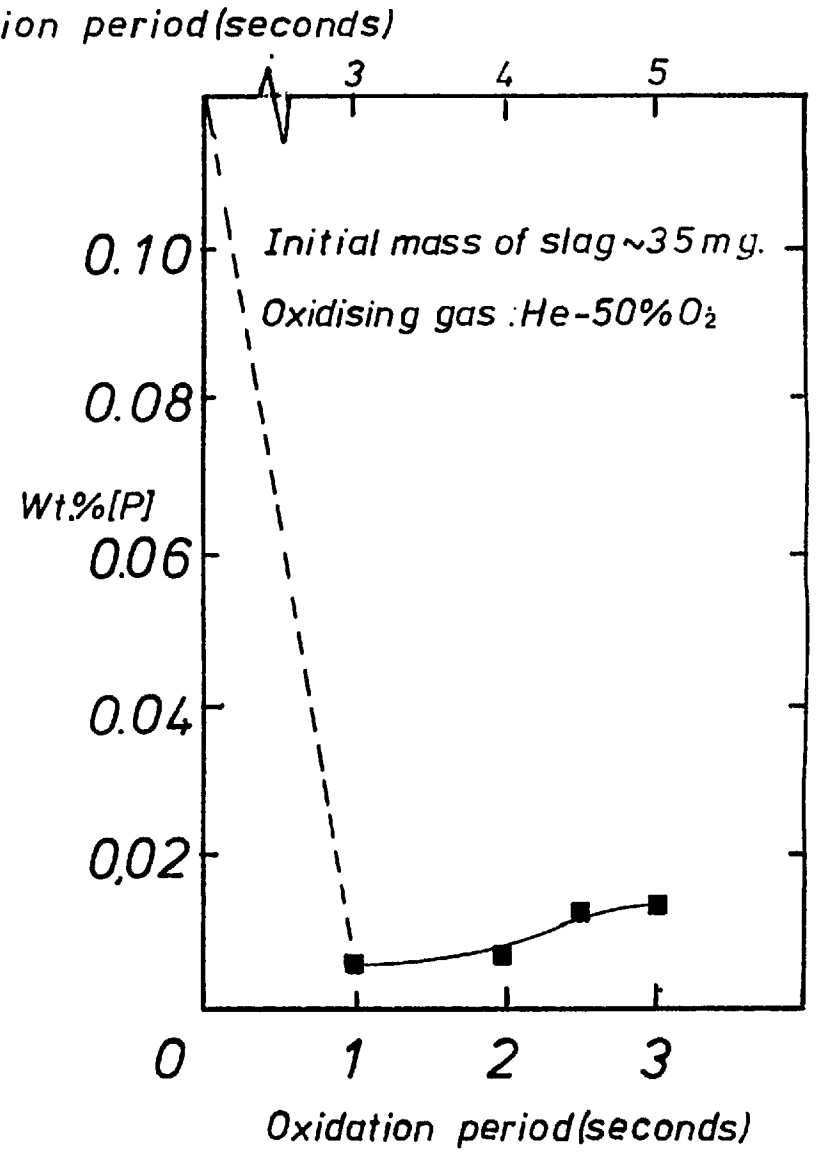
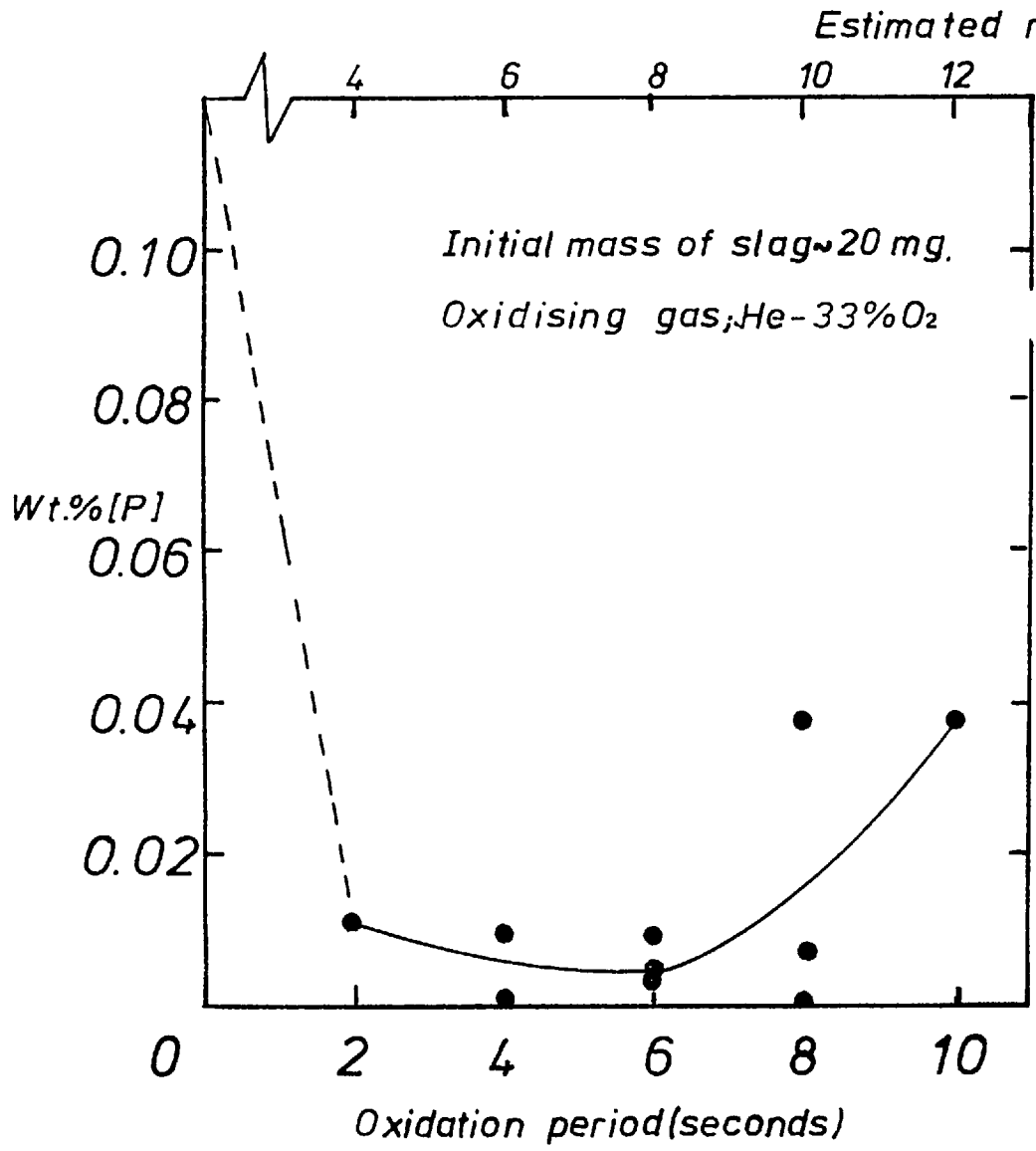


Figure 7.10 Variation of the phosphorus concentration in the iron drops, in equilibrium with $\text{CaF}_2\text{-CaO-P}_2\text{O}_5\text{-FeO}$ slags at 1600°C .

consisting of 46% CaF_2 -38% CaO -15.4% SiO_2 , in streams of He-33% O_2 and He-50% O_2 are shown in Tables 7.9 and 7.10 and in Figures 7.11 and 7.12 respectively. These results show a high degree of dephosphorization in a very short period of time so that if the rates are interpreted in terms of mass transfer coefficients a value of $0.2 \text{ cm}\cdot\text{s}^{-1}$ would be obtained. This value is approximately an order of magnitude greater than those typically found in well stirred systems, hence on such grounds it is reasonable to consider a levitated drop to be vigorously stirred. On the other hand, if these results are interpreted in terms of the eddy diffusivity of P a value of $1.2 \times 10^{-2} \text{ cm}^2 \cdot \text{s}^{-1}$ would be obtained. This value is about two orders of magnitude greater than the atomic diffusivity of phosphorus in liquid iron at 1550°C ⁽¹⁰⁴⁾, and about an order of magnitude greater than the estimated value of the effective diffusivity of carbon in levitated drops of iron by El-Kaddah et al. ⁽¹⁰⁵⁾, when interpreting the rates of carburization of iron by CO/CO_2 gas mixtures. Both these considerations lead to the conclusion that the levitated iron drops are well stirred and that the rate of transport of phosphorus in levitated drops of iron is very rapid. Considering the kinetics of dephosphorization, it is to be expected that the rate of transport in the metal phase does not become the rate controlling step until very low levels of phosphorus concentrations in the metal are obtained.



Figures 7.11 & 7.12 Dephosphorization of Fe-P drops by streams of oxidising gases in the presence of a basic slag (46%CaF₂-38.6%CaO-15.4%SiO₂).

The initial rates of dephosphorization in these series of experiments were about 1.6×10^{-5} and 2.6×10^{-5} moles, cm⁻², s⁻¹, (these rates were calculated by allowing 2 seconds for the "back mixing" of the gases (106) and the delay time prior to quenching). Although the ratio of these rates is very close to the ratio of the partial pressures of the oxygen in the gas streams, they are about one tenth of the rates calculated; if they were controlled by gaseous diffusion of oxygen through the boundary layer. Thus it may be concluded that the observed rates of removal of phosphorus from these drops were controlled by chemical reactions at the interface and/or transport of phosphorus in the slag phase. It is interesting to note that the rate of dephosphorization observed by Gaye and Riboud, (107) when drops of Fe-1.5%P were reacted with CaO-Al₂O₃-FeO_t-SiO₂ slag at 1550°C was about 2.3×10^{-5} moles, cm⁻² s⁻¹. This rate is very similar to the rates observed in this investigation.

7-6.5. Kinetics of Transfer of Phosphorus between the Fe-P Drops and Lime

In order to discuss the mechanisms controlling the rates of transfer of phosphorus between the metal and the slag phases, a diagram illustrating the general form of dephosphorization and re-phosphorization by slags containing CaO-P₂O₅-FeO has been drawn and is shown

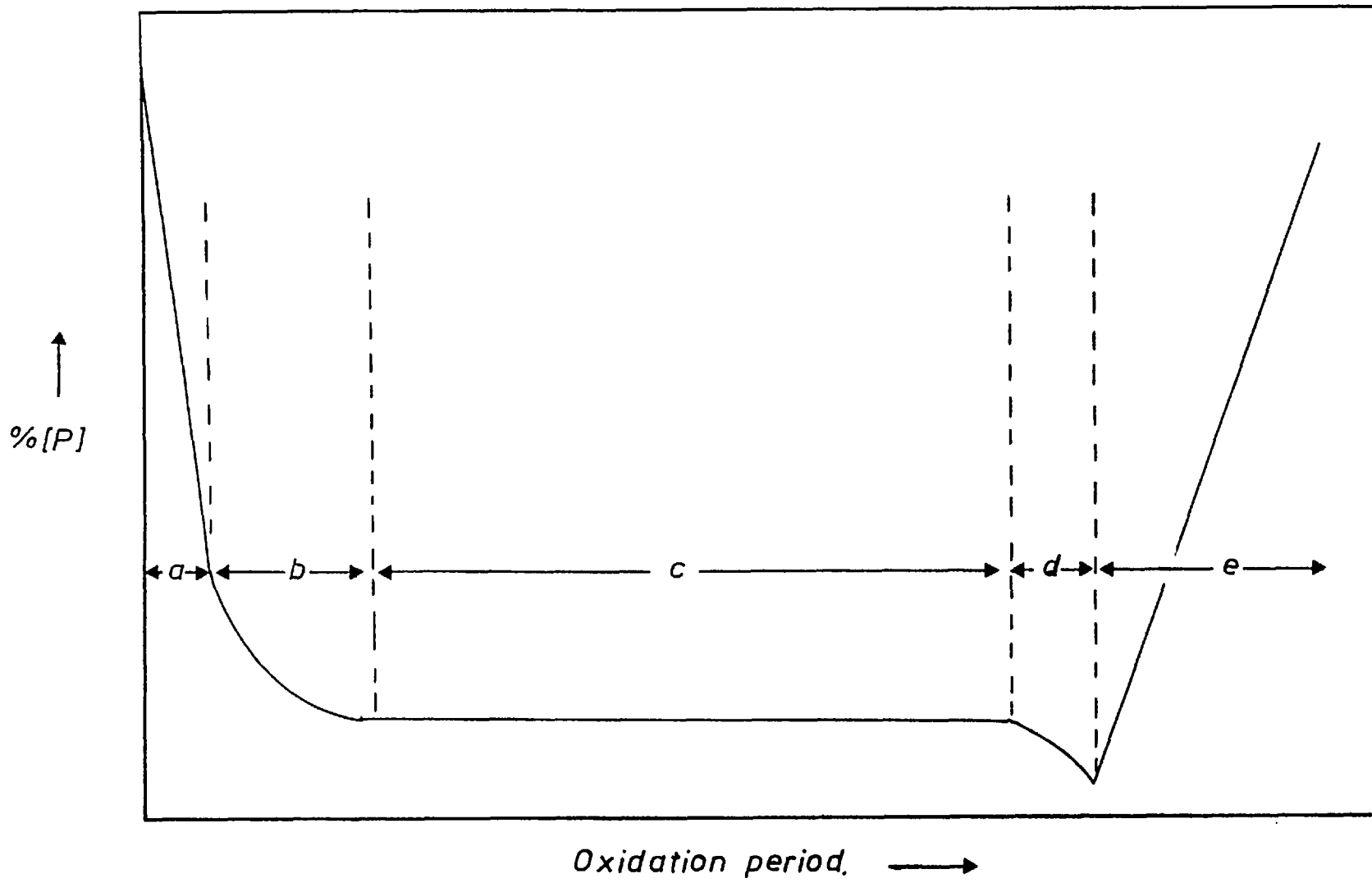


Figure 7.13 A possible form of the dephosphorization and rephosphorization curve.

in Figure 7.13. As can be seen the diagram is divided into the following five separate regions:

a. Initial fast dephosphorization period

In this period a high degree of dephosphorization is being achieved in a relatively short period of time. The rate is controlled by transport of phosphorus in the slag phase.

b. Slow dephosphorization period

The rate begins to slow down as the reaction period increases, due to the formation of a solid calcium phosphate phase at the lime/slag interface, as well as the transport of phosphorus in the metal and slag phases.

c. Lull period

The reaction of phosphorus practically ceases due to the slow dissolution of the solid calcium phosphate phase in the iron oxide being produced during this period.

d. Final dephosphorization period

The dephosphorization begins again once the solid phosphate phase had dissolved in the liquid slag and more lime also dissolves.

e. Rephosphorization period

The slag loses its phosphate capacity due to the

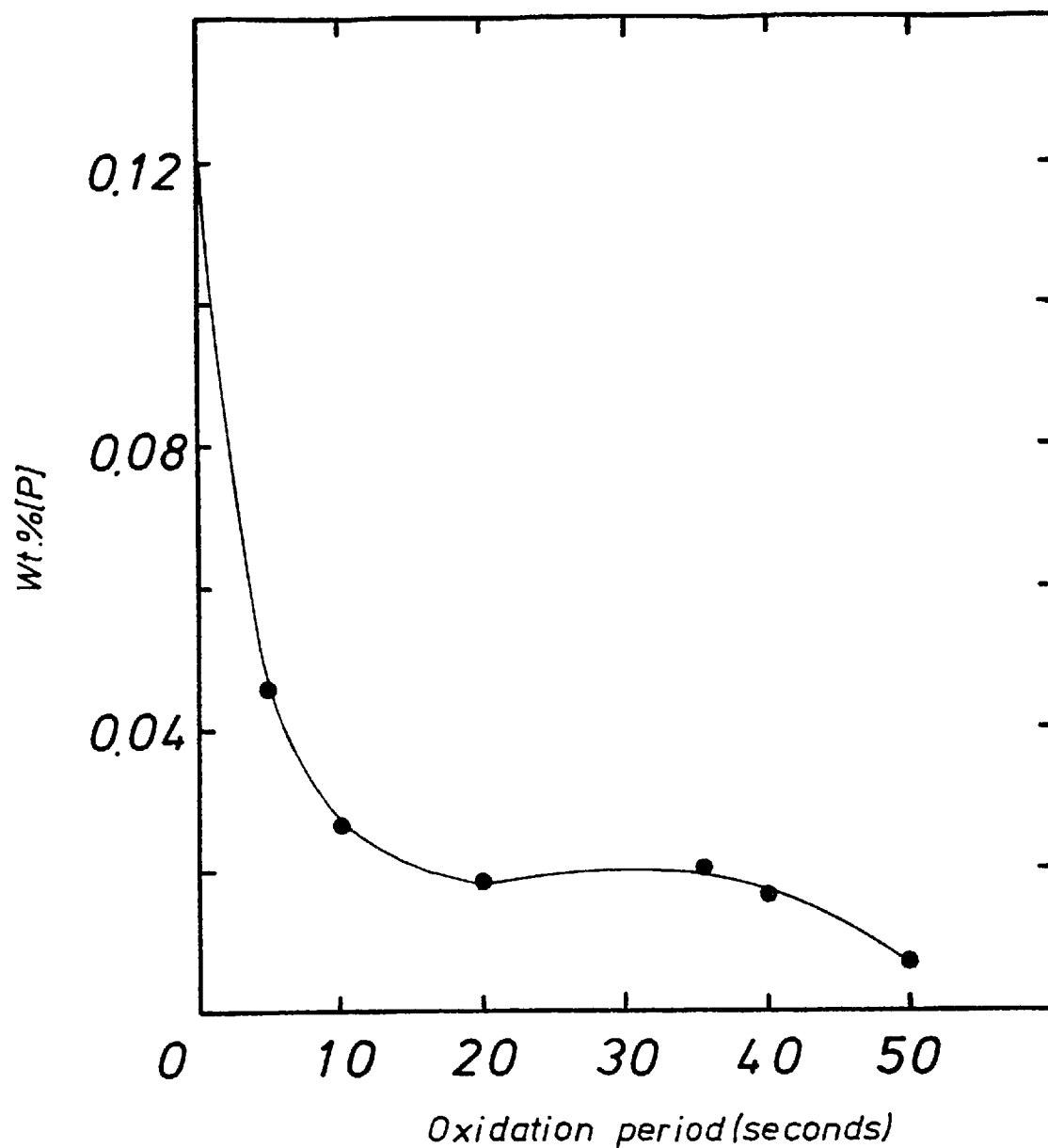


figure 7.14 Oxidation of Fe-P in a stream of He-5%O₂; (flowing at 0.75 l. min⁻¹) with approx. 20 mg of lime.

excessive dilution of the lime by iron oxide, and reversion occurs.

On considering the dephosphorization reaction in a stream of He-5%O₂, it can be seen from Figure 7.14, that during the first 5 seconds a rapid rate of dephosphorization is achieved, since the dephosphorization proceeds at the metal/slag interface and under the conditions of the experiment, the rate of supply of oxygen to the drop is slow, hence the rate of oxidation of iron is also slow. This results in a very little amount of lime dissolving in the iron oxide, and because of the tendency for the phosphate formed to move towards the iron oxide/lime interface, formation of calcium phosphate at the lime/slag interface is very likely to occur. However, until sufficient calcium phosphate is formed at the interface the rate of removal of phosphorus would not be effected considerably, but once most of this interfacial area is covered by a layer of calcium phosphate, then the reaction will begin to slow down, and eventually ceases when the calcium phosphate layer covers the entire interfacial area. During this lull period, because of the relatively low solubility of lime (~15%) and P₂O₅ (~3%) in the iron oxide, when in contact with solid tricalcium phosphate, the oxidation of iron continues with practically no removal of phosphorus from the metal. However, once a sufficient quantity of iron oxide is formed to dissolve

the calcium phosphate layer, then dissolution of lime begins to take place and further dephosphorization is achieved. If these drops were further oxidised, then reversion of phosphorus to the metal would be expected to occur as the phosphate capacity of the slag falls.

The results obtained on oxidation of Fe-P drops with approximately 20 mg of lime attached, in a stream of He-50%O₂ as shown in Table 7.8 and Figure 7.15. Once again a high degree of dephosphorization (94%) is observed in a few seconds, but the rate of dephosphorization observed in this case is about 1.9×10^{-5} moles.cm⁻².s⁻¹, which is about one seventh of the rate expected if it were controlled by the supply of oxygen by gaseous diffusion. Thus it is reasonable to expect a high rate of oxidation of iron to occur simultaneously. Since the measured rate of dissolution of lime, from a pellet of 0.2 cm in diameter, in iron oxide was about 5×10^{-5} moles.cm⁻² s⁻¹, thus it is possible that complete dissolution of lime had occurred during the first few seconds of the oxidation period, and formation of the solid tricalcium phosphate phase was avoided. This in turn had resulted in preventing the stopping of the dephosphorization reaction. However as shown in Figure 7.15 further oxidation of the drop results in reversion of phosphorus by the mechanism noted above. The overall rate of reversion of phosphorus observed in this series of experiments is about 2.3×10^{-5} moles.cm⁻² s⁻¹, (i.e. 0.091% in 2 + 1 sec.) is slightly faster than the

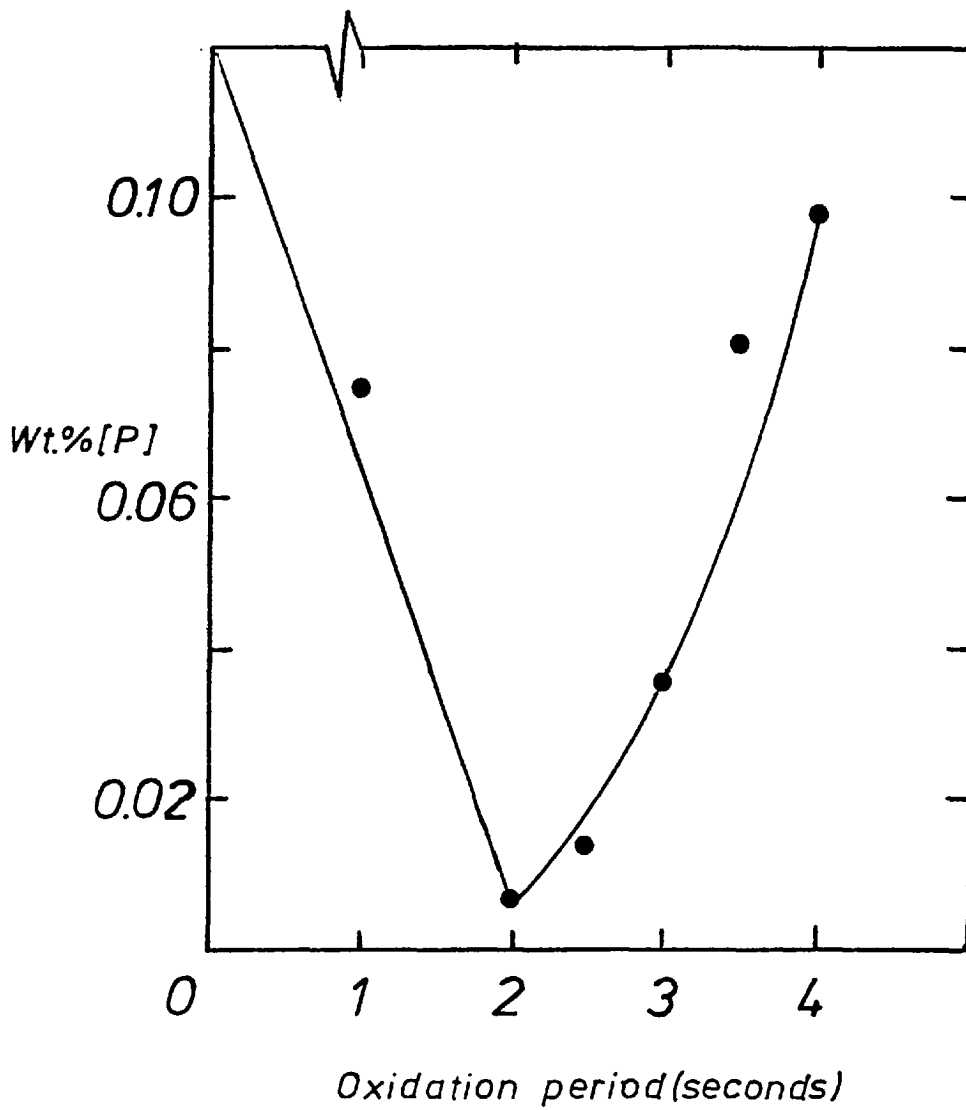


Figure 7.15 Dephosphorization and rephosphorization of Fe-P drops by a stream of He-50%O₂, with approximately 20 mg of lime attached.

observed rate of dephosphorization. On the other hand when rates of rephosphorization of Fe-P drops by $\text{Ca}_4\text{P}_2\text{O}_9$ + liquid was measured, by the free fall technique, the observed rates were about $5 \times 10^{-5} \text{ moles.cm}^{-2}\text{s}^{-1}$, indicating that the rate of the reaction was dependent on the phosphorus concentration in the slag, and hence the transport of phosphorus in the slag phase may be the rate controlling step, during the reversion process.

7-6.6. Reactions of Fe-C-P with Basic Slags

The growing attention towards the simultaneous removal of phosphorus and carbon from melts containing relatively high carbon concentrations (2-4%) has been the reason for the number of studies made in this field, by oxidation of Fe-C-P drops in the presence of a basic slag. The results of the experiments with Fe-C-P and CaO-50%Al₂O₃ slags are of interest in view of the recent theory of coupled reactions.^(99,100) As can be seen from Table 7.12 a small fall in the phosphorus concentration of the metal was observed before and after the oxidation of the levitated drops by gaseous oxygen. This loss of phosphorus from the metal was accompanied by a small loss of carbon during the levitation period prior to the commencement of oxidation. During this period a gas bubble (presumably of CO) nucleated and grew at the metal/slag interface. This bubble grew to about 0.7 cm in diameter over a period of 7 minutes.

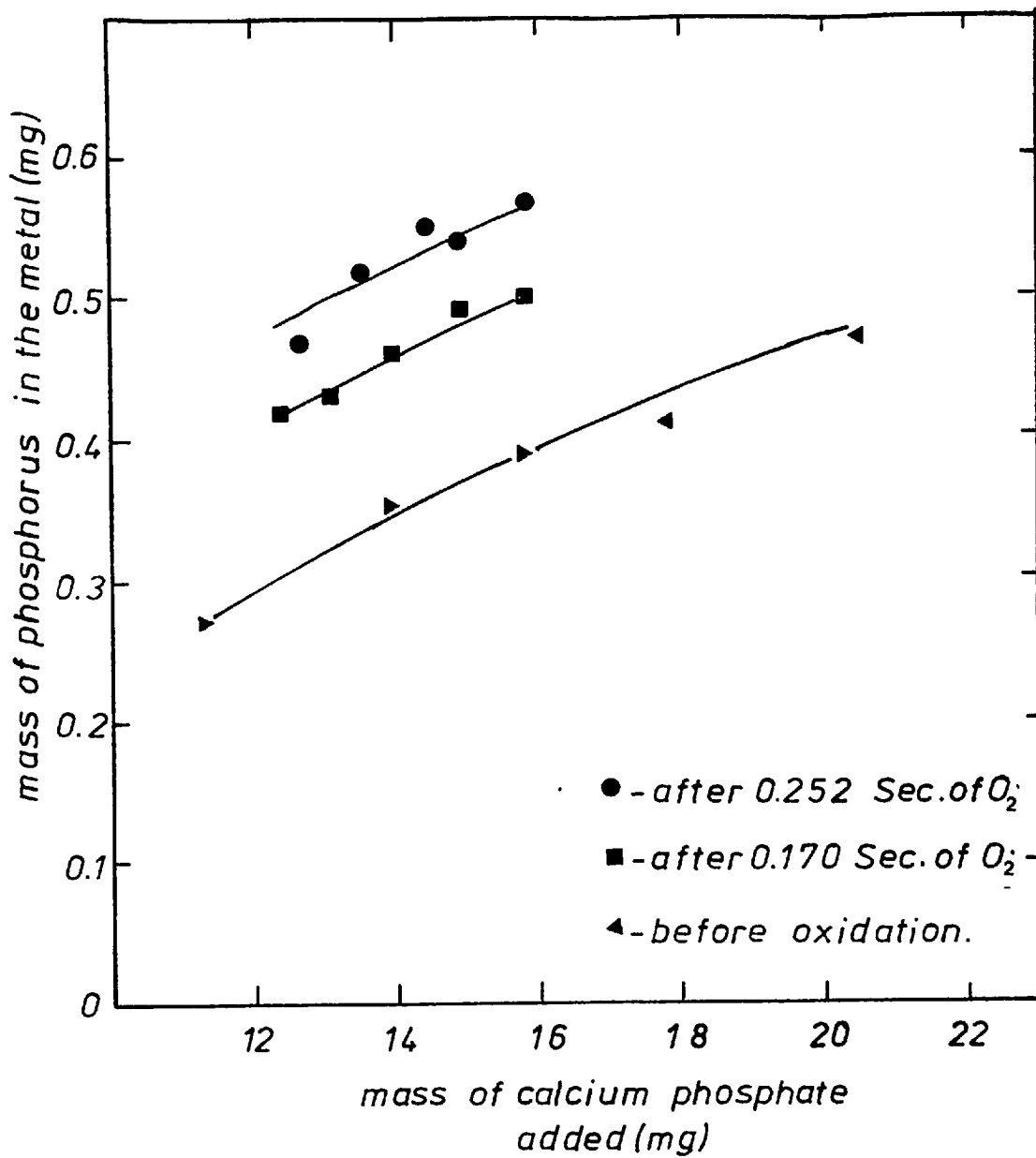
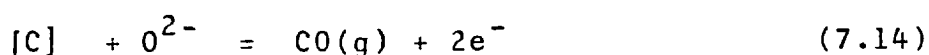
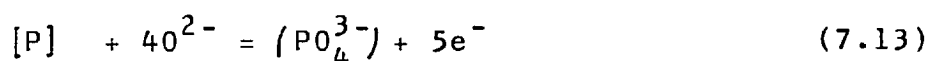


Figure 7.16 Kinetics of rephosphorization of iron drops by the $CaO-P_2O_5-FeO$ slags.

By comparison, when a CaO-CaF₂ slag was used, no nucleation and growth of the gas bubble was observed. Furthermore there was no significant change in the phosphorus or carbon concentrations in the metal. It is, therefore, possible that the phosphorus and carbon losses from the drops, with CaO-Al₂O₃ slags attached, may have been due to coupled reactions expressed in ionic form as:



From the results obtained in the present investigation it is thought that the presence of phosphorus in the metal promotes the reduction of alumina to a greater extent than that predicted thermodynamically.

However as is shown in Tables 7.12 and 7.13, the oxidation of these drops in a stream of oxygen led to practically no removal of phosphorus, although considerable loss of carbon from the metal was observed. Considering the reactions at the gas/metal interface, the theory of oxidation of phosphorus at the "fire spot" postulated by Fuji et al. appears to be incorrect, as this reaction was discussed in Chapter 5 and no significant loss of phosphorus was observed. However if the conditions were such that dephosphorization could

be achieved locally, then one would expect that oxidation at the metal/slag interface would be most likely. It appears that the technique of levitation would provide some of the conditions required for the promotion of the reaction, particularly the occurrence of the carbon boil at the metal/slag interface which would prevent reversion by the dissolved carbon of any phosphate formed. However as was noted above no dephosphorization was achieved during the oxidation and removal of carbon. It may be argued that perhaps some local oxidation and removal of phosphorus at the metal/slag interface may have occurred, but at the same time as the carbon boil occurred, not only the phosphate phase in the slag was ejected, but also some of the metal phase near the metal/slag interface, which was depleted of phosphorus was ejected, so that the overall metal phosphorus concentration in the drops did not change significantly. However, due to the relatively high rates of transport of species in levitated drops, one would expect some change in the metal phosphorus concentration, and it was not observed. It appears that the oxygen potential of the slag at the metal/slag interface did not reach a high enough value to oxidise the phosphorus, before the commencement of the carbon boil. Most workers who have achieved simultaneous dephosphorization and decarburization have used slags containing $\text{CaO/Fe}_2\text{O}_3$, with or without other constituents such as CaF_2 , SiO_2 and MnO . However, Fuji et al.⁽⁹⁷⁾ reported that under the conditions of

blowing an oxygen jet on to the surface of a melt containing 2-1.5% carbon and about 0.3% phosphorus, oxidation of the carbon and the phosphorus occurred when no liquid slag had been formed. On the other hand it is evident from the work of Turkdogan and Leake⁽¹⁰⁸⁾ on enhanced vaporization of iron from iron-carbon melts by blowing oxygen gas on the surface, that when more than 2% carbon is present in the iron the formation of an iron oxide film does not take place, but at carbon concentrations below 2% a thin layer of iron oxide is formed and hence vaporization practically ceases. It is likely, therefore that the formation of an oxide layer on the surface of the melts used by Fuji et al. did occur and that a locally high oxygen potential in the oxide layer caused the oxidation of the phosphorus to take place, and the oxide was then stabilized by the lime. Or in other words the removal of phosphorus was coupled with the reduction of ferrous, ferric and oxygen ions in the slag.

7-7. CONCLUSIONS

It is considered that the results obtained in this investigation has improved our knowledge of the Fe-P/ CaO-P₂O₅-FeO system, particularly the role of the miscibility gap in the slag system studied, and it may be concluded that its effect on the dephosphorization power of the slag can be beneficial as compared to a

single phase liquid slag. The results obtained indicate that it is incorrect to use an algebraic correlation to predict the metal phosphorus concentration over a wide range of slag compositions, particularly when slags containing less than 15% SiO_2 are considered, because of the phase separation.

It has been found that chemical equilibrium between levitated drops of iron alloys and slags can be achieved in a very short period of time, and rates of mass transfer in the metal phase are very high. Thermal equilibrium may not be achieved between levitated drops and liquid slags, when large quantities of slags are being used.

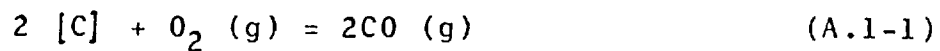
The rates of transfer of phosphorus between liquid iron drops and basic slags are very fast and it is controlled by the mass transfer in the slag phase. It has also been concluded that the oxidation of phosphorus from Fe-C-P alloys in the absence of iron oxide in the basic slag is unlikely.

APPENDICES

APPENDIX 1

Theoretical Prediction of the rate of Decarburization
when gaseous diffusion is the controlling factor

On the supposition that when oxygen is used the reaction at the interface is:



it can be shown that the flux of oxygen (J_{O_2}) to the interface is:

$$J_{O_2} = \frac{D_{O_2}/CO}{Z \cdot RT} \ln \left(\frac{1 + P_{O_2}^b}{1 + P_{O_2}^i} \right) \quad (A.1-2)$$

Assuming that transport in the gas phase is rate controlling for the reaction (A.1-1), and ignoring any contribution due to CO combustion in the boundary layer, then one may further assume that the partial pressure of oxygen at the metal/gas interface is zero, and hence the partial pressure of CO is one atmosphere. Furthermore the partial pressure of oxygen in the bulk gas ($P_{O_2}^b$) is always one atmosphere. (A schematic representation of the concentration profiles in the metal and gas phases is presented in Figure A.1-1). Thus the equation (A.1-2) simplifies to

$$J_{O_2} = \frac{D_{O_2}/CO}{Z \cdot RT} \ln 2 \quad (A.1-3)$$

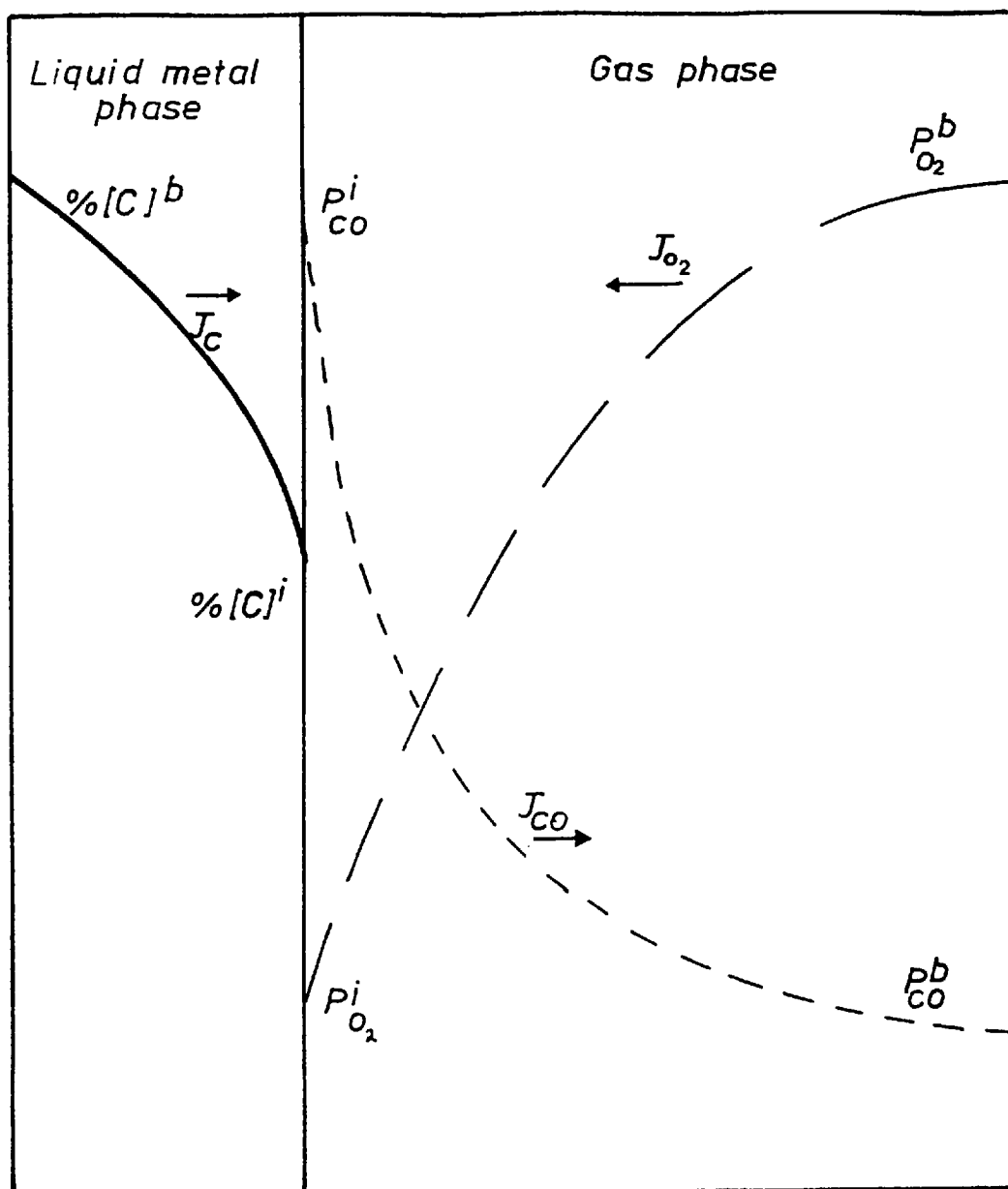


Figure A.1-A

A schematic representation of the concentration profiles.

From the stoichiometry of the reaction (A.1-1) the flux of oxygen and carbon can be expressed as:

$$J_C = -2J_{O_2} \quad (A.1-4)$$

Hence by combining equations (A.1-3) and (A.1-4), the rate of decarburization can be expressed in the following equation:

$$\begin{aligned} -J_C &= 2J_{O_2} = \frac{2 \times D_{O_2/CO}}{Z \cdot RT} \ln 2 \\ \therefore -J_C &= \frac{D_{O_2/CO}}{Z} \times \frac{2 \ln 2}{RT} \end{aligned} \quad (A.1-5)$$

On taking the arithmetical mean between the temperature of the metal surface and the gas, as the film temperature (T_f), then at a constant T_f and flow rate of oxygen, the decarburization rate (J_C) should be linear and is only dependent on the quantity $\frac{D_{O_2/CO}}{Z}$, which can be defined as the gas mass transfer coefficient (K_g). As was discussed earlier the mean mass transfer coefficient can be expressed in terms of a Sherwood number (Sh), which may be correlated in terms of controlling variables in the form of dimensionless groups of numbers. The relative importance of these groups of dimensionless numbers are dependent on the regime for the transport of materials (e.g. at high pressures and/or low flow rates, natural convection plays the major role in the mass transfer, hence the terms with Grashof numbers become more important,

whilst at lower pressures and higher flow rates, forced convection terms become more predominant.)

Evaluation of the gaseous mass transfer coefficient

To evaluate the mass transfer coefficient (K_g) of the species in a gas mixture, a knowledge of the coefficient of interdiffusivity of the species in the gas mixture ($D_{O_2/CO}$), of the coefficient of the viscosity of the gas mixture (ρ_{CO/O_2}), of the densities of the gaseous species, at the surface of the molten iron (ρ_s), in the boundary layer (ρ_f), and in the bulk gas stream (ρ_b) is necessary.

a. Evaluation of interdiffusivity of CO/O₂

It has been shown from the molecular theory of gaseous gases⁽³⁶⁾ that the interdiffusivity (D_{CO/O_2}) of a binary gas mixture can be expressed by the following equation:

$$D_{CO/O_2} = \frac{2.628 \times 10^{-3} \times [(T^3 (M_{CO} + M_{O_2}) / 2M_{CO}M_{O_2})]^{0.5}}{P \times \sigma_{CO,O_2}^2 \times \Omega_{T^*,CO/O_2}^{(1,1)}} \quad (A.1-6)$$

where D_{CO/O_2} is interdiffusivity in cm^2/sec .

T is temperature in $^{\circ}\text{C}$.

M_{CO} and M_{O_2} are molecular weights of the species CO and O_2 .

P is total pressure in atmospheres.

σ_{CO, O_2} is the collision diameter in A° .
 $\Omega_{T^*}^{(1,1)}(CO, O_2)$ = dimensionless function of temperature
 and intermolecular potential energy
 for one molecule of CO and one molecule
 of O_2 .

Tabulated values of σ_{CO} , σ_{O_2} , ϵ_{CO} , ϵ_{O_2} , and $\Omega_{T^*}^{(1,1)}(CO, O_2)$
 are given by Hirshfelder et al. (36) and Bird et al. (37).

b. Evaluation of the coefficient of viscosity of a
 binary gas mixture

Once again it can be shown, by the molecular theory
 of gases, (36) that the coefficient of the viscosity of a
 binary gas mixture (μ_{CO, O_2}) can be expressed by the
 following equation.

$$\mu_{CO, O_2} = \frac{N_{CO} \cdot \mu_{CO}}{N_{CO} + N_{O_2} \cdot \phi_{CO, O_2}} + \frac{N_{O_2} \cdot \mu_{O_2}}{N_{O_2} + N_{CO} \cdot \phi_{O_2, CO}} \quad (A.1-7)$$

where $\mu_{CO} = 2.6693 \times 10^{-5} \frac{\sqrt{(M_{CO} \cdot T_f)}}{\sigma_{CO}^2 \times \Omega_{T^*}^{(2,2)}(CO)}$

$\mu_{O_2} = 2.6693 \times 10^{-5} \frac{\sqrt{(M_{O_2} \cdot T_f)}}{\sigma_{O_2}^2 \times \Omega_{T^*}^{(2,2)}(O_2)}$

$$\phi_{CO, O_2} = \frac{1}{\sqrt{8}} \cdot \left(1 + \frac{M_{CO}}{M_{O_2}} \right)^{-0.5} \cdot \left[1 + \left(\frac{\mu_{CO}}{\mu_{O_2}} \right)^{0.5} \cdot \left(\frac{M_{O_2}}{M_{CO}} \right)^{0.25} \right]^2$$

$$\phi_{O_2, CO} = \frac{1}{\sqrt{8}} \cdot \left(1 + \frac{M_{O_2}}{M_{CO}} \right)^{-0.5} \cdot \left[1 + \left(\frac{\mu_{CO}}{\mu_{O_2}} \right)^{0.5} \cdot \left(\frac{M_{CO}}{M_{O_2}} \right)^{0.25} \right]^2$$

c. Evaluation of the density of the gas mixture

The density of the gas mixtures at the surface, film, and bulk gas temperatures were evaluated using the following equation:

$$\rho_{CO, O_2}^T = N_{CO} \cdot \rho_{CO}^T + N_{O_2} \cdot \rho_{O_2}^T \quad (A-1.9)$$

d. Evaluation of the approach gas velocity

The approach gas velocity (u) at the bulk temperature was corrected for the obstruction in the tube due to the levitated drop. This was done by using the mean flowing area i.e.

$$u = 4Q/\pi(D^2 - d^2) \quad (A-1.10)$$

where Q = volume flow rate ($\text{cm}^3 \cdot \text{s}^{-1}$)

D = inner diameter of the silica tube (cm)

d = diameter of the levitated drop (cm).

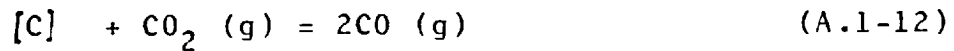
The calculated properties of the gases and the metal drops are summarized in Table A-1.1.

TABLE A-1.1 Metal and gas properties used in the calculation of the predicted gas mass transfer coefficients for decarburization of 1.15 g drops of Fe-C in streams of oxygen.

Mean surface temperature, T_s	1973 ⁰ K
Mean density of the drops ⁽³⁸⁾	6.7 g.cm. ⁻³
Diameter of the drops, d,	0.69 cm.
ρ_s^{CO}	1.73 x 10 ⁻⁴ g.cm. ⁻³
T_b	293 ⁰ K.
$\rho_b^{O_2}$	13.53 x 10 ⁻⁴ g.cm. ⁻³
T_f	1133 ⁰ K.
ρ_f^{CO, O_2}	3.26 x 10 ⁻⁴ g.cm. ⁻³
μ_f^{CO, O_2}	4.84 x 10 ⁻⁴ g.cm. ⁻¹ . s. ⁻¹ .
$(D_{CO/O_2})_f$	2.0 cm ² . s. ⁻¹ .
Pr	0.75
Sc	0.74
Gr ^h	216.8
Gr ^m	529
\overline{Gr}	745
Gas flow rate (l.min ⁻¹)	3.0 5.0 10.3
Approach gas velocity(cm.s ⁻¹) ⁵⁶	93.3 192.3
$(Re)_f$	26.0 43.4 89.4

Calculation of the gaseous diffusion mass transfer between iron-carbon drops and a stream of CO₂

On considering that the reaction at the interface is:



then it can be shown that the flux of CO₂ to the interface is

$$J_{CO_2} = \frac{D_{CO_2/CO}}{Z \cdot RT} \cdot \ln \left(\frac{1 + P_{CO_2}^b}{1 + P_{CO_2}^s} \right) \quad (A.1-13)$$

and on simplification this equation yields:

$$J_{CO_2} = \frac{D_{CO_2/CO}}{Z} \cdot \ln \left(\frac{1 + P_{CO_2}^b}{RT} \right) \quad (A.1-14)$$

on taking $k_g^{CO_2/CO} = \frac{D_{CO_2/CO}}{Z}$

and from the stoichiometry of the reaction (A.1-12)

$$-J_C = J_{CO_2} \quad (A.1-15)$$

hence $-J_C = \frac{k_g^{CO,CO_2}}{RT} \cdot \ln \left(1 + P_{CO_2}^b \right) \quad (A.1-16)$

TABLE A-1.2 Metal and gas properties used to calculate the gaseous mass transfer coefficient between the levitated drops and stream of CO_2 flowing at 0.75 l, min^{-1}

$$T^b = 20^\circ\text{C} \equiv 293^\circ\text{K}$$

$$\rho_{\text{CO}_2}^b = 18.11 \times 10^{-4} \text{ g.cm}^{-3}$$

$$T^s = 1645^\circ\text{C} \equiv 1918^\circ\text{K}$$

$$\rho_{\text{CO}}^s = 1.78 \times 10^{-4} \text{ g.cm}^{-3}$$

$$T^f = 833^\circ\text{C} \equiv 1106^\circ\text{K}$$

$$\rho_{\text{CO,CO}_2}^f = 3.98 \times 10^{-4} \text{ g.cm}^{-3}$$

$$(D_{\text{CO,CO}_2})_f = 1.48 \text{ cm}^2/\text{sec.}$$

$$\rho_{\text{CO,CO}_2}^f = 4.27 \times 10^{-4} \text{ g.cm}^{-3} \cdot \text{sec}^{-1}$$

for a 1.15 g drop: $r = 0.34$ $d = 0.68$

$$u = 14.2 \text{ cm.s}^{-1}$$

$$\text{Re} = 9.0$$

$$\text{Sc} = 0.73 \quad \text{Pr} = 0.76$$

$$\text{Gr}^h = 394$$

$$\text{Gr}^m = 1100 \quad \overline{\text{Gr}} = 1486$$

APPENDIX 2

Theoretical prediction of the critical oxygen partial pressure for the maximum rate of vaporization of iron in a stream of Helium-oxygen at 1600°C

Data :

$$T_b = 293^{\circ}\text{K}, \quad T_s = 1873^{\circ}\text{K}, \quad T_f = 1083^{\circ}\text{K}$$

$$D_{\text{He},\text{O}_2} = 6.3 \text{ cm}^2 \cdot \text{s}^{-1}, \quad \mu_{\text{He},\text{O}_2} = 4.53 \times 10^{-4} \text{ g} \cdot \text{cm} \cdot \text{s}^{-1} \quad d = 0.68 \text{ cm}$$

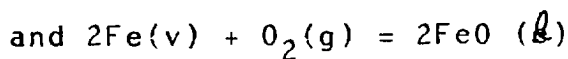
$$\text{Pr} = 0.67 \quad \text{Sc} = 1.54 \quad \text{Gr}^h = 4.84$$

$$\text{Gr}^m = 10.31 \quad \overline{\text{Gr}} = 17.67 \quad \text{Re} = 6.51$$

using $\text{Sh} = 2 + 0.52 (\text{Re}^{0.62} \text{Sc}^{0.31})$

$$\text{Sh} = 3.9 \quad K_g^{\text{He-O}_2} = 36.1 \text{ cm} \cdot \text{s}^{-1}$$

Since $J_{\text{Fe}}^{\text{max}} = \frac{P_{\text{Fe}}}{\sqrt{2\pi RT} M_{\text{Fe}}}$
 $= 1.03 \times 10^{-5} \text{ moles} \cdot \text{cm}^{-2} \cdot \text{s}^{-1}$



$$\therefore J_{\text{Fe}}^{\text{max}} = -2J_{\text{O}_2}^{\text{max}}$$

$$\therefore 2 \frac{K_g}{RT_f} \cdot \ln(1 + p_{\text{O}_2}^b) = 1.03 \times 10^{-5}$$

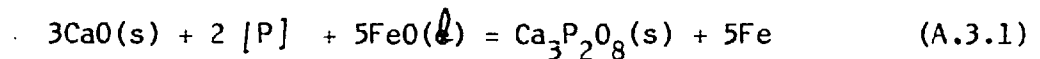
$$\therefore p_{\text{O}_2} = 0.013$$

$$(p_{\text{O}_2})^{\text{max}} = 1.3 \times 10^{-2} \text{ Atm.}$$

APPENDIX 3

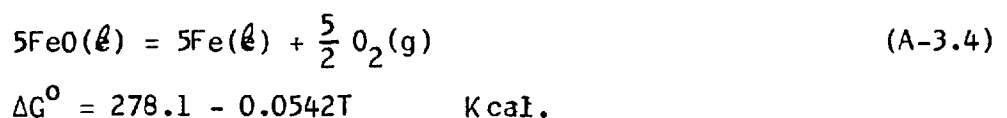
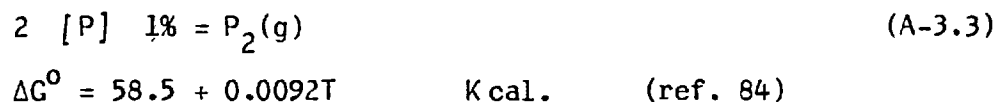
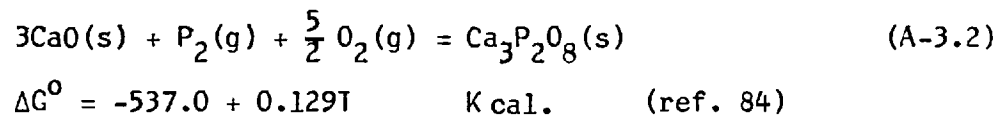
Calculation of equilibrium phosphorus concentration
in liquid iron at 1600°C

On the supposition that there is no temperature difference between the metal and the slag phase, and the activity of CaO in the slags containing low concentrations of P₂O₅ behaves ideally, then for the reactions

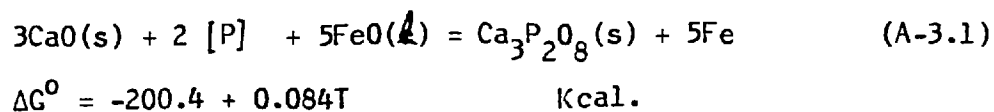


the equilibrium phosphorus concentration in the metal can be calculated provided the activities of CaO and FeO in the slag and the equilibrium constant for the above reaction are known.

For the reactions



∴ for the reaction:



∴ at 1600°C $\Delta G^\circ_{\text{A-3.1}} = -43.068 \quad \text{Kcal.}$

$$\text{and } K_{\text{A-3.1}} = 11.497 = \frac{a_{\text{Ca}_3\text{P}_2\text{O}_8}}{a_{\text{CaO}}^3 \times [\text{P}]^2 \times a_{\text{FeO}}^5}$$

on considering point "g" (79%FeO-19.5% CaO-1.5% P₂O₅)

then $a_{\text{FeO}} \sim 0.56$ (ref.89)

$a_{\text{CaO}} \sim 0.13$ (ref.109)

∴ $[\text{P}]_{\text{calc.}} = 0.290\%$

$[\text{P}]_{\text{obs.}} = 0.035\%$

on considering point "r" (90% FeO-7%CaO-3%P₂O₅)

then $a_{\text{FeO}} \sim 0.91$ (ref. 89)

$a_{\text{CaO}} \sim 0.029$ (ref. 109)

$a_{\text{Ca}_3\text{P}_2\text{O}_8}(s) = 1$

∴ $[\text{P}]_{\text{calc.}} = 0.817\%$

$[\text{P}]_{\text{obs.}} = 0.094\%$

As can be seen the degree of reversion between the calculated and the observed ones are in very good agreement:

$$\text{i.e.} \quad \left(\frac{\% [P]_r}{\% [P]_g} \right)^{\text{calc.}} \div \left(\frac{\% [P]_r}{\% [P]_g} \right)^{\text{obs.}} = 1.05$$

However the difference between the calculated and the observed concentrations of phosphorus in the metal is probably due to the difference in the temperature of the metal and the slag. In fact when a temperature difference of 150°C was chosen and the above calculations were repeated an excellent agreement between the calculated and the observed phosphorus concentrations in the metal were obtained:

$$\text{i.e.} \quad \Delta G_{A-3.1}^{\circ} = 54.288 \quad \text{Kcal.}$$

$$\ln K_{A-3.1} = 15.754$$

$$\text{then} \quad [P]_g^{\text{calc.}} = 0.035\%$$

$$\text{and} \quad [P]_r^{\text{calc.}} = 0.097\%$$

ACKNOWLEDGEMENTS

Sincere gratitude is made to my supervisor, Dr. J.H.E. Jeffes and Professor P. Grieveson for the invaluable advice, guidance, and encouragement received throughout the work.

I am indebted to Dr. D.G.C. Robertson for his advice, assistance and interest towards this work. I am also thankful to Dr. R.J. Hawkins for the helpful discussions and to Dr. J. Williamson for assistance on the X-ray analyses of the slags.

I am grateful for the award of a Bursary from the British Steel Corporation.

I extend my thanks to Mr. A.J. Tipple, and L.E. Leake for their helpful suggestions, and to Sylvia Greenwood for typing the thesis so carefully.

I am also especially grateful to my mother, Mrs. M.D. Jahanshahi for the financial assistance to enable me to complete this thesis in the United Kingdom.

REFERENCES

REFERENCES

1. Peifer, W.A. Levitation melting... A survey of the State of the Art. *Journal of metals*. May 1965, 17, pp. 487-493.
2. McLean, A.
Metallurgical Journal. University of Strathclyde. 1968, 18, pp. 36-44.
3. Roston, A.J. Levitation melting. *Science Journal*. July 1967, 3, pp. 69-73.
4. Lewis, J.C., Newmayer, H.R.J. and Ward, R.G.
The stabilization of liquid metal during levitation melting. *J. of Sci. Instrum.*, 1962, 39, p. 569.
5. Holsey, W.J.
A.E.C. Report Y-1413, 1963, Union Carbide Nuclear Company, Y-12 plant, Oak Ridge Tennessee.
6. Okness E.C., Wroughton, D.M. Comenetz, P.H., Brace, P.H. and Kelly, J.C.R.
Journal of applied physics. 1952, 23, pp.545-552.
7. Jenkins, A.E., Harris, B., and Baker, L.A.
Electromagnetic levitation and its uses in physico-chemical studies at high temperatures. "Symposium on metallurgy at high pressures and high temperatures." *Met. Soc. A.I.M.E. Conference*, 1964, 22, pp. 23-43.
8. Yavoskii et al. An apparatus for investigating the kinetics of steel refining processes. *Izv. Vaz. Chern. Met.* 1975, 9, pp. 179-182. (B151 14040 March 1976).
9. Baker, L.A., Warner, N.A. and Jenkins, A.E.
Kinetics of decarburization of liquid iron in an oxidizing atmosphere using the Levitation Technique. *Trans. A.I.M.E.* 1964, 230, pp. 1228-1235.
10. Baker, L.A., Warner, N.A. and Jenkins, A.E.
Decarburization of a levitated iron droplet in oxygen. *Trans. A.I.M.E.*, 1967, 239, pp. 857-864.
11. Swisher, J.H. and Turkdogan. Decarburization of iron-carbon melts in CO₂-CO atmospheres. *Trans. A.I.M.E.* 1967, 239, pp. 602-610.
12. Distin, P.A., Hallett, G.D., Richardson, J.D.
Some reactions between drops of iron and flowing gases. *J.I.S.I.* 1968, 206, 821-833.

13. Ito, K. and Sano K. Decarburization of molten iron with oxidising gases and oxidation of co-existing metallic elements. Trans. I.S.I. J. 1968, 8, pp. 165-171.
14. Goto, K., Kawakami, M., and Someno, M. On the rate of decarburization of liquid metals with CO/CO₂ gas mixture. Trans. A.I.M.E. 1969, 245, pp. 293-301.
15. Kaplan, R.S. and Philbrook, W.D. The kinetics of gaseous oxidation of binary and ternary alloys of liquid iron. Trans. A.I.M.E. 1969, 245, pp. 2195-2204.
16. Ghosh, D.N. and Sen, P.K. Kinetics of decarburization or iron carbon melts in oxidizing gas atmospheres. J.I.S.I. 1970, 208, pp. 911-916.
17. Nomura, H., Mori, K. Kinetics of decarburization of liquid iron at low concentration of carbon. Trans. I.S.I.J. 1973, 13, pp. 325-332.
18. Fruehan, R.J. and Martonik, L.J. The rates of decarburization of liquid iron by CO₂ and H₂. Trans. A.I.M.E. 1974, 5, 1027-1032.
19. Achari, A. and Richardson, i). Reactions involving levitated drops of iron and nickel. Private Communication 1973.
ii) The carbon oxygen reaction in liquid iron. Physical chemistry and steelmaking. 1978, Vol. 3, pp. 48-51.
20. Sain, D.R. and Bolton, G.R. Interfacial reaction kinetics in the decarburization of liquid iron by carbon dioxide. Trans. A.I.M.E. 1976, 78, pp. 235-244.
21. Sain, D.R. and Bolton, G.R. The influence of sulphur on interfacial reaction kinetics in the decarburization of liquid iron by carbon dioxide. Trans. A.I.M.E. 1978, 98, pp. 403-408.
22. Fruehan, R.J. The effect of sulphur and phosphorus on the rate of decarburization of solid iron in hydrogen. Met. Trans. AIME, 1972, 3, 1447-53.
23. Hayes, P. and Grievson, P.
Met. Science Journal. 1975, 9, 332 -
24. Kootz, T.
Arch. Eisenhüttenw 1941, 15, p. 77.
25. Maxwell, J.C.
Collected Scientific Papers, Cambridge, 1890, 11, 625.

26. Langmuir, I.
Phys. Rev., 1918, 12, 368.
27. Ranz, W.E. and Marshall, W.R.Jr., Evaporation from drops II. Chem. Eng. Progress, 1952, 48, 173-180.
28. Steinberger, R.L. and Treybal, R.E. Mass transfer from a solid soluble sphere to a flowing liquid stream. A.I. Ch.E. Jnl. 1960, 6, 227-232.
29. Topley, B. and Whytelaw-Gray,
Phil. Mag. 1927, 4, 873.
30. Frocessling, N.
Gerlands Beit & Geophys. 1938, 52, 170.
31. Skelland, A.H.P., and Cornish A.R.H.
A.I. Ch.E. Jnl. 1963, 9, 73.
32. Merk, H.J. and Prins, J.A. Thermal convection in laminar boundary layers III. Appl. Sci. Res. 1954, 4A, 207-221.
33. Piret, G.L., Kyte, J.R.A., and Madden, A.J.
Chem. Eng. Progress. 1953, 49, 653.
34. Mathers, W.G., Madden, A.J., and Piret, E.L.
Simultaneous heat and mass transfer in free convection. Ind. Eng. Chem. 1957, 49, 961.
35. El-Kaddah, N.H. Carbon-oxygen equilibrium and homogeneous nucleation of carbon monoxide bubbles in levitated molten drops.
Ph.D. Thesis, Imperial College, London, 1975.
36. Hirshfelder, J.O., Curtiss, C.F. and Bird R.B.
Molecular Theory of Gases and Liquids.
John Wiley, New York (1964).
37. Bird, R.B., Stewart, W.E., and Lightfoot, E.N.
Transport phenomena. Wiley International Edition, 1967.
38. Lucas, L.D. Density of iron-carbon alloys.
Compt. Rend. 1959, 248, pp. 2336-38.
39. Richardson, F.D. Interfacial phenomena in metallurgical reactions. Trans. I.S.I.J. 1974, 14, pp.1-8.
40. Kozakevitch, P. Surface activity in liquid metal solutions (surface phenomena of metals).
S.C.I. Monograph, No. 28, 1968, pp.223-245.

41. Kozakevitch, P. & Urbain G. Surface Tensions of liquid iron and its alloys. Mem. Sci. Rev. Metallurgy 1961, 7, pp. 517-534.
42. Kozakevitch, P. & Urbain G. Surface tensions of liquid iron and its alloy. Mem. Sci. Rev. Metallurgy 1961, 12, pp. 931-947.
43. Hondros, E.D.
Proc. Roy. Soc. 1965, A286, pp. 479-98.
44. Hondros, E.D.
Acta. Met. 1968, 16, 377.
45. Robertson, D.G.C. Heterogeneous Reactions and mass transfer from liquid metal drops in gases. Ph.D. Thesis, University of New South Wales 1968.
46. See, J.B. and Warner, N.A. Reactions of iron alloy drops in free fall through oxidising gases. J.I.S.I. 1973, 211, pp. 44-52.
47. Robertson, D.G.C., Warner, N.A., and Jenkins, A.E. Basic oxygen and spray steelmaking. Chemeca. 1970. Aust. Acad. Sci., Butterworths, Sydney, 1971, pp. 54-69.
48. Roddis, P.G. Mechanism of decarburization of iron-carbon alloy drops falling through an oxidising gas. J.I.S.I. 1973, 211, pp. 53-58.
49. El-Kaddah, N.H. and Robertson, D.G.C. Homogeneous nucleation of carbon monoxide bubbles in iron drops. Jnl. Colloid and Interface Science, 1977, 60, pp. 349-360.
50. El-Kaddah, N.H. and Robertson, D.G.C. The nucleation of CO bubbles in molten iron-carbon drops reacting with oxidising gases. To be published in Met. Trans. B.
51. Turkdogan E.T., Grieveson, P., and Darken, L.S. Enhancement of diffusion-limited rates of vaporization of metals. J. Physical Chemistry, 1963, (67), pp. 1647-1654.
52. Turkdogan, E.T. The theory of enhancement of diffusion-limited vaporization rates by a convection-condensation process, Part I - Theoretical. Trans. A.I.M.E. 1964, 230, pp. 740-749.

53. Turkdogan, E.T. and Mills K.C. The theory of enhancement of diffusion-limited vaporization rates by a convection-condensation process. Part II - Experimental. Trans. A.I.M.E. 1964, 230, pp. 750-753.
54. Turkdogan, E.T., Grieveson, P., and Darken, L.S. Mechanism of the formation of iron oxide fumes. Open Heart Proc. A.I.M.E., 1962, 45, pp. 470-490.
55. Turkdogan, E.T. Reflections on research in pyrometallurgy and metallurgical chemical engineering. Trans. I.M.M. 1974, 83, Part C, pp. 67-81.
56. Kor, J.W. and Turkdogan, E.T. Vaporization of iron and phosphorus from iron-phosphorus melts in oxygen-bearing gas streams. Trans. A.I.M.E., 1975, 68, pp. 411-418.
57. Stull, D.R. and Prophet, H.
JANAF thermodynamic tables, June 1971.
58. Bookey, J.B. The free energies of formation of tricalcium and tetracalcium phosphates. J.I.S.I. 1952, 172, pp. 61-66.
59. Zellar, G.R., Payne S.L., Morris, J.P. and Ripp, R.L. The activities of iron and nickel in liquid Fe-Ni alloys. Trans. A.I.M.E. (1959), 215 pp. 181-185.
60. Speiser, R., Jacobs, A.J., and Spertnak, J.W. Activities of iron and nickel in liquid iron-nickel solutions. Trans. A.I.M.E. 1959, 215, pp. 185-192.
61. Turkdogan, E.T. and Leake, L.E. Preliminary studies on the evolution of fumes from iron at high temperatures. J.I.S.I. 1959, 192, pp. 162-170.
62. D.R. Creehan. The effect of MgO additions on the dephosphorizing capacity of steelmaking slags. Private Communication, 1980.
63. Olesen, W., and Maety, H.
Arch. f. Eisenhüttenwe, 1948, 19, pp. 111-117.
64. Kaiser, W., and Breslin, J. Factors determining the oxygen content of liquid silicon at its melting point. J. Appl. Phys. 1958, (29), p. 1292.

65. Wagner, C. Passivity during the oxidation of silicon at elevated temperatures. *J. Appl., Phys.* 1958, (29), p. 1295.
66. Sano, N., Matsushita, Y. Kinetics of silicon oxidation from liquid iron droplets. *I.S.I.J.* 1971, 11, pp. 232-239.
67. Filippov, S.I. and Martynov, S.Z. Kinetics of direct oxidation of impurities in liquid iron. *Izvest, vuz Chern. Met.* 1961, No. 1, p. 5. Brucher, H., Translation 5134.
68. Robertson, D.G.C.R. Heterogeneous reactions and mass transfer from liquid metal drops in gases. Ph.D. thesis, University of New South Wales, 1968, pp. 39-59.
69. Baker, R. Oxidation studies of molten iron alloy drops. *J.I.S.I.* 1967, , pp. 637-641.
70. Toop, G.W.
Ph.D. Thesis, University of London, 1964.
71. Forster, A., and Richardson, F.D.R. Oxidation of copper and nickel drops by carbon dioxide. *Trans. I.M.M.* 1975, C, pp. 116-122.
72. Glen, C.G. and Richardson, F.D. "Homogeneous kinetics at elevated temperatures". A symposium, G.R. Belton and W.L. Wornel, eds., 369-391. Plenum press, 1970.
73. Harvey, R.L. Kinetics of reactions of gases with levitated metal droplets. Ph.D. thesis, University of London, 1973.
74. Fruehen, R.J. The thermodynamic properties of liquid Fe-Si alloys. *Trans. A.I.M.E.* 1970, (1), pp. 865-870.
75. Kubaschewski, O., Evans, E.L.I. & Alcock, C.B. *Metallurgical thermochemistry*. Pergamon Press, 4th edition, Oxford, 1967.
76. Elliott, J.F., Gleiser, M. and Ramakrishna, V. *Thermochemistry for steelmaking*. (thermodynamic and transport properties). Addison-Wesley Publishing Company Inc., Pergamon Press, 1963, Vol. 2.
77. Zea, Y.K. The phosphorus reaction in basic open-hearth practice. *J.I.S.I.* 1945, No. I, pp. 459p-504p.

78. Winkler, T.B. and Chipman, J. Equilibrium study of distribution of phosphorus between iron and basic slags. Trans. A.I.M.E. 1946, 167, pp. 111-133.
79. Balagiva, K., Quarrell, A.G. & Vajragupta, P. A laboratory investigation of the phosphorus reaction in the basic steelmaking process. J.I.S.I. 1946, No. I, pp. 115-145.
80. Balagiva, K. and Vajragupta, P. The effect of temperature on the phosphorus reaction in the basic steelmaking process. J.I.S.I. 1947, 155, pp. 563-567.
81. Najragupta, P. Note on further work on the phosphorus reaction in basic steelmaking. J.I.S.I. 1948, 158, pp. 494-496.
82. Fischer, W.A. and Vom Ende, H.
Stahl u. Eisen, 1952, 72, pp. 1398-1408.
83. Bookey, J.B. The free energy of formation of magnesium phosphate. J.I.S.I. 1952, 172, pp. 66-68.
84. Bookey, J.B. The free energies of formation of tricalcium and tetracalcium phosphates. J.I.S.I. 1952, 172, pp. 61-66.
85. Turkdogan, E.T. and Pearson, J. Activities of constituents of iron and steelmaking slags. Part III - phosphorus pentoxide. J.I.S.I. 1953, 153, pp. 398-401.
86. Healy, G.W. A new look at phosphorus distribution. J.I.S.I. 1970, pp. 664-668.
87. Flood, H., and Grjothcim, K. Thermodynamics calculation of slag equilibria. J.I.S.I. 1952, 171, pp. 64-72.
88. Trömel, G., Fritze, H.W. Further experiments on the dephosphorization of iron with lime rich slags. Arch. f. Eisenhütten 1957, 28, pp. 489-495.
89. Trömel, G., and Fritze, H.W. Equilibria between iron and lime containing phosphate slags. Arch. f. Eisenhütten 1959, 30, pp. 461-72.
90. Trömel, G., Fix, W., and Fritze, H.W. Summary of equilibrium between iron and lime containing phosphate slags. Arch. f. Eisenhütten. 1961, 32, pp. 353-359.

91. Drewes, E.J. and Olette, M.
Arch. Eisenhuettenw 1967, 38, No. 3, pp.163-75.
92. Schwerdtfeger, K. and Turkdogan, E.T. Miscibility gap in the system iron oxide-CaO-P₂O₅ in air at 1625°C. Trans. A.I.M.E. 1967, 239, pp.589-590.
93. Olette, M. and Vancon, G. Studies of the miscibility gap in the system P₂O₅-CaO-FeO-Fe₂O₃. Circulaire Informations techniques (France) 1961, No. 7-8, pp. 1739-54.
94. Kawai, Y. and Nakajima, H. Rate of dephosphorization of liquid iron by solid lime. Trans. I.S.I.J., 1974, 14, pp. 96-101.
95. Yoshii, C. and Miura, F.
Tetsu-to-Hagane, 1966, 52, p. 521.
96. Kawai, Y., Mori, K., and Nakashima, H.
Proc. ICSTIS, Suppl. Trans. I.S.I.J., 1971, 11, p. 520-
97. Fuji, T., Araki, T., and Marukawa, K.
Analysis of oxidising reactions in an oxygen top blowing convertor. Trans. I.S.I.J. 1969, 9, p.437.
98. Aratani, F., and Sanbongi, K.
Tetsu-to-Hagane 1972, 58, p. 1225.
99. Inoue, H., Shigeno, Y., Tokuda, M., and Ohtani, M.
Simultaneous desulphurization and dephosphorization of hot metal by CaCl₂-CaO flux. Proceedings to the 2nd international conference on injection metal. June 1980, Lulea, Sweden.
100. Mori, K., Doi, S., Kaneko, T., and Kawai, Y.
Rates of transfer of phosphorus between metal and slag. Trans. I.S.I.J. 1978, 18, pp. 261-268.
101. Knights, C.F. and Perkins, R. Distribution of metallic elements between slags and metals at temperatures up to 2000°C. Trans. I.M.M. 1970, C, pp. 197-206.
102. Oelsen, W. and Wiemer, H. Exsolution occurrence in ferrous oxide-sodium phosphate slags. Mitt. Kais-Wilhelm-Inst. f. Eisenforsch. 1942, 24, pp. 167-210.

103. Oelsen, W. and Maetz, H.
Mitt. Kaiser-Wilhelm-inst. Eisenforsch.
Düsseldorf 1941, 23, (No. 12), pp.195-245.
104. Turkodgan, E.T. Physical chemistry of oxygen
steelmaking thermochemistry and thermodynamics.
Monograph series on BOF steelmaking U.S. steel
Co. Dec. 1970.
105. El-Kaddah, N.H. and Robertson, D.G.C. The kinetics
of gas-liquid metal reactions involving
levitated drops. Carburization and
decarburization of molten iron in CO/CO₂
gas mixtures at high pressures.
Met. Trans. A.I.M.E. 1978, 9B, pp. 191-199.
106. Satyanarayana, Rao, G. Kinetics and mechanisms of
gas-metal-slag reactions relevant to
steelmaking. Ph.D. Thesis, Imperial College,
London, 1979.
107. Gaye, H., and Riboud, P.V. Oxidation kinetics of
iron alloy drops in oxidizing slags. Trans.
A.I.M.E. 1977, 8B, pp. 409-415.
108. Turkdogan, E.T. and Leake, L.E. Preliminary studies
on the evolution of fumes from iron at high
temperatures. J.I.S.I. 1959, 192, pp. 162-170.
109. Turkdogan, E.T. Activities of oxides in CaO-FeO-
Fe₂O₃ melts. Trans. A.I.M.E. 1961, 221,
pp. 1090-95.

FUTURE WORK

The effect of phosphorus, at higher concentrations in the metal drops, on the rate of decarburization of iron-carbon and nickel-carbon alloys need further investigation. It is suggested that such studies should be carried out at higher temperatures, to show the effect of the phosphorus on the rate of vaporization of iron or nickel. It is also recommended that CO_2 should be used instead of O_2 to overcome any contributing factor due to the combustion of CO in the gaseous boundary layer, and to clarify the contribution due to natural convection, under the conditions of $\text{Gr}/\text{Re}^2 < 1.3$.

The nucleation of CO bubbles in levitated drops of iron-carbon alloys needs to be further studied, under the conditions of relatively low decarburization rates $\sim 2 \times 10^{-5} \text{ moles.cm}^{-2} \text{ s}^{-1}$ and at lower temperatures to verify the occurrence of the carbon boil (if any) in the absence or presence of an oxide phase.

The removal of phosphorus from liquid iron or nickel alloys by a vapour phase reaction needs further study. It is difficult to suggest any better experimental technique for carrying out such investigations than levitation or free fall. It is thought that removal of phosphorus via volatile chlorides may be possible, in which case the experiments should be carried out in streams of chloride with or without the presence of other oxidising gas mixtures. If the above experiments result

in an efficient dephosphorization of the alloys, then it is worthwhile to consider the simultaneous removal of carbon, silicon and phosphorus by such a vapour phase reaction.

Dephosphorization of iron based alloys by basic slags of various compositions requires further attention, in order to establish the true equilibrium constants for distribution of phosphorus between the metal and complex slags. It is suggested that these experiments should be carried out in crucibles rather than by the levitation technique to overcome any contribution due to the temperature gradient in the slag phase.

Finally, the kinetics of removal of silicon and phosphorus from iron drops in the presence of lime requires some investigation to clarify the simultaneous removal of silicon and phosphorus in the Q-BOP.